

The Structures of Cellulose

ACS SYMPOSIUM SERIES **340**

The Structures of Cellulose

Characterization of the Solid States

Rajai H. Atalla, EDITOR
Institute of Paper Chemistry

Developed from a symposium sponsored by
the Cellulose, Paper, and Textile Division
at the 190th Meeting
of the American Chemical Society,
Chicago, Illinois,
September 8-13, 1985



American Chemical Society, Washington, DC 1987



Library of Congress Cataloging-in-Publication Data

The structures of cellulose.

(ACS symposium series; 340)

Includes bibliographies and indexes.

I. Cellulose—Congresses.

I. Atalla, Rajai H., 1935- . II. American Chemical Society. Cellulose, Paper, and Textile Division. III. American Chemical Society. Meeting (190th: 1985: Chicago, Ill.) IV. Series.

TS933.C4S77 1987 547.7'82 87-11537

ISBN 0-8412-1032-2

Copyright © 1987

American Chemical Society

All Rights Reserved. The appearance of the code at the bottom of the first page of each chapter in this volume indicates the copyright owner's consent that reprographic copies of the chapter may be made for personal or internal use or for the personal or internal use of specific clients. This consent is given on the condition, however, that the copier pay the stated per copy fee through the Copyright Clearance Center, Inc., 27 Congress Street, Salem, MA 01970, for copying beyond that permitted by Sections 107 or 108 of the U.S. Copyright Law. This consent does not extend to copying or transmission by any means—graphic or electronic—for any other purpose, such as for general distribution, for advertising or promotional purposes, for creating a new collective work, for resale, or for information storage and retrieval systems. The copying fee for each chapter is indicated in the code at the bottom of the first page of the chapter.

The citation of trade names and/or names of manufacturers in this publication is not to be construed as an endorsement or as approval by ACS of the commercial products or services referenced herein; nor should the mere reference herein to any drawing, specification, chemical process, or other data be regarded as a license or as a conveyance of any right or permission, to the holder, reader, or any other person or corporation, to manufacture, reproduce, use, or sell any patented invention or copyrighted work that may in any way be related thereto. Registered names, trademarks, etc., used in this publication, even without specific indication thereof, are not to be considered unprotected by law.

PRINTED IN THE UNITED STATES OF AMERICA

American Chemical Society
Library
1155 16th St., N.W.

In **Washington, D.C. 20036**, D.C.

ACS Symposium Series; American Chemical Society: Washington, DC, 1987.

ACS Symposium Series

M. Joan Comstock, *Series Editor*

1987 Advisory Board

Harvey W. Blanch
University of California—Berkeley

Alan Elzerman
Clemson University

John W. Finley
Nabisco Brands, Inc.

Marye Anne Fox
The University of Texas—Austin

Martin L. Gorbaty
Exxon Research and Engineering Co.

Roland F. Hirsch
U.S. Department of Energy

G. Wayne Ivie
USDA, Agricultural Research Service

Rudolph J. Marcus
Consultant, Computers &
Chemistry Research

Vincent D. McGinniss
Battelle Columbus Laboratories

W. H. Norton
J. T. Baker Chemical Company

James C. Randall
Exxon Chemical Company

E. Reichmanis
AT&T Bell Laboratories

C. M. Roland
U.S. Naval Research Laboratory

W. D. Shults
Oak Ridge National Laboratory

Geoffrey K. Smith
Rohm & Haas Co.

Douglas B. Walters
National Institute of
Environmental Health

Foreword

The ACS SYMPOSIUM SERIES was founded in 1974 to provide a medium for publishing symposia quickly in book form. The format of the Series parallels that of the continuing ADVANCES IN CHEMISTRY SERIES except that, in order to save time, the papers are not typeset but are reproduced as they are submitted by the authors in camera-ready form. Papers are reviewed under the supervision of the Editors with the assistance of the Series Advisory Board and are selected to maintain the integrity of the symposia; however, verbatim reproductions of previously published papers are not accepted. Both reviews and reports of research are acceptable, because symposia may embrace both types of presentation.

Preface

“We must love them both, those whose opinions we share and those whose opinions we reject. For both have labored in the search for truth and both have helped us in the finding of it.”

—Saint Thomas Aquinas

CONTROVERSY HAS BEEN A CONSTANT IN THE STUDY OF CELLULOSE since it began in the middle of the past century, during its growth with expansion of industrial use of cellulosic raw materials, and with advances in plant biology. The early controversies involved many hypotheses concerning the chemical nature of cellulose and culminated in the acceptance of the polymer hypothesis during the first decades of this century. More recent controversies have dealt with hypotheses concerning the physical structures of cellulose as well as the mechanisms of its biogenesis.

The symposium upon which this book is based was an attempt to promote convergence among the structural hypotheses toward a useful paradigm. Such a model would be helpful to practitioners in other areas of cellulose science who are seeking to organize chemical or biological data concerning cellulose in relation to its structure. The symposium also sought to bring together reports from the leading laboratories active in structural studies on the many forms and complexes of cellulose. The objective was to incorporate discussion of new methodologies that have been applied to cellulose in the past decade and to include the most recent results based on more traditional methods of structural investigation. Furthermore, the organizers of the symposium wanted to include some presentations representative of the uses of structural studies to complement investigations of other aspects of cellulose.

Another objective of the symposium, in addition to promoting further studies in the field, was to provide those in related fields with a sense of the origin of the controversies and the questions that remain open.

In a review published in 1970, D. W. Jones wrote, “After extensive studies by many crystallographers over the last 50 years. . . many uncertainties remain about the crystal structures of the celluloses and their derivatives.” Later in the same review he added, “When evidence from spectroscopy and stereochemistry is taken into account, the X-ray data from cellulose I, modest as they are, have not been shown to be consistent with any conventional crystal structure.” The diversity of views represented

in the chapters of this book suggests that the observations made by Jones remain valid today, though perhaps some convergence of views can be perceived.

Investigators attempting to interpret the diffractometric data seek the simplest structure consistent with the data. On the other hand, neither recent spectroscopic results nor some of the earlier data concerning allomorphic transformation could be rationalized in terms of the simple structures that were fitted to the diffractometric data. Thus, to the extent that a structural model is to be used to organize and interpret patterns of behavior, the simple structural models are inadequate. Yet the diffractometric data have not provided a sufficient basis for refinement of a structural model with a larger number of internal degrees of freedom. The chapters in this book are at the leading edge of the effort to resolve the questions that remain in this area.

Readers familiar with the traditional terminology in the field of cellulose structures will note that, in many chapters, the commonly used *polymorph* has been replaced with *allomorph*. This term was suggested by A. D. French, who pointed out that this differentiation is more consistent with correct usage in crystallography. This usage has not been required of authors, however, so both forms occur in the book.

The cooperation of many individuals has been central to completion of this volume. R. St. John Manley first suggested the symposium when he was program chairman for the Cellulose, Paper, and Textile Division. More recently, as chairman of the division, he supported publication of this volume in the ACS Symposium Series. The referees provided an important measure of refinement for the manuscripts beyond the initial drafts. A. D. French was willing to undertake a disproportionate share of the review process and provided helpful editorial assistance for a number of manuscripts. The Institute of Paper Chemistry provided valuable assistance with respect to correspondence and preparation of a number of manuscripts not originating at the Institute; Grace Kessler was particularly helpful. Robin Giroux of the ACS Books Department provided support and helpful suggestions at many stages during the publication process. Finally, the authors, who invested time and effort in the preparation of the manuscripts, are the individuals without whom the publication would not be possible. I extend to all my deepest appreciation.

RAJAI H. ATALLA
Institute of Paper Chemistry
Appleton, WI

March 1987

Chapter 1

Structures of Cellulose

Rajai H. Atalla

Institute of Paper Chemistry, Appleton, WI 54912

An overview of studies of the structure of cellulose is presented and begins with a historical perspective, developed with particular emphasis on the early diffractometric studies. More recent studies are then described, and the key questions confronted in any analysis of diffractometric data are discussed. The central questions are concerned with the validity of the assumption that the unit cells of cellulose belong to space group $P2_1$, and whether the twofold screw axis associated with this space group coincides with the molecular chain axes. The diversity of the interpretations which occur in the literature and in following chapters is noted. More recent spectroscopic investigations are then discussed, with emphasis on the degree to which they may provide additional information concerning structure. It is noted that although both Raman spectroscopy and CP-MAS ^{13}C NMR cannot provide direct information concerning the positions of molecules in the unit cells, they are sensitive to the values of the internal coordinates. Thus, they provide information complementary to the diffractometric data in that it serves to constrain the acceptable structural models to a smaller subset than that otherwise admissible on the basis of diffractometric observations alone. In this respect, the spectroscopic information complements the diffractometric data in the same way as the assumptions concerning the symmetry of the unit cell. Furthermore, it appears that the structures suggested by the spectroscopic studies represent relatively small although significant departures from those derived on the basis of diffractometry alone. In anticipation of future directions in studies of celluloses, it is noted that multidisciplinary approaches, similar to some described in later chapters, hold great promise for future progress in understanding the structural diversity that is characteristic of cellulose.

0097-6156/87/0340-0001\$06.00/0
© 1987 American Chemical Society

Since the occurrence of cellulose as a distinct substance was first recognized by Anselme Payen in 1842 the evolution of ideas concerning its structure has been closely related to advances in structural chemistry and its methodologies. The pattern of close relation continues into the present time and is well reflected in the following chapters which include contributions from most of the major laboratories active in the field. In this chapter, we discuss the structural problem in general and place those of the following chapters which are concerned with the problem in perspective relative to recent developments in the field, with particular emphasis on the past decade.

The procedures for structural studies on cellulose have much in common with investigations of structure in polymers in general. In most instances diffractometric data are not sufficient for a solution of the structure in a manner analogous to that possible for lower molecular weight compounds which can be made to form single crystals. It becomes necessary, therefore, to complement diffractometric data with structural information derived from studies carried out on the monomers or oligomers.

Kakudo and Kasai have summarized the central problem well (1): "There are generally less than 100 independently observable diffractions for all layer lines in the x-ray diagram of a fibrous polymer. This clearly imposes limitations on the precision which can be achieved in polymer structure analysis, especially in comparison with the 2000 or more diffractions observable for ordinary single crystals. However, the molecular chains of the high polymer usually possess some symmetry of their own, and it is often possible to devise a structural model of the molecular chain to interpret the fiber period in terms of the chemical composition by comparison with similar or homologous substances of known structure. Structural information from methods other than x-ray diffraction (e.g., infrared and NMR spectroscopy) are also sometimes helpful in devising a structural model of the molecular chain. The majority of the structural analyses which have so far been performed are based on models derived in this way. This is, of course, a trial and error method". Similar perspectives have been presented by Arnott (2), Atkins (3), and Tadokoro (4,5).

An acceptable fit to the diffractometric data is not the ultimate objective, however. Rather it is the development of a model that possesses a significant measure of validity as the basis for organization, explanation and prediction of experimental observations. With respect to this criterion, the models of cellulose which have been developed so far leave much to be desired, for their capacity to integrate and unify the vast array of information concerning cellulose is limited indeed. One of the objectives of this symposium is to facilitate identification of points of departure for further studies in search of models which are more useful.

To help place the proceedings in perspective we begin with a brief historical review, and continue with a discussion of recent contributions based on the key methodologies which have been used. The methodologies are in three broad, complementary categories, which include diffractometry, spectroscopy, and theoretical model building on the basis of conformational analysis. Although, significant structural information is inferred from patterns of chemical

reactions under a wide range of conditions, we limit this chapter to studies based on physical methods.

In order to achieve greater clarity in the following discussion, it is well to note that questions of structure arise at three different levels. The first, that of the chemical structure, reflects the pattern of covalent bonding in cellulose molecules and is generally well established. While the evolution of concepts at this level is of historical interest, it is not under discussion in these proceedings. The next level of structure is that of the relative organization of the repeat units in an individual molecule, under constraints of conformational energy considerations, as well as considerations of packing of the molecules in a particular state of aggregation. This level of structure is particularly important in spectroscopic studies wherein the energy levels between which transitions are observed are determined by the values of the internal coordinates which define molecular conformations. The final level of structure is that reflecting the arrangement of the molecules relative to each other in a particular state of aggregation, whether it be amorphous, or represents one or another of the crystalline allomorphs which occur because of the polymorphy characteristic of the crystallinity of cellulose. This is the level of structure probed by diffractometric measurements which are inherently most sensitive to the three dimensional organization represented by a particular state of aggregation.

Historical Overview

The evolution of ideas concerning the nature of cellulose and the models of its chemical structure have been described by Purves (6) in an excellent overview, beginning with the first observations by Payen and leading up to those which finally won acceptance of the polymer hypothesis in the decade immediately preceding the Second World War. Another valuable perspective is presented by Flory (7) in his general review of the evolution of the polymeric hypothesis, highlighting investigations of the three common natural homopolymers: starch, cellulose, and natural rubber. Finally, the first chapter in the treatise by Hermans (8) focuses on the physical chemical aspects of the early structural studies, in an account which is an excellent complement to the review by Purves with its emphasis on the classical organic chemical phase in the structural studies.

Among more recent reviews of structure, those by Jones (9), and by Tonessen and Ellefsen (10,11) are the most comprehensive. Preston (12) and Frey-Wyssling (13) in their respective treatises on plant cell walls, have also touched upon the problem of the structure of cellulose. The reader is referred to these sources for comprehensive presentations of the range of proposals concerning the structures of cellulose which have been under discussion in recent decades. A representative subset will be presented here as a point of departure for following discussions.

Quite early in the x-ray diffractometric studies of cellulose it was recognized that its crystallinity is polymorphic. It was established that native cellulose, on the one hand, and both regenerated and mercerized celluloses, on the other, represent two distinct crystallographic allomorphs (14). Little has transpired

since the early studies to change these perceptions. There has been, however, little agreement regarding the structures of the two forms. For example, Petitpas *et al.* (15) have suggested on the basis of extensive analyses of electron-density distributions from x-ray diffractometric measurements that chain conformations are different in celluloses I and II. In contrast, Norman (16) has interpreted the results of his equally comprehensive x-ray diffractometric studies in terms of similar conformations for the two allomorphs.

At a more basic level than the comparison of celluloses I and II, the structure of the native form itself has remained in question. Among recent studies, for example, Blackwell and Gardner (17), in their analysis of the structure of cellulose from Valonia ventricosa, assumed a lattice belonging to the $P2_1$ space group, with the twofold screw axis coincident with the molecular chain axis. Hebert and Muller (18), on the other hand, in an electron diffractometric study of a number of celluloses including Valonia, confirmed the findings of earlier investigators who found no systematic absences of the odd order reflections forbidden by the selection rules of $P2_1$, and concluded that the cellulose unit cells do not belong to that space group.

Even when $P2_1$ is taken to be the appropriate space group, the question of chain polarity remains. As noted by Jones (19), and by Howson and Sisson (20), the structure initially proposed by Meyer and Mark (21) assumed that the chains were parallel in polarity. The structure later proposed by Meyer and Misch (22) was based on the reasoning that the rapidity of mercerization, and its occurrence without dissolution required that the polarity of the chains be the same in both celluloses I and II. It was reasoned further that regeneration of cellulose from solution is most likely to result in precipitation in an antiparallel form, and that the similarity between x-ray diffraction patterns of mercerized and regenerated cellulose required that they have the same polarity. It was thus inferred that native cellulose must also have an antiparallel structure.

Although the argument that regeneration in the antiparallel mode is more probable was found invalid within a decade of its first presentation (23), the relative organization of molecules suggested by Meyer and Misch remained the point of departure for most subsequent investigators.

When the models incorporating antiparallel arrangement of the chains are extended to native cellulose, they pose serious questions concerning proposed mechanisms for the biosynthesis of cellulose. It is difficult to envision a plausible mechanism for simultaneous synthesis and aggregation of antiparallel chains. It is perhaps for this reason that more recent proposals of parallel structures for native cellulose have been embraced by investigators of the mechanism of biosynthesis.

The contribution of spectroscopy to the early studies of structure was quite limited. An important contribution was made in the studies by Liang and Marchessault (24-26) wherein measurements of dichroism in infrared absorption of oriented specimens led to proposal of a particular hydrogen-bonding scheme. The differences between the spectra of celluloses I and II were explained in terms of differences in the packing of molecular chains and associated

variations in the hydrogen-bonding patterns. In another application, infrared absorption measurements were used as the basis of a crystallinity index by Nelson and O'Connor (27,28).

More recently, a number of new structure sensitive techniques have been developed, and they have been applied to studies of cellulose. These include Raman spectroscopy and Solid State ^{13}C Nuclear Magnetic Resonance, in the experimental arena, and conformational energy calculations in the theoretical domain. These are more recent contributions and are the subjects of subsequent sections in this chapter and later chapters in these proceedings.

Diffractometric Studies

As noted by Kakudo and Kasai, the primary difficulty in structural studies on polymeric fibers is that the number of reflections usually observed in diffractometric studies are quite limited. In the case of cellulose it is generally difficult to obtain more than 50 reflections. Consequently it becomes necessary to minimize the number of structural coordinates to be determined from the data by adopting plausible assumptions concerning the structure of the monomeric entity. The limited scattering data are then used to determine the orientation of the monomer units with respect to each other. In the majority of diffractometric studies of cellulose published so far, the monomeric entity has been chosen as the anhydroglucose unit. Thus, structural information from single crystals of glucose is implicitly incorporated in the analyses of the structure of cellulose. The coordinates which are adjusted in search of a fit to the diffractometric data include those of the primary alcohol group at C6, those of the glycosidic linkage, and those defining the positions of the chains relative to each other.

In addition to selection of the structure of the monomer as the basis for defining the internal coordinates of the repeat unit, the possible structures are usually further constrained by taking advantage of any symmetry possessed by the unit cell. The symmetry is derived from the systematic absence of reflections which are forbidden by the selection rules for a particular space group. In the case of cellulose, the simplification usually introduced is the application of the symmetry of space group $P2_1$, which includes a twofold screw axis parallel to the direction of the chains. The validity of this simplification remains the subject of controversy, however, because the reflections which are disallowed under the selection rules of the space group are in fact frequently observed. In most of the studies these reflections, which are usually weak relative to the other main reflections, are assumed to be negligible. The controversy continues because the relative intensities can be influenced by experimental conditions such as the periods of exposure of the diffractometric plates. Furthermore, the disallowed reflections tend to be more intense in electron diffractometric measurements than in x-ray diffraction measurements. Thus, more often than not, investigators using electron diffraction challenge the validity of the assumption of twofold screw axis symmetry.

The key assumption with respect to symmetry, however, is not the existence of the twofold screw axis as an element of the symmetry of the unit cell, but rather the additional assumption that

this axis coincides with the axis of the molecular chains of cellulose. This latter assumption has, implicit in it, a number of additional constraints on the possible structures which can be derived from the data. It requires that adjacent anhydroglucose units are related to each other by a rotation of 180 degrees about the axis, accompanied by a translation equivalent to half the length of the unit cell in that direction; it is implicit, therefore, that adjacent anhydroglucose units are symmetrically equivalent and, correspondingly, that alternating glycosidic linkages along the chain are symmetrically equivalent.

If the assumption concerning coincidence of the twofold screw axis and the molecular chain axis were excluded for example by locating the twofold screw axis between the molecular chains though still parallel to the chain axes, the diffractometric patterns would admit nonequivalence of alternate glycosidic linkages along the molecular chain, as well as the nonequivalence of adjacent anhydroglucose units. This possibility has been ignored, however, in large part because it requires expansion of the number of internal coordinates which have to be determined from the diffractometric data. Furthermore, it excludes the possibility of antiparallel alignment of chains in the unit cell.

The assumptions that the unit cell possesses the symmetry of space group $P2_1$ and that the twofold axis is coincident with the chain axis, do in fact meet a criterion long honored in scientific studies, namely, William of Ockham's principle of economy, which requires that the most simple hypothesis consistent with observations should always be adopted. Clearly the structure based on the anhydroglucose as the repeat unit is the most simple structure that accounts for the majority of the diffractometric data. Furthermore, the diffractometric data available are not sufficient to allow refinement of a structure possessing many more degrees of freedom, as would be the case if the twofold axis were not assumed coincident with the chain axis.

The assumptions concerning the symmetry of the unit cell noted above have been the basis of recent refinements of the structure of cellulose I. In one such refinement (17) the forbidden reflections were simply assumed negligible, and the intensity data from Valonia cellulose were used to arrive at a final structure. In another study, the inadequate informational content of the diffractometric data was complemented with analyses of lattice packing energies (29); the final structures were constrained to minimize the packing energy as well as optimizing the fit to the diffractometric data. Here the assumptions implicit in the weighting of the potential functions which are used in the energy calculations, further complicate the interpretations. As noted by French, et al. in a subsequent chapter in these proceedings, the structures derived in these two studies, though both based on parallel chain arrangements, are nevertheless very different crystal structures. When the same convention is applied in defining the axes of the crystal lattice, the structure most favored in one analysis is strongly rejected in the other. Furthermore, neither of these is strongly favored over yet a third, antiparallel structure (30).

The structures of oligomers are another important source of relevant information cited by Kakudo and Kasai. The implications of

the structures of the disaccharides have been considered by Atalla (31) and were the basis for reassessment of the second assumption concerning symmetry noted above. Structures with alternating non-equivalent glycosidic linkages were found more consistent with spectroscopic data (32).

Studies of oligomers have been extended in two chapters in the present volume, with the comparisons made primarily with structures proposed for cellulose II. Sakthivel, *et al.* applied the Rietveld crystal structure method to cellotetraose. Their results favor a parallel arrangement of chains in the unit cell, with individual chains possessing near twofold screw axis symmetry.

In a study of a number of oligomers, Henrissat, *et al.* used a multidisciplinary approach to examine the matter of the valid repeat unit. Their conformational analyses and ^{13}C NMR spectra were interpreted in terms of nonequivalent glycosidic linkages in the individual chains, but the diffraction data were found most consistent with an antiparallel structure.

Spectroscopy

Spectroscopic studies are useful in structural investigations because they provide information which is complementary to that derived from diffractometric data. The information derived from spectra is not directly related to the coordinates of molecules in the unit cell. The spectra are, however, sensitive to the values of internal coordinates which define molecular structure. Thus they provide a basis for testing the degrees of equivalence of structures. Very often also, specific spectral features can be identified with particular functional groups defined by distinctive sets of internal coordinates.

Two classes of spectral studies have been applied for the first time during the past decade as the basis of structural studies of cellulose. These are Raman spectroscopy, and solid state ^{13}C NMR using the CP/MAS technique. Both have raised questions concerning the assumptions about symmetry incorporated in the diffractometric studies. And while they cannot provide direct information concerning the structures, they establish criteria that any structure must meet to be regarded as an adequate model. The information from spectroscopic studies represents one of the major portions of the phenomenology that any acceptable structural model must rationalize.

Although the new spectral methods have also found application in investigations of structural changes induced by mechanical treatments or by treatments with swelling agents, the following discussion will be limited to studies which have focused on questions of structure. The results of such studies have to be rationalized by any model derived from crystallographic investigations and thus provide tests of consistency complementary to the diffractometric data, in the sense set forth by Kakudo and Kasai.

Raman Spectroscopy. Raman spectroscopy is the common alternative to infrared spectroscopy for investigating molecular vibrational states and vibrational spectra. It has enjoyed a significant revival since the development of laser sources for excitation of the spectra. Its key advantage in the present context is that it is

primarily sensitive to the skeletal vibrations of the cellulose molecule, with the mode of packing in the lattice having only secondary effects. This feature is a consequence of the dependence of Raman spectral activity of molecular vibrations on changes in the polarizability of vibrating bond systems, rather than changes in associated molecular dipoles. The most intense contributions to the spectra are due to bond systems which are predominantly covalent in character, with the more polar systems resulting in much weaker bands.

In the first detailed comparison of the Raman spectra of celluloses I and II, it was concluded that the differences between the spectra, particularly in the low frequency region, could not be accounted for in terms of chains possessing the same conformation but packed differently in the different lattices (33). As noted above, that had been the general interpretation of diffractometric studies of the two most common allomorphs. The studies of the Raman spectra led to the proposal that two different stable conformations of the cellulose chains occur in the different allomorphs.

In order to establish the differences between the conformations, information from other sources was considered. The results of published conformational energy calculations suggested two stable conformations for the glycosidic linkages (34,35). These represent relatively small left-handed and right-handed departures from the conformation of the glycosidic linkage in a twofold helical structure. They are well approximated, respectively, by the experimentally observed conformations of the glycosidic linkages in the crystal structures of the model disaccharides cellobiose (36) and methyl- β -cellobioside (37).

An analysis of the vibrational spectra in the OH stretching region for both the model disaccharides and for celluloses I and II suggested that nonequivalent glycosidic linkages alternate along the molecular chains (31). The solid state ^{13}C NMR spectra were found consistent with this model (38), although alternative interpretations are also possible. Finally the Raman spectra in the methylene bending region indicated that the C6 carbons occur in two nonequivalent environments in cellulose I but appear merged into a single set in cellulose II (39).

The results of the spectroscopic studies were interpreted in terms of nonequivalence of adjacent anhydroglucose units in the molecular chains, requiring the basic repeat unit of structure to be taken as the dimeric anhydrocellobiose unit. The difference between cellulose I and II was associated with the locus of the nonequivalence. In cellulose II it was thought to be at the glycosidic linkages, while in cellulose I it was taken to be centered at C6 and the adjacent segment of the pyranose rings.

To reconcile the conclusions outlined above with the requirements of chain packing, the proposal was made that cellulose chains possess alternate left-handed and right-handed glycosidic linkages in sequence along the chain axes. The left-handed and right-handed linkages were envisioned as representing relatively small departures of the dihedral angles from those prevailing for a twofold helix. The degree of departure from the parameters of a twofold helix was seen as somewhat greater for cellulose II than for cellulose I. The

model is discussed in somewhat more detail in the chapter by Wiley and Atalla, later in this volume.

Solid State ^{13}C NMR Spectra.

The second important spectroscopic method which has been applied in investigating the structure of cellulose during the past decade is high resolution ^{13}C NMR of the solid state based on the CP-MAS technique. In this technique, cross polarization (CP) is used to enhance the ^{13}C signal, high power proton decoupling to eliminate dipolar couplings with protons, and magic angle spinning (MAS) of the sample about a particular axis relative to the field to eliminate chemical shift anisotropy. Application of this method results in acquisition of spectra of sufficiently high resolution so that chemically equivalent carbons which occur in magnetically nonequivalent sites can be distinguished.

Though the technique has been used by a number of different investigators (38,40-43), we focus here on the studies by VanderHart and Atalla as representative of the structural questions addressed (44,45). Some resonance multiplicities for chemically equivalent carbons occur in the spectra of all the celluloses investigated.

The spectra of high crystallinity samples of cellulose II showed clear splittings of the resonances associated with C4 and C1. These have been interpreted as evidence of nonequivalent glycosidic linkages along the molecular chains (38), though it has also been suggested that the splittings may be evidence for nonequivalent chains in the unit cell (43). The latter argument leaves open the question as to why the resonances for carbons 2, 3, 5, and 6 do not display similar splittings.

Perhaps the most significant new information derived from the CP-MAS spectra is that relating to the native celluloses. The spectra reveal multiplicities that cannot be interpreted in terms of a unique unit cell, even though they arise from magnetically nonequivalent sites in crystalline domains. The narrow lines observed have relative intensities which are neither constant among the samples of different native celluloses, nor are they in the ratios of small whole numbers as would be expected if they arose from different sites within a relatively small unit cell. VanderHart and Atalla proposed that native celluloses are composites of two distinct crystalline forms (44,45).

Spectra of the two forms were resolved through linear combination of the spectra of native celluloses possessing the two forms in different proportions. The two types were designated celluloses I_{α} and I_{β} . The I_{α} form was found to be dominant in celluloses from lower plant forms and bacterial celluloses, while the I_{β} form was found dominant in celluloses from higher plants.

In studies of the Raman spectra of different native celluloses, Atalla (32) concluded that the two forms I_{α} and I_{β} consist of molecular chains which have the same molecular conformation. In the chapter by Wiley and Atalla in the present volume, evidence is presented to suggest that though the molecular conformations are the same, the hydrogen-bonding patterns differ in the two forms.

VanderHart and Atalla also present additional ^{13}C NMR CP-MAS experiments in a subsequent chapter. These provide strong evidence for the existence of the I_{α} and I_{β} forms in native celluloses,

particularly those from the lower plants and bacterial cellulose. They do raise, however, some questions about the earlier estimates of the amount of I_{α} form in the native celluloses from the higher plants.

In yet another application of the CP-MAS ^{13}C NMR spectroscopy in studies of the structure of celluloses, Horii, *et al.* have introduced correlations between the chemical shifts and dihedral angles as the basis of developing new structural information. In a subsequent chapter in these proceedings they provide an overview of their studies correlating the chemical shifts of specific carbons with the values of the dihedral angles about bonds involving those carbons. By examining the values of chemical shifts for monomeric and oligomeric compounds of known structures, they have developed correlations which may be applied in translating the spectral information in a manner that is complementary to the diffractometric studies.

Multidisciplinary Studies

In addition to the studies outlined above, with primary focus on diffractometry or on spectroscopy, there have been, recently, a number of studies which recognize at the outset the type of constraints summarized by Kakudo and Kasai, and which begin with an integrated approach to the investigation of structure. Perhaps the best illustration of this approach is the work of Henrissat and coworkers noted earlier and outlined in a later chapter, focusing on oligomers clearly related to the structure of cellulose II.

In the work of Henrissat, *et al.*, the x-ray diffractometric data of Poppleton and Mathieson (46) on cellotetraose was complemented with structural data on other oligomers, with CP-MAS ^{13}C NMR spectroscopy, with conformational energy calculations, and with molecular orbital calculations to determine some of the favored conformations. The difficulty of the problem of the structures of cellulose is perhaps best illustrated by some of the remaining ambiguities cited in this study.

Yet another set of interdisciplinary studies are represented by the work of Hayashi and coworkers, wherein they attempt to shed light on the questions of reversibility, or lack thereof, in transformations between the allomorphs of cellulose and its derivatives. In addition to their diffractometric studies reported in prior publications, they add in their contribution to the present symposium analyses of the infrared spectra as well as analyses of the CP-MAS ^{13}C NMR spectra. Their thesis is not inconsistent with the proposals of Atalla and coworkers concerning differences between the conformations of celluloses I and II. However, Hayashi and coworkers go beyond this by proposing that the differences in conformation can be preserved in the course of heterogeneous derivatization reactions, and also in the process of generating the other allomorphs of cellulose, namely celluloses III and IV, from the two primary allomorphs I and II.

The adoption of multidisciplinary approaches in the effort to shed light on the complex questions of structures is likely to expand in the future. The proceedings of this symposium are clear evidence both for the need and the value of such approaches.

Future Directions

The studies reviewed briefly above place the problem of the structures of cellulose in a promising perspective. Until the development of the new spectroscopic methods, the crystallographic studies were undertaken with little additional information from other sources, with the exception of some of the conformational energy calculations. These are useful, but they are sensitive to the nature of the potential functions used in the calculations and particularly to the manner in which the different potential functions are weighted.

As noted earlier, the crystallographic studies have sought the most simple model structure consistent with observations. Clearly the structure based on the anhydroglucose as the repeat unit is the most simple structure that accounts for the majority of the diffractometric data. Furthermore, the data available did not provide a basis for introducing departures from the most simple model, nor suggestions for its revision.

The new information from spectroscopic studies sheds new light in two key areas. The first is related to the complexity of the structures of the native celluloses. The second is that of the relationship between the structures of celluloses I and II.

It has been known for some time that the more crystalline native celluloses from algae and from *Acetobacter xylinum* produce diffraction patterns that have many features in common with those of the crystalline celluloses from the higher plants, such as ramie, but that cannot be indexed as simply or on the basis of the same unit cell. The new information from the CP-MAS ^{13}C NMR spectra, together with that from the Raman spectra, suggests some bases for understanding these differences, and directions for further explorations.

The key conclusion that is relevant here is that the native celluloses are composites of more than one crystalline form, but that the difference between the two forms lies not in the molecular conformation but in the hydrogen bonding patterns. Thus, it is possible that the native celluloses have unit cells with very similar atomic coordinates for the heavy atoms, but with different coordinates for the hydrogens. The similarities in the heavy atom locations could account for the many commonalities in the diffraction patterns, while the differences in the coordinates of the hydrogen atoms could be responsible for the differences between the patterns. This would account for the greater incidence of nonallowed reflections in the electron diffraction patterns.

It is not clear that a polymeric system with a composite structure, such as the one proposed above, represents a tractable crystallographic problem. However, any new insights concerning the discrepancies between the proposed simple structures and the observations are important, for they may suggest departures in new directions for investigation. A very significant implication of the proposal suggested above, to explain the discrepancies between the diffraction patterns, is that the primary determining factor in the structure of the native celluloses may be the shape of the molecules rather than the hydrogen bonding pattern. The proposal clearly implies that more than one hydrogen bonding pattern is consistent

with the organization of the heavy atoms in the molecular skeleton in the unit cell. The proposal has a number of other implications for further investigation, discussion of which is beyond the scope of the present chapter.

With respect to the comparison between celluloses I and II, the spectral data leave little question that the molecular conformations are indeed different. The chapter by Wiley and Atalla sets forth some of the evidence based on Raman spectroscopy. The validity of the theoretical arguments developed in support of the hypothesis that two distinct conformations do indeed occur has been demonstrated through its application in studies of model compounds. The most comprehensive is a study of the vibrational spectra of the inositols (47), wherein spectra of seven of the isomers were investigated and the effects of conformational differences accounted for.

The hypothesis that conformational differences occur is also supported by the differences between the CP-MAS ^{13}C NMR spectra of celluloses I and II. It is indeed not likely that the differences in the chemical shifts of the different carbons and the differences in the degrees of splittings of the C1 and C4 resonances can be accounted for in terms of structures adhering strictly to the assumption that the twofold screw axes coincide with the axes of the molecular chains.

The data arising from both spectroscopic methods clearly point to the need to explore the degree to which the diffraction data can be accounted for in terms of structures wherein the anhydrocellobiose unit is assumed to be the basic repeat unit in the crystallographic structure. The spectroscopic studies and the conformational energy calculations suggest that the departures from equivalence of the two anhydroglucose units need not be very large ones. This may indeed be the reason why the disallowed reflections appear to be weak in the diffraction patterns. On the other hand, the spectroscopic evidence suggests that the nature of these minor departures from symmetric equivalence of adjacent anhydroglucose units may be the key to some of the anomalies encountered in the structural studies.

It is clear that the new information developed from spectroscopic and multidisciplinary studies provides a basis for initiating diffractometric studies with a different set of constraints than those used in the past. The refinements are likely to be more complex, but the expectation is that the structures thus derived will more closely approximate the molecular structure of cellulose. Such models may then provide more comprehensive rationalizations of the phenomenology of cellulose.

Literature Cited

1. Kakudo, M.; Kasai, N. X-ray diffraction by polymers, Elsevier, New York, 1972, p. 285.
2. Arnott, S. In Fiber Diffraction Methods; ACS Symposium Series No. 141, American Chemical Society, Washington, DC, 1980, p. 1.
3. Atkins, E. D. T. In Fiber Diffraction Methods, ACS Symposium Series No. 141, American Chemical Society, Washington, DC, 1980, p. 31.

4. Tadokoro, H. In Fiber Diffraction Methods, ACS Symposium Series No. 141, American Chemical Society, Washington, DC, 1980, p. 43.
5. Tadokoro, H. Structure of crystalline polymers, Wiley, New York, 1979, p. 6.
6. Purves, C. B. In Cellulose and Cellulose Derivatives, Pt. I; Ott, E.; Spurlin, H. M.; Graffline, M. W., Eds., Interscience, New York, 1954, p. 29.
7. Flory, P. J. Principles of polymer chemistry, Cornell University Press, Ithaca, New York, 1953, p. 3.
8. Hermans, P. H. Physics and chemistry of cellulose fibers, Elsevier, New York, 1949, p. 3.
9. Jones, D. W. In Cellulose and Cellulose Derivatives, Pt. IV; Bikales, N. M.; Segal, L.; Eds., Wiley-Interscience, New York, 1971, p. 117.
10. Ellefsen, O.; Tonessen, B. A. In Cellulose and Cellulose Derivatives, Pt. IV, Bikales, N. M.; Segal, L.; Eds., Wiley-Interscience, New York, 1971, p. 151.
11. Tonessen, B. A.; Ellefsen, O. In Cellulose and Cellulose Derivatives, Pt. IV, Bikales, N. M.; Segal, L.; Eds., Wiley-Interscience, New York, 1971, p. 265.
12. Preston, R. D. The physical biology of plant cell walls; Chapman and Hall, London, 1974.
13. Frey-Wyssling, A. The plant cell wall; Gebruder Borntraeger, Berlin, 1976.
14. Howsmon, J. A.; Sisson, W. A. In Cellulose and Cellulose Derivatives, Pt. I; Ott, E.; Spurlin, H. M.; Graffline, M. W.; Eds., Interscience, New York, 1954, p. 231.
15. Petipas, T.; Oberlin, M.; Mering, J. J. Polym. Sci. C 1963, 2, 423.
16. Norman, M. Text. Res. J. 1963, 33, 711.
17. Gardner, K. H.; Blackwell, J. Biopolymers 1974, 13, 1975.
18. Hebert, J. J.; Muller, L. L. J. Appl. Polym. Sci. 1974, 18, 3373.
19. Ref. 9; p. 138.
20. Ref. 14; p. 237.
21. Meyer, K. H.; Mark, H. Z. Physik. Chem. 1929, B2, 115.
22. Meyer, K. H.; Misch, L. Helv. Chim. Acta 1937, 20, 232.
23. Pierce, F. T. Trans. Faraday Soc. 1946, 42, 545.
24. Liang, C. Y.; Marchessault, R. H. J. Polym. Sci. 1959, 37, 385.
25. Liang, C. Y.; Marchessault, R. H. J. Polym. Sci. 1959, 39, 269.
26. Marchessault, R. H.; Liang, C. Y. J. Polym. Sci. 1960, 43, 71.
27. Nelson, M. L.; O'Connor, R. T. J. Appl. Polym. Sci. 1964, 8, 1311.
28. Nelson, M. L.; O'Connor, R. T. J. Appl. Polym. Sci. 1964, 8, 1325.
29. Sarko, A.; Muggli, R. Macromol. 1974, 7, 486.
30. French, A. D. Carbohydrate Res. 1978, 61, 67.
31. Atalla, R. H. Advances in Chemistry Series 1979, 181, 55.
32. Atalla, R. H. In Structure, Function and Biosynthesis of Plant Cell Walls, Dugger, W. M.; Bartinicki-Garcia, S.; Eds.,

- American Society of Plant Physiologists, Rockville, MD, 1984, p. 381.
33. Atalla, R. H. Appl. Polym. Symp. 1976, 28, 659.
 34. Reese, D. A.; Skerrett, R. J. Carbohydrate Res. 1968, 7, 334.
 35. Melberg, S.; Rasmussen, K. Carbohydrate Res. 1979, 71, 25.
 36. Chu, S. S. C.; Jeffrey, G. A. Acta Crystallogr. 1968, B24, 830.
 37. Ham, J. T.; Williams, D. G. Acta Crystallogr. 1970, B29, 1373.
 38. Atalla, R. H.; Gast, J. C.; Sindorf, D. W.; Bartuska, V. J.; Maciel, G. E. JACS 1980, 102, 3249.
 39. Atalla, R. H. Proceedings of the International Symposium on Wood and Pulping Chemistry, SPCI Rept. No 38, Stockholm 1981, Vol. 1, p. 57.
 40. Earl, W. L.; VanderHart, D. L. JACS 1980, 102, 3251.
 41. Earl, W. L.; VanderHart, D. L. Macromol. 1981, 14, 570.
 42. Maciel, G. E.; Kolodziejcki, W. L.; Bertran, M. S.; Dale, B. E. Macromol. 1982, 15, 686.
 43. Fyfe, C. A.; Dudley, R. L.; Stephenson, P. J.; Deslandes, Y.; Hamer, G. K.; Marchessault, R. H. JACS 1983, 105, 2469.
 44. Atalla, R. H.; VanderHart, D. L. Science 1984, 223, 283.
 45. VanderHart, D. L.; Atalla, R. H. Macromol. 1984, 17, 1465.
 46. Poppleton, B. J.; Mathieson, A. McL. Nature 1968, 219, 1946.
 47. Williams, R. M.; Atalla, R. H. J. Phys. Chem. 1984, 88, 508.

RECEIVED March 5, 1987

Chapter 2

X-ray Diffraction Studies of Ramie Cellulose I

A. D. French¹, W. A. Roughead², and D. P. Miller²

¹Southern Regional Research Center, U.S. Department of Agriculture, P.O. Box 19687,
New Orleans, LA 70179

²Department of Physics and Astronomy, Clemson University, Clemson, SC 29631

Current fiber x-ray diffraction studies, including new calculations by the authors, are reviewed. Because of different conventions used to describe the crystal structure of native cellulose, the preferred parallel structure described as "up" by Gardner and Blackwell for Valonia corresponds to the "down" structure that was strongly rejected for ramie by Woodcock and Sarko. A variety of assumptions were tested, as were results from the different computer programs used for fiber diffraction. These results were compared with those from a computer program written for single crystal work, and the comparisons were satisfactory. A major reason for the differences in reported structures for celluloses comes from differences in the diffraction intensity data sets taken at the various institutions.

Cellulose fibers have been studied with x-ray diffraction since 1913 (1). Over the past dozen years, a number of full-fledged studies of native cellulose have been published, each without apparent fault, but with contradictory indications of chain packing mode. At the same time, spectroscopists have challenged some of the fundamental assumptions and apparently clear results of the diffraction studies.

This report is part of an effort by several fiber crystallographers to better understand the variable outcome from these studies and specifically to ascertain that results are not dependent on the particular computer program used. R. Millane at Purdue and A. Sarko at Syracuse are also analyzing a data set obtained by Roughead and Miller from diffraction photographs taken by French (the RMF data) (2) in order to learn more about the methodology and about cellulose itself. In this report some results will be discussed based on that data as well as some comparative results based on other data sets.

Selection of Ramie Cellulose for Study. Ramie cellulose was selected for study because it is highly oriented and fairly

0097-6156/87/0340-0015\$06.50/0
© 1987 American Chemical Society

crystalline. Although ramie is not as commercially important as cotton, cotton fibers have a complicated extra level of structure that decreases the amount of information available from a diffraction study. If this fiber structure in cotton is destroyed with a Waring blender (making x-ray fiber diffraction impossible), an electron diffraction pattern nearly identical to that from ramie may be obtained (3). In contrast, electron diffraction patterns (and x-ray patterns, too) from algal and bacterial celluloses differ from ramie and cotton, even though they all have the main features in common. Infrared spectra from ramie and cotton are also similar to each other and different from those of the algal and bacterial celluloses (4). Thus, the structure of ramie should accurately resemble cotton at the molecular and crystallite levels, while there is some doubt as to whether such close similarity applies between the structures of algal and cotton celluloses.

Review of Previous Work

Unit Cell. Various workers (2,5-6) have determined similar dimensions for the ramie unit cell. As shown in Table I, however, the a and b dimensions have ranges of about 0.07 Å. (The a and b dimensions of the MGW (Mann, Gonzalez and Wellard) and RMF cells have been interchanged to conform to standard crystallographic notation (7) as discussed below.)

Table I. Unit Cells for Ramie

Authors	Mann* Gonzalez Wellard (MGW)	Woodcock Sarko (WS)	Roughead* Miller French (RMF)
Dimension			
a	7.846	7.78	7.794
b	8.171	8.20	8.248
c	10.34	10.34	10.33
γ	96.38	96.5	96.77

* The a and b dimensions have been interchanged from the reported values for this comparison.

The base plane of the unit cell for cellulose I is often drawn with the origin of the axes placed in the lower left corner, with the x axis to the right and the y axis up and to the left with monoclinic angle being obtuse. However, Sarko's group in Syracuse has used standard crystallographic convention, with the origin in the upper left, the y axis to the right, and the x axis down and to the left. In both cases, the z axis is toward the viewer if the x and y axes are in the plane of the paper. This paper uses the standard convention, shown in Figure 1, as used in Syracuse. The a, b, and c

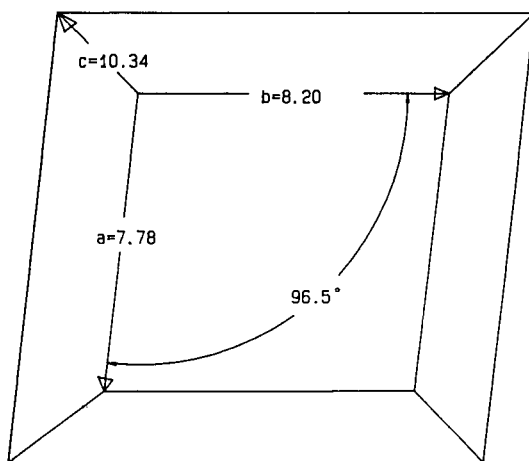


Figure 1. Drawing of the cellulose I unit cell, according to the standard crystallographic convention in ref. 7, by Bill Garner, Martin Marietta Corporation.

dimensions are the repeating distances along the x , y , and z axes, respectively.

Chain Conformation. From computer modeling studies of cellulose (8), we know that the cellulose molecule has limited flexibility. Only a few regular (internally symmetric) conformations are allowed for cellulose, a beta 1,4-linked glucan, and structures similar to the traditional 2-fold helix are the only ones in accord with the observed z axis spacing. Such chains resemble flat ribbons.

Crystal Structure. In the current models from x-ray diffraction, a total of two cellulose chains having atomic positions close to those resulting from 2-fold screw symmetry pass through each of the unit cells. These chains are bound into sheets by hydrogen bonding between the edges of the ribbons; there are no hydrogen bonds proposed to connect the sheets to each other (6,9-11). The remaining cohesiveness is apparently provided by vander Waals attraction.

In order to form these sheets, the O6 hydroxyl group is rotated into the tg position, where it forms both intra- and inter-molecular hydrogen bonds. Although the tg O6 position is somewhat controversial because it is rarely found in single crystal studies of smaller carbohydrates, it has been reported in all recent x-ray studies of cellulose I.

Packing Mode. The structures for native ramie cellulose described by Woodcock and Sarko (6) (WS) and for *Valonia* cellulose by Gardner and Blackwell (11) have been called "parallel-up", as opposed to "parallel-down" and to "antiparallel" arrangements (11). However, their proposed structures used the different axial conventions described above. If both structures are described using the same convention, the packing in one of the cells is parallel-up and the other is packed parallel-down. In other words, the parallel-up structure preferred by Gardner and Blackwell corresponds to the parallel-down structure strongly rejected by Woodcock and Sarko. Work by French (9) showed a small preference for an antiparallel arrangement. Identical, hydrogen-bonded sheet structures can be formed in each of these packing arrangements, but the between-sheet interactions are different.

Cell Symmetry. For many years, it was accepted that the cellulose molecule embodied 2-fold screw symmetry (space group $P2_1$). Later, Honjo and Watanabe (12) showed electron diffraction diagrams that indicate that *Valonia* cellulose crystallizes in the $P1$ space group that does not contain symmetric chains. The unit cell also contained 8 chains. Other diffraction work showed the presence of faint meridional reflections on the odd layer lines that also indicate that the chains do not have exact 2-fold screw symmetry. While the validity of this evidence has been accepted for *Valonia*, it has not been used in structural studies because of the low intensities of the spots that indicate the large cell and that break the symmetry. It has been argued that the deviations from symmetry must be relatively small (11); assumptions regarding the cell size have been necessary in order for the needed computations to be manageable.

In Woodcock and Sarko's work on ramie (6) and in unpublished work by French, the improvement in fit between observed and calculated intensities was insignificant when the model was allowed to deviate from 2-fold symmetry. On the other hand, splitting in the nmr peaks and other spectral evidence (13,14) has given strong indication that the molecules are not nearly as symmetric as thought.

Given the above contradictions, questions of general interest regarding cellulose structure include:

- a. What is the packing mode of the chains? Is the packing mode different in cellulose I and II? If so, how is the conversion effected?
- b. What is the extent of deviation from a symmetric P2₁ structure?
- c. What is the nature of fibrils? Are they extended or folded; what is the source of levelling off degree of polymerization? Why is it different for cellulose I and II?
- d. What is the fibrillar structure from the standpoint of mild reactions? Which oxygen atoms are available for mild reactions such as crosslinking a fabric? Is the hydrogen bonding scheme important in determining the reactivity?
- e. What is the cause of differences in results among the other physical methods? What are the differences among the various celluloses that cause differences in their IR and nmr spectra?

Some other aspects are primarily of interest to fiber crystallographers:

- a. What is the source of the substantial error remaining in our studies?
- b. What is the meaning of the temperature factors that result?

Fiber x-ray diffraction can be expected to provide at least some evidence relative to all the above questions. With the available ratio of data to parameters, however, some questions may well remain unanswered. Samples of far higher crystallinity would be needed to accomplish a complete determination, and there is some danger that such samples would not completely correspond to samples of more general interest.

Computer Techniques

Program Description. In order to determine polymer crystal structures, each of the participating institutions uses computer programs that reflect different resources and abilities as well as philosophies. Models to be used for calculation of intensities are constructed in various ways, and each has a different strategy for finding the best result. Each of the methods has some unique abilities and some disadvantages.

The SHELX program (15) is used at Clemson University. It was designed for single crystal studies and can swiftly reach a good match between observed and calculated data but has no stereochemical component in the determination and was not designed to accommodate polymers which have the same molecule passing through many unit cells. It was slightly modified for overlapped

intensities. Starting models must be fairly close, because there is no searching based on overall parameters of a polymer, such as chain rotation or chain translation.

The program used at the Southern Regional Research Center (SRRC) was written for simple cellulose structures (9) mostly by V. G. Murphy, now at Colorado State University. It quickly calculates R values for changes in variables such as chain rotation and chain translation. Like SHELX, it has no stereochemical component. Modeling is based on the virtual-bond method (16), and relies on substitution of different coordinate sets from single-crystal studies of model compounds such as cellobiose in order to provide fine internal adjustments of atomic coordinates. The SRRC program uses variation space searching to find the best combination of chain rotation and translation instead of a least squares minimization. Because individual atomic positions (except O6) are not varied directly by the program, such a simple program is not well-suited for determining structures with relatively high ratios of data to variable parameters. It is, however, useful for examining the effects of different assumptions or quickly furnishing starting models for a more elaborate program. It is also very easy to prepare a new data set.

At Syracuse and Purdue, the computer programs are highly sophisticated for study of polymers in general. Both can combine diffraction intensity calculations and stereochemistry to optimize intermolecular interactions for structures that simultaneously yield a good fit between the observed and calculated diffraction intensities. These studies usually weight the diffraction data and the stereochemical studies equally. The PS-79 program used at Syracuse was written by Peter Zugenmaier and Tony Sarko (17). It uses techniques designed for speed and implementation on a relatively small computer. The modeling method allows variation in monomeric geometry through changes in the distance between the linkage oxygen atoms. All the atomic positions can be varied with constraints to accommodate stereochemical and x-ray data.

The Linked Atom Least Squares (LALS) program (18,19) by Arnott and coauthors is used at several institutions, including Purdue, where it was developed, and Case Western Reserve University, where it was used by Gardner and Blackwell. It is best implemented on a large computer; the Control Data Corporation supercomputer at Purdue handles it very rapidly. Setting up a new model with LALS is more complicated than with the other programs, but LALS appears to provide realistic molecular flexibility.

R Factors. Each program determines the extent of agreement between the observed and calculated intensities (the R factor) in a slightly different way. The exact method of calculation is important in the magnitude of R that is attained, making it difficult to compare results from different laboratories. While the minima in these different R factors usually arise from very similar structures, each algorithm may, as seen below, indicate a different preference among competing models. Differences in the magnitude of R arise from different methods for calculating the contributions from spots that are too weak to be observed but have a calculated intensity greater than the threshold of observation. Such reflections are called the unobserved data. Very minor

differences result from the technique used to supply the scattering factors to the calculations. Two other sources of difference in the magnitude of reported R values are the method used to scale the observed intensities to the calculated ones (scale factor), and the method for compensating for thermal motion and positional disorder (temperature factor).

The SRRC program calculates 5 different R values, shown in Table II. They are: a simple R, (Robs), based on only reflections that are observed, an R for only the unobserved data (Runobs), their total (Rtot), the weighted total R" (R"wt) and the unit- (or un-) weighted total R" (R"unwt). A weighted Rtot is calculated in some other programs. By keeping the Robs and Runobs separate, the effects of two somewhat independent sets of data may be observed. At SRRC the square roots of the observed and calculated intensities are scaled to each other with a least squares fit that incorporates an exponential term (9). This simultaneously produces a low magnitude of R", a scale factor, and a temperature factor. As shown in Figure 2, coarse determinations of chain rotational position could be accomplished with any of these R values. When R values are calculated at fine increments of rotation (Figure 3), however, the choice of type of R factor determines which chain rotations are chosen to represent the best structure.

Weighting Schemes. R"wt is preferred by statisticians because it gives extra penalty to proposed structures that have a few large discrepancies between observed and calculated intensities instead of a normal distribution of errors. This effect arises from the use of the square of the differences. Also, the weighting increases R"wt heavily when the discrepancy pertains to the more accurately determined spots and penalizes lightly when the spots are poorly resolved.

Only the RMF data set includes standard deviations for the intensity measurements. These values, divided by the square root of the observed intensity and inverted, can be used to weight the R value calculation. For cellulose I, which has a few dominant spots, this inevitably results in a large range of weights. Other weighting schemes can be adopted. For the Mann, Gonzalez and Wellard (20) (MGW) and the WS data sets, the 4th root of the intensity was used to give a small range in weights that would partially reflect the errors due to counting statistics. The scheme finally adopted for the RMF data used the reciprocals of the fractional error, except that a ceiling was set at 0.20 of the weight otherwise calculated for the strongest reflection. Such weightings typically decrease the sensitivity of the R factor to variations in the model. Also, the weighted R" is usually numerically smaller than the unit-weighted R" which, in turn, is smaller than Rtot.

Comparison of Programs. The purpose of the comparison of the results derived through these 4 different computer programs is to learn to what extent results are independent of the computer program. There are actually two similar questions. The first is whether similar R factors will result from identical input structures. The second considers the similarity of structures selected as the final best model in each program. At present, we can comment best on the first question.

Table II. R FACTORS CALCULATED BY THE SRRC PROGRAM⁺

$$R_{\text{obs}} = \frac{\Sigma (I_{\text{obs}}^{1/2} - I_{\text{calc}}^{1/2})}{\Sigma I_{\text{obs}}^{1/2}}$$

$$R_{\text{unobs}}^* = \frac{\Sigma (I_{\text{calc}}^{1/2} - 2/3 (I_{\text{Threshold}}^{1/2}))}{\Sigma I_{\text{obs}}^{1/2}}$$

$$R_{\text{Total}} = R_{\text{obs}} + R_{\text{unobs}}$$

$$R''_{\text{unwt}}^* = \sqrt{\frac{\Sigma (I_{\text{calc}}^{1/2} - I_{\text{obs}}^{1/2})^2}{\Sigma I_{\text{obs}}}}$$

$$R''_{\text{wt}}^*{}_{\text{@}} = \sqrt{\frac{\Sigma w (I_{\text{calc}}^{1/2} - I_{\text{obs}}^{1/2})^2}{\Sigma w I_{\text{obs}}}}$$

+ Because of overlapped reflections, it is not possible to obtain observed structure factors (F_{obs}). In order to have a familiar range for the calculated R values, the values in the calculation were $I^{1/2}$. The $I_{\text{calc}}^{1/2}$ term was calculated by squaring the F_{calc} values of a composite reflection, summing the squares, and calculating the square root of the sum.

* When considering reflections that have an intensity below threshold, the calculation was performed with $I_{\text{calc}}^{1/2} - I_{\text{obs}}^{1/2}$ terms that had zero value if the calculated term was below threshold and a value of $I_{\text{calc}}^{1/2} - 2/3 (I_{\text{Threshold}}^{1/2})$ if the calculated term was above threshold. This procedure was described by Gardner and Blackwell (11).

@ Various weighting schemes were used. See the text.

Center															Corner																																																																																																																																																																																													
10°															10°																																																																																																																																																																																													
159.130	90.73	64.60	57.53	57.63	56.47	46.53	58.86	64.116	159.	249.182	119.88	73.65	60.58	61.66	64.56	56.59	64.79	104.156	249.	182.200	130.91	71.80	60.54	52.57	66.67	62.60	65.71	81.102	132.	119.130	112.81	61.49	43.43	51.61	64.60	60.64	60.80	64.60	73.	85.101	119.	98.91	80.65	68.36	40.30	60.83	60.81	64.66	69.	73.81	61.60.	64.60	50.43	34.64	64.66	62.59	56.55	54.55	61.64.	73.71	61.49	41.43	43.57	57.48	64.65	65.67	68.67	69.72	73.	65.60	49.38	42.54	64.69	80.79	72.09	70.69	67.65	66.65.	60.54	63.36	42.57	77.115	145	123.96	79.73	69.64	61.60.	53.47	60.30	55.72	93.103	104.	90.80	64.72	65.58	51.55	53.	57.55	48.47	56.87	99.103	127	116.95	83.86	87.72	64.56	50.57.	63.61	56.56	64.78	121.106	116	141.112.	99.104.	78.68	59.61	63.	56.59	57.57	66.77	1104.	90.95	1132.130	110	103.100.	73.62.	55.56	56.	47.51	55.55	62.68	81.60	83.98	110.104.	96.78	59.52	47.66	47.	43.53	55.55	64.66	64.66	65.103.	79.62	60.79	62.52	41.40	40.	53.58	56.54	56.63	69.72	87.104.	100.78	60.52	52.45	60.45.	53.	58.65	62.57	55.56	65.73	78.79	59.49	45.42	40.43.	68.58.	68.71	64.60	54.52	54.68	62.52	41.40	40.44	46.60.	68.	64.81	60.57	53.50	51.56	59.53	47.38	30.43	48.41.	70.86.	116.102	82.70	61.58	56.55	58.61	56.46	42.45	68.60.	76.116.	159.130	90.73	64.60	57.53	57.63	56.47	46.53	58.86	64.116	159.
51.40	38.36	29.31	30.29	32.33	35.36	34.35	33.32	37.39	41.51.	193.144	92.67	53.66	42.43	30.54	53.42	56.38	44.56	79.124	193.	144.136	103.71	53.42	38.38	47.57	55.46	43.66	30.59	75.102	144.	92.103	87.61	43.33	29.31	42.52	55.48	44.45	48.52	60.74	92.	67.71	61.66	35.23	22.39	30.51	45.43	44.44	46.49	57.67.	53.53	43.33	22.29	42.54	53.47	44.44	44.42	42.44	49.53.	66.42	33.25	27.28	38.53	63.61	51.66	45.43	43.43	66.66.	42.58	23.42	27.28	48.60	58.01	64.95	66.52	46.44	42.43.	43.26	31.27	29.28	58.51	106.104	85.71	50.52	66.44	42.43.	30.47	42.39	42.53	90.106	136	127.96	78.89	67.53	50.49	30.	53.53	53.51	53.81	93.85	96.102	137	109.81	81.50	50.48	51.	42.66	46.45	47.61	66.71	78.93	109.103	87.61	42.56	35.28	42.	36.43	44.43	44.66	52.50	68.81	91.87	78.43	31.27	26.36.	38.46	43.44	44.43	46.52	67.82	81.61	43.34	29.27	26.38.	44.50	46.42	43.43	44.66	53.61	58.42	31.29	29.29	28.34.	56.29	52.44	42.42	44.30	55.30	36.27	27.30	31.36	44.56.	79.75	80.49	44.43	41.42	49.34	48.35	28.28	34.66	63.79.	124.102	74.37	49.66	43.43	46.55	51.38	30.30	34.44	63.96	124.	193.144	92.67	53.66	42.43	30.54	53.42	56.38	44.56	79.124	193.																									
219.171	131.109	93.91	86.91	98.96	90.86	90.96	108.128	161.219.	219.171	131.109	93.91	86.91	98.96	90.86	90.96	108.128	161.219.	171.127	131.108	94.85	82.77	86.98	90.91	86.95	90.105	115	126.131.	131.131	116.96	83.74	68.68	79.97	92.86	91.95	80.85	86.93	99.	108.108	94.79	69.55	63.76	69.95	80.85	82.86	93.99	109.109.	98.86	83.69	61.49	57.87	69.103.	96.91	89.89	89.89	96.	93.85	74.36	49.63	40.95	108.100	95.87	82.81	82.93.	91.82	68.55	57.87	80.102	133	136.140	117	104.101	95.82	79.	86.77	68.43	72.80	102.127	136	137.113	93.104.	91.96	79.85.	86.	91.86	78.67	87.95	133.136	146	153.127	117	118.121.	101.85.	90.	90.98	92.89	99.108	136	137.133	170	147	129	127	141.	110.97	91.96.	96.	98.97	95.103	104	121.141	145	118.	95.	80.95	91.85.	89.95	101.104	121	141.145	118.	95.82	74.67	87.	90.99	95.86.	86.87	93.91	100.110	109.95	81.72	45.76	91.96.	108.108	100.93	89.82	82.96	91.97	93.83	76.64	65.71	81.103.	109.	128.1135	99.89	81.79	85.93	88.78	64.67	76.91	80.120	128.	161.148	136.109	92.80	85.90	96.93	85.78	95.91	103.120	145	161.	219.171	131.109	93.91	86.91	98.96	90.86	90.96	108.128	161.219.																																		

Figure 2. R factors for parallel-down chains using RMF data. 06 was in the tg position. All five R factors calculated by the SRRC program are shown, calculated at 10° increments of rotation (0° to 180°) of the corner (rows) and center (columns) chains. At each increment of rotation, the shift of the center chain along the z axis was varied in 10 increments of 0.1 z (1.03 Å) and the lowest R calculated for any shift is reported. The minimum (circled) for each R (indicative of the most likely structure) occurs when both chains are rotated about 50°.

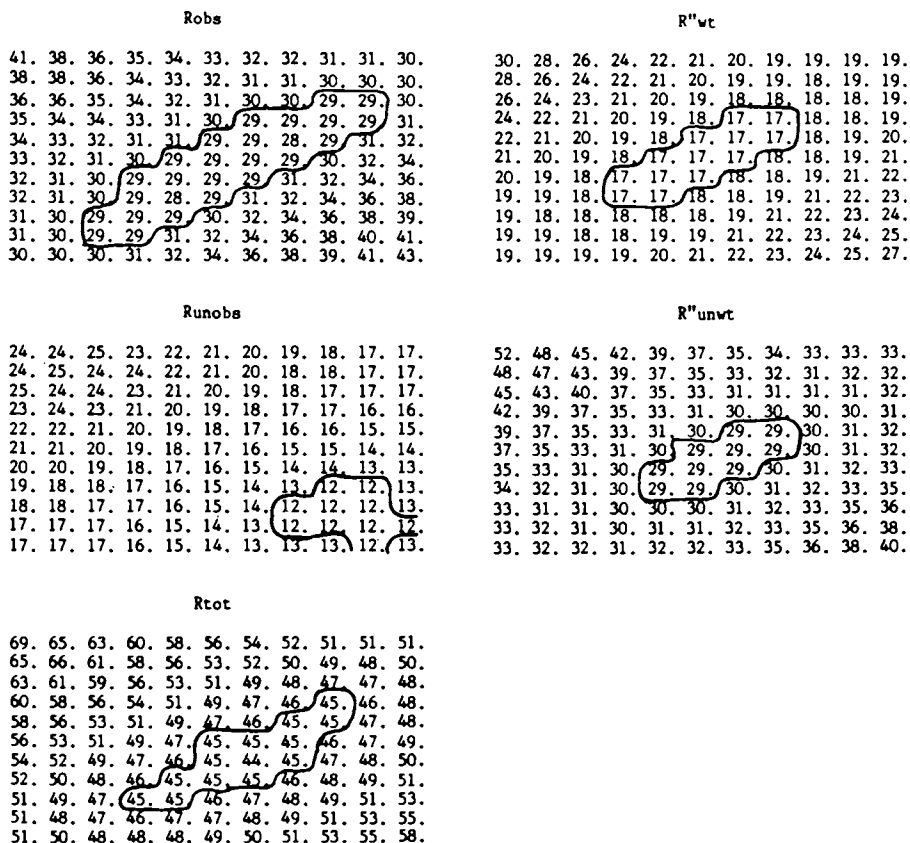


Figure 3. R factors for the same models as in Figure 1, examined at increments of 2° . The minimum occurs in different locations, depending on which R is chosen to select the best model. On both Figure 1 and Figure 2, some factors have sharper minima than others.

Table III shows that similar results are furnished by each of the computer programs designed for modeling polymers (LALS, PS-79, SRRC), once attention is given to the matter of axial convention. All of the programs yield comparable calculated R" factors if identical atomic positions and observed intensities are supplied. Preliminary calculations by R. Millane at Purdue and A. Sarko at Syracuse, using the RMF data and LALS or PS-79, respectively, produced R values similar to those of the SRRC program. When the single-crystal program, SHELX, was used to calculate R" based on fixed atomic positions from the SRRC program, similar results were also obtained. However, SHELX gave much lower R" values when rigid restraints were relaxed, albeit with some cost in polymeric integrity (see below).

Sources of Variation in Results

Monomeric Geometry. Previous work (21) showed that the overall conclusions are not substantially affected by small differences in coordinates for the glucose ring used in the starting model. We have reexamined this point since the WS and RMF data sets have become available for ramie cellulose, along with the WS monomeric geometry that was internally adjusted to best agree with the WS diffraction and stereochemical analysis of ramie.

As shown in Table IV, each of the stereochemically reasonable models composed of different monomeric geometries gave similar R factors regardless of chain polarity. The R values do differ slightly, based on the different monomeric geometries used for the starting model. Because of the sensitivity of the R factors to variations in atomic coordinates, it seems reasonable to use a model that can be refined under influence of the diffraction data. Calculations at SRRC using the WS data showed that the Sarko-Muggli (averaged) monomeric geometry produced R values about 0.05 higher than the WS geometry which was refined to best fit the WS data. However, R values were not similarly improved when the WS geometry was used with the other data sets.

Data Set. Wide variations (30 to 50 percent) in the x-ray data collected at different labs for Valonia were reported previously (9). These different data sets affect the results on such major questions such as selection of chain polarity. There are now three different data sets for ramie, and these are compared:

Details of Collection

- a. MGW used scanning densitometry over the entire flat film. Supplemental techniques were enlisted to obtain absolute intensities and the intensities of four meridional reflections. They observed 29 spots (1960). The formulae of Cox and Shaw (23) were used to make the Lorentz [geometric] and polarization (Lp) corrections.
- b. WS used layer-line scans and computer curve resolution to find 34 measurable spots on a flat film (6). No meridional data were quantified. (1979) The Lp corrections of Cella, Lee and Hughes (24) were used.

Table III. Comparisons of LALS, PS-79 and SHELX with the SRRC Program, Using the Same X-Ray Data and Models for Each Comparison

Authors	Program	Study	R Factor (R ^u nwt)		
			UP	DOWN	ANTI
Gardner Blackwell	LALS	Valonia ^a 1974	----	.180	.244
French Murphy	SRRC	Valonia ^a 1977	.179	.165	.215
Woodcock Sarko	PS-79	Ramie 1979	.193	.338	.246
Present Work	SRRC	Above Data, Model ^b	.172	.289	.253
Roughead Miller French	SHELX	Ramie 1983, Flexible Model	----	.030 ^c	.045 ^c
Present Work	SRRC	Above Data, Rigid Except 06	.126 ^c	.149 ^c	.137 ^c

a. Gardner and Blackwell¹¹ observed only data, fixed temperature factor

b. A lack of exact symmetry in the Woodcock and Sarko model prevented exact match of the structure at SRRC.

c. R^uwt values are reported here.

Table IV: Comparison of the Effect of Different Monomeric Geometries in Rigid Models

RMF Data - SRRC Program

Smallest R Values Found (06 tg)

Monomeric Geometry		R _{tot}	R ^{"wt}	R ["]
Sarko-Muggli	UP	.38	.16	.26
	DOWN	.42	.18	.28
	ANTI	.39	.15	.26
Non-Reducing ^a Cellobiose	UP	.46	.18	.30
	DOWN	.45	.15	.30
	ANTI	.47	.16	.29
Methyl Beta ^b Maltoside	UP	.49	.18	.31
	DOWN	.44	.17	.29
	ANTI	.48	.17	.28
Woodcock-Sarko	UP	.45	.15	.30
	DOWN	.41	.16	.28
	ANTI	.46	.15	.28

a. Reference 26.

b. Reference 27.

- c. RMF also scanned the whole film and used NASA image enhancement programs to smooth data (2). They added a sophisticated background correction. A total of 29 spots were resolved, including meridionals on the second to fifth layer lines (1983). The photographs were made with a precession camera, and standard Lp corrections for precession photography were modified for fibers by Miller.

Table V. Intensity^{1/2} Data Reported for
Ramie, Equatorial (0th) Layer Line

RMF*	WS*	MGW
1.6	**	**
60.4	55.3	59.0
53.0	45.6	59.0
158.0	158.0	158.0
4.0	30.8	9.5
5.6	35.0	12.3
**	37.8	7.1
65.2	92.2	26.9

* Data were scaled so that the most intense spot was 158 to match the strongest peak of MGW.

** No comparable spot reported.

In addition to the differences in the number of spots and the choices of Miller indices (compare the original reports after correcting for differences in cell conventions) the intensity values differ. An important example is furnished by the equatorial layer-line data, shown in Table V. The extent of variation in the measurement is best assessed after remembering that the determined values are the intensities, whereas Table V reports their square roots. These variations are similar to those found for the Valonia data, and can be assumed to apply to other fiber diffraction data from polysaccharides.

Certain structural features arise from a cursory analysis of any of the data sets. Each of the 3 above data sets yields maps similar to those in Figures 2 and 3 that clearly show an area of optimal chain rotation. (Because of the overlapped reflections, there is a false minimum at about 140° , 140° that aligns the chains along the shorter x axis. Chains rotated to the position of the false minima have short interatomic distances.) With similar clarity, the gg 06 position is eliminated by all of the above data sets, as exemplified in Table X, below.

The other two staggered 06 positions, gt and tg, have different z coordinates but similar x and y coordinates (9). The R factors calculated for models having 06 in either of these two positions are similar because much of the intensity is on the equator, where the z coordinates have no effect. This

ambiguous result is independent of the packing mode as well as which data set is used.

Table VI. Comparison of Structures Arising from Different Data Sets

Sarko - Muggli Residue Geometry, 06 **tg**
SRRC Computer Program

	UP		DOWN		ANTI	
	RMF	MGW	RMF	MGW	RMF	MGW
Corner Chain Rotation ($^{\circ}$)	61	62	123	119	59	60
Center Chain Rotation ($^{\circ}$)	62	62	118	116	59	60
Center Chain Translation (fraction of \underline{c})	.300	.280	.275	.275	.375	.360
06 Position ($^{\circ}$)	0	-3	10	-3	0	-3

Table VI shows that the data sets do produce slightly different structures. The SRRC program was used with the RMF and MGW data sets and the Sarko-Muggli (22) monomeric coordinates to determine the best values of chain rotation, translation and 06 rotation (06 was restricted to the **tg** range of positions) for up, down and antiparallel models. The scale factors ranged between 0.7 and 1.0.

The shift of the center chain is difficult to ascertain, as shown by Figure 4. One particular cause for the different values reported is that the weighting schemes diminish the variation in the R value to position of the center chain. Questions as to whether the weighting is appropriate and whether the information is present in the data must both be considered. Since the strong and heavily weighted equatorial reflections of cellulose I contain no information regarding the chain shift (z coordinates), this problem is inevitable.

The results from the three different data sets show (Table VII) that the conclusions regarding packing mode depend on which data set is used. The MGW data set favors antiparallel packing; the WS data clearly favors parallel up, and the RMF data set shows a slight preference for the parallel up over the antiparallel mode. These results must be considered in the context of the restrictions on 06 (only **tg** positions were used) and the constraint to $P2_1$ symmetry.

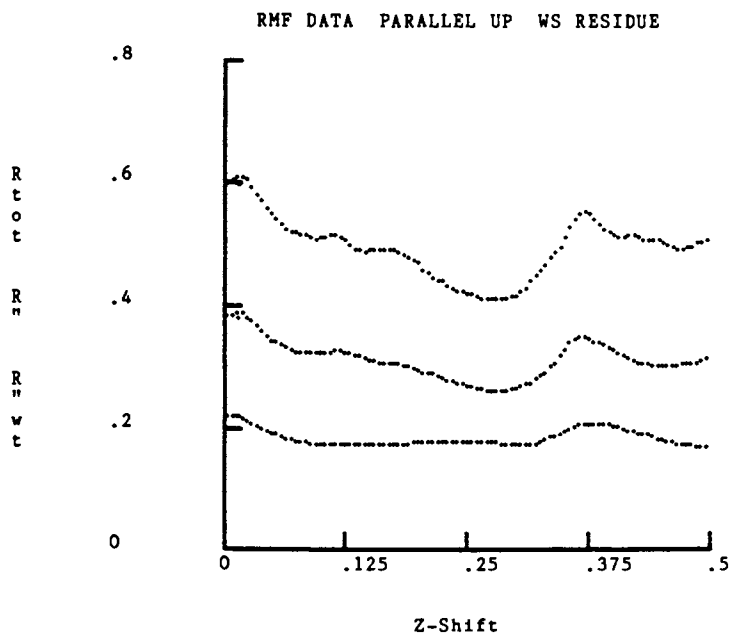


Figure 4. R factors (R_{tot} , R'' , and $R''wt$) for 100 increments of shifts of the center chain along the z axis (RMF data, parallel up model, WS monomeric geometry). $R''wt$, preferred by statisticians, provides little indication of the best value of the shift.

Table VII. R Factors for Symmetrical Models With 06 tg*

Data Set	Packing Mode	Robs	Runobs	Rtot	R"wt	R"unwt
MGW	Up	.208	.055	.264	.114	.186
	Down	.198	.072	.270	.128	.194
	Anti	.181	.062	.242	.109	.168
WS	Up	.142	.035	.177	.126	.172
	Down	.246	.056	.302	.226	.293
	Anti	.201	.064	.293	.181	.244
RMF	Up	.260	.125	.384	.158	.264
	Down	.303	.118	.421	.184	.284
	Anti	.275	.124	.399	.162	.267

*Monomeric geometry used was from Sarko and Muggli except for WS, which used WS geometry. The up-down notation matches standard notation.

The three different data sets produce extreme differences in the temperature factors (Table VIII). This difference is not characteristic of just the SRRC program, as a similar range for cellulose is in the literature. The temperature factor (B) is important because it indicates systematic error in the Lp correction or other aspect of data gathering and reduction, for at least two of the data sets. Negative temperature factors, as found in the WS data, typically indicate either that additional atoms, such as water molecules, are needed in the structure, or, when that is known to be incorrect, that there is a flaw in some overall aspect of intensity measurement, such as background correction. The root mean displacements (μ) of the atoms are shown in parentheses underneath the positive values of the temperature factor ($\mu = [B/(8 \pi^2)]^{1/2}$). Although temperature factors of 9 and 23 Å^2 seem large compared to the values of 3 or 4 Å^2 found for crystals of small organic molecules, the high values reflect additional disorder in the small and imperfect crystallites of polysaccharides. The expression of these uncertainties in atomic position in terms of the mean displacement could diminish the objection to the high B values. Such high values of B are frequently reported for studies of single crystals of proteins.

Table VIII. Isotropic Temperature Factors, B, and Mean Displacements (in parentheses), μ , From Different Data Sets

SRRC Computer Program			
Data Set	UP	DOWN	ANTI
Mann			
Gonzalez	22.06	23.09	24.05
Wellard	(.53)	(.54)	(.55)
Woodcock	-4.33	-3.24	-2.92
Sarko			
Roughead	9.66	9.55	8.70
Miller	(.35)	(.35)	(.33)
French			
Typical Organic Structure		4.00	(.22)

Units of B are A^2 . Units of μ are A.

Some idea of the ultimate ability of x-ray data to distinguish among models can be obtained by substituting calculated data from one model for the observed data in the program. This simulates having "perfect" data that arise from one chain polarity. The other models (parallel down and antiparallel) are then adjusted to produce the calculated patterns that best match the calculated intensities from the parallel up model. Table IX shows that the number of reflections observed by RMF should be sufficient to provide a differentiation among the models if the data and chain models are accurate.

Table IX. Fit of Parallel Down and Antiparallel Models to Intensities Calculated from Parallel Up Model with 06 tg.

	Robs	Runobs	Rtot	R ^u wt	R ^u nwt
Parallel Down	.106	.098	.233	.088	.200
Anti-Parallel	.075	.115	.230	.057	.160

06 Position. One of the major outstanding issues is the exact position of the primary alcohol group. Because of the indications of the lack of symmetry from the spectral work (13-14), a new look at this issue is in order.

Models that must be examined include those where both the **tg** and **gt** positions are present within each chain, and those with corner chains having one 06 position while the center chains have the other. A third variation is that each chain may have alternate deviations from, for example, pure **gt** conformations from one residue to the next.

Table X. Change in Distance to 06 Due to Chain Rotation*
Distances are between corner chains in a direction essentially parallel to the **b** axis.

Chain Rotations (Degrees)	Atom Pair	Interatomic Distance (Angstroms)		
		06=220° (gt)	06=210° (gt)	06=-3° (tg)
69	06-02"	2.62	2.83	3.36
	06-03"	**	**	2.93
65	06-02"	2.47	2.66	3.28
	06-03"	**	**	2.89
63	06-02"	2.21	2.38	3.19
	06-03"	**	**	2.90
61	06-02"	2.11	2.26	3.17
	06-03"	**	**	2.92
59	06-02"	2.04	2.16	3.17
	06-03"	**	**	2.96

* WS unit cell. Add 0.05 A to each distance for RMF cell.

** Distance more than 3.49 A.

The **gt** 06 position was previously ruled out because of short contacts that occur when the chains are rotated into the 61-63° positions that give the best R factors (Table VI). The questioned interaction is within the sheets, where the chain centers are spaced apart by about 8.2 A (the unit cell **b** dimension). Table X shows that the chains need only be rotated 2° from the positions of lowest R in order to provide sufficient (>2.6 A) clearance. The historic Meyer-Misch cell has a dimension of 8.35 A, providing even more clearance. Therefore, the unit cell dimensions are critical to such determinations.

Table XI. Effect of O6 Position on R Value

All Models Parallel-Down, Sarko-Muggli
Geometry, SRRC Computer Program, RMF Data

O6 Position	tg	gt	gg	gt, tg in chain
Type of R				
Rtot	.415	.387	.556	.385
R"wt	.179	.149	.314	.148
R"unwt	.283	.269	.421	.259

The R factors obtained at SRRC do not rule out a structure containing a mixture of O6 positions. The lowest values of R in Table XI were obtained for a mixed structure. Note that structures with O6 in the **gg** position, as mentioned earlier, are clearly ruled out by high R values.

Table XII. Parallel Down Models from
Clemson University

Sarko-Muggli Residue, RMF Data

	Rtot	Rw"				
All gt	.4415	.0730				
All tg	.4348	.0556				
gt tg in chain	.4747	.0525				
gt gt corner	.4313	.0297				
tg tg center						
Corner	gt gt	gt gt	gt tg	gt tg	gt tg	tg tg
Center	gt tg	tg gt	gt tg	tg tg	tg gt	tg gt
R"	.0416	.0469	.0525	.0545	.0655	.0684

The most recently computed R values from Clemson (Table XII) indicate that a lower figure can be obtained for a structure that has the same O6 positions within individual chains but with O6 positions for the center chains being different from O6 positions of the corner chains. However, in the best model from Clemson, the polymer continuity is disrupted by about 0.2 Å at the top of the unit cell due to lack of polymeric constraints in the SHELX program.

Although the R" values from SHELX are very low, the conventional R values computed with this program are still quite high, indicating substantial error in gathering the data rather

than the results of using a model with more variables than can be supported by the data.

Conclusions

This work has shown that the variations in crystal structures of cellulose are not likely to arise from the computer techniques used. When care was taken to make reasonable comparisons of results of the four programs studied, the results were essentially the same. The data is the main factor in determining which of the competing models is selected as best.

New work on cellulose should draw upon some of the observations herein. Unit cells should conform to crystallographic convention. The temperature factor is a valuable gauge of the validity of the data set. Perhaps some electron diffraction studies of the hk0 plane will be able to give precise values of the a and b dimensions to aid in the stereochemical analyses. It is of substantial value to be able to know the error in the measurement of the intensity data as well as the intensity data. However, the use of error estimates for weighting the R calculations must be used with caution. The outstandingly low R^{wt} values obtained by the SHELX method must be reconciled with the slightly non-polymeric result. The LALS and PS-79 programs should be able to closely duplicate this result but have not yet done so.

This study has identified a difficulty in use of crystallographic convention that raises the question as to whether the ramie and cotton celluloses have the same packing as the algal and bacterial celluloses. The structure proposed by Woodcock and Sarko for ramie is not the same parallel-up packing as proposed by Gardner and Blackwell for *Valonia*. Work herein with simulated, "perfect" data indicates that distinction between the two parallel models is possible, at least with rigid models. It will be useful to repeat this experiment with the flexible modeling programs.

The high R_{tot} values that are associated with the extremely low R^{wt} values obtained at Clemson indicate that there is still substantial error in the data or that a different model for the unit cell is needed, perhaps a larger one with more chains. The discontinuous chain is suggestive of two different linkages in the chains, which may point the way towards models of the different chains in 8-chain unit cells.

An indication of systematic error in at least two of the currently available data sets is furnished by the various temperature factors, as well as the more random discrepancies in the square roots of the intensities.

The failure of the present work to identify the correct packing mode or 06 position should not be taken as an indication of the futility of the fiber diffraction experiment for native cellulose. The use of calculated data as an observed data set for fitting alternate models demonstrated that there is sufficient difference between the models to permit a distinction. If the maintenance of conventional stereochemistry by the LALS and PS-79 programs prevents LALS and PS-79 from discerning the correct model, one must lay the blame on the high error in the data and redouble efforts to decrease it.

Besides the issues tackled in the present study which fall within the traditional scope of cellulose structural studies, there are two remaining items that need to be incorporated in future work.

The first is the re-determination of the data, with a higher degree of resolution of overlapping peaks together with clarification of the issue of the 8-chain vs. 2-chain unit cell. Because of the greater number of peaks reported by Woodcock and Sarko, along with less overlapping of the peaks, the indication for the parallel-up packing mode was stronger than the indications from the other studies.

The second is the incorporation of some technique to compensate for the fact that cellulose crystallites are not infinite. This fact modifies the intensities and should be included before fine distinctions can be made with confidence. A whole pattern fitting technique as proposed by Fraser et al (25) may solve both problems.

Literature Cited

1. Nishikawa, S.; Ono, S. Proc. Tokyo Math. Physic. Soc. 1913, 7, p. 131.
2. Miller, D. P.; Roughead, W. A.; French, A. D. Proc. 1983 Dissolving and Specialty Pulps Conf., TAPPI Press, Atlanta GA, p. 233.
3. Hebert, J. J.; Muller, L. L. J. Appl. Polym. Sci. 1974, 18, p. 3373.
4. Marrinan, H. J.; Mann, J. J. Polym. Sci. 1956, 21, p. 301.
5. Wellard, H. J. J. Polym. Sci. 1956, 13 p. 471.
6. Woodcock, C.; Sarko, A. Macromolecules 1980, 13 p. 1183.
7. Klug, H. P.; Alexander, L. E. X-Ray Diffraction Procedures; 2nd ed., John Wiley and Sons: New York, 1974, p. 13.
8. French, A. D. In Polymers for Fibers and Elastomers; Arthur, J. C., Ed.; ACS Symposium Series No. 260; American Chemical Society: Washington, DC, (1984) p. 43.
9. French, A. D. Carbohydr. Res. 1978, 61, p. 67.
10. Takahashi, Y.; Suzuki, H.; Tadokoro, H. Polymer Preprints in Japan 1980, 29 p. 2079.
11. Gardner, K. H.; Blackwell, J. Biopolymers, 1974, 13 1975.
12. Honjo, G.; Watanabe, M. Nature, 1958, 181, p. 326.
13. VanderHart, D. L.; Atalla, R. H. Macromolecules 1984, 17, p. 1465.
14. Atalla, R. H. In Hydrolysis of Cellulose: Mechanisms of Enzymatic and Acid Catalysis, Brown, R. D.; Jurasek, L. Ed.s; ACS Symposium Series 181; American Chemical Society, Washington, DC, 1979; p. 55. 181 (1979) 55.
15. Sheldrick, G. M. "The Chemistry Laboratory", Cambridge U., Cambridge, England. 1974. Available from the Author.
16. French, A. D.; Murphy, V. G. Carbohydr. Res., 1973, 27, p. 391.
17. Zugenmaier, P.; Sarko, A. In Fiber Diffraction Methods; A. D. French and K. H. Gardner, Ed.s; ACS Symposium Series No. 141; American Chemical Society: Washington, DC, 1980; p. 225.
18. Arnott, S.; Wonacott, A. J. Polymer 1966, 7 p. 157.
19. Smith, P. J. C.; Arnott, S. Acta Crystallogr. 1978, A34, p. 3.

20. Mann, J.; Roldan-Gonzalez, L.; Wellard, H. J. J. Polym. Sci. 1960, 42 p. 165.
21. French, A. D.; Murphy, V. G. In Cellulose Chemistry and Technology; ACS Symposium Series No. 48, American Chemical Society, Washington, DC, 1977, p. 12.
22. Sarko, A.; Muggli, R. Macromolecules 1974, 7, p. 486.
23. Cox, E. G.; Shaw, W. F. B. Proc. Royal Soc. (London) 1930, 127A, p. 71.
24. Cella, R. J.; Lee, B.; Hughes, R. E. Acta Crystallogr. 1970, A26, p. 118.
25. Fraser, R. B. D.; MacRae, T. P.; Miller, A.; Suzuki, E.; Tullock, P. A. J. Appl. Cryst. 1977, 10 p. 64.
26. Chu, S. S. C.; Jeffrey, G. A. Acta Crystallogr. 1968, B24, p. 830.
27. Chu, S. S. C.; Jeffrey, G. A. Acta Crystallogr. 1967, 23, p. 1038.

RECEIVED March 31, 1987

Chapter 3

Multidisciplinary Approaches to the Structures of Model Compounds for Cellulose II

Bernard Henrissat¹, Serge Perez^{1,2}, Igor Tvaroska³, and William T. Winter⁴

Centre de Recherches sur les Macromolécules Végétales, Centre National de la Recherche Scientifique, B.P. 68, 38402 Saint Martin d'Hères Cedex, France

The 3-dimensional structural features of macromolecules such as cellulose are often preserved in oligomeric model compounds which provide the opportunity for more accurate characterization through the occurrence of larger crystalline domains. We have been examining cellobiose, methyl β -D-cellobioside and cellotrioside, and cellotetraose using X-ray and electron diffraction, CP-MAS NMR spectroscopy and computer modeling with the PCILO and MM2 algorithms. The geometry of the pyranose ring in oligomers was shown by modeling to vary with linkage conformation. Thus, selecting either the cellobiose or methyl β -D-cellobioside conformation alters the geometry of the ring selected by the program to have minimal energy. When these different ring geometries are incorporated in the molecular mechanics program, they influence, in turn, the conformational energy surface, even altering the relative levels of minima. X-ray and electron diffraction studies have established the packing similarity of both methyl β -D-cellotrioside and cellotetraose to cellulose II. Finally, we have examined proposals that correlate chemical shift data from ^{13}C CP-MAS NMR spectroscopy with conformations and with differences in the charge distribution in the individual conformers.

¹Current address: Institut National de la Recherche Agronomique, rue de la Géraudière, F-44072 Nantes, France

²Correspondence should be addressed to this author.

³On a leave of absence from the Institute of Chemistry, Center of Chemical Research of the Slovak Academy of Sciences, 84238, Bratislava, Czechoslovakia

⁴On a leave of absence from the Department of Chemistry, Polytechnic University, 333 Jay Street, Brooklyn, NY 11201

Introduction

Characteristics of macromolecules are often preserved in oligomeric model compounds. As one example, X-ray powder diffraction patterns (1) and the infrared spectra (2) of the cellodextrins beginning with cellotetraose are very similar to those of cellulose II. Such a similarity implies a close relationship in their molecular structures. While these model compounds should permit more accurate characterization because of their macroscopic, single-crystal domains (3), cellodextrins form non-centrosymmetric crystals and analysis of their diffraction data is a serious challenge.

Since single-crystal diffraction is the only method that provides bond lengths, bond angles and the characteristic geometry, it is the ultimate structural method. On the other hand, polymer X-ray studies depend on a proposed model, and hence are not absolute. Therefore, it is important to refer to single crystal studies for data on which to base cellulose models. The crystal and molecular structures of cellobiose (4) and methyl β -D-cellobioside (5) have been reported. We also wish to know the detailed structures of the higher oligomers, which are more analogous to cellulose II. After pioneering work on cellotetraose (6,7), Poppleton and Gatehouse (8) proposed a larger, triclinic unit cell, containing 2 molecules. The full structure is not yet determined.

Recently, new approaches such as molecular mechanics have been applied to structural characterization of native and regenerated celluloses. Among these, the most promising may be "magic angle spinning" for recording the NMR spectra of solid cellulose samples (9-17) and cellodextrins (10,18-19). The characteristics of spectra from cellulose II were found to be very similar to oligomers of DP > 4 (10,11). In addition, conclusions were drawn regarding the asymmetric unit in the crystalline region. Nevertheless, several points are still obscure.

The major aim of the present work was to characterize crystalline cellodextrins using several methods in order to reach a consistent description of the structural features and to establish the workability of each approach to the more complex case of cellulose.

Materials and Methods

Nomenclature. The numbering of the atoms and torsion angles of interest for cellobiose is shown in Fig. 1. Numbering proceeds from the nonreducing end (unprimed) to the reducing end (primed). The signs of the torsion angles agree with the rules of the IUPAC-IUB Commission of Biochemical Nomenclature (20).

The torsion angles of interest are defined as follows :

$$\phi : \theta \{O5 - C1 - O1 - C4'\}$$

$$\psi : \theta \{C1 - O1 - C4' - C5'\}$$

The conformation of the primary hydroxyl group at C6 (χ) is referred to as either gauche-trans, gauche-gauche or trans-gauche (21). In this terminology, the torsion angle : $\theta \{O5 - C5 - C6\} - O6$ is stated first, then the torsion angle $\theta \{C4 - C5 - C6 - O6\}$. The unit cell dimensions of cellulose II, as determined from X-ray and electron diffraction studies (22-25) on Rayon, Fortisan,

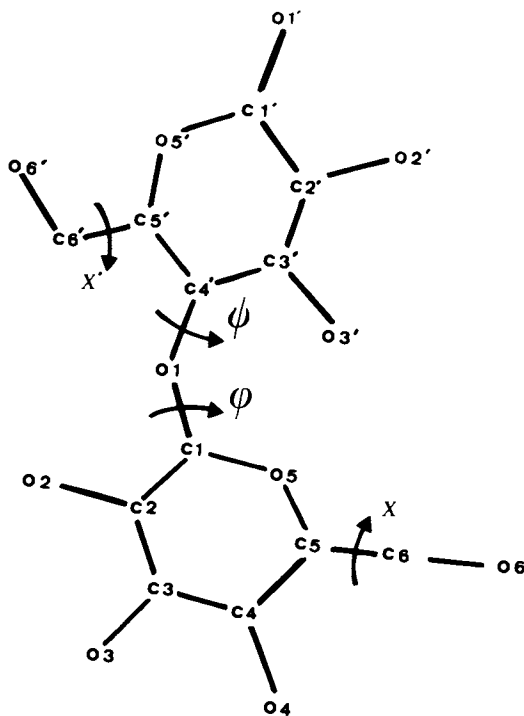


Figure 1. Schematic representation of cellobiose, along with the atom labeling and the torsional angles of interest.

mercerized cotton and single crystals are : $a = 8.01$, $b = 9.04$, $c = 10.36$ Å and $\gamma = 117.1^\circ$. Following the most accepted crystallographic models (22, 24), the unit cell requires two cellulose chains packed with antiparallel polarity.

Sample Preparation. Cellobiose was purchased from Fluka Company. Samples were dissolved in water and crystallization resulted from slow diffusion of ethanol.

Methyl β -D-cellobioside, a gift from Dr. M. Vincendon (Grenoble, France), was dissolved in hot methanol and crystallized by slowly cooling the solution.

Hendeca-O-acetyl celotriose and tetradeca-O-acetyl cellotetraose were obtained by acetolysis of cotton cellulose according to Wolfrom et al. (26) and were purified by preparative HPLC. Methyl deca-O-acetyl- β -D-celotrioside was prepared according to the method described by Takeo et al. (27). Deacetylation of the acetylated sugars was achieved in methanol containing catalytic amounts of sodium methylate. The high purity of the samples and their anomeric configuration were confirmed by high-resolution solution ^{13}C NMR.

Solid State NMR. The samples under investigation were obtained from crystals which were ground into homogeneous powder. In each case, wide angle X-ray scattering diagrams were recorded in order to confirm the unit cell dimensions previously found.

Solid state ^{13}C NMR spectra were recorded at 50.3 MHz with a Bruker CXP-200 spectrometer equipped with a Doty probe. Proton 90° pulse widths were 4 μs , and cross-polarization times were 1 ms. Matching conditions were checked with an adamantane standard. The magic angle was set by monitoring the ^{79}Br NMR spectrum of KBr (28). Sample containers were made of aluminum oxide with Kel-F caps and were spun at 2.5-3.5 KHz. Characteristically, 200-10000 acquisitions were obtained per spectrum, with recycle time of 4 s. All peaks in the spectra were referenced to the peak of linear polyethylene (33.6 ppm). A small amount of polyethylene was added to each sample (29).

Conformational Analysis Calculations. PCILO method : The standard version of the semiempirical quantum-chemical method (30, 31) adopted for the optimization of the geometry according to Powell-Zangwill's (32, 33) algorithm through bond lengths, bond angles and torsion angles was applied. (PCILO : Perturbative Configuration Interaction with Localized Orbitals).

Force Field method : MM2CARB is the MM2 (Molecular Mechanics) Force Field program (34) modified with the Jeffrey-Taylor acetal segment parameters (35) and intramolecular hydrogen bonding (36). It was utilized, following the strategy outlined by Tvaroska and Pérez (37). To obtain better agreement between calculated C-O bond lengths and those observed by X-ray or neutron diffraction methods, the following equilibrium bond lengths for bond stretching energy were used : C1-O5 from 1.396 to 1.422 Å, C1-O1 from 1.380 to 1.388 Å, C5-O5 from 1.412 to 1.420 Å , and C4-O1 from 1.388 to 1.415 Å.

"Empirical" method: (PFOS : Potential Functions Oligosaccharide Structures). The potential energy is calculated by including the

partitioned contributions arising from the van der Waals, torsional and hydrogen bond contributions. The van der Waals interactions are evaluated by using 6-12 potential functions with the parameters proposed by Scott and Scheraga (38). A three-fold potential is used for rotation about the aglycon bond O1-C4' with a barrier of 1.0 kcal/mol. For rotation about glycosidic bond C1-O1, the intramolecular mechanism responsible for exo-anomeric effect, is taken into account using the potential function proposed by Tvaroska (39); a three-fold rotational barrier of 1.0 kcal/mol is also included. Hydrogen bond energy is computed by an empirical expression :

$$V_{HB} = 33.14 (R - 2.55) (R - 3.05)$$

where R is the distance between oxygen atoms which should lie between 2.55 and 3.05 Å. No electrostatic interaction is taken into account. The energy map is calculated as a function of ϕ and ψ at intervals of 5°. With respect to the relative energy minimum, iso-energy contours are drawn by interpolation at 1 kcal/mol increments. Helical arrangements are customarily described in terms of a set of helical parameters (n , h), n being the number of residues per turn of the helix and h being the translation along the helix axis. These parameters are calculated following our algorithm reported previously (40).

Diffraction and related Methods. Methyl β -D-celotriose was dissolved in water (10 mg.ml⁻¹). Crystallization into hexagonal platelets was achieved by a slow diffusion of ethanol. A crystal of dimensions ca. 0.5 x 0.5 x 0.1 mm was mounted on a Nonius CAD4 diffractometer. The radiation was nickel-filtered Cu K α . The unit-cell dimensions were obtained as part of the alignment process on the diffractometer by a least-squares fit to the setting of 20 well-centered reflexions. The monoclinic space group P2₁ was assigned, based upon the systematic absences : 0 k 0, $k \neq 2n$. 4310 independent reflexions were measured, of which 616 were assigned zero weight as the net count of each was less than 1.99 (I) where $\sigma(I)$ is the standard deviation estimated from counting statistics. Because of the low value of the absorption coefficient, no absorption correction was applied. Scattering factors were obtained from International Tables for X-ray crystallography (41). The MULTAN computer program (42) was used for normalization and attempts to solve the structure through direct methods.

Crystallization of cellotetraose from aqueous solution was done by slow diffusion of ethanol. Crystals thin enough for electron diffraction were prepared by epitaxial crystallization of cellotetraose onto Valonia microfibrils in a solution containing 1% of cellotetraose in a 3:2 mixture of ethanol in water. Crystallization took place within a few weeks, at room temperature. A shish-kebab type of structure (43) was obtained from which lamellar fragments of cellotetraose crystals could be detached by mild sonication. The fragments were mounted on carbon-coated grids and were observed on a Philips EM 400T Electron Microscope operating at 120 kV. A full determination of the unit-cell parameters was achieved through a series of tilt experiments and subsequent analysis of the resulting electron diffractograms (Roche, E.; unpublished data).

About 1 cm³ of highly crystalline powdered cellotetraose was used to obtain a neutron diffraction pattern from the high resolution D1A machine at the Institute Laue Langevin in Grenoble. Since the material could not be deuterated, the effective absorption was important, as was the "incoherent" background scattering. In order to obtain good statistics in the background region, only a single powder pattern was collected in the whole of our allocated three days. We had hoped to be able to extract at least 50 Bragg intensities from such a pattern by using a relatively long wavelength of 3 Å to spread out the lower orders over the whole angular range. However, most of the Bragg intensity goes into six strong peaks, with the remainder all very small and barely above the background level. Furthermore, it appears that the widths of the lines may depend on the $(h\ k\ l)$ direction in the structure: near $2\theta = 85^\circ$, neighboring lines have very different widths. This effect, presumably due to directional differences in short range crystalline order, complicates the application of profile refinement methods to resolve individual reflexions.

Linked-Atom-Least-Squares Procedure. Molecular models having standard bond lengths, bond angles and ring conformations (43) were generated using the linked-atom-least-squares method previously described (44). In the present application of this method for non-helical structures, the variable parameters include all the torsion angles and valence angles about glycosidic linkages, and those defining the orientations of rotatable substituents, notably the primary hydroxyl groups. For each molecule, two variable parameters, u and v define the point where the molecular axis intersects the orthogonal crystallographic plane of the unit cell; additional parameters μ and ν define the orientation about, and relative translation parallel to that axis. Any or all of these parameters may be varied so as to minimize the following function:

$$\Omega = \sum W_m (oF_m - F_m)^2 + S \sum \epsilon_j$$

The first summation is used to optimize agreement between observed structure amplitudes, oF_m , with those calculated from the model, F_m after scaling by a factor $1/k$. In calculating F_m , all atoms were assumed to vibrate isotropically and 4Å^2 was assigned as the value of B in the attenuation factor, $\exp(-B\sin^2\theta/\lambda^2)$. Unit weights, W_m , were assigned to all measurable reflections within a given resolution sphere. The second term is used to ensure the stereochemical acceptability of the model by minimizing a quantity, $\sum \epsilon_j$, which approximates the non-bonded repulsion energy. This term is also used to optimize weak attractive interactions such as hydrogen bonds. The precise formulation of ϵ_j and empirical constants employed in its evaluation have been described elsewhere (44). The calculations were performed on an EC-1045.01 machine, at the Computer Centre of the Slovak Academy of Sciences, Bratislava, and on a Honeywell-Bull CII-HB68 mainframe at the University of Grenoble. The molecular drawings shown throughout this article were obtained with the aid of the PITMOS program (45). The perspective drawing of the three dimensional shape of the mirror image of the conformational energy well of cellobiose (Fig. 2) was obtained with the CARTOLAB program (46).

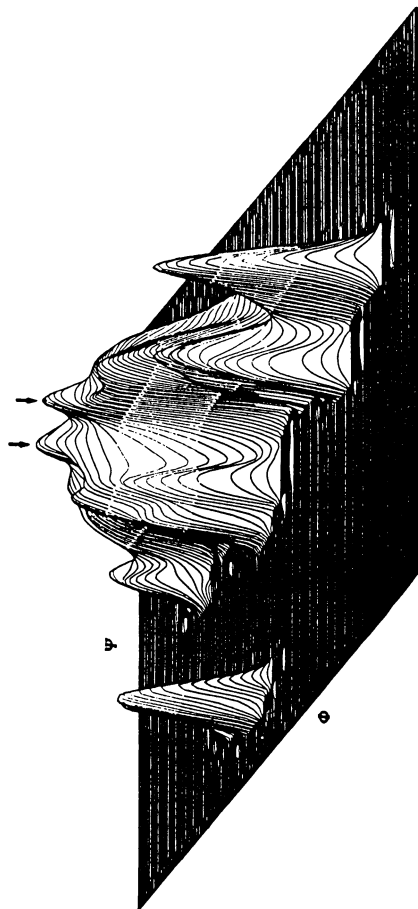


Figure 2. Perspective drawing of the three-dimensional shape of the mirror image of the conformational energy well for the full angular range for ϕ and ψ . The volume was constructed using the following scheme:

$$V(\phi, \psi) > 15 \text{ kcal/mol} : V(\phi, \psi) = 0 ;$$

$$V(\phi, \psi) < 15 \text{ kcal/mol} : V^p(\phi, \psi) = -(V(\phi, \psi) - 15) .$$

V being the energy expressed relative to the minimum.

Proceeding from top to bottom of the three-dimensional shape, we note: the very low energy region (the arrows point towards the conformations observed for crystalline cellobiose and methyl β -D-cellobioside). The 5 kcal/mol to the 10 kcal/mol energy contours correspond to the light grey region of the volume.

Results and Discussion

Conformational Analysis. Comparison of results shows that the locations of the energy minima on the (ϕ, ψ) map are almost independent of the function used for calculating energy, whereas the differences in energy levels of the various minima are strongly dependent on this choice. The differences are most pronounced in the low-energy regions. This suggests that energy surfaces are valuable in refining the pertinent portion of the map embodying "allowed" conformations, but relative energy values should be treated with caution.

Figure 2 shows the energy map for cellobiose, as calculated from PFOS method; the two deepest minima are indicated by arrows. These two minima correspond to crystalline conformations found for cellobiose (4) and methyl- β -D-cellobioside (5). For these models of the two stable conformations, an intramolecular hydrogen bond of the type O3'...O5 is present, with O3'...O5 distance of about 2.60 Å, compared to 2.76 Å in the crystal structures.

We next studied the influence of the orientation of the hydroxyl groups at C6 on the conformations at the glycosidic junction. Because the trans-gauche (tg) position of O6 seldom occurs, probably as the result of repulsive interaction between O4 and O6 (21), we considered only the gauche-gauche (gg) and gauche-trans (gt) conformers. The role of the primary hydroxyl group differs depending on whether it is on the reducing or the non-reducing residue. For values of ϕ and ψ corresponding to the crystalline conformations of either cellobiose (4) or methyl β -D-cellobioside (5), a gt orientation of the primary hydroxyl group of the non-reducing residue brings an O2-H...O6 hydrogen bond. Crystalline methyl cellobioside (5) has this bond; cellobiose does not.

Previous work revealed that cellobiose can exist in several stable conformations. Conformers corresponding to the eight lowest minima (Fig. 2) were used as starting points for calculations with MM2CARB. Seven conformers resulted; their relative energies are given in Table I. In Table II are selected characteristics of

Table I. Relative energies (kcal/mol) of stable conformers for cellobiose and methyl β -D-cellobioside calculated by MM2CARB method with and without hydrogen bond energy (V_{HB}).

Conformer	cellobiose		methyl β -D-cellobioside	
	without V_{HB}	with V_{HB}	without V_{HB}	with V_{HB}
C1	1.33	0.93	1.45	0.84
C2	0.00	0.50	0.00	0.36
C3	3.42	0.00	1.60	0.00
C4	1.52	1.75	2.20	1.68
C5	4.24	2.11	4.48	2.09
C6	6.39	2.94	2.69	3.04
C7	2.88	2.24	3.34	1.67

Table II. MM2CARRB calculated energies E (kcal/mol), dipole moments μ (D), and selected geometrical parameters: bond lengths (Å), bond angles (deg), for methyl β -D-cellobioside conformers.

Conformers	$\underline{C1}$	$\underline{C2}$	$\underline{C3}$	$\underline{C4}$	$\underline{C5}$	$\underline{C6}$	$\underline{C7}$
E	32.06	31.58	31.22	32.89	33.31	34.26	32.89
ϕ	-87.6	-66.3	48.2	-74.4	-147.9	-171.9	-46.6
ψ	178.9	-120.4	-114.9	55.1	-145.0	-176.0	-83.0
ϕ^H	32.8	49.9	161.4	44.5	-35.9	-62.1	70.1
ψ^H	-66.1	16.7	5.8	171.7	-26.9	-60.6	-164.3
χ	63.6	58.2	61.0	64.3	64.2	62.6	63.7
χ'	62.9	-64.1	61.2	68.0	63.7	-67.2	60.4
C(5)-O(5)	1.4315	1.4289	1.4286	1.4305	1.4296	1.4299	1.4280
C(5)-C(1)	1.4264	1.4237	1.4240	1.4221	1.4273	1.4314	1.4188
C(1)-O(1)	1.3923	1.3997	1.3989	1.3973	1.3956	1.3963	1.3944
O(1)-C(4')	1.4289	1.4308	1.4283	1.4328	1.4269	1.4281	1.4318
C(5)-O(5)-C(1)	112.7	113.1	112.9	112.3	112.6	113.2	112.8
O(5)-C(1)-O(1)	107.2	108.1	108.8	109.4	102.6	101.2	108.6
C(1)-O(1)-C(4')	117.1	114.9	114.9	117.3	115.6	118.7	116.2
μ	4.3	3.5	4.3	4.9	5.9	2.2	5.2

$\phi^H = H1-C1-O1-C4'$; $\psi^H = C1-O1-C4'-H4'$

methyl β -D-cellobioside. Note (Table 1) that the inclusion of hydrogen bonding energy (V_{HB}) changes the relative stability of the conformers.

Because all possible intramolecular hydrogen bonds were considered, it is of interest to compare the various patterns that resulted from the three best conformations. The hydrogen bonding in C2 corresponds to that of crystalline of methyl β -D-cellobioside, with O3'H...O5 and O3'H...O6 hydrogen bonds with interoxygen distances of about 2.77 and 2.80 Å, respectively. On the other hand, the C1 conformation does not have an O3'H...O5 hydrogen bond. The interoxygen distance is 3.0 Å but the hydrogen atom on O3' is not positioned favorably. Instead it forms a bond to O6, the distance being 2.90 Å. In the C3 conformer, O3'H...O5 and O6'H...O6 were formed.

The parameters in Table II demonstrate an interaction between the ring geometry and the conformation around the glycosidic and aglycon bonds. The calculated bond lengths agree with the values observed in the crystal structures except for O5-C1 and C1-O1 and for C5-O5-C1 and C1-O1-C4'. The C1-O1 bonds are shorter than observed values and vary with ϕ and ψ . At the same time, the O5-C1-O1 bond angles vary from 101.2 to 109.5° and glycosidic bond angles from 113 to 120°. These variations of internal geometry owing to changes in linkage torsion angle are consistent with statistical analysis of carbohydrate crystal structures (47,48). Dipole moments range from 3.4 to 6.0 D.

When the torsion angles ϕ , ψ are identical for all the pairs of glucose residues along the chain, the polymer chain assumes a regular helical shape. From the geometrical parameters defining the repeat unit, it is possible to calculate, for each ϕ , ψ the values of the helical parameters n , h . In turn, these values may be compared to those derived from X-ray diffraction of oriented fibrillar material which, in the case of cellulose chains are $n = 2$ and $h = 5.15$ Å. None of the stable cellobiose conformers as derived from either energy minimization or crystal structure elucidations can generate such a helical structure.

Charge Densities - CP/MAS NMR Spectroscopy. Recent ^{13}C NMR studies of solid carbohydrates using the cross-polarization/magic angle spinning (CP/MAS) technique (15) demonstrates that ^{13}C NMR chemical shifts of the C1, C4 and C6 carbon atoms are considerably displaced, up to 10 ppm, depending on the particular structure. A relation of these shifts to conformation would be valuable in learning whether a conformation is retained in non-crystalline or solution states.

A simple linear relationship has been proposed between the chemical shift for C6 and the torsion angle χ about the exo-cyclic C5-C6 bond. The chemical shifts fell into 3 groups of 60-62 ppm, 62.5 ppm and 65.5-66.6 ppm for the gg, gt and tg conformations (18). In a more sophisticated empirical observation, it was proposed that chemical shifts in a series of closely related molecules are related to charge density (50,51).

As a first step in understanding the relationship of chemical shift to conformation, we calculated charge densities for α and β -D-glucose, cellobiose, and methyl β -D-cellobioside, using the PCILO program. Charge densities for C6 of α - and β -D-glucose

American Chemical Society
Library

1155 16th St., N.W.
In The Structures of Cellulose: Atlanta, R.;
ACS Symposium Series; American Chemical Society: Washington, DC, 1987.

were, respectively, 0.1195 and 0.1173 (gg), 0.1189 and 0.1169 (gt), and 0.1182 and 0.1164 (tg). These values correlate well with the observed chemical shifts, above.

Calculated electron densities on selected carbon and oxygen atoms of methyl β -D-cellobioside (in the crystalline conformation) as a function of conformation of the primary alcohol groups are given in Table III. The results for cellobiose are similar. While conformational change results in changed density within the glucose residue, there is no effect on the other residue. However, the correlation of charge density and chemical shift observed above for glucose is not observed in this case. There are several possible explanations. Owing to the rarity of tg conformations, the chemical shift data is insufficient. (The values reported are from cellulose I, determined by fiber diffraction, and may not be reliable). Also, chemical shift should be a continuous function of torsional angle. Therefore, the proposed linear relationship cannot be correct. Our understanding of a relationship between electron density and chemical shift may be very approximate. Many more calculations are needed, using fine increments of torsional rotation. Such attempts will also provide information on chemical shifts of unstable conformers that cannot be isolated.

Packing features of known oligomers. X-ray data on crystalline oligomers provides information about some features of the packing habits as well as on molecular conformation. For a full understanding of any packing arrangement, the energy between a reference molecule and all its neighbors in the crystal is evaluated, taking into account the hydrogen bonds and the non-bonded interactions (52). These calculations use the same parameters as in the conformational analysis of single molecules using the PFOS method. Contributions to the energy were broken down into the pure, non-bonded part and the intermolecular hydrogen bonding.

The packing in crystals of cellobiose is very dense, each molecule is surrounded by 10 neighbors that occur in pairs (Fig. 3a). The strongest interactions are calculated for molecules related by pure translational symmetry along the crystallographic c axis (c = 5.091 Å). The energy of pairing of parallel molecules is due only to van der Waals interactions. The remaining packing energy arises from molecules related by symmetry operations about the 2_1 axis, with appropriate translations along the a and/or c axes. In these instances, the intermolecular associations are obtained through van der Waals and hydrogen bonding contributions.

Some of these same features are also found in methyl β -D-cellobioside, which also crystallizes in the $P2_1$ space group. Each molecule has 10 paired neighbors (Fig. 3b). The strongest intermolecular pairing is also obtained for molecules related to each other by pure translation along the crystallographic c axis (c = 4.496 Å). The pairing energy again arises from van der Waals forces. Other pure translational operations, such as $-\underline{a}$ or $-\underline{a} - \underline{c}$ result in strong cohesive energy, provided by comparable magnitudes of van der Waals and hydrogen bonding. Here, the only interactions along the 2_1 axis (b = 25.532 Å) occur via the methanol molecule through hydrogen bonding with subsequent bridging in the disaccharide molecules.

Table III. PCILO calculated electron densities for selected carbon and oxygen atoms as a function of hydroxymethyl groups orientations of methyl β -D-cellobioside in crystal conformation.

	$\rho_C(5')$	$\rho_C(6')$	$\rho_O(6')$	$\rho_C(5)$	$\rho_C(6)$	$\rho_O(6)$
g _L ,tg	3.8842	3.8851	6.1692	3.8979	3.8857	6.1672
tg,gt	3.8837	3.8837	6.1580	3.8981	3.8857	6.1674
gg,gt	3.8798	3.8847	6.1657	3.8980	3.8856	6.1670
gt,tg	3.8839	3.8851	6.1691	3.8979	3.8846	6.1666
tg,tg	3.8834	3.8837	6.1578	3.8981	3.8846	6.1668
gg,tg	3.8795	3.8847	6.1658	3.8980	3.8846	6.1666
gt,gg	3.8840	3.8850	6.1691	3.8940	3.8852	6.1680
tg,gg	3.8835	3.8837	6.1574	3.8942	3.8852	6.1678
gg,gg	3.8795	3.8846	6.1661	3.8941	3.8852	6.1683

g and t stand for gauche and trans, respectively (see text for explanation).

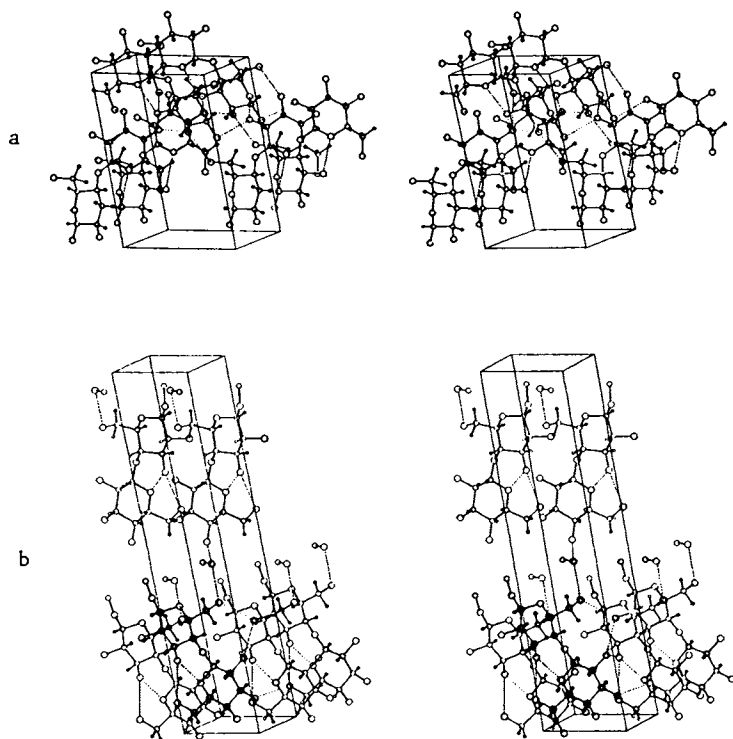


Figure 3. Stereoscopic representations of the molecular surrounding found in the crystalline state of :

a Cellobiose (4)

b Methyl β -D-cellobioside (5).

Methyl β -D-celotrioside. Fig. 4 shows a typical hexagonal crystalline platelet of methyl β -D-celotrioside, which upon reduction to powder gives rise to the diffraction pattern of Figure 5. The unit cell data are in Table IV. From the observed

Table IV. Crystal data for methyl β -D celotrioside.

$C_{19} H_{34} O_{16}$	$Mr = 518.46$
$a = 8.005 (2) \text{ \AA} ; b = 76.403 (9) \text{ \AA} ; c = 8.995 (2) \text{ \AA}$	
$\beta = 116.39 (5)^\circ ; \text{ monoclinic} ; P2_1 ; Z = 8$	

density of 1.50 Mg.m^{-3} , the asymmetric unit contains four independent molecules. Solving a non-centrosymmetrical structure with 140 non-hydrogen atoms from only 3694 reflections is a formidable challenge. Preliminary attempts to resolve the structure with conventional direct methods were unsuccessful; the work is still being pursued in our laboratory.

The crystal morphology (Fig. 4) and the dimension of the unit cell b parameter of 76.403 Å lead to the conclusions that:

- the molecules are in extended conformations and are placed parallel to the b axes. In some respect, they form a pseudo-chain structure.
- the base plane parameters (a , c and β) resemble those of cellulose II and of cellotetraose.

Fig. 6 summarizes the possible molecular features in terms of parallel and antiparallel arrangements compatible with the unit cell data for methyl β -D-celotrioside. By analogy with the antiparallel type of packing proposed for cellulose II and for cellotetraose, one would favor type d in Fig. 6.

Owing to its high crystallinity and the similarity of its X-ray diffractogram with that of cellotetraose, methyl β -D-celotrioside was used as a model for cellulose II in a study using ^{13}C NMR spectroscopy. It was thought that the aglyconic methyl group would also be useful in providing information about the variety of linkage conformations in the structure. Fig. 7 shows the spectra, along with some related oligomers. The spectra are similar, especially the chemical shifts for C4, which occur at lower field than in the lower oligomers. The resonance attributed to the C6 nuclei gives rise to a single broad peak centered at 64.2 ppm; three signals appear at 108.3, 106.0 and 104.0 ppm for the 3 C1 atoms.

At high field, the methyl groups produce two peaks, at 58.4 and 56.7 ppm. This important observation signifies that there are two main magnetic environments, and therefore, conformations, for the aglyconic moieties. Moreover, these two peaks are themselves composites of two or three peaks, consistent with the large unit cell. This supports model d , which has both "head-to-head" and "head-to-tail" environments for the methyl groups. By comparing

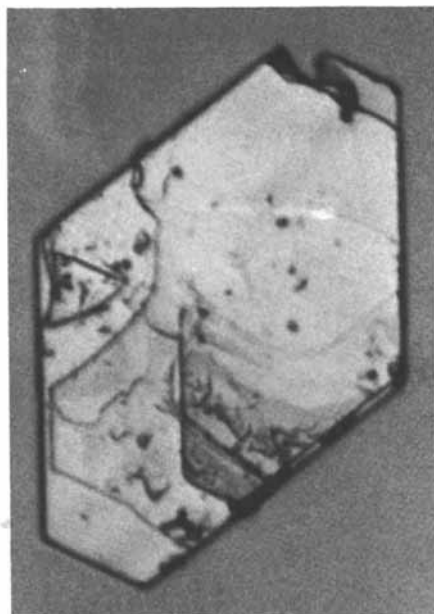


Figure 4. Typical hexagonal crystalline platelet of methyl β -D-cellotriside.

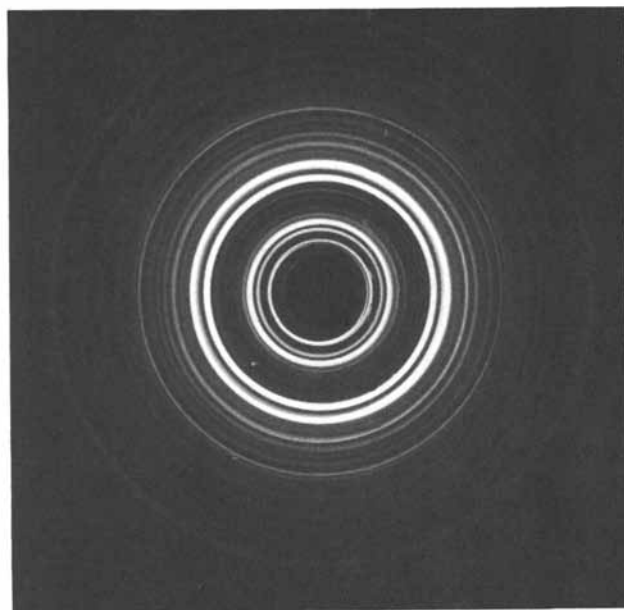


Figure 5. X-ray powder diffraction pattern of methyl β -D-cellotriside.

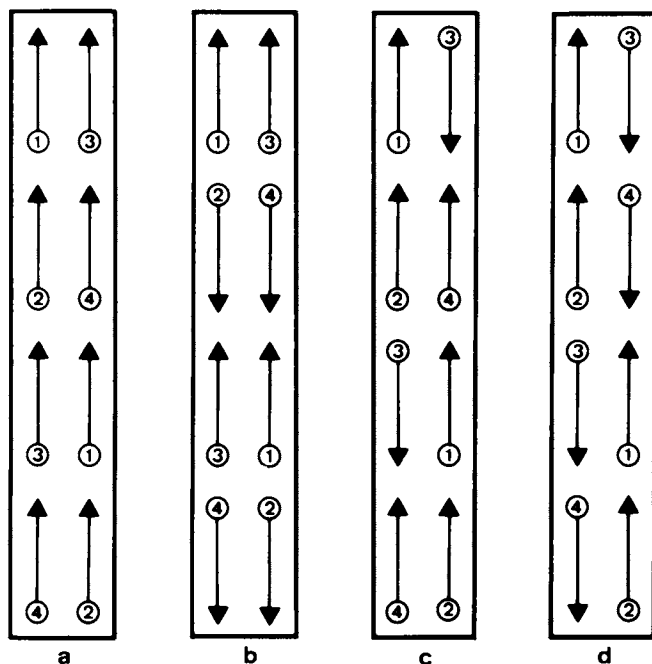


Figure 6. Schematic drawings of the possible molecular arrangements for crystalline methyl β -D-celotrioside consistent with a $P2_1$ space group symmetry. The 4 independent molecules are numbered from 1 to 4; the arrows point towards the methyl groups. For obvious crystallographic reasons the 2_1 axis of symmetry cannot coincide with any of the molecular axis.

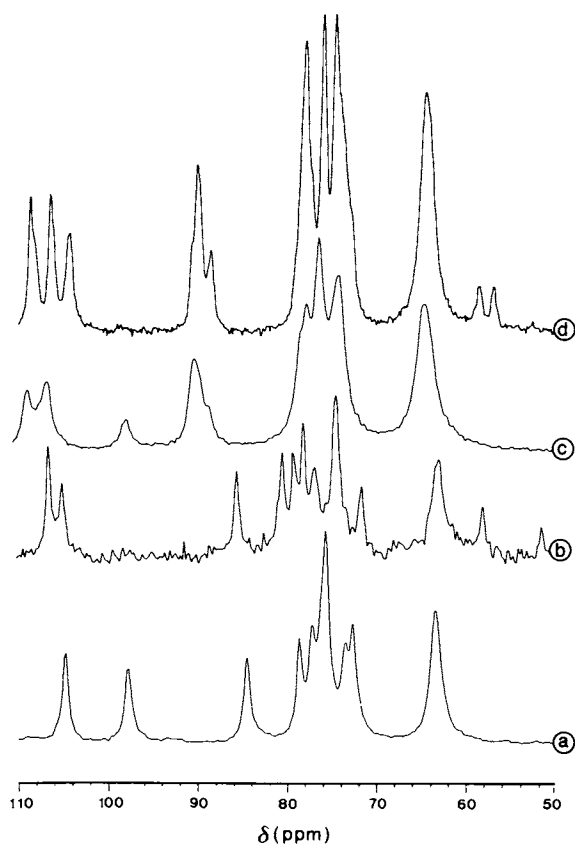


Figure 7. CP/MAS ^{13}C NMR spectra of some cellulose oligomers recorded at 50.36 MHz : a/ cellobiose, b/ methyl β -D-cellobioside, c/ cellotetraose and d/ methyl β -D-cellotrioside.

this spectrum with that of methyl β -D-cellobioside we could attribute the signal at 58.1 ppm to the aglyconic methyl group; the signal at 51.6 ppm then arises from the methanol molecule that co-crystallizes with methyl β -D-cellobioside.

Cellotetraose. Despite several years of steady effort, no single crystal adequate for conventional X-ray crystallography could be grown. Fig 8. shows a powder diffraction photograph; the wide angle neutron diffractogram is in Fig. 9. Crystal data are in Table V. Fig. 10 shows both a lamellar fragment of cellotetraose

Table V. Crystal data for cellotetraose.

$C_{24} H_{41} O_{21}$,		Mr = 665.57
a =	8.963 (3) Å	; b = 8.033 (3) Å ; c = 22.473 (7) Å
α =	94.98 (10) °	; β = 89.34 (10) ° ; γ = 116.13 (10) °
triclinic ; P1 ; Z = 2		

and the corresponding electron diffractogram. The base plane pattern has two-dimensional p1 symmetry which is consistent with both triclinic and monoclinic space groups. The fact that recording diffraction data from the base plane required tilting the crystal by 9-11° indicated that the correct choice was the triclinic space group. For a chiral molecule this could only be P1. The unit cell parameters agreed with previous values (8). We also confirmed that this triclinic cell fits the neutron data.

Observed structure factors were kindly provided by Poppleton. We found that only 869 of 2951 measured reflections could be considered as "observed" ($I/\sigma(I) > 1.99$). Since there are two tetramers per cell, determination of the structure requires location of 90 non-hydrogen atoms with only 869 observed reflections. Preliminary calculations produced a negative temperature factor, indicating an unreliable data set, as if from a damaged crystal. The crystal used by Poppleton was only 0.01 mm thick, and it required 900 hours of exposure to a high-intensity beam to record the data. Because the data were not likely to be accurate enough for conventional methods, we decided to attempt to solve the structure with one of the "Real-Space Crystal Structure Resolution" procedures with the 70 reflections corresponding to 3 Å resolution.

The Linked-Atom Least-Squares (LALS) procedure (44) was used to generate molecular models of cellotetraose. The glucose residues were kept in the standard 4C_1 conformation; all bond angles and bond lengths were fixed at standard values (43). The constrained model of the crystal structure was optimized against both X-ray data and non-covalent interatomic interactions, as described by Smith and Arnott (44).

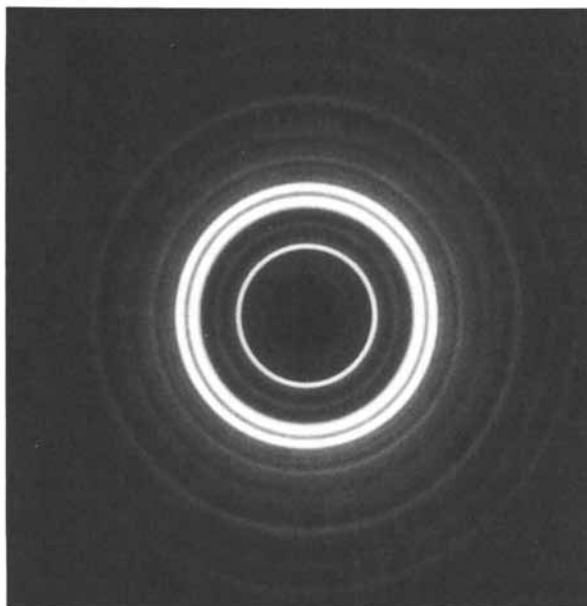


Figure 8. X-ray powder diffraction pattern of cellotetraose.

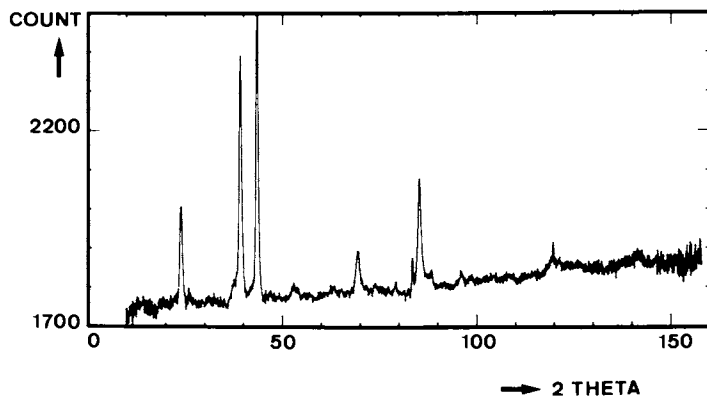


Figure 9. Wide angle neutron powder diffractogram of cellotetraose.

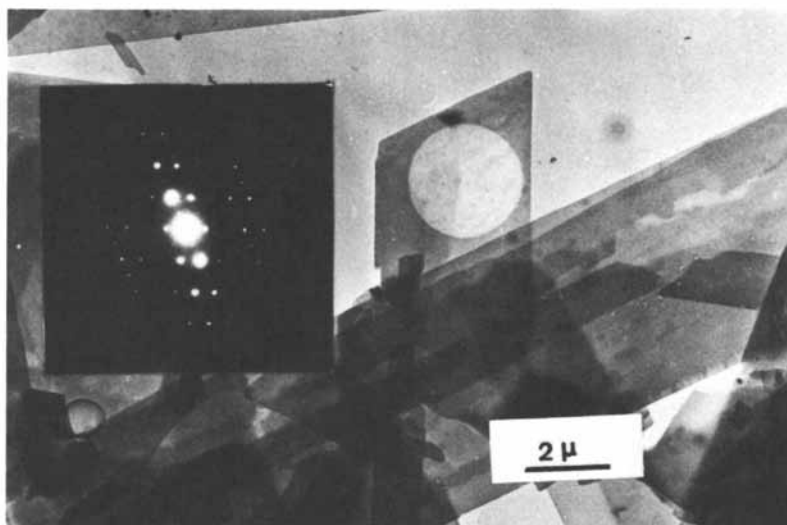


Figure 10. Electron micrograph of microcrystals of cellotetraose. Insert : corresponding electron diffraction diagram properly oriented.

The preliminary molecular models were treated as rigid bodies and the relative orientations about and translation along the long crystal axis were varied in increments. At each step, the magnitude of steric interference was calculated. The values of packing parameters corresponding to local minima were used as starting points for refinement that varied some of the molecular and packing parameters along with the X-ray scale factor. We concluded at this stage that the structure contains antiparallel molecules.

Further refinement varied molecular parameters such as torsion angles of the primary hydroxyl groups and the torsion and valence angles at the glycosidic linkages. The final R was 0.21; the observed and calculated structure factors are in Table VI. Atomic coordinates are in Table VII; labeling of the atoms proceeds from the non-reducing residue (a and e in the first and second molecules, respectively) to the reducing residue (d and h respectively).

Only the main features can be assessed without ambiguity at 3 Å resolution. The chief one is the antiparallel arrangement of the two independent molecules in the unit cell. Fig. 11 is a stereoscopic drawing of the structure, Fig. 12 shows the projection onto the a, b base plane. This projection is consistent with the platelet morphology of the crystals shown in Fig. 10.

Because all glucose residues were treated as rigid bodies in the refinement, the variable linkage torsion angles and glycosidic bond angles had to accommodate all variations required to produce the best structure. They may therefore suffer some loss of accuracy. All the (ϕ , ψ) angles, however, fall into the very low-energy region of the map (see Fig. 13). Going from residue to residue, ϕ and ψ were not similar enough to suggest local pseudo-symmetry. The glycosidic angles ranged from 117.2 to 121.8°.

Distances between O3 and O5 on the preceding unit ranged from 2.47 to 3.02 Å, indicating hydrogen bonding. Proceeding from the non-reducing end, distances spanning disaccharide residues are 10.43, 10.55 and 10.38 Å (molecule 1) and 10.36, 10.48, and 10.41 Å (molecule 2). While there is scatter in the distribution of ϕ and ψ , partly due to the low accuracy, some of the conformations are near the C1 conformer (methyl β -D-cellobioside) and some are near C2 (cellobiose).

Conclusion

The multidisciplinary approaches described in the present work are all aimed at describing, and understanding the structural features of cellulose oligomers at a molecular level. Intimate details are indeed taken into account in the conformational analysis calculations. The utilization of highly parametrized molecular mechanics programs, including the contribution of intramolecular hydrogen bonding to the total energy, produced conformations in agreement with observed crystal structures. The very same method was also very powerful in demonstrating the interactions between ring geometry and rotations about the glycosidic and aglycon linkages. When the hydrogen bond is considered, it appears that the pyranose ring undergoes small

Table VI. Structure factor table for cellotetraose at 3 Å resolution.

<u>h</u>	<u>k</u>	<u>l</u>	F-calc	F-obs	<u>h</u>	<u>k</u>	<u>l</u>	F-calc	F-obs
0	0	2	41.03	19.56	1	-1	3	23.45	38.39
1	0	0	12.12	14.28	-1	0	5	35.84	28.27
-1	0	1	22.48	14.62	2	0	1	33.76	25.37
0	0	3	28.67	20.42	1	-1	5	27.01	39.77
0	1	0	127.23	101.05	1	-2	2	12.17	28.07
1	-1	0	22.69	22.91	1	0	5	15.93	25.74
0	-1	1	45.58	48.63	-2	0	2	23.48	23.81
0	1	1	29.38	16.32	-2	1	3	34.10	27.95
-1	0	2	49.74	40.51	2	0	2	56.59	49.18
0	-1	2	48.73	99.01	0	0	6	11.54	23.65
1	-1	2	30.88	17.84	0	2	0	17.05	22.46
0	1	2	19.88	27.46	-2	0	3	18.07	23.20
0	0	4	30.80	34.60	2	-2	0	45.81	34.62
-1	0	3	33.77	40.05	2	-2	1	42.48	32.61
1	0	3	21.08	25.08	0	-2	2	21.73	31.18
0	1	3	19.42	23.04	0	2	1	22.37	23.81
-1	0	4	75.26	101.92	-2	1	4	14.20	22.05
0	-1	4	30.20	32.20	-1	0	6	25.14	26.39
1	0	4	91.85	97.10	1	-1	6	33.34	35.35
-1	-1	1	52.42	43.09	1	-2	4	16.96	20.34
2	-1	0	243.12	224.51	1	1	4	78.75	112.36
2	-1	1	83.26	78.40	0	-2	3	24.16	42.68
2	1	1	31.31	43.04	-2	2	2	34.27	40.22
1	1	1	31.12	36.83	0	2	2	41.33	50.74
-1	1	4	15.41	31.30	2	-2	3	29.25	28.65
-1	-1	2	56.27	54.58	-1	-1	5	59.45	87.40
0	1	4	31.47	34.21	-1	1	6	68.13	81.51
2	-1	2	62.66	50.98	0	1	6	40.29	45.66
-2	1	2	51.92	54.34	0	-2	4	14.84	30.40
1	1	2	39.63	51.39	-1	2	4	52.79	64.98
2	0	0	256.80	245.83	0	2	3	42.20	58.31
-1	2	0	20.21	20.66	1	-2	5	57.56	56.06
1	-2	1	21.00	25.12	-2	1	5	28.68	28.89
-2	0	1	38.89	34.66	-2	0	5	20.49	21.60
0	-1	5	21.25	34.86	-1	0	7	36.51	34.90

Table VII. Fractional coordinates of C and O atoms for cellotetraose model obtained at 3 Å resolution.

a-C1	0.0624	0.4084	-0.9037	e-C1	0.5370	0.4817	-0.4833
a-O1	-0.0243	0.3739	-0.8510	e-O1	0.5944	0.4398	-0.5375
a-C2	-0.0468	0.2672	-0.9534	e-C2	0.5992	0.4067	-0.4342
a-O2	-0.0767	0.0851	-0.9403	e-O2	0.5292	0.2092	-0.4440
a-C3	0.0350	0.3112	-1.0134	e-C3	0.5548	0.4662	-0.3731
a-O3	-0.0765	0.1891	-1.0600	e-O3	0.6289	0.4108	-0.3275
a-C4	0.0815	0.5126	-1.0241	e-C4	0.6160	0.6764	-0.3655
a-O4	0.1785	0.5616	-1.0764	e-O4	0.5549	0.7298	-0.3117
a-C5	0.1832	0.6429	-0.9709	e-C5	0.5550	0.7400	-0.4181
a-O5	0.0932	0.5914	-0.9170	e-O5	0.6065	0.6800	-0.4733
a-C6	0.2214	0.8440	-0.9766	e-C6	0.6234	0.9497	-0.4157
a-O6	0.0741	0.8651	-0.9869	e-O6	0.7946	1.0352	-0.4306
b-C1	0.0717	0.4925	-0.6679	f-C1	0.5693	0.5068	-0.7178
b-O1	0.1568	0.5298	-0.6134	f-O1	0.5000	0.5000	-0.7735
b-C2	0.1687	0.6525	-0.7057	f-C2	0.5307	0.6391	-0.6748
b-O2	0.1738	0.8202	-0.6771	f-O2	0.6074	0.8210	-0.6945
b-C3	0.0906	0.6126	-0.7683	f-C3	0.5898	0.6400	-0.6115
b-O3	0.1931	0.7544	-0.8049	f-O3	0.5368	0.7490	-0.5710
b-C4	0.0699	0.4234	-0.7960	f-C4	0.5207	0.4420	-0.5933
b-O5	-0.0206	0.2739	-0.7537	f-O5	0.5576	0.3177	-0.6404
b-C5	0.0658	0.3239	-0.6967	f-C5	0.4931	0.3243	-0.6979
b-O6	-0.0319	0.0856	-0.7766	f-O6	0.4791	0.1155	-0.6273
b-C6	-0.0047	-0.0078	-0.7298	f-O6	0.3077	0.0227	-0.6455
c-C1	0.0701	0.4546	-0.4334	g-C1	0.5378	0.3450	-0.9522
c-O1	-0.0125	0.4329	-0.3798	g-O1	0.6127	0.3303	-1.0055
c-C2	-0.0286	0.2848	-0.4767	g-C2	0.5783	0.2381	-0.9073
c-O2	-0.0320	0.1235	-0.4538	g-O2	0.5071	0.0459	-0.9282
c-C3	0.0462	0.3099	-0.5383	g-C3	0.5148	0.2663	-0.8459
c-O3	-0.0580	0.1586	-0.5798	g-O3	0.5694	0.1817	-0.8032
c-C4	0.0653	0.4931	-0.5596	g-C4	0.5780	0.4732	-0.8269
c-O5	0.1579	0.6535	-0.5122	g-C5	0.5395	0.5702	-0.8757
c-C5	0.0743	0.6168	-0.4565	g-O5	0.6085	0.5379	-0.9311
c-C6	0.1678	0.8368	-0.5287	g-C6	0.6124	0.7792	-0.8615
c-O6	0.2222	0.9753	-0.4791	g-O6	0.5230	0.8576	-0.8918
d-C1	0.0209	0.6793	-0.2070	h-C1	0.5775	0.3976	-1.1852
d-O1	0.0931	0.7968	-0.1557	h-O1	0.5081	0.4129	-1.2382
d-C2	0.0242	0.7979	-0.2568	h-C2	0.6044	0.5657	-1.1419
d-O2	-0.0755	0.8914	-0.2411	h-O2	0.7217	0.7304	-1.1656
d-C3	-0.0366	0.6784	-0.3159	h-C3	0.6632	0.5464	-1.0808
d-O3	-0.0159	0.7945	-0.3630	h-O3	0.6705	0.6950	-1.0392
d-C4	0.0596	0.5642	-0.3290	h-C4	0.5456	0.3604	-1.0587
d-O5	0.0569	0.4580	-0.2756	h-C5	0.5194	0.2014	-1.1061
d-C5	0.1204	0.5846	-0.2228	h-O5	0.4604	0.2320	-1.1613
d-O6	0.1630	0.3547	-0.2840	h-C6	0.3921	0.0144	-1.0888
d-C6	0.2370	0.3757	-0.3412	h-O6	0.2414	0.0203	-1.0704

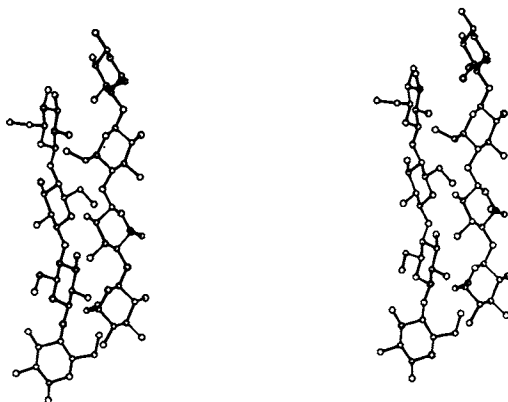


Figure 11. Stereoscopic representation of the unit cell content of crystalline cellotetraose.

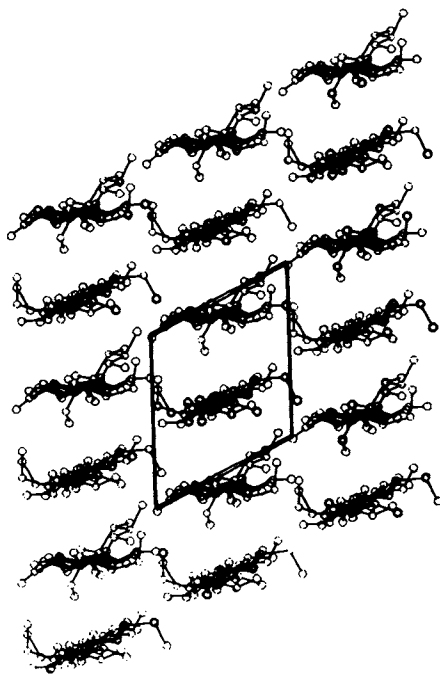


Figure 12. Projection of the cellotetraose structure onto the a,b base plane.

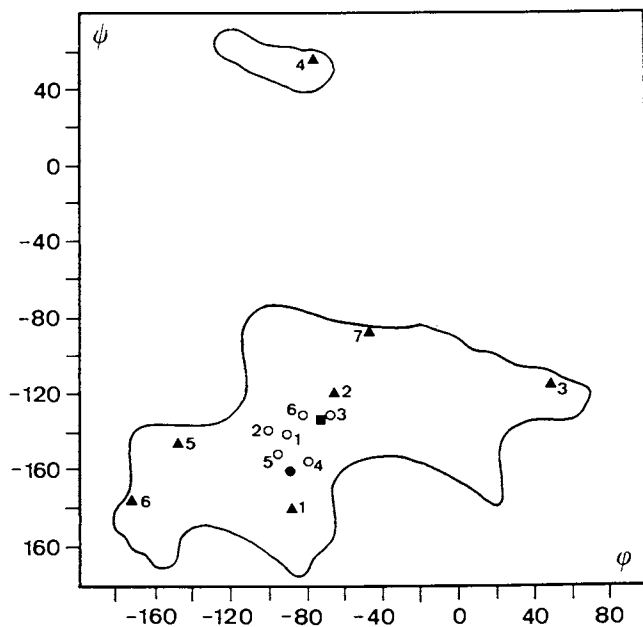


Figure 13. Calculated and observed (ϕ, ψ) conformations of linear cellodextrins.

▲ : calculated conformations from Molecular Mechanics labeled from 1 to 7 and refer to conformers C1 to C7 listed in Table II.

Observed (ϕ, ψ) conformations :

■ : cellobiose	-73.3	-132.3
● : methyl β -D-cellobioside	-88.9	-160.7
○ : cellotetraose, unit a to b; 1	-90	-141
unit b to c; 2	-103	-138
unit c to d; 3	-68	-129
unit e to f; 4	-80	-156
unit f to g; 5	-94	-150
unit g to h; 6	-83	-131

The external contour corresponds to 10 kcal/mol expressed relative to the minimum.

distorsions. The present results offer a picture which is a compromise between the extreme distorsions mentioned by Melberg and Rasmussen (53) on the one hand, and the lack of such distorsions reported by Pizzi and Eaton (54) on the other hand. Conventional X-ray crystallography on oligomers is in fact the ultimate method since, upon completion of a three-dimensional structure, the coordinates of all the atoms in a molecule are determined with a high accuracy. This, simply, results from the fact that there is usually a far greater number of observables, i. e. diffraction intensities, than parameters to be found. Unfortunately, such a situation is not found in the case of cellulose oligomers with a DP higher than two. Neither the three dimensional structure of cellotetraose, nor that of methyl β -D-cellotrioside have been solved and refined to an acceptable accuracy. Nevertheless, crucial structural information has been gained since the antiparallel orientation of cellotetraose molecules has been determined. Also, our results strongly suggest that several distinct conformations about the glycosidic bonds are found in the cellotetraose molecules. To what extent such a behaviour may explain the splitting of the ^{13}C NMR resonance of the C1 atoms is still not well established. Whereas it was well known that cellotetraose was a good model for cellulose II, we have clearly shown that methyl β -D-cellotrioside is also quite an adequate model. Such an adequacy is based on the similarity between the high resolution solid state NMR spectra together with the dimensions of the crystal unit cell. Crystal structure elucidation of methyl β -D-cellotrioside represents quite a challenge, but at least, single crystals good enough for X-ray analysis can be grown in a reproducible manner, which is not the case yet for cellotetraose. The high resolution solid state spectrum of methyl β -D-cellotrioside exhibits a distinct splitting of the C1 atoms resonances and this may reflect the occurrence of distinct conformations at the glycosidic linkages. This very same spectrum also shows how the methyl groups of methyl glycosides may be used as convenient probes in establishing gross structural features. Nevertheless, drawing definite conclusions about any direct correlation between an observed splitting and known structural features as derived from X-ray investigation should be handled with caution. Whereas it appears that the occurrence of split resonances reflects conformational inhomogeneity (55), the converse is not necessarily true. This statement is illustrated by the methyl β -D-cellobioside case, for which two distinct conformations of the C6 carbon atoms are observed in the crystal structure whereas only one resonance at 63.1 ppm can be assigned to the corresponding atoms in the ^{13}C CP/MAS NMR spectrum. Our calculations, although still primitive, appear to explain such a behavior.

Despite the lack of high accuracy, some consistent features can be drawn from the study of cellulose oligomers through our approach. The results indicate clearly that the glycosidic linkages in cellulose oligomers have different conformations. It is also clear that the glycosidic linkage does not exist in a conformation consistent with a "two-fold" helix symmetry. These conclusions which are essentially reached through conformational analysis calculations are supported by the appearance of the solid state

¹³C NMR spectra of both cellotetraose and methyl β -D-cellobioside, and cellulose II as well. Despite a large difference between the unit cell contents of methyl β -D-cellobioside and cellotetraose, their respective base plane dimensions, i.e. normal to the direction parallel to the molecular axis, are strikingly comparable; this must reflect strong packing habits, of not only long cellulose chains but cellulose-like chains as cellotetraose or methyl β -D-cellobioside (at the exclusion of metastable arrangements resulting from biosynthetic pathways and organizations).

There has been considerable discussion regarding the crystal structure of cellulose II and two models have been proposed; they both are based upon a monoclinic $P2_1$ space group. In one, the unit cell is postulated to contain two¹ independent chains (22-24) (model A), while in the other, the chain conformation is thought to be such that a cellobiosyl unit does indeed constitute the repeating unit (17) (model B). In model A, the two-fold helical conformation is assumed, i.e. all atoms (including C1 carbon atoms) are conformationally identical with respect to the polymer axis. Since the chains are located on the crystallographic axes of symmetry they may have different conformations. Model A has an antiparallel arrangement, in agreement with our finding on cellotetraose. Therefore, each atom in a chain would have a different packing environment than the corresponding atom in the neighboring chains. Can such features, involving differences in distances greater than 3 Å, explain the significant splitting of the C1 resonances on the NMR spectra? Why is similar splitting not observed for the other carbon atoms? In model B, a cellobiosyl unit constitutes the repeating unit (11), in agreement with the results of conformational analysis performed on isolated molecules. Therefore, two pairs of glycosidic torsion angles alternate along the polymer chain, thereby providing a rational explanation for the observed splitting of the C1 resonances. No longer can the macromolecular chain have a two-fold helical symmetry and hence the coincidence between polymer axis and crystallographic two-fold axis is forbidden. To keep monoclinic symmetry, the cellulose chains would have to be located between the crystallographic axes; the chains are no longer independent and have to be in a parallel register which is not consistent with the arrangement found for cellotetraose and postulated for methyl- β -D cellobioside. The only way would be to consider the triclinic P_1 space group, with two independent, antiparallel chains traversing the unit cell. This would be consistent with all the features displayed by the cellulose oligomers. This would also explain why the (0 0 1) reflection is not absent from the X-ray fiber diffraction pattern of cellulose II as it should really be in a monoclinic $P2_1$ space group.

Addendum : Subsequent to the presentation of this work, a report by D.L. VanderHart (J. Chem. Phys. (1986) 84, 1196) established a field dependency for ¹³C NMR chemical shifts of polyethylene in the solid state. At the 50.3 MHz frequency used in the present work, the correct value is 32.9 ppm not 33.6 and hence all chemical shifts should be decreased by 0.7 ppm from the values reported above.

Acknowledgments

The authors are much indebted to Dr. H. Chanzy of this Institute for initiating some parts of the work reported here and his untiring support. Appreciation is extended to Dr. E. Ohleyer for his expertise in the preparation of considerable amounts of the celloextrins, and to Dr. E. Roche who made available some unpublished results on electron diffraction of cellotetraose.

Dr. B. Poppleton, Commonwealth Scientific and Industrial Research Organization, Melbourne, Australia, kindly supplied a list of measured intensities on cellotetraose. The help of Dr. A. Hewatt, Institut Laue Langevin, Grenoble, France, was invaluable for recording the neutron powder diffraction pattern of cellotetraose. Dr. R. H. Marchessault, Xerox Research Centre, Mississauga, Canada, gave us access to the high resolution solid state NMR spectrometer.

Grants for supporting the sabbatical stays of two of us (I. T. and W. T. W.) were supplied by the Centre National de la Recherche Scientifique.

Literature Cited

1. Wellard, H. J., J. Polym. Sci. (1954) **13**, 471.
2. Marrinan, H. J. and Mann, J. J., J. Appl. Chem. (1954) **4**, 204.
3. Pérez, S. and Brisse, F., Biopolymers (1978) **17**, 2083.
4. Chu, S. S. C. and Jeffrey, G. A., Acta Crystallogr. (1968) **B24**, 830.
5. Ham, J. T. and Williams, D. G., Acta Crystallogr. (1970) **B26**, 1373.
6. Poppleton, B. J. and Mathieson, A. McL., Nature (1968) **219**, 1946.
7. Williams, D. G., J. Polym. Sci., A-2 (1972) **8**, 637.
8. Poppleton, B. J. and Gatehouse, J., J. Polym. Sci., A-2 (1972) **10**, 375.
9. Schaefer, J., Stejskal, E. O. and Buchdahl, R., Macromolecules (1977) **10**, 384.
10. Fyfe, C. A., Dudley, R. L., Stephenson, P. J., Deslandes, Y., Hamer, G. K. and Marchessault, R. H., J. Am. Chem. Soc. (1983) **105**, 2469.
11. Atalla, R. H., Gast, J. C., Sindorf, D. W., Bartuska, F. J. and Maciel, G. E., J. Am. Chem. Soc. (1980) **102**, 3249.
12. Earl, W. L. and VanderHart, D. L., J. Am. Chem. Soc. (1980) **102**, 3251.
13. Earl, W. L. and VanderHart, D. L., Macromolecules (1981) **14**, 570.
14. Atalla, R. H. and VanderHart, D. L., Science (1984) **223**, 283.
15. Horii, F., Hirai, A. and Kitamaru, R., Adv. Chem. Ser. (1984) **260**, 27.
16. Cael, J. J., Kwok, D. L. W., Bhattacharjee, S. S. and Patt, S. L., Macromolecules (1985) **18**, 821.
17. Teeäär, R. and Lippmaa, E., Polym. Bull. (1984) **12**, 315.
18. Horii, F., Hirai, A. and Kitamaru, R., Polym. Bull. (1983) **10**, 357.

19. Fyfe, C. A., Stephenson, P. J., Veregin, R. P., Hamer, G. K. and Marchessault, R. H., J. Carbohydr. Chem. (1984) 3, 663.
20. IUPAC-IUB Commission on Biochemical Nomenclature, Arch. Biochem. Biophys. (1971) 145, 405.
21. Marchessault, R. H. and Pérez, S., Biopolymers (1979) 18, 2369.
22. Kolpak, K. J. and Blackwell, J., Macromolecules (1976) 9, 273.
23. Kolpak, K. J., Weih, M. and Blackwell, J., Polymer (1978) 19, 123.
24. Stipanovic, A. J. and Sarko, A., Macromolecules (1976) 9, 851.
25. Buleon, A. and Chanzy, H., J. Polym. Sci., Polym. Phys. Ed. (1978) 16, 833.
26. Wolfrom, M. L., Dacons, J. C. and Fields, D. L., TAPPI (1956) 39, 803.
27. Takeo, K., Okushio, K., Fukuyama, K. and Kuge, T., Carbohydr. Res. (1983) 121, 163.
28. Frye, J. S. and Maciel, G. E., J. Magn. Reson. (1982) 53, 615.29. Earl, W. L. and VanderHart, D. L., J. Magn. Reson. (1982) 48, 35.
30. Diner, S., Malrieu, J.P. & Claverie, P., Theoret. Chim. Acta, (Berl.) (1969), 13, 1.
31. Malrieu, J.P., Claverie, P. & Diner, S., Theoret. Chim. Acta (Berl.) (1969), 13, 18.
32. Powell, M.J.D., Computer J. (1964), 7, 155.
33. Zangwill, V.I., Computer J. (1965), 8, 293.
34. Allinger, N. L., J. Am. Chem. Soc. (1977) 99, 8127.
35. Jeffrey, G. A. and Taylor, R., J. Comput. Chem. (1980) 1, 99.
36. Taylor, R., J. Molec. Struct. (1981), 71, 311.
37. Tvaroska, I. and Pérez, S., Carbohydr. Res. (1986) 149, 389.
38. Scott, R. A. and Scheraga, H. A., J. Chem. Phys. (1965) 42, 2209.
39. Tvaroska, I., Carbohydr. Res. (1984) 125, 155.
40. Gagnaire, D., Pérez, S. and Tran, V., Carbohydr. Res. (1980) 78, 89.
41. International Tables for X-ray Crystallography (1962) Vol. III, Birmingham, U.K., Kynoch Press.
42. Main, P., Lessinger, L., Woolfson, M. M., Germain, G. and Declercq, J. P. (1977) MULTAN 77. A System of Computer Programs for the Automatic Solution of Crystal Structures from X-ray Diffraction Data. University of York, U.K. and Louvain, Belgium.
43. Arnott, S. and Scott, W. E., J. Chem. Soc., Perkin Trans. II (1972) 324.
44. Smith, P. J. C. and Arnott, S., Acta Crystallogr. (1978) A34, 3.
45. Dheu, M. L. and Pérez, S. (1980) Programmes Interactifs de Tracés de Molécules et de Structures, C.E.R.M.A.V., Grenoble, France. Pérez, S. and Scaringe, R., J. Appl. Cryst. (1986) 19, 65.
46. Mallet, J. L. (1976) Programmes de Cartographie Automatique. Présentation de la Bibliothèque CARTOLAB, Sciences de la Terre, Série Informatique Géologique, N°7, Nancy, France.
47. Tvaroska, I. and Kozar, T., Chemicke Zvesti (1981) 35, 425.

48. Fuchs, B., Schleifer, L. and Tartakovski, E., Nouv. J. Chim. (1984) 8, 275.
49. Ebaheem, K. A. K. and Webb, G. A., Progr. Nucl. Magn. Reson. Spectrosc. (1977) 11, 149.
50. Cyr, N., Perlin, A. S. and Whitehead, M. A., Can. J. Chem. (1972) 50, 814.
51. Korpi-Tommola, S. L. and Lindberg, J. J., Comm. Phys. Math. (1973) 43, 167.
52. Mackie, W., Sheldrick, B., Akrigg, D. and Pérez, S., Int. J. Biol. Macromol. (1986) 8, 43.
53. Melberg, S. and Rasmussen, K., Carbohydr. Res. (1979) 71, 25.
54. Pizzi, A. and Eaton, N., J. Macromol. Sci.- Chem. (1984) A21, 1443.
55. Taylor, M. G., Marchessault, R. H., Pérez, S., Stephenson, P. J. and Fyfe, C. A., Can. J. Chem. (1985) 63, 270.

RECEIVED March 17, 1987

Chapter 4

Application of the Rietveld Crystal Structure Refinement Method to Cellotetraose

A. Sakthivel¹, A. D. French², B. Eckhardt^{3,4}, and R. A. Young³

¹School of Textile Engineering, Georgia Institute of Technology, Atlanta, GA 30332

²Southern Regional Research Center, U.S. Department of Agriculture, P.O. Box 19687, New Orleans, LA 70179

³School of Physics, Georgia Institute of Technology, Atlanta, GA 30332

The Rietveld method of structure refinement from x-ray powder diffraction data was applied to cellotetraose, which gives a diffraction pattern similar to that of cellulose II. Unit cell dimensions were consistent with earlier work. The space group was shown to be P1 rather than P2₁. Models, rigid except for the positions of the O(6) atoms, were used to test the effects on the calculated diffraction patterns of parallel and antiparallel packing modes, O(6) positions, and the presence of hydrogen atoms. The hydrogen atoms had a negligible effect on the calculated x-ray diffraction pattern. The intensities of specific individual Bragg reflections were sufficiently affected by the O(6) positions so that they may help to indicate those positions, even though the net effect on the overall pattern-fitting was small. Results from refinements of an antiparallel model against intensities calculated from a parallel model indicated that differentiation may be difficult on the basis of x-ray powder diffraction patterns. Preliminary results based on simple models with tetramer symmetry close to 2₁ suggested that the two tetramers in the unit cell are slightly inclined to the *c* axis.

It has long been known that cellotetraose, the β 1,4-linked tetramer of D-glucose, yields a powder diffraction pattern exhibiting more crystallinity but otherwise similar to that of cellulose II, the allomorph resulting from treatment of cellulose I in strongly alkaline solution or from regeneration from solution. In the quest to obtain structural information applicable to cellulose II, previous workers, using tiny single crystals, e.g., 0.2 x 0.1 x 0.01 mm³ "usually of poor quality but

⁴Current address: Fachbereich Physik, Universität Bremen, Bibliothekstrasse, Postfach 330440, 2800 Bremen 33, Federal Republic of Germany

0097-6156/87/0340-0068\$06.00/0
© 1987 American Chemical Society

with well developed (001) faces" (1), suggested (2) that the space group of cellotetraose was P1 and determined the unit cell of cellotetraose accordingly. Further single-crystal diffraction work has, however, been thwarted by x-radiation damage occasioned by the long exposures required because of the small size of the crystals.

Rietveld refinement (3,4) permits structural study with powder diffraction data. The entire diffraction pattern is calculated from a model consisting of the unit cell parameters, crystallite size (line width), proposed atomic positions and thermal parameters. The validity of the proposed model is measured by comparison of the observed and calculated intensity at each step-scan increment, including background correction, and the model parameters are systematically refined in order to provide the best agreement in a least squares sense.

In Immirzi's version (5), the molecule is described in terms of generalized coordinates so that the model can be refined when the data are limited and the molecule is complex. This is similar to the analyses of fiber diffraction data in which the monomers are kept rigid except for rotating side groups. However, powder diffraction data are less likely to be affected by errors in collection, correction and reduction than fiber data. Errors from preferred orientation produced in sample preparation are possible, but can be tested for.

Although the Rietveld method has been used successfully with hundreds of materials, including some polymers such as polypropylene (6), it is believed that this is the first attempt to perform a thorough structural study of an oligosaccharide with powder x-ray diffraction data. In this paper, we describe some of the details of the Rietveld method, as modified by Immirzi for polymers and further modified locally, and discuss our assessments of various assumptions used in such a study. A preliminary structural result is also presented.

EXPERIMENTAL PROCEDURE

The samples of cellotetraose studied herein were provided by Dr. Fred Parrish, Southern Regional Research Center, Dr. Ross Brown, University of Florida, and Dr. John Vercellotti, V-Labs, Covington, LA. They were made by hydrolysis of cellulose in hydrochloric acid and separated from the other resulting oligomers through column chromatography.

The step-scanned, wide-angle diffraction data were obtained (reflection mode) with a standard θ - 2θ x-ray powder diffractometer using a diffracted beam monochromator and $\text{CuK}\alpha$ radiation from a standard sealed-off x-ray tube. The scanning range was from 7° to 43.40° 2θ ; no clearly recognizable peaks were observed beyond 43.40° . The step width was 0.04° and the counting time was 250 seconds per step. Since little improvement in the data resulted from maintaining the specimen near liquid nitrogen temperatures, all results reported here were obtained from room temperature data.

The absorption factor $\exp(-\mu t)$ (equal to $I_{\text{transmitted}}/I_{\text{incident}}$ for a normally incident beam) was measured as 76.4%. The wide-angle diffraction pattern is shown in Figure 1.

Small-angle data were collected with a small angle x-ray diffractometer equipped with a position sensitive detector placed 25.0 cm away from the sample (transmission mode). The result is shown in Figure 2.

RIETVELD REFINEMENT METHOD

Given the atomic positions from a model, the intensity y_i at the i^{th} step is

$$y_i = y_{i,b} + \sum y_{i,H}$$

$$y_{i,H} = G(\theta_i - \theta_H) |F_H|^2 P_H T_H (LP)_i$$

where

$y_{i,b}$ = background at the i^{th} step
 H = Miller indices h, k, l for a Bragg reflection
 $G(\theta_i - \theta_H)$ = Bragg reflection profile function (a Pearson VII function was used, see references 4 and 6 for more details)
 θ_i = scattering angle at the i^{th} step
 F_H = structure factor
 P_H = multiplicity of H
 $(LP)_i$ = Lorentz and polarization factor at step i
 T_H = $\exp(-P(\alpha_H)^2)$, preferred orientation function
 P = preferred orientation parameter
 α_H = acute angle between the preferred orientation direction and the reciprocal lattice vector for H

The background intensity ($y_{i,b}$) is calculated as

$$y_{i,b} = b_1 + (b_2 - b_1)(2\theta_1 - 2\theta_i) / (2\theta_1 - 2\theta_2) + b_3 * G(2\theta_3 - 2\theta_i)$$

where

$2\theta_1$ and $2\theta_2$ are the limits of the scanning range,
 $G(2\theta_3 - 2\theta_i)$ is a Pearson VII function with 3 refinable parameters, and
 $b_1, b_2, b_3, 2\theta_3$ are also parameters that are refined.
 The equation given above for $y_{i,b}$ is empirical and a graphical representation of it can be found in reference 6.
 The structure factor F_H , is calculated as follows:

$$F_H = \sum M_j f_j \exp\{-2\pi i(hx_j + ky_j + lz_j)\} \exp\{-B_j (d_H^*/2)^2\}$$

j = ranges from 1 to no. of atoms in the unit cell
 M_j = site occupancy (of the j^{th} atom site)
 f_j = atomic scattering factor for the j^{th} atom
 x_j, y_j, z_j = fractional coordinates of the atom j
 B_j^* = temperature factor
 d_H^* = $2 \sin\theta / \lambda$
 λ = wavelength of the radiation used

The difference between the observed and calculated patterns is measured by the residual,

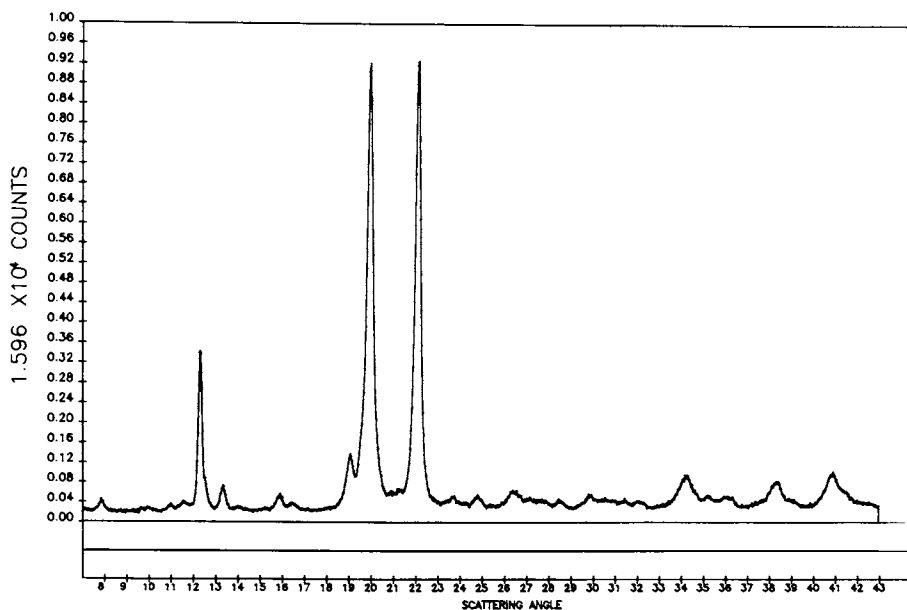


Figure 1. Wide angle x-ray powder diffraction pattern of cellotetraose at room temperature. CuK radiation.

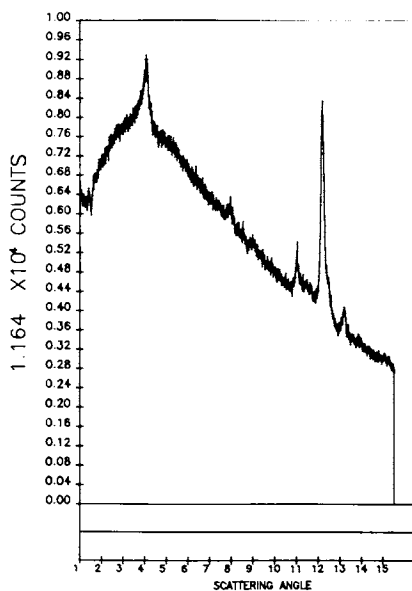


Figure 2. Small-angle powder-diffraction pattern of cello-tetraose at room temperature (transmission mode). CuK radiation and a position sensitive detector at 25.0 cm from the sample were used.

$$\chi^2 = \sum w_i (y_{i,obs} - y_{i,calc})^2 \quad (1)$$

where the sum extends over all scattering angles 2θ at which a measurement of the diffracted intensity $y_{i,obs}$, was made. w_i is a weight factor, usually chosen to be $1/y_{i,obs}$. A minimum in χ^2 is sought. A necessary condition for termination of refinement is that the gradient of χ^2 with respect to each of the M refined parameters, x_k , has vanished. The resulting equations are nonlinear in the x_k 's and cannot be solved analytically for the parameter shifts dx_k which will minimize χ^2 . Therefore, the calculated intensities are expanded in the x_k 's and only linear terms are kept. Letting braces denote matrices and parentheses denote vectors, one ends up with an equation of the form

$$\{A\} (dx) = b \quad (2)$$

from which,

$$(dx) = \{A\}^{-1} (b) \quad (3)$$

The various quantities are:

$$A_{jk} = \sum w_i \frac{\delta y_{i,calc}}{\delta x_j} \frac{\delta y_{i,calc}}{\delta x_k} \quad (4)$$

$$b_j = \sum w_i \frac{\delta y_{i,calc}}{\delta x_j} (y_{i,obs} - y_{i,calc}) \quad (5)$$

$$dx_k = x_k^{old} - x_k^{new} \quad (6)$$

This clearly shows several important features of the Rietveld refinement procedure. Firstly, it involves inversion of an $M \times M$ matrix. Secondly, it works only if the starting values are already close to a minimum, because of the linear approximation in the derivation of equation (2). Thirdly, whatever minimum is obtained, it is not necessarily the global minimum one is looking for but may be a local minimum, since the method is a local one. Finally, because of finite width of every reflection, the calculated intensity at each step contains contributions from several neighboring reflections. In our case up to 45 possible reflections can contribute to the intensity calculated at a single point in the diffraction pattern. The program used for Rietveld refinement in this work is an extensively modified version of REFIN (FORTRAN V), written by A. Immirzi (5).

In order to assess the agreement between the calculated and observed pattern, several numbers can be calculated. Most commonly used are R_{wp} and R_p .

$$R_{wp} = \left[\frac{\sum w_i (y_{i,obs} - y_{i,calc})^2}{\sum w_i y_{i,obs}^2} \right]^{1/2} \quad (7)$$

and

$$R_p = \frac{\sum |y_{i,obs} - y_{i,calc}|}{\sum y_{i,obs}} \quad (8)$$

On a strictly statistical basis R_{wp} is the preferred indicator because its numerator is the function that is being minimized (equation 1). Note that these R values are normally larger than those reported for fiber and single-crystal studies because they are based on the intensities at all steps in the pattern and not just on individually observed Bragg reflection intensities.

Another indicator can be calculated which is more akin to the conventional 'R value' with which some readers will be familiar from the literature on single crystal structure refinement:

$$R_B = \frac{\sum (I_{i,"obs"} - I_{i,calc})}{\sum I_{i,"obs"}} \quad (9)$$

In its formulation, R_B is comparable to the conventional R value based on intensities which, for a normal distribution of errors, is larger than the most quoted R value based on structure factors by a factor of $\sqrt{2}$.

In equation 9, $I_{i,"obs"}$ is written with quotation marks because it is not actually observed directly. Rather, the total intensity observed for a set of overlapping reflections is apportioned among the reflections in the ratios of the calculated intensities (3,4). R_B is, therefore, biased in favor of the model being used. However, it is useful because it is relatively insensitive to features, such as profile shape errors, which produce an inflation of R_p and R_{wp} without crystal structural significance.

COMPUTER MODEL BUILDING

The molecular formula for cellotetraose, the β 1,4-linked tetramer of D-glucose, is $C_{24}H_{42}O_{21}$. Since the contributions of the hydrogen atoms to the x-ray pattern may be safely disregarded (Figure 3), structural determination consists of defining the x, y, and z coordinates (plus any thermal parameters) for each of the remaining 45 atoms in each tetramer. Even though 910 data points were taken, no more than about 30 intensity "peaks" can be observed, most of which are composites of several Bragg reflections. Therefore, only a very limited number of parameters in the model can be meaningfully refined.

The coordinates of the atoms in the monomer were assumed to be known from single crystal studies of glucose (7). Each monomer was treated as a rigid body with 3 degrees, each, of rotational and translational freedom.

The origin of the coordinate system (for example, coinciding with the center of the first monomer) can be freely chosen. The first monomer then has only 3 rotational degrees of freedom. The other three monomers are described by 3 translational and 3 angular parameters, each.

One parameter for each monomer describes the orientation of the oxygen of the primary hydroxyl group (O(6)), with respect to the C(4) - C(5) bond.

With this selection of parameters, the tetramer is described in terms of 25 parameters. Specification of its orientation with respect to the unit cell requires another three angles. (In a strictly mathematical sense, these three parameters are redundant. Hence, they are never refined simultaneously with the orientation parameters of the monomers). Thus, the total number of parameters for the first tetramer is 28. It is then easy to describe many tetramers per unit cell; all one has to do is to take 28 parameters for the first tetramer and 28 parameters plus three for the additional translational degrees of freedom for each additional tetramer. For two tetramers this adds up to 59 parameters. In most of our refinements, the number of parameters actually refined in any one cycle was limited to about 20.

Only β -cellotetraose has been modeled in this study. The cellotetraose sample could also be a mixture of α - and β -cellotetraoses or even all α . In the case of mixtures, the anomers may occur in the same crystals as in the case of α - β maltose (8), or the powder sample may contain two types of similar crystals that differ at the anomeric carbon. This is among the topics that will be examined during the second phase of this study.

RESULTS AND DISCUSSION

Space Group and Unit cell parameters. According to Poppleton and Mathieson (1), the space group for cellotetraose is either $P1$ and $P2_1$. The fairly strong 001 reflection observed at 3.90° (Figure 2) eliminates the $P2_1$ space group. Starting from those in the literature (2), the lattice parameters refined to

$$\begin{array}{lll} \underline{a} = 8.98 \text{ \AA} & \underline{b} = 8.01 \text{ \AA}, & \underline{c} = 22.34 \text{ \AA} \\ \alpha = 94.31^\circ & \beta = 89.27^\circ & \gamma = 116.45^\circ \end{array}$$

These parameters agree well with the reported lattice parameters (2), except for \underline{c} , which is smaller by 0.25Å in our study. The density calculated from our parameters is 1.55 g/cm³, that from (2) is 1.52 g/cm³ and the measured density is reported (1) to be 1.49 g/cm³.

The large, asymmetric ($P1$) unit cell permits 338 possible reflections in the angular range studied. Most peaks are composed of many unresolvable reflections. For instance, the major peaks at 12.3 , 19.9 , 22.0 , and 40.8° (to which $1\bar{1}0$, 110 , 200 , and 310 , respectively, are the major contributors) contain 6, 9, 10 and 40 reflections, respectively. In the Rietveld method, the intensity at any point in the calculated diffraction pattern is the sum of contributions from neighboring reflections. In the diffraction

patterns calculated in this work, the range of influence of any reflection was limited to twice the width of the profile at half the maximum height.

Number of Tetramers per Unit Cell.

A: Trials with one tetramer per cell. We first tried several models containing one tetramer per unit cell (of half the cell volume finally used), as proposed by Poppleton and Mathieson (1). However, we could not produce the roughly equal intensities of the two very strong peaks at 20° and 22° along with a strong one at 12°. We therefore concluded that the number of tetramers per unit cell is greater than one.

B: Trials with two tetramers per cell. As described by Gardner and Blackwell for cellulose (9), two tetramers can be packed in the unit cell in 3 ways: Parallel-up, antiparallel, and parallel-down. In parallel-up models, z-coordinates of the atoms at the reducing ends of both the tetramers are greater than those of the nonreducing ends, and conversely for the parallel-down models. Antiparallel models contain one "up" and one "down" tetramer. In their studies, Sarko and Muggli (10) have used a and b axes which are interchanged compared to ours, those in the Blackwell-Gardner system, and those in references (1,2). This results in the c axis pointing in a direction opposite to that in the Blackwell-Gardner system. This has caused some confusion in that a parallel-up model in one system comes to be called a parallel-down model in the other system and vice versa.

We have refined several parallel-up and antiparallel models against the diffraction data and the best agreements between the calculated and the experimental data are shown in Figures 4 and 5. The ab and ac projections of the corresponding models are shown in Figures 6 and 7.

The R values for the best models are given in Table I. Since

Table I. R values for the best available models

Model	R _p	R _{wp}	R _{Bragg}
Parallel-up	0.141	0.190	0.185
Antiparallel	0.171	0.226	0.235

the R values are fairly low (for x-ray Rietveld refinement), especially for the parallel up model, we believe that the general features of the models are correct. Before a final model can be proposed, however, factors such as the parallel down model, the O(6) position, the possibility of the α anomeric form, and the conformation angles between monomers in the tetramers must be more thoroughly examined. The cartesian and the fractional coordinates

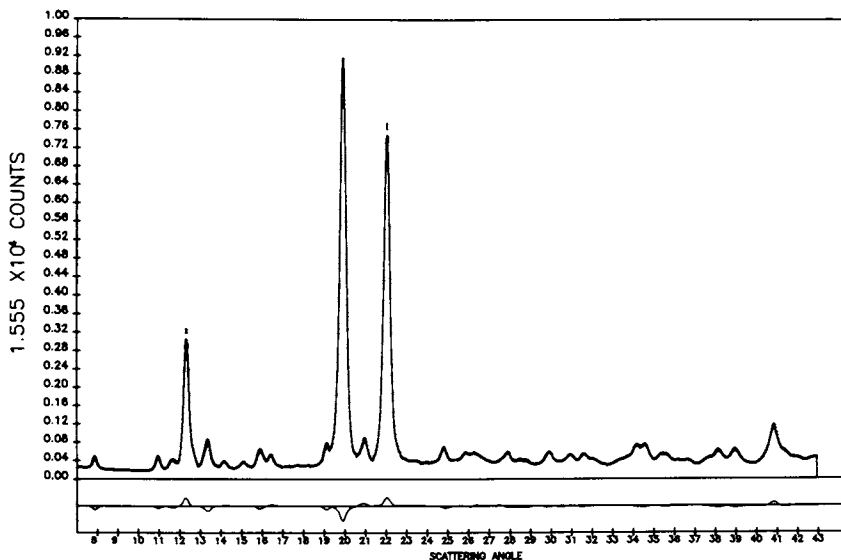


Figure 3. Calculated x-ray powder diffraction patterns for models with or without the hydrogen atoms. The pattern for the model not including hydrogen is shown in the same field, and their difference is shown in the lower field.

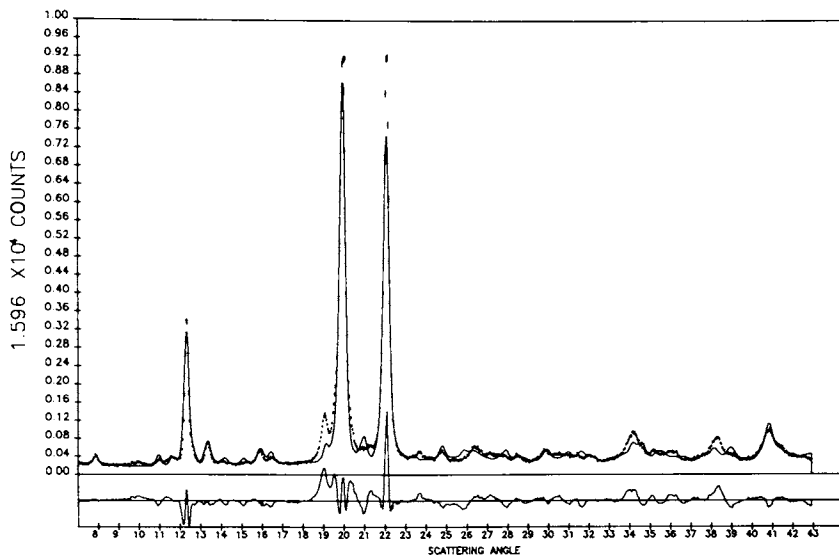


Figure 4. Calculated and observed patterns for the best parallel model. The observed pattern is shown by dots with vertical error bars based on counting statistics. The calculated pattern is shown by a continuous curve in the same field and the difference between the observed and the calculated patterns is shown in the lower field. R_{wp} for this model is 0.19.

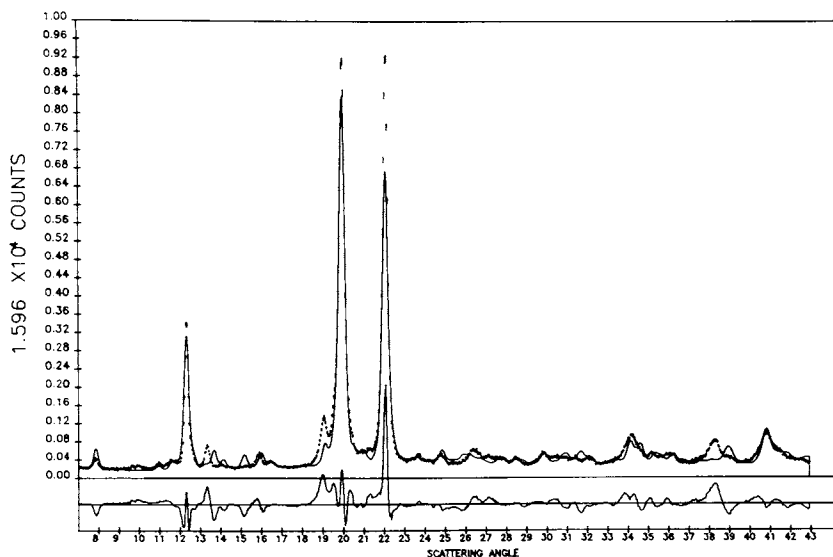


Figure 5. Calculated and observed patterns for the best anti-parallel model. The observed pattern is shown by dots with vertical bars based on counting statistics. The calculated pattern is shown by a continuous curve in the same field and the difference between the observed and the calculated patterns is shown in the lower field. R_{wp} for this model is 0.226.

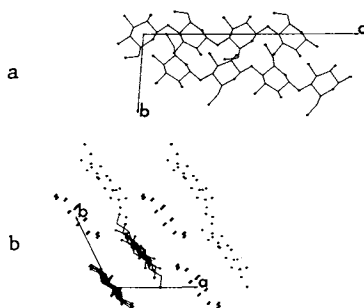


Figure 6. Best parallel model obtained from Rietveld refinement against observed pattern ($R_{wp} = 0.19$). a) bc projection and b) ab projection. All the carbon and the oxygen atoms are shown for one corner and one central molecule only, in the unit cell. Only the oxygen atoms are shown for other molecules.

of the best available parallel-up and antiparallel models are given in Tables II and III, respectively. In all the models, the molecular axes of the tetramers are slightly inclined with respect to the c axis.

O(6) position.

The position of the O(6) is described by the conformation of the C(6)-O(6) bond with respect to the C(5)-O(5) and the C(4)-C(5) bonds. For example, if the C(6)-O(6) bond is trans to C(5)-O(5) and gauche to C(4)-C(5), then the position of O(6) is described as "tg".

The position of O(6) atoms in cellulose structures is at the center of several controversies. In an exploratory way, we have exploited the continuous dependence of the features of the powder diffraction pattern on crystal structural details to investigate the sensitivity of the diffraction pattern to changes in O(6) position. In the work reported in the following paragraphs, all R_{wp} values are for comparison of parallel-up models with the observed pattern. The position of O(6) was fixed as gg,tg,gt by specifying the torsion angle describing its position as 0, -120, and 120°, respectively. Also, the individual tetramers were close to having a 2-fold screw symmetry.

A: "tg" vs. "gt" models. A powder diffraction pattern for a model with all O(6) atoms located in the "tg" position was calculated. R_{wp} was 0.20. This value is slightly higher than that of the best parallel model because in the best parallel model the O(6)'s are all positioned slightly away from "tg".

With all other parameters in the model kept unchanged, all the O(6) positions were changed to "gt". R_{wp} was 0.22, which indicates that the overall change in the pattern was small.

The calculated patterns for both the "tg" and the "gt" models are given in Figure 8. The patterns are similar but a noticeable difference occurs in the peaks arising from the 004, 104 and 104 reflections (at 15.9°, 19.1° and at 19.6°, respectively). The sensitivity of the calculated pattern to changes in internal conformation, such as the O(6) position, makes it seem probable that a systematic study of the various O(6) positions and other internal changes will lead to lower R_{wp} values.

B. "tg" vs "tg, gt, tg, gt" models. In the next model, the O(6) conformations were tg, gt, tg, gt (from the non-reducing to the reducing end). Again, the overall effect on the pattern was small ($R_{wp} = 0.22$) but there were perceptible changes in non-zero l reflections (Figure 9), e.g., 002 has vanished. It is small but significant changes such as this that may ultimately lead to the correct model.

C. "tg" vs "tg, gg, tg, gg" models. Figure 10 shows that the very strong 110 and 200 reflections have changed considerably from the "tg" model. R_{wp} for this model was 0.25.

These computational experiments show that changes in the O(6) position produce changes in the reflections at small 2θ which are

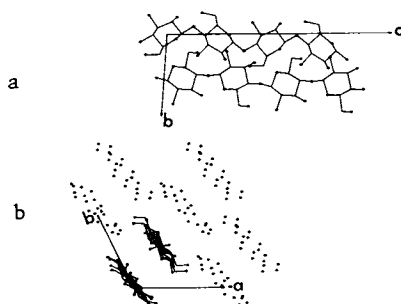


Figure 7. Best antiparallel model obtained from Rietveld refinement against observed pattern ($R_{wp} = 0.226$). a) bc projection b) ab projection. All the carbon and the oxygen atoms are shown for one corner and one central molecule only, in the unit cell. Only the oxygen atoms are shown for other molecules.

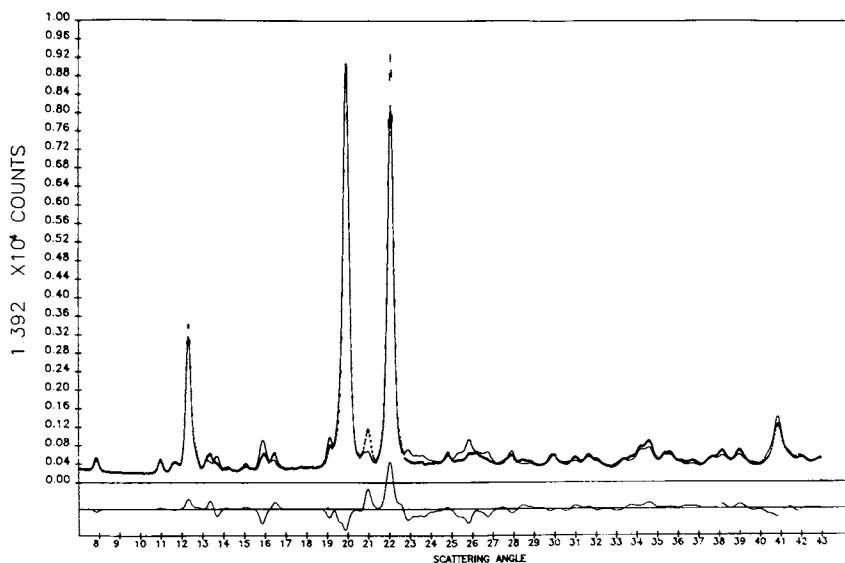


Figure 8. Calculated diffraction patterns with different C(6)-O(6) conformations. The pattern for the "tg" model is given by dots. The pattern for the "gt" model is given by the continuous curve. The difference is shown in the lower field.

Table II. Fractional and cartesian coordinates of the best parallel model. Species 1 is oxygen and species 2 is carbon. The first 45 atoms are in the corner molecule and the rest are in the center molecule. In each tetramer the first three monomers consist of 6 carbon atoms and 5 oxygen atoms and the monomer at the reducing end has 6 carbons and 6oxygens

No.	Species	Fractional Coordinates			Cartesian Coordinates		
1	1	-.121	.297	-.076	-2.142	2.123	-1.879
2	2	-.001	.164	-.008	-.587	1.170	-.273
3	2	-.095	.278	-.014	-1.841	1.987	-.500
4	2	-.024	.020	-.060	-.282	.142	-1.362
5	2	.074	-.087	-.048	.974	-.621	-1.009
6	2	.029	-.170	.013	.863	-1.213	.385
7	2	.039	-.024	.063	.438	-.172	1.417
8	1	-.060	.064	.045	-.766	.457	.960
9	1	.032	.116	-.113	-.130	.832	-2.593
10	1	.035	-.236	-.094	1.154	-1.689	-1.947
11	1	.139	-.246	.028	2.123	-1.757	.780
12	1	.127	-.291	.138	2.175	-2.082	3.268
13	2	.013	-.153	.215	.664	-1.092	4.892
14	2	.108	-.266	.201	1.916	-1.905	4.652
15	2	.029	-.014	.169	.314	-.102	3.783
16	2	-.068	.093	.189	-.938	.662	4.152
17	2	-.016	.182	.252	-.787	1.300	5.521
18	2	-.019	.041	.295	-.321	.296	6.572
19	1	.079	-.047	.271	.874	-.337	6.098
20	1	-.032	-.116	.113	-.130	-.832	2.580
21	1	-.035	.237	.149	-1.157	1.697	3.186
22	1	-.125	.258	.274	-2.040	1.845	5.940
23	1	-.095	.320	.386	-1.993	2.287	8.415
24	2	.025	.187	.454	-.440	1.334	10.022
25	2	-.069	.301	.447	-1.693	2.151	9.795
26	2	.002	.043	.401	-.134	.306	8.933
27	2	.100	-.064	.413	1.122	-.457	9.285
28	2	.054	-.147	.474	1.010	-1.050	10.682
29	2	.065	-.001	.524	.586	-.009	11.712
30	1	-.035	.087	.506	-.619	.621	11.257
31	1	.057	.139	.348	.017	.995	7.702
32	1	.061	-.213	.368	1.302	-1.524	8.347
33	1	.165	-.223	.489	2.270	-1.592	11.077
34	1	.152	-.268	.599	2.322	-1.918	13.565
35	2	.039	-.130	.676	.811	-.927	15.189
36	2	.133	-.243	.662	2.064	-1.740	14.949
37	2	.055	.009	.630	.462	.062	14.077
38	2	-.042	.116	.650	-.790	.826	14.447
39	2	.010	.205	.714	-.640	1.464	15.817
40	2	.006	.064	.757	-.174	.460	16.867
41	1	.104	-.024	.733	1.022	-.172	16.393
42	1	-.006	-.093	.574	.277	-.667	12.874
43	1	-.009	.260	.611	-1.010	1.861	13.481
44	1	-.099	.281	.735	-1.892	2.008	16.237
45	1	.083	.162	.810	.165	1.160	18.012

Table II. Continued

No. Species		Fractional Coordinates			Cartesian Coordinates		
46	1	.576	-.003	.107	5.183	-.023	2.458
47	2	.555	.266	.156	4.031	1.905	3.390
48	2	.656	.158	.148	5.325	1.130	3.275
49	2	.566	.389	.105	3.695	2.783	2.183
50	2	.462	.492	.120	2.398	3.518	2.431
51	2	.511	.598	.181	2.456	4.274	3.747
52	2	.512	.473	.229	2.912	3.383	4.899
53	1	.616	.387	.210	4.153	2.766	4.533
54	1	.509	.272	.051	3.598	1.948	1.040
55	1	.490	.624	.076	2.183	4.459	1.372
56	1	.396	.671	.198	1.165	4.796	4.063
57	1	.528	.900	.327	1.539	6.437	6.815
58	2	.539	.657	.383	2.500	4.700	8.216
59	2	.444	.765	.368	1.261	5.470	7.814
60	2	.524	.503	.335	2.916	3.595	7.243
61	2	.622	.404	.355	4.145	2.888	7.765
62	2	.570	.337	.418	3.917	2.406	9.190
63	2	.572	.492	.462	3.387	3.516	10.090
64	1	.474	.571	.437	2.220	4.082	9.482
65	1	.585	.586	.280	3.168	4.188	5.978
66	1	.590	.245	.314	4.424	1.754	6.937
67	1	.679	.269	.440	5.143	1.922	9.737
68	1	.563	.136	.569	4.569	.975	12.689
69	2	.541	.406	.618	3.417	2.901	13.622
70	2	.643	.298	.609	4.711	2.127	13.506
71	2	.553	.529	.567	3.082	3.779	12.416
72	2	.449	.632	.582	1.785	4.515	12.662
73	2	.498	.737	.643	1.843	5.271	13.978
74	2	.499	.613	.691	2.299	4.380	15.130
75	1	.603	.526	.672	3.540	3.762	14.765
76	1	.496	.412	.513	2.985	2.944	11.271
77	1	.477	.763	.538	1.570	5.455	11.603
78	1	.383	.810	.660	.551	5.794	14.294
79	1	.515	1.040	.788	.926	7.434	17.046
80	2	.526	.797	.845	1.887	5.696	18.447
81	2	.431	.904	.830	1.647	6.466	18.045
82	2	.511	.642	.797	2.303	4.592	17.475
83	2	.609	.543	.817	3.532	3.885	17.999
84	2	.557	.476	.879	3.303	3.403	19.421
85	2	.559	.631	.924	2.774	4.513	20.324
86	1	.461	.710	.899	1.607	5.079	19.713
87	1	.572	.725	.742	2.554	5.184	16.210
88	1	.577	.385	.776	3.810	2.751	17.168
89	1	.666	.408	.901	4.530	2.919	19.968
90	1	.483	.552	.976	2.371	3.943	21.518

Table III. Fractional and cartesian coordinates of the best antiparallel model. Species 1 is oxygen and species 2 is carbon. The first 45 atoms are in the corner molecule and the rest are in the center molecule. In each tetramer the first three monomers consist of 6 carbon atoms and 5 oxygen atoms and the monomer at the reducing end has 6 carbons and 6 oxygens

No.	Species	Fractional Coordinates			Cartesian Coordinates		
1	1	-.145	.249	-.089	-2.189	1.782	-2.157
2	2	-.015	.152	-.013	-.675	1.088	-.388
3	2	-.123	.246	-.027	-1.980	1.759	-.754
4	2	-.020	.005	-.062	-.192	.033	-1.386
5	2	.091	-.081	-.043	1.102	-.578	-.897
6	2	.044	-.153	.019	.944	-1.095	.522
7	2	.036	-.006	.065	.346	-.044	1.451
8	1	-.074	.061	.041	-.876	.433	.873
9	1	.035	.092	-.116	-.016	.660	-2.645
10	1	.069	-.234	-.085	1.454	-1.675	-1.750
11	1	.165	-.208	.040	2.217	-1.484	1.037
12	1	.123	-.260	.149	2.029	-1.858	3.490
13	2	.007	-.108	.220	.447	-.769	4.978
14	2	.102	-.223	.210	1.710	-1.592	4.846
15	2	.025	.020	.170	-.147	.146	3.791
16	2	-.073	.130	.185	-1.119	.928	4.053
17	2	-.023	.231	.247	-1.030	1.654	5.385
18	2	-.028	.101	.295	-.610	.723	6.517
19	1	.071	.009	.275	-.606	.064	6.140
20	1	-.035	-.093	.116	.016	-.661	2.632
21	1	-.039	.265	.142	-1.297	1.898	3.015
22	1	-.133	.311	.265	-2.300	2.221	5.713
23	1	-.107	.395	.376	-2.363	2.824	8.154
24	2	.012	.277	.450	-.881	1.983	9.885
25	2	-.082	.389	.438	-2.122	2.780	9.550
26	2	-.010	.124	.401	-.527	.887	8.880
27	2	.088	.021	.418	.712	.152	9.338
28	2	.041	-.049	.480	.539	-.348	10.759
29	2	.050	.106	.526	.070	.756	11.702
30	1	-.049	.189	.505	-1.113	1.351	11.153
31	1	.047	.209	.346	-.322	1.495	7.614
32	1	.050	-.136	.376	.934	-.974	8.479
33	1	.151	-.120	.499	1.781	-.861	11.246
34	1	.135	-.143	.611	1.724	-1.024	13.749
35	2	.020	.009	.682	.142	.066	15.237
36	2	.114	-.106	.673	1.404	-.757	15.105
37	2	.037	.137	.633	-.159	.981	14.052
38	2	-.061	.247	.648	-1.425	1.763	14.314
39	2	-.011	.348	.710	-1.335	2.489	15.646
40	2	-.016	.218	.757	-.916	1.557	16.778
41	1	.083	.126	.737	.300	.899	16.398
42	1	-.023	.024	.578	-.289	.174	12.891
43	1	-.027	.382	.605	-1.603	2.732	13.274
44	1	-.121	.427	.727	-2.605	3.056	15.972

Table III. Continued

No.	Species	Fractional Coordinates			Cartesian Coordinates		
45	1	.059	.326	.809	-.627	2.331	17.888
46	1	.400	.969	.844	-.143	6.925	18.324
47	2	.494	.762	.788	1.718	5.450	17.204
48	2	.516	.960	.802	1.218	6.865	17.398
49	2	.566	.690	.836	2.628	4.930	18.317
50	2	.538	.493	.816	3.078	3.523	17.997
51	2	.604	.485	.754	3.698	3.464	16.611
52	2	.540	.574	.709	2.803	4.103	15.555
53	1	.576	.760	.733	2.470	5.431	15.982
54	1	.488	.695	.891	1.906	4.969	19.538
55	1	.625	.435	.857	4.058	3.112	18.957
56	1	.555	.294	.732	3.933	2.104	16.244
57	1	.718	.310	.602	5.340	2.219	13.344
58	2	.606	.492	.553	3.688	3.518	12.123
59	2	.592	.300	.562	4.244	2.148	12.444
60	2	.538	.576	.604	2.783	4.115	13.200
61	2	.557	.765	.589	2.275	5.466	12.753
62	2	.478	.750	.527	1.622	5.362	11.383
63	2	.538	.651	.479	2.518	4.651	10.375
64	1	.512	.474	.499	2.909	3.385	10.923
65	1	.628	.591	.657	3.532	4.225	14.400
66	1	.474	.830	.633	1.300	5.937	13.691
67	1	.518	.933	.510	1.329	6.669	10.889
68	1	.353	.887	.382	.007	6.344	8.042
69	2	.446	.681	.326	1.580	4.868	6.924
70	2	.469	.879	.340	1.081	6.283	7.118
71	2	.519	.608	.373	2.492	4.349	8.035
72	2	.491	.411	.354	2.940	2.941	7.715
73	2	.557	.403	.291	3.562	2.883	6.331
74	2	.492	.493	.247	2.666	3.522	5.273
75	1	.529	.678	.271	2.334	4.850	5.700
76	1	.440	.614	.429	1.769	4.388	9.256
77	1	.577	.354	.395	3.922	2.531	8.675
78	1	.507	.213	.270	3.797	1.523	5.962
79	1	.670	.229	.140	5.203	1.637	3.062
80	2	.558	.411	.091	3.552	2.936	1.843
81	2	.544	.219	.100	4.108	1.567	2.164
82	2	.491	.494	.142	2.647	3.533	2.920
83	2	.509	.683	.126	2.138	4.885	2.471
84	2	.431	.669	.065	1.486	4.781	1.103
85	2	.491	.569	.017	2.382	4.070	.093
86	1	.464	.392	.037	2.773	2.804	.641
87	1	.580	.510	.195	3.396	3.644	4.118
88	1	.427	.749	.171	1.164	5.355	3.409
89	1	.471	.852	.048	1.193	6.088	.607
90	1	.393	.532	-.034	1.633	3.806	-1.040

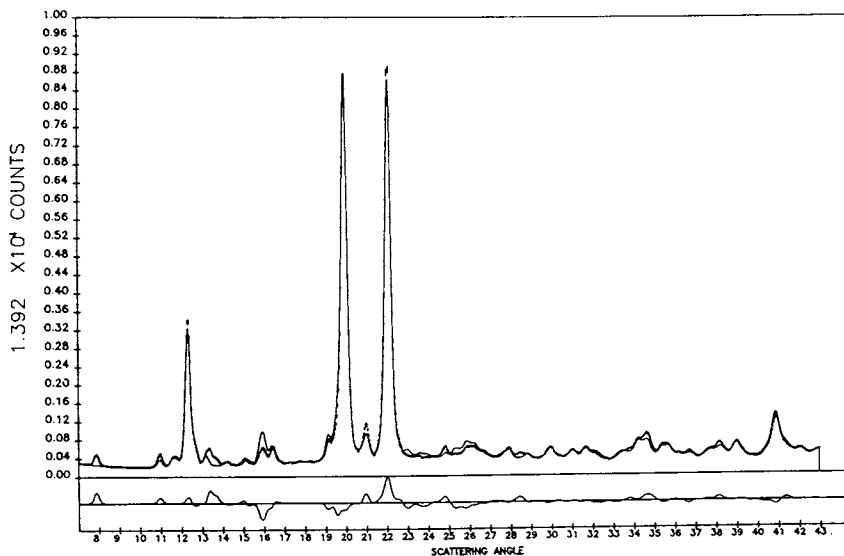


Figure 9. Calculated diffraction patterns for models with different C(6)-O(6) conformations. The pattern for the "tg" model is given by dots. The pattern for the "tg, gt, tg, gt" model is given by the continuous curve. The difference is shown in the lower field.

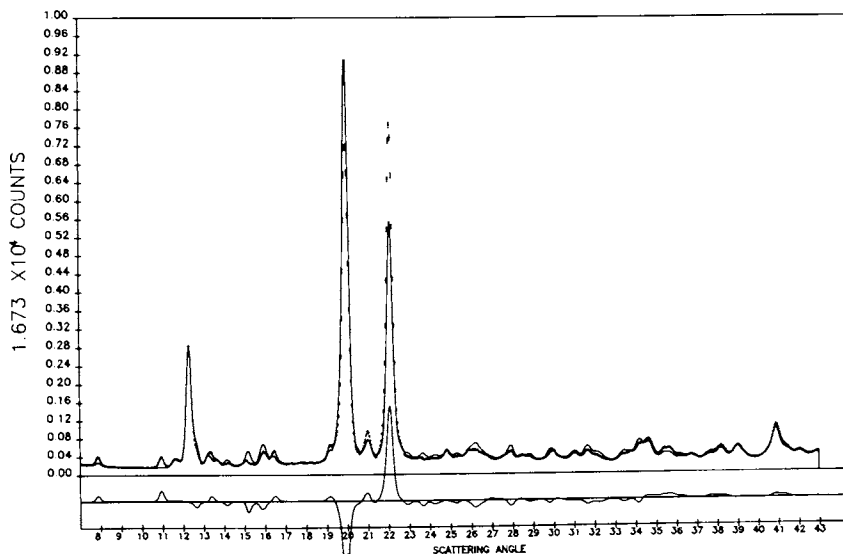


Figure 10. Calculated diffraction patterns with different C(6)-O(6) conformations. The pattern for the "tg" model is given by dots. The pattern for the "tg, gg, tg, gg" model is given by the continuous curve in the same field. The difference is shown in the lower field.

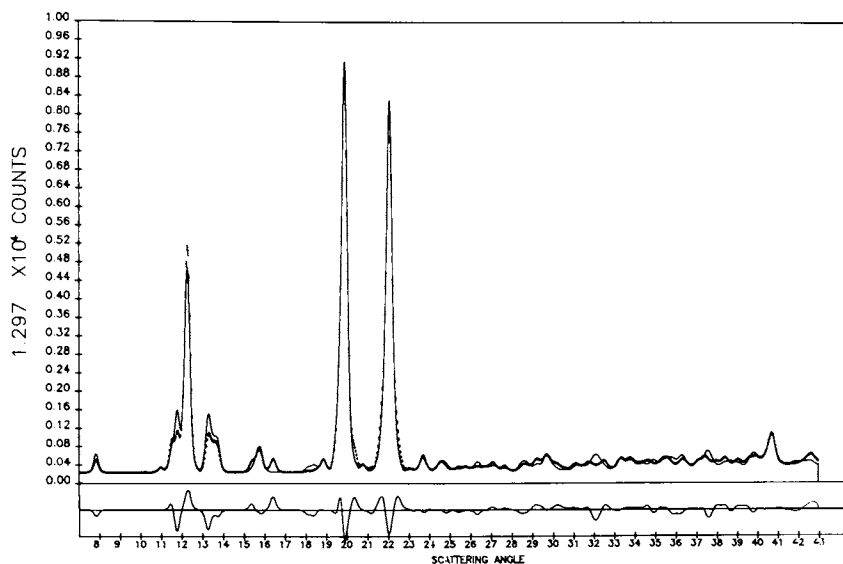


Figure 11. Calculated diffraction patterns for parallel and antiparallel models refined against each other. The pattern for the parallel models is given by dots. The pattern for the antiparallel model is given by the continuous curve in the same field. The difference is shown in the lower field.

potentially analyzable even though the R_{wp} 's for all of these models are fairly close.

Refinement of Parallel against Antiparallel Models.

In an attempt to learn how much information regarding chain polarity is available from powder diffraction data such as ours, we refined an antiparallel model against intensities calculated from a parallel model. Next, we refined the parallel model against the intensities calculated from that antiparallel mode. The R_{wp} was only 14% in both cases. The similarity of these two calculated patterns (Figure 11) underlines the difficulty of choosing a model based on diffraction data alone. Packing energy calculations, along with spectroscopic data and hydrogen bonding possibilities should be useful in making a final choice. In particular, packing energy minimization will be helpful to eliminate the poor contacts present in the model proposed here.

CONCLUSIONS

X-ray powder diffraction data indicate that the unit cell for cellotetraose is triclinic (space group P1) with two tetramers per unit cell. Although there is a small preference for a parallel structure at this stage, similarities between patterns calculated for parallel and antiparallel models make it difficult to choose one over the other. In addition to the rather insensitive R values, the differences in specific reflections in the observed and the calculated patterns for different models may be used as criteria in selection of a model.

For fairly crystalline powders, such as cellotetraose, the Rietveld method seems to have a power comparable to fiber diffraction for a typical cellulose samples. Peak overlap is even more severe, but the data are known with greater confidence because of less probable error in collection and correction of the data. Therefore, it is likely to be a worthwhile complement to the fiber method for highly crystalline samples, even if oriented samples are available.

Acknowledgments We thank Professor A.F. Turbak for helpful discussions and advice.

This material is based upon work supported in part by the U.S. Department of Agriculture under Co-operative Agreement No. 58-7b30-3-564.

Literature Cited

1. Poppleton P.J., Mathieson A.McL., Nature., 219,1046-1049, (1968)
2. Poppleton P.J., Gatehouse B.M., J. Polym. Sci., A2,375-376, (1972)
3. Rietveld H.M., J. Appl. Cryst., 2, 65-71, (1969)
4. Young R.A., Wiles D.B., Advances in X-ray Analysis, 24,1-23, (1981)
5. Immirzi A., Acta Cryst., B36,2378-2385, (1980)

6. Young R.A., Lundberg J.L., Immirzi A., ACS Symposium Series, No. 141, 69-91, Fiber Diffraction Methods, Eds. French A.D., Gardner K.H., (1980)
7. Chu S.S.C., Jeffrey G.A., Acta Cryst., B24, 830-838, (1968)
8. F. Takusagawa and R.A.Jacobson, Acta Cryst., B34, 213, (1978)
9. Gardner K.H., Blackwell J., Biopolymers, 13, 1975-2001, (1974)
10. Sarko A., Muggli R., Macromolecules, 7, 486-494, (1974)

RECEIVED March 5, 1987

Chapter 5

Further Carbon-13 NMR Evidence for the Coexistence of Two Crystalline Forms in Native Celluloses

D. L. VanderHart¹ and Rajai H. Atalla²

¹National Bureau of Standards, Polymers Division, Gaithersburg, MD 20899

²Institute of Paper Chemistry, Appleton, WI 54912

The hypothesis that all native celluloses are composites of two crystalline allomorphs, I_{α} and I_{β} , is further explored using solid state ^{13}C NMR techniques. Spectra of several algal and higher plant celluloses and the effects of acid hydrolysis and mechanical beating are investigated. No significant alteration of the I_{α} and I_{β} ratios is seen upon hydrolysis of a cellulose from cotton linters. However, both beating and hydrolysis enhance the I_{β} proportion in an algal cellulose obtained from *Cladophora*. Methods of enhancing the crystalline core resonances, based on proton rotating frame relaxation and carbon longitudinal relaxation, are used to verify that unit cell inequivalence rather than crystal surface chains determines the crystalline resonance profiles. These studies indicate that the C4 resonance region, from 88-92 ppm in all native celluloses is a faithful monitor of the relative numbers of inequivalent sites within the cell(s). Also, the higher plant celluloses contain a much smaller fraction of the I_{α} crystalline form than originally proposed. The possibility even exists that the higher plant celluloses represent the pure I_{β} form. If this is true, then it follows from the C4 lineshape that this unit cell contains more than four non-equivalent anhydroglucose residues.

Experiments based on weak ^{13}C - ^{13}C spin exchange were also conducted in order to probe the spatial environment, within a 0.7-1.0nm radius, around carbons identified with individual multiplet components, which are assumed to belong exclusively to the I_{α} or I_{β} forms. It is expected that only those carbons belonging to that form will be able

0097-6156/87/0340-0088\$08.50/0

© 1987 American Chemical Society

to undergo spin-exchange during a time of 50-70s. The spectrum of such 'nearest neighbors' is isolated for three different multiplet lines in an algal cellulose and two lines in a higher plant cellulose. Results rule out the possibility that tertiary morphology can give rise to any multiplicity in these spectra. Moreover, the results strongly reinforce the hypothesis of polymorphy in the algal celluloses; however, no clear evidence for multiple crystalline forms in the higher plant cellulose is found by this method. The spin-exchange results raise a few minor questions about the details of the spectrum belonging to each allomorph. On the basis of all of these results, revised spectra for the I_{α} and I_{β} allomorphs are presented. These represent minor departures from the previously published spectra.

Finally, the spectrum of the *Cladophora* cellulose which survived the strong acid hydrolysis closely resembled the cotton hydrocellulose spectrum except that the resolution was much better in the former spectrum. A contrast in resolution is consistent with a difference in the average lateral dimensions for the crystallites; this difference is corroborated by electron microscopy. The close similarity of multiplet relative intensities in these two samples, in spite of their different crystallite surface-to-volume ratios verifies that surface resonances are not determining the apparent multiplet intensities, particularly, for the 88-92 ppm region of the C4 resonance.

In previous publications (1-3) we have proposed, principally on the basis of ^{13}C NMR evidence, that native celluloses are composites of two crystalline forms occurring in different proportions. These allomorphic forms were designated I_{α} and I_{β} . The ^{13}C solid-state spectra proposed for the I_{α} and I_{β} allomorphs are shown in Figure 1. Although these spectra contain non-crystalline resonance contributions, the crystalline resonance profiles can be distinguished from the non-crystalline resonances due to the greater linewidth and lower total intensity of the latter resonances. The sharp features of the resonance profile are the expression of the two crystalline forms.

The previous studies (1-3) suggested that the higher plant celluloses, like cotton and ramie, were rich in I_{β} while the I_{α} content was appreciable if not dominant in the algal celluloses and the bacterial cellulose obtained from *Acetobacter xylinum*. In Figure 2 the considerable contrast between the spectra of cotton linter cellulose, both dry (2A) and wet (2B), and algal cellulose (2C) from *Valonia ventricosa* is illustrated. Because the lateral dimensions of the crystallites in cotton are 3.5-5 nm (4-6) and in

Valonia are approximately 12-20nm (7-9), the chains in the former crystallites will have a less defined array of nearest neighbors and be more subject to interfibrillar drying stresses than the Valonia chains. Therefore, the crystalline resonances in spectrum 2A are significantly broader than 2C. Wetting the cellulose relieves drying stresses and sharpens the resonances (10-11) as shown in 2B where the relative multiplet intensities are seen more clearly. The very different multiplet intensities are most obvious at C1 and C4 in spectra 2B and 2C. The postulate that multiple crystalline forms coexist in a given cellulose, arose from the extensive coincidence in the multiplet peak positions and the variation in relative multiplet intensities from cellulose to cellulose. Although other investigators have observed variations of unit cell parameters for the different native celluloses (12-13), differences in numbers of chains per unit cell (14-18), and differences in the -OH stretching regions of IR spectra (19), the possibility that every native cellulose may be polymorphic has only been proposed by us (1-3).

Why an organism should produce more than one kind of crystalline cellulose is not obvious. Moreover, if two crystalline forms coexist, the morphological expressions of each form are not yet recognized, nor have electron diffraction patterns from, say, individual Valonia fibrils yet shown any obvious difference from fibril to fibril (20-21). Therefore, we thought it desirable to examine further the evidence supporting the composite model since the hypothesis has important implications for both biosynthetic and morphological studies.

Background

At the heart of the interpretation of the ^{13}C spectra is the postulate that sharper multiplet features associated with chemically equivalent carbon atoms in the cellulose spectra are expressions of magnetically inequivalent sites within the unit cells. If this "fine structure" were due to some other cause, then the conclusion of multiple crystalline forms would be called into serious question. The fact that the ratios of multiplet intensities for given resonances, such as that of C4 or C1, vary from sample to sample and rarely have ratios of small whole numbers, reinforces the crystalline composite hypothesis.

In order to establish further the validity of the hypothesis it is necessary to exclude alternate explanations for the resonance multiplicities. Two possible explanations have been considered in earlier papers and we repeat these here.

The first alternate explanation was that the tertiary structure, i.e. the natural assembly and interweaving pattern of the elementary fibrils may give rise to small shifts and or broadening because of anisotropic bulk magnetic susceptibility (ABMS) (22). This mechanism has been argued previously (23) to give rise to shifts of the order of 0.1 ppm in cellulose; however, this calculation assumed that cellulose possesses an ABMS tensor identical to sucrose. One characteristic of ABMS shifts originating in the tertiary structure is that all carbons within a

given monomer unit should be affected equally by this perturbation. With respect to this measure, the experimental splittings certainly dismiss the dominance of the ABMS mechanism since the lineshapes for, say, C1, C4, and C6 are each different (see Figure 2). However, the possibility that the fine structure is due to a combination of unit cell inequivalence and ABMS effects is more difficult to dismiss and certain results described herein bear directly on this possibility.

The second (and, in our opinion, more likely) alternate explanation is that the surface layers of the crystallites may be well ordered, like those in the crystal interior, and therefore give rise to sharp resonance features which are present in addition to multiplicities arising from inequivalence in those unit cells in the interior of the crystallites. Since the shape and surface-to-volume ratio of native cellulose crystallites vary, the observation that the ratios of multiplet intensities are often not whole numbers could then be explained. In previous reports we have argued (3,23) that surface resonances are not sharp and do not contribute to the multiplicities in the above sense. As evidence against a sharp surface resonance, the intensities of the C4 resonance multiplets in Valonia ventricosa are too large to be explained in this manner. The elementary fibrils of Valonia have typical lateral crystal dimensions of 12x20 nm, so that the outer unit cell layer, assumed for simplicity to be a two-chain unit cell, contains about 20% of the total number of crystal chains. Since the least intense multiplet line represents at least 20% of that carbon's crystalline lineshape intensity, one would have to postulate that both chains in the unit cell on all lateral faces of the crystallite contribute to the same sharp resonance features. This is unlikely. Moreover, in the spectrum of Valonia the broad wings of C4 and C6 are found to comprise about 16-20% of their total intensity and are the most likely manifestations of surface chain resonances. Further evidence regarding this interpretation was sought in the present study.

Our approach to investigating the multiple crystalline form hypothesis in native celluloses is fourfold. First, ^{13}C spectra of additional native celluloses are examined and further variations are evaluated in the light of the polymorphy hypothesis. Second, variations in the ratio of I_{α} to I_{β} arising from chemical or mechanical treatments are studied. The crystalline forms may have different sensitivities to chemical attack or mechanical stress so that the I_{α} to I_{β} ratios could be altered in a given cellulose. This approach requires an independent measurement of any changes in surface-to-volume ratios.

In the third approach, we attempt to isolate or at least enhance those resonances arising from the crystalline interior. If such resonances are enhanced or isolated, then any resonances arising from crystalline surface layers are correspondingly reduced or suppressed.

The fourth and final approach is to probe directly, via ^{13}C NMR spin exchange techniques, the ^{13}C resonances lying in the immediate neighborhood, (in this case a sphere of radius 0.7-1.0

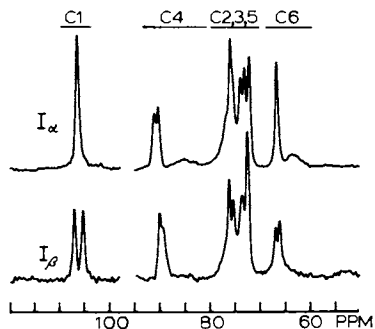


Figure 1. Originally proposed ^{13}C CP-MAS NMR spectra for the crystalline allomorphs, I_α and I_β ; included are the assignments of the various carbon resonances. These spectra were generated by linear combination and were based on spectra of Acetobacter xylinum cellulose and a low-DP regenerated cellulose I. Gaps in the spectra appear where the first spinning sideband of polyethylene, the chemical shift standard, occurred.

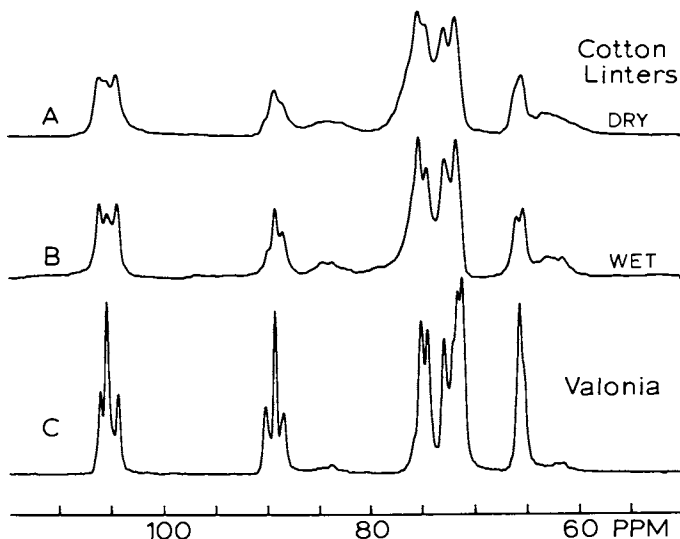


Figure 2. 50 MHz CP-MAS ^{13}C spectra of cotton linters (A: dry; B: wet) and Valonia ventricosa (C). All spectra are normalized to the same total intensity.

nm) of the set of ^{13}C nuclei giving rise to a particular multiplet component. The idea is that those ^{13}C nuclei in the immediate neighborhood of, say, a C1 resonance belonging solely to the I_α crystal phase, will also belong principally to the I_α form. However, most of these neighboring ^{13}C nuclei will not themselves be in the C1 position since ^{13}C isotopic distributions at natural abundance (1.1%) are quite random. In view of the 0.7-1.0 nm distance involved, several monomer units with their random ^{13}C site occupation contribute to the C1 neighbors. Thus, if one could isolate the resonance profile of the set of neighbors to the C1 carbons of the I_α form, one would identify all of the carbon resonances associated with the I_α unit cell provided that the unit cell is not too large. Furthermore, the smaller the unit cell, the more faithfully these 'near-neighbor' multiplet intensities would reflect the true multiplet intensities for each carbon in the I_α phase. On the other hand, if ABMS broadening is responsible for producing some multiplet splitting, then the 'near-neighbor' carbon spectrum would show a reduced multiplicity relative to the spectrum of the entire sample.

In this report we present experimental evidence derived from these four approaches. In the end, the hypothesis that unit cell inequivalence alone causes the observed multiplicity for chemically equivalent carbons is supported. Therefore, the crystalline composite hypothesis, although slightly revised, is strongly supported, particularly for the algal celluloses.

Experimental

^{13}C spectra were obtained on a spectrometer which operates at a magnetic field of 4.7T (50.3 MHz for carbon). ^{13}C magnetization was initially generated by spin-lock cross-polarization (24,25) (CP). Magic-angle spinning (26,27) (MAS) speeds were in the range of 3-4 KHz. The rotating rf field strengths for both protons and carbons fell in the range of 60-70 kHz for each nucleus, except for the Dante (28-30) pulses in the ^{13}C spin exchange experiments. During the Dante pulses rotating rf carbon fields of approximately 10kHz in strength were used in order to suppress CP. CP times of 1 ms were typical. Decoupling periods of 52 ms were employed for signal observation.

Pulse sequences have been described adequately in the literature. In this paper CP or CP-MAS spectra are those obtained via the usual spin-lock CP method (24,25). Spectra relating to the longitudinal relaxation times for carbons (T_1^{C}) were obtained via the method of Torchia (31). In these latter spectra, signals obtained at longer times have enhanced contributions from those carbons with longer T_1^{C} 's.

The 'Dante' irradiation is a 'comb' of equally spaced pulses each of which produces a nuclear nutation of only a few degrees (28,29). The object of the sequence is to perturb the Zeeman population of a carbon line at the rf carrier or separated from the rf carrier by the inverse of the time between pulses. In our case a comb of 50 pulses, 1 μs in length and separated by

approximately 0.4 ms, was used to invert (to an extent of about 60% of the original signal amplitude) the multiplet resonance centered on the rf carrier. The inversion of this line is quite efficient, first, because the carbon resonance is well defined due to the presence of proton decoupling during this period and secondly, because the intrinsic T_2 of each frequency is much greater than the apparent T_2 (deduced from linewidth of each multiplet component). A more complete description of the DANTE sequence and its use in selectively perturbing carbon spin populations, even those carbons with sizeable chemical shift anisotropy, may be found in Ref. 30. The Dante sequence is inserted at the beginning of the variable delay time in Torchia's T_1 ^{13}C sequence (31).

In this paper, the ^{13}C spin exchange experiments, which employ the Dante sequence, are used to probe the ^{13}C resonance profile of those carbons which lie in an 0.7-1.0 nm sphere surrounding the resonance perturbed by the Dante sequence. A detailed description of the method and a consideration of the spatial extent of ^{13}C spin exchange (or spin diffusion) as a function of time are beyond the scope of this paper. Such information may be found in a forthcoming paper (32). In the present paper the Dante sequence will be viewed as a method for very selectively perturbing the Zeeman spin population within a multiplet. ^{13}C spin exchange in cellulose will be looked upon simply as the mechanism whereby, over the course of the 50-70s mixing period selected for the results shown in this paper, the original spin population disturbance, localized to a given multiplet line in the Dante preparation, spreads to other resonances belonging to carbons within 0.7-1.0 nm of the originally perturbed carbon spins. The method whereby the signals of these neighboring carbons are isolated will be illustrated in the results section. Further details on the validity of this method of separation can also be found elsewhere (32).

All cellulose samples were purified by Browning's method (33) for wood cellulose. Sugar analyses of several of the purified higher plant celluloses revealed a qualitative correlation between the non-glucose pyranoses and the non-crystalline content indicated by the ^{13}C CP-MAS spectra. The algal celluloses and the bacterial cellulose had negligible amounts of non-glucose sugars. With a few noted exceptions, all samples were equilibrated with normal laboratory relative humidity which ranged between 35% and 50%.

Mechanical beating of an algal cellulose from Cladophora glomerata was carried out for 5 hr in a Waring blender at 1% and 3% solids consistency. Beating was judged more efficient in the latter case based on a greater retention of water.

Hydrolysis of the beaten Cladophora was carried out in boiling 4N HCl for 44 hr; mass recovery was 22%. In another preparation, an unbeaten sample from a different strain of Cladophora glomerata, which was harvested from a different location at a different time of year, was subjected to the same hydrolysis conditions; mass yield was 12%. In the latter case, electron microscopic investigation (21) of sonicated and dispersed

fibrils of the original material and of the hydrolyzed material showed no significant change in cross-sectional area. Thus, it appears that the hydrolysis somehow managed to leave the cross sectional area of the remaining fibrils unaffected despite the low mass yield.

The assignment of ^{13}C resonances to different carbons in the anhydroglucose has been discussed previously (34,35); assignments are also indicated in Figure 1. The broad resonance features upfield from C4 and C6 are due to disorder (3,23,34-36). Non-crystalline resonances associated with the other four carbons more strongly overlap their respective crystalline lines; therefore, the shape of the pure crystalline resonance is most obvious for the C4 and C6 carbons.

Results

Spectra of Several Native Celluloses. In Figure 3 the CP-MAS spectra of several higher plant celluloses are compared and are also contrasted to the spectrum of algal cellulose from Cladophora glomerata (bottom spectrum). In Figure 4, the spectra of two samples of bacterial cellulose from two different sources of Acetobacter xylinum, several algal celluloses, and the Cladophora, beaten at 1% solids consistency, are shown.

The spectra of the higher plant celluloses in Figure 3 lack resolution in comparison with the algal cellulose spectrum. This poor resolution is most likely attributed to the relatively small lateral dimensions of the crystalline fibrils in these materials. This lack of resolution is generally correlated with the intensity of the broad wings in the C4 and C6 regions. These wings indicate the amount of non-crystalline and/or crystal-surface residues. In Figure 3, the cactus spines and the Benares hemp exhibit the greatest crystallinity, and, to the extent that the downfield portion of the resonance at C4 can be recognized as consisting of three overlapping peaks, the relative heights of the shoulders seem similar to those for cotton (see Figure 2A) suggesting similar I_{α} to I_{β} ratios. The appearance of a single maximum in certain spectra at C1, for example that of Kenaf, is more an indication of a larger non-crystalline contribution than a greater proportion of the I_{α} form. This is reasonable since the central maximum is rather broad. The lack of resolution makes measurements of the apparent ratios of I_{α} to I_{β} difficult.

The lower four spectra in Figure 4 represent four different algal species, Cladophora glomerata, Valonia macrophysa, Rhizoclonium hieroglyphicum, and Valonia ventricosa. These spectra are all quite similar although Cladophora seems to have a slightly larger portion of I_{α} as judged by the larger downfield shoulder at C4 compared with the upfield shoulder (see Figure 1). The spectrum of Acetobacter at the top of the figure strongly resembles that of Cladophora cellulose. The Acetobacter cellulose contains a larger proportion of non-crystalline material in addition to having a slightly higher proportion of the I_{α} form according to the spectra of Figure 1. The greater proportion of non-crystalline chains in Acetobacter cellulose is consistent with

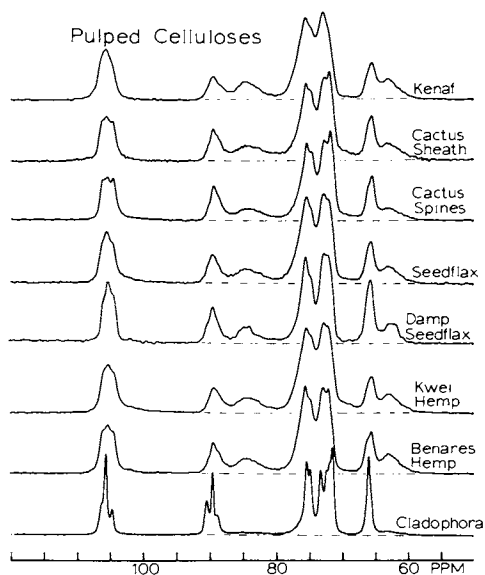


Figure 3. CP-MAS ^{13}C spectra of various higher plant celluloses in comparison with the algal cellulose spectrum of Cladophora (lower).

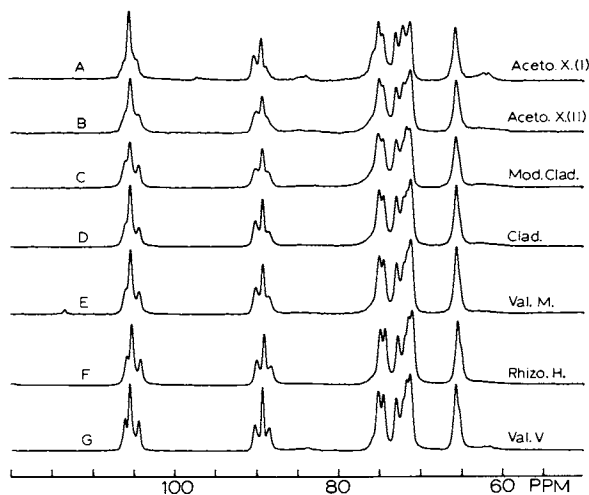


Figure 4. 50 MHz ^{13}C CP-MAS spectra of bacterial and algal celluloses: A and B: two preparations of Acetobacter xylinum; C: Cladophora glomerata, beaten at 1% solids consistency, D: Cladophora glomerata, E: Valonia macrophysa, F: Rhizoclonium hieroglyphicum, and G: Valonia ventricosa.

a greater surface to volume ratio for the latter since Acetobacter fibrils are approximately 6 nm wide (37) whereas Cladophora fibrils are about 20 nm wide (21). The Valonia, Cladophora, and Rhizoclonium algal spectra each exhibit non-crystalline resonance intensity in the C4 region of the order of 12-20% of the total C4 intensity. The wings of the C4 and C6 resonances in spectrum 4A are more prominent and the crystalline carbon resonances are a bit sharper than in spectrum 4B because the sample in 4A had a higher level of hydration than in 4B.

The spectra of Figure 4 are quite similar, although variations in the heights of the central C1 peaks and the upfield and downfield shoulders of the C4 resonance are outside of experimental error. If the multiplet intensities arise from unit cell inequivalence alone, then these variations support the hypothesis of multiple crystalline forms in the algal and bacterial celluloses.

Spectral Changes Resulting from Mechanical Beating and/or Acid Hydrolysis. The premise underlying this second group of explorations is that two crystalline forms may differ in their response to mechanical or chemical stresses. Thus, one might hope to alter the I_{α} to I_{β} ratio in a given material after exposure to such stress. On the other hand, the demonstration of such changes would not, in itself, constitute a proof for polymorphy if the multiplet structure in the NMR spectra had its origin, at least partially, in the tertiary morphology or the crystallite surface layers. A complete argument would require that the effect of the applied stresses on these characteristics also be followed.

Figure 5 shows the spectral changes accompanying acid hydrolysis of cotton linters. The hydrocellulose which results from this 30-minute hydrolysis in 2.5N HCl at 100C achieves the leveling-off DP and represents a mass fraction at least 90% of the original (38). Judging by the constant shape of the C4 crystalline resonance (88-92 ppm), no change in the I_{α} to I_{β} ratio has occurred as a result of hydrolysis. The bottom linear-combination spectrum gives proof that, within experimental error, the C4 (and C6) crystalline resonances are unchanged by the hydrolysis. This linear combination spectrum is very similar to a spectrum of ball-milled, decrystallized cellulose (3) implying that hydrolysis has mainly attacked the 3-dimensionally disordered regions. Since the C4 crystalline resonance is unchanged upon hydrolysis, the corresponding reduction in intensity of the central feature of C1 reflects a decrease in the underlying non-crystalline resonance rather than a change in the I_{α} to I_{β} ratio.

Figure 6 shows spectra of five preparations of algal celluloses obtained from Cladophora: spectrum A is from the original purified cellulose, spectrum B is that of the same cellulose beaten in a Waring Blender for 5 h while dispersed in water at 1% solids consistency, spectrum C is like B except that the beating was carried out at 3% solids consistency, spectrum D is that of the beaten cellulose in spectrum B following acid hydrolysis in 4N HCl for 44 h at 100 C (22% mass recovery), and

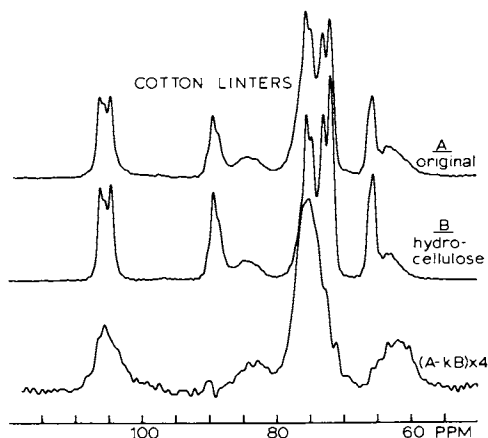


Figure 5. Effect of acid hydrolysis on the ^{13}C CP-MAS spectrum of cotton linters. A: Original material, B: subjected to 2.5N HCl for 30 min, and C: a renormalized linear combination spectrum $[4x(A-.72B)]$. Spectrum A and B are normalized to the same total intensity.

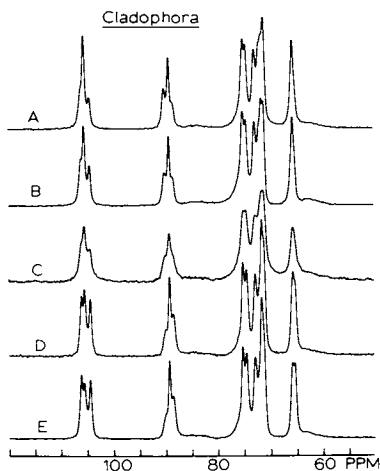


Figure 6. ^{13}C CP-MAS spectra, normalized to the same intensity, of various preparations of Cladophora cellulose: A: original, B: after beating in a Waring Blender at 1% solids consistency, C: after beating in a Waring Blender at 3% solids consistency, D: after acid hydrolysis (4N HCl, 100C, 44h) of the beaten (1%) sample (22% mass recovery), E: after acid hydrolysis, as above, of an unbeaten second strain of Cladophora (12% mass recovery).

spectrum E is that of the second strain of Cladophora cellulose after purification and exposure only to the above acid hydrolysis (12% mass recovery). The spectrum of the purified cellulose of this second strain is not shown because it is not significantly different from spectrum 6A. Judging by both measures of the I_{α} content, i.e. the downfield shoulder of C4 (at 90.3 ppm) and the central multiplet feature of C1 (at 105.5 ppm), the I_{α} content decreased noticeably as a result of beating at both 1% and 3% solids consistency. The degradation of resolution in Figure 6C probably results from a greater alteration of the tertiary morphology in the sample beaten at 3% solids consistency compared with the sample beaten at 1% solids consistency since the former sample retained more water. The strain on the fibrils resulting from the drying of a disordered network would be expected to cause line broadening. Spectrum 6B suggests that some conversion of I_{α} to I_{β} can be accomplished by mechanical stress since the non-crystalline spectral intensities are very similar in spectra 6A and 6B. However, mass recovery following beating was difficult to monitor. Therefore, while conversion of the I_{α} to the I_{β} crystalline form via mechanical stress is strongly suggested, the alternate possibility of a preferential mass loss of the I_{α} form cannot be entirely dismissed.

Scanning transmission electron micrographs of the materials corresponding to spectra 6A and 6B were also acquired. Even though resolution was insufficient for imaging the lateral dimensions of individual crystallites, these micrographs revealed that beating disrupts the fibrillar network. While the original lateral dimensions of most of the fibrillar aggregates were in the 80-200 nm range, aggregates as small as 30 nm could be seen after beating, although the average lateral fibril dimension was about 100 nm. The disruption of tertiary structural organization was thus clear, yet the question of possible alterations of the lateral dimensions of individual crystallites remained unanswered because of insufficient resolution.

The more dramatic spectral changes in Figure 6 are caused by strong acid hydrolysis, rather than beating. Spectra 6D and 6E appear to be "sharper-featured" (more crystalline) versions of the higher plant cellulose spectra (see Figures 2, 3 and 5). There is a dominant upfield shoulder at C4 compared to the downfield shoulder; the central component of C1 is also greatly reduced. The hydrolysis, however, is harsh and a mass loss of 78-88% raises questions about the corresponding changes in lateral crystallite dimensions. If the resonance multiplicity were due, in part, to surface chains, then changes in the lateral dimensions of the crystallites would affect the multiplet intensities. An electron microscopic investigation (21) of the lateral dimensions of sonicated and dispersed individual crystallites showed no significant difference between the celluloses corresponding to spectra 6A and 6E; the lateral dimensions average 20 nm in both cases. The narrower linewidths in spectrum 6E compared with 5A provide additional qualitative support that the average lateral dimensions of the crystallites in the hydrolyzed Cladophora cellulose are substantially greater than those in cotton linters

(3.5-5 nm) (4-6) and that the sampling of the crystallites in the electron microscopic investigation is representative of the whole material. Thus, the spectral differences between Figures 6A and 6E cannot arise from changes in the number of chains on the crystal surfaces. It follows that the spectra of Figure 6 strongly reinforce the hypothesis that multiple crystalline forms coexist in *Cladophora* cellulose. Furthermore, they suggest that the I_{α} form is more susceptible to hydrolysis than the I_{β} form or the I_{α} form, for morphological reasons, is more exposed to the acid attack.

Methods for Emphasizing Resonance Intensity from Carbons in the Crystalline Interior. The experiments described in this section explore further the possibility that ordered surface layers on crystallites might give rise to sharp resonances, although strong arguments to the contrary have already been given. If one could suppress those resonances arising from crystallite surfaces, then one could isolate the resonance profile corresponding to the true interior unit cell(s) and directly address the question of crystalline polymorphy.

The key assumption in the following experimental approaches is that a chain at the crystalline surface experiences less well-defined, and, on average, weaker intermolecular potentials than an interior crystalline chain. Hence, the surface chain will have a greater molecular mobility and its spins will undergo relaxation more efficiently.

If one further assumes that each nucleus relaxes independently, then one can enhance resonances arising from the crystalline core by isolating those signals corresponding to the most slowly relaxing spins. Observation of ^{13}C spins only need not limit the study to relaxation characteristics of carbons since the use of CP for ^{13}C signal generation also gives signals proportional to proton polarization levels (25). Thus, proton relaxation may also be monitored indirectly.

Two questions must be considered when attempting to isolate the crystalline core ^{13}C spectrum. First, do both protons and ^{13}C nuclei relax independently? Second, which relaxation parameter will offer the highest contrast between surface and interior resonances?

Observations based on proton spin diffusion. Protons, by virtue of their 100% natural abundance are strongly coupled to one another by dipolar coupling. This coupling gives rise to spin exchange which, in turn results in spin diffusion (39) whereby magnetization is transported in a diffusion-like process. When protons are quantized along the static field, a diffusion constant of about $5 \times 10^{-12} \text{ cm}^2/\text{s}$ is appropriate for cellulose (40); in the presence of a strong, resonant proton rf field, the diffusion constant is halved. We find that the longitudinal and rotating frame relaxation times ($T_{1\text{H}}$ and $T_{1\text{H}}$) in cellulose are respectively in the ranges of 0.5-1.0s and 15-120ms. Proton spin diffusion will thus maintain very uniform spin polarization levels during a $T_{1\text{H}}$ recovery so that monitoring ^{13}C spectra as a function

of proton recovery time will not reveal any contrast in intensity between surface and interior chains. On the other hand, times like 15-20ms, which are typical (41) values for $T_{1\rho}^H$ in higher plant celluloses are comparable to times expected for magnetization transport across a crystallite 3.5-5 nm in lateral dimension (42,43). Therefore, if one obtains CP spectra using a fixed CP time applied at the end of a variable proton spin-locking time, the core crystalline resonances would be enhanced at longer spin-locking times. However, the spectra would never be entirely free of the surface resonances. (A superior experiment and one which we did not do because of its technical difficulty is to monitor the CP spectrum following a period of relaxation under multiple pulse (43,44). The multiple pulse irradiation simultaneously attenuates spin diffusion very strongly.)

Figure 7 shows spectra of hydrocellulose obtained from cotton linters using a CP time of 0.5 ms. For spectrum A the spin locking time prior to CP was 0.01 ms while in spectrum B it was 25 ms. The 'A-B' spectrum shows that the shapes of the C4 crystalline resonances in A and B are indistinguishable in spite of the proton magnetization gradient between the surface and the interior of the crystallites. The existence of this gradient is confirmed by the preferential reduction of the broad resonances in B relative to A. Most of the intensity in these broad resonances in the hydrocellulose, we believe, arises from crystal surface chains, although alternative interpretations have been proposed (36), namely, that all intensity in the wings of C4 and C6 arises from non-crystalline carbons. In support of our point of view, we note the contrast in shape between this difference spectrum in Figure 7 and that of Figure 5C, particularly in the C2,3,5 region. In cotton linters the C2,3,5 carbons in three-dimensionally disordered regions contribute to the single broad resonance; but these regions are attacked preferentially during hydrolysis. In the difference spectrum of Figure 7, the C2,3,5 resonance region has much more definition as one might expect from more ordered surface chains. The other difference spectrum at the bottom of Figure 7 indicates that there is no further lineshape change occurring for spin-locking times longer than 15 ms. Stabilization of the lineshape by proton spin diffusion at about 15 ms is quite consistent with expectations (42) if most of the disordered, more mobile material were on the surface of crystallites whose lateral dimensions were in the 3.5-5 nm range. Thus, under the assumption that the surface chain protons have shorter intrinsic $T_{1\rho}^H$ values than do the interior chain protons, these results indicate that the shape of the C4 resonance contains no sharper features (in the range from 88-92 ppm) associated with surface chains. Also, since the proton polarization is not expected to vary appreciably over dimensions of monomer units, the resonance profiles for each carbon in the difference spectrum arise from the same spatial regions. Therefore, the monomer units which give rise to the broad C4 resonance also produce a corresponding contribution to the central region of the C1 resonance.

A similar $T_{1\rho}^H$ experiment was conducted on algal cellulose from Rhizoclonium. Figure 8 shows these results and the difference spectrum. Because the lateral crystallite dimension in Rhizoclonium is 25-30 nm, the contrast, after an extended period of spin-locking, between average proton magnetization at the surface and in the crystallite interior can become larger than in hydrocellulose, even though the apparent $T_{1\rho}^H$ increases fivefold to about 100 ms. Nevertheless, no change in the C4 lineshape is observed as a function of spin-locking time. Again we conclude that surface resonances are not contributing to the fine structure at C4. In fact, none of the sharp resonances seem to change relative intensity with spin locking times. The implication is that these sharp features are the expression of the true unit cell(s).

Observations based on ^{13}C longitudinal relaxation with spin exchange. Depending on the type of native cellulose, the ^{13}C longitudinal relaxation time, T_{1C} , for each crystalline carbon at 50 MHz can become quite long. In hydrocellulose, for example, crystalline T_{1C} 's are of the order of 200s (45) while in the algal celluloses we find that corresponding T_{1C} 's are closer to 1000s. Thus, the T_{1C} 's in these systems are sufficiently long to allow some ^{13}C - ^{13}C spin exchange to occur.

The influence of ^{13}C spin exchange on T_{1C} is non-existent when all carbons have the same intrinsic relaxation time. However, at 50MHz the T_{1C} values for the broad resonance of C6 are less than 1s and the T_{1C} for the broad resonance of C4 is about 10-20s (45). A fraction of faster relaxing intensity, comparable to that at C4, is also visible in the other resonances at C1 and C2,3,5. If one assumes that most of this faster relaxation is occurring at the crystalline surface and in 3-dimensional regions of disorder, then, by ^{13}C spin exchange, crystalline carbons about 1 nm from the surface will also relax more efficiently. Therefore, the most slowly relaxing carbons in a T_{1C} experiment will be those associated with the crystalline core.

Figures 9 and 10 show spectra of cotton hydrocellulose and cellulose from Cladophora, respectively, as a function of delay time in Torchia's T_{1C} method (31). At longer delay times, these spectra represent the ^{13}C nuclei not yet relaxed. The disappearance of the broad features and the slight sharpening of the crystalline resonances are consistent with an enhancement of the crystalline core resonances since the most highly ordered chains should produce the sharpest resonances (22).

Figure 9 raises an important question concerning crystalline polymorphism in the native celluloses. The hypothesis that higher plant celluloses like cotton and ramie are crystalline composites was suggested, in part, by the outer doublet and the sharper central feature of the C1 resonance in spectrum 9A. However, comparison of spectra 9A and 9C shows the central peak at C1 to be less intense at 200s compared with 1 ms, while the shape of the crystalline resonance at C4 remains constant. Since carbons C1-C5 relax at very nearly the same rates (32) in a T_{1C} experiment, it is very likely that the signals for each of these carbons in

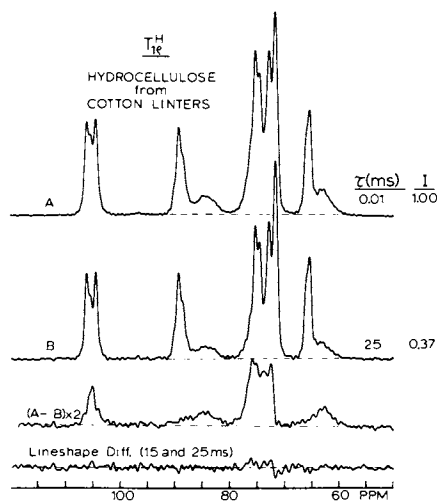


Figure 7. CP-MAS spectra of cotton hydrocellulose following the two indicated periods of proton spin locking; the CP time was 0.5 ms. Spectrum B is renormalized to match the intensity in A for the crystalline C4 resonance; true total intensities are also given. The difference spectrum, (A-B), shows the profile of resonances with shorter $T_{1\rho}$ values. The lower lineshape involving the spectrum (not shown) with a 15 ms proton spin lock, indicates that there are no further lineshape changes after 15 ms of spin locking.

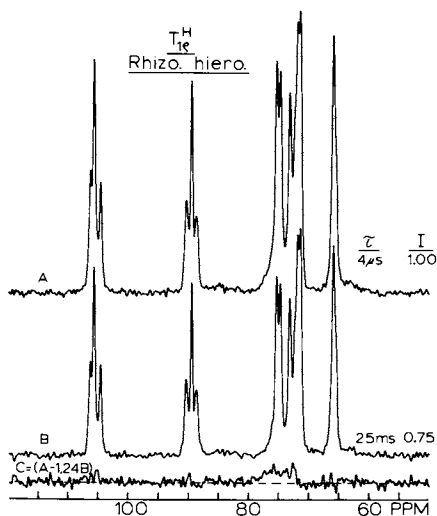


Figure 8. CP-MAS spectra of the highly crystalline algal cellulose, Rhizoclonium hieroglyphicum as a function of proton spin locking time.

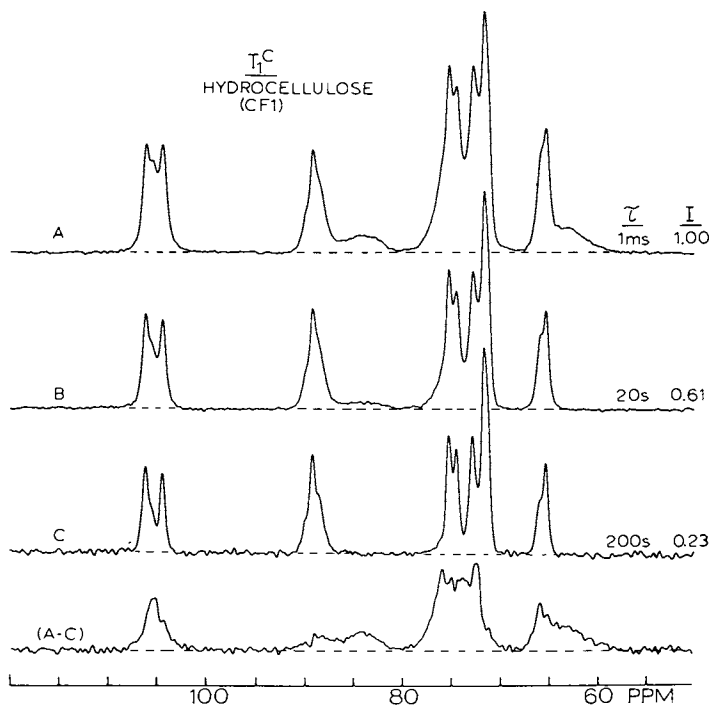


Figure 9. CP-MAS spectra of hydrocellulose from cotton linters as a function of the indicated delay time in a T_1^C experiment [Ref. 31].

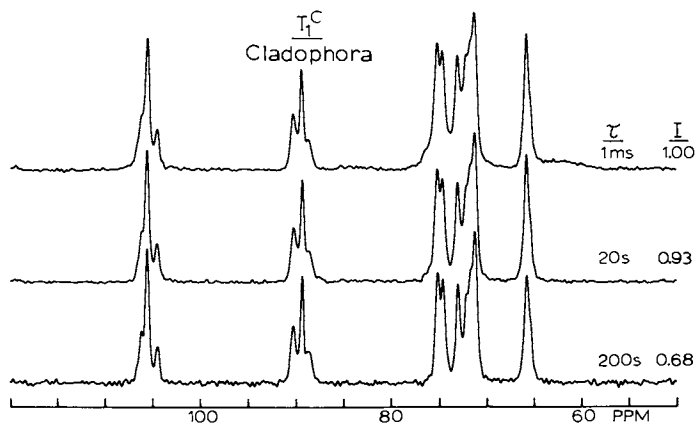


Figure 10. CP-MAS spectra of Cladophora cellulose as a function of the indicated delay times in a T_1^C experiment. Total intensities are also given.

spectrum 9C arise from the same spatial regions. Thus, the composite hypothesis would lead one to expect a smaller downfield shoulder at C4 than is observed in Figure 9C. The difference spectrum, A-C, is very similar to the difference spectrum in Figure 7 and shows that the change of shape at C1 does not involve any particularly sharp component; in fact, the corresponding resonance change at C4 involves the broad upfield shoulder. Therefore, the lineshape change at C1 is attributed to anhydroglucose residues in disordered regions, probably including the crystal surface. This leaves less of the central resonance intensity at C1 which can be ascribed to the presence of the I_{α} phase. If there is an I_{α} crystalline polymorph present, it is of the order of 15% or less.

Since we believe that spectrum 9C, in all regions except C6, possesses undistorted relative intensities whose dominant contributions arise from chains in the crystalline core, the following alternative interpretation must be considered: (a) The originally postulated (1-3) I_{α} phase in cotton or ramie is no more than a minor component. (b) Because the downfield shoulder of C4 and the central component of C1 are becoming comparable in intensity, the originally suggested spectrum of the I_{β} form may not be accurate (see Figure 1) since the intensity of the C1 resonance in the I_{α} phase should be twice that of the downfield shoulder of C4. (c) Because of (b) the possibility exists that Figure 9C is the correct I_{β} lineshape (except in the C6 region). (d) If Figure 9C represents the true I_{β} lineshape, then the multiplet ratios of C4 require that the unit cell must contain more than four anhydroglucose units in order to generate these intensity profiles. (e) The C4 crystalline resonance (88-92 ppm) in spectrum 9A is a good indicator of the number of carbons at each magnetically distinct site in the unit cell.

In contrast to the difference in the behavior of the C1 and C4 lineshapes for cotton hydrocellulose in Figure 9, the changes in lineshape for Cladophora cellulose in Figure 10 are very minor. Since the crystallite width in Cladophora cellulose is about 20 nm (21), the intensity change related to crystal surface resonances is expected to be reduced. Thus, the principal changes between spectra 10A and 10C involve a slight sharpening of the resonances in spectrum 10C and a disappearance of the weak, broad C4 and C6 wings. All the celluloses represented in Figure 4 showed similar T_1^C behavior. Again, we interpret spectrum 10C as arising principally, from chains in the crystalline interior. In Figure 10 there is no anomalously fast decay associated with the sharp central feature of C1 as there was in Figure 9. The overall decay of intensity for Cladophora cellulose during the 200s was 32% compared with 77% for the hydrocellulose in Figure 9. Much of this difference in extent of decay can be explained by the larger crystallites in Cladophora cellulose, the associated reduction in the number of more mobile surface chains and the diminished opportunity for spin exchange with these surface chains.

Figure 10 indicates that: (a) If two allomorphs coexist in the Cladophora cellulose, the T_1^C behavior of both allomorphs is the same. (b) If the reduction of intensity in the T_1^C

experiments is principally due to ^{13}C - ^{13}C spin exchange with surface chains, then the stability of the lineshapes in Figure 10 suggests that the surface-to-volume ratios, or the lateral dimensions of the I_α and I_β crystallites are comparable. (c) The resonance profiles, especially for C4 (88-92 ppm), in spectrum 10A give a good indication of the relative number of carbons at each of the magnetically inequivalent sites in the unit cell(s).

Isolation of Spectra from Carbons Within 0.7-1.0 nm of a Carbon in a Single Multiplet Line. ^{13}C - ^{13}C spin exchange is quite slow in a natural abundance sample when proton decoupling is absent. The rate of exchange depends, among other things, on the inverse sixth power of the ^{13}C - ^{13}C internuclear distance (39,46). At natural abundance, these distances are statistically determined; moreover, the nearest ^{13}C neighbors to a given carbon, say C1, will generally not be C1 carbons. Because a more complete treatment of this experiment and its interpretation will appear elsewhere (32), we will simply take a descriptive approach.

Isolation of the spectra of neighboring ^{13}C nuclei is as follows: a) The Zeeman population of one line within a multiplet is perturbed using the Dante (28,29) sequence. b) After the perturbation a 50s-70s mixing time follows during which magnetization changes occur due to both T_1^{C} processes and ^{13}C - ^{13}C spin exchange. c) The spin exchange and the T_1^{C} effects are monitored independently to isolate the 'near-neighbor' spectra associated only with those carbons which have undergone spin exchange as a result of the original perturbation.

These 'near-neighbor' spectra arise from carbons primarily lying within a radius of 0.7-1.0 nm from the perturbed carbons (32). Such 'near-neighbor' spectra are a simultaneous test of the alternate explanations for the observed differences in native cellulose spectra, namely, that some sharp spectral features originate from chains on crystallite surfaces or that ABMS effects give rise to sharp features because of special tertiary morphology. The choice of the perturbed line is based on the I_α and I_β spectra of Figure 1 such that the perturbed line belongs either to the I_α or I_β spectrum. For this purpose, the C1 and C4 resonances are best since there is significant overlap elsewhere.

Figure 11 illustrates the application of this technique to a sample of Rhizoclonium cellulose. Spectrum 11A and 11B are different only in that the low-level 'comb' of ^{13}C Dante pulses is absent (11A) or present (11B). Proton decoupling was applied for 20ms during the Dante sequence; this decoupling was also present in the experiment without the Dante pulses in order to make comparison between these two experiments most meaningful. The 3ms interval indicated in Figure 11 refers to the period between the end of the Dante pulses and the beginning of signal observation. Spectra 11C and 11D are pairs similar to 11A and 11B except that the mixing time was 70s instead of 3ms. Spectra 11E-11G are each difference spectra based on spectra 11A-11D. Spectrum 11E represents the profile of the original population disturbance produced principally at the central C1 multiplet in Rhizoclonium cellulose (an ' I_α ' perturbation ~ see

Figure 1). Spectrum 11F is the 'near-neighbor' spectrum which also includes a rather large peak corresponding to the C1 sites which have not yet exchanged. Figure 11G is a more amplified (x2) near-neighbor spectrum obtained by subtracting a portion of spectrum 11E from 11F in order to decrease the intensity in the central C1 region and also look for possible 'near-neighbor' lines corresponding to the outer wings of the C1 resonance which are thought to belong to the I_{β} allomorph. In other words, spectrum 11G tests whether the profile of the C1 resonance has changed as a result of ^{13}C - ^{13}C spin exchange with other C1 multiplets. The lack of wing intensity at C1 argues against the suggestion of Cael, et al. (47) that the central resonance of C1 belongs to a unit cell possessing a 1:2:1 triplet.

Several conclusions may be drawn from Figure 11. First, this Dante sequence is quite selective. Spectrum 11E shows that the population disturbance is centered quite well on the central C1 multiplet. Second, the 'near-neighbor' spectrum may be isolated (Spectrum 11F) and even tested for spin exchange within the C1 multiplet (spectrum 11G). Third, given that the perturbation is thought to be an ' I_{α} ' perturbation (see Figure 1), the 'near-neighbor' spectrum contains many characteristics typical of an I_{α} -rich spectrum, i.e. weak C1 doublets, a strong downfield shoulder at C4, and a sharp maximum at the correct position for C6. The profile of the C2,3,5 region deviates somewhat from the I_{α} spectrum of Figure 1; however, this region in Figure 1 has a substantial non-crystalline contribution and a lower intrinsic resolution which makes comparison more difficult. Qualitatively, the departure of the 'near-neighbor' spectrum (11G) from the parent spectrum (11A) supports the idea of crystalline polymorphy. Fourth, from a qualitative point of view, ^{13}C - ^{13}C spin exchange seems quite uniform in the sense that the 'near-neighbor' spectra have intensities at C4 and C2,3,5 which are in the ratio 1:3 with C6 being slightly less intense (80% of C4 intensity), as expected. Moreover, the total intensity in spectrum 11F was found to be 90% of the total intensity in spectrum 11E which corresponds quite well with expectations based on the 15% decay over 70s of the central C1 multiplet due to T_1^{C} processes (spectra 11A and 11C). This agreement ensures that the 'near-neighbor' spectrum is not due to a change in spectrometer characteristics. The ratio of the C1 intensity to the total intensity in spectrum 11F indicates that slightly more than half of the intensity at C1 in spectrum 11E has, over 70s, made its way to other carbon sites via ^{13}C - ^{13}C spin exchange. Fifth, most of the multiplet lines seen in the parent spectrum (11A) are also seen in the 'near-neighbor' spectrum (11F, 11G). It follows that ABMS effects are probably insignificant (this is shown more rigorously later).

In order to demonstrate crystalline polymorphy more fully, Figure 12 shows the results of three Rhizoclonium cellulose experiments, like those of Figure 11, in which three different lines were initially perturbed. Spectrum 12A is the parent spectrum (like spectrum 11A). The remaining six spectra, in pairs, consist of profiles of an original population perturbation (like spectrum 11E) caused by the Dante inversion followed by the

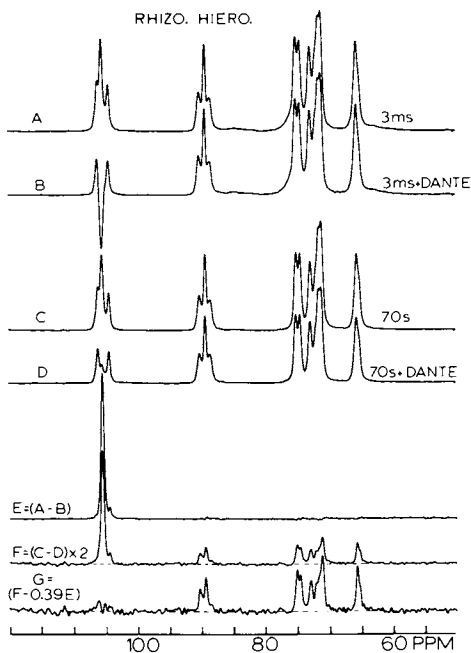


Figure 11. Spectral method for isolating the 'near-neighbor' spectrum of an I_{α} line in Rhizoclonium cellulose. The number of scans is 1200 for spectra A and B, 600 for C and D. See text for other details.

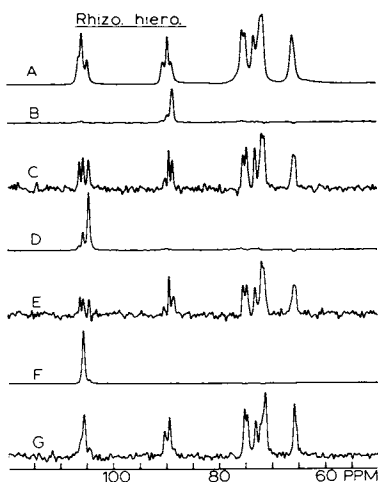


Figure 12. CP-MAS spectra of Rhizoclonium cellulose associated with three different 'near-neighbor' experiments.

corresponding 'near-neighbor' spectrum. The 'near-neighbor' spectra are like those of spectrum 11G except that a null in the position of the perturbed site is not sought; rather, an intensity comparable to the site intensities at the neighboring sites is left at the originally perturbed site, i.e. an 'equilibrium' spectrum is approximated. Spectra 12B and 12C as well as 12D and 12E correspond to ' I_{β} ' perturbations (see Figure 1) while spectra 12F and 12G correspond to the ' I_{α} ' perturbation of Figure 11. The Dante sequences used here are not ideal in their ability to select a multiplet line; there is some perturbation of the adjacent line as well. This non-ideality is more apparent when the perturbed line is weaker than the adjacent line as is the case in spectra 12C and 12E. In spite of this non-ideality, the 'near-neighbor' spectra resulting from these ' I_{β} ' perturbations are very similar to one another in resonance position and reasonably similar in intensity profiles. These two 'near-neighbor' spectra also show many features which indicate that the I_{β} content (see Figure 1) of each spectrum is much higher than in the parent spectrum (12A) as expected for a mixture of crystalline polymorphs. The strongly emphasized C1 doublet, the dominant upfield shoulder of C4, and the flatter profile for the C6 maximum are all consistent with an I_{β} -rich spectrum. These spectra stand in contrast to the previously discussed I_{α} -rich spectrum (12G). The upfield portion of the C2,3,5 resonances in the 'near-neighbor' spectra also follows expectations based on the spectra of Figure 1. The non-trivial central component of C1 in spectra 12C and 12E may be no accident since the results of Figure 9, as discussed earlier, may point to an I_{β} spectrum which includes a weak central C1 resonance.

A number of conclusions follow from Figure 12. These are: a) Assuming that the pure I_{α} and I_{β} spectra are given in Figure 1, an ' I_{α} ' or ' I_{β} ' initial perturbation yields a 'near-neighbor' spectrum which is richer, compared with the parent spectrum, in the corresponding ' I_{α} ' or ' I_{β} ' resonances. This is illustrated most clearly in the C4 crystalline resonance profiles of the 'near-neighbor' spectra. b) The two 'near-neighbor' spectra resulting from the I_{β} perturbation are very similar to one another indicating that the intensities in the 'near-neighbor' spectra are not very dependent on the line which is perturbed. c) The insignificance of ABMS shifts is indicated by the 'near-neighbor' spectrum, 12C. For if it is postulated that ABMS shifts appear in discrete bands (as opposed to a continuum) as a result of well-defined fibril patterns, and if unit cell multiplicity also exists, then the resonance profile for a given carbon is the convolution of the two effects. Since the origin of the ABMS effects is postulated to be the fibril packing geometry, the dimensions involved are much larger than the unit cell. This implies that all spectral lines associated with unit cell inequivalence are, within any given unit cell, shifted to the same extent as a result of ABMS effects; moreover, if two outer bands exist (e.g. for C1 and C4) each outer band must belong to a different set of ABMS-shifted sites. The fact that the 'near-neighbor' spectrum, 12C, resulting from the perturbation of

one outer C4 band shows spin-exchange with both outer C1 bands is, therefore, a contradiction of the original postulate since spin exchange is too slow to occur between fibrils. So ABMS effects and the importance of fibril geometry are dismissed as a possible cause of any multiplet character for all resonances. d) None of the minor resonances at C1 or C4 are exclusively due to surface chains because the crystallites in Rhizoclonium cellulose have lateral dimensions of the order of 25-30 nm; therefore, the total fraction of surface chains is less than 13%, considering both chains in a two chain unit cell at the crystalline surface to be surface chains. No minor resonance at C4 or C1 is as small as 13% in spectrum 12A. Moreover, the 'near-neighbor' spectra (12C and 12E) resulting from the perturbation of minor resonances at C4 and C1 indicate spatial proximity with carbons resonating at several multiplet lines of the unperturbed carbons (C1 or C4). These demonstrated proximities to carbons, if by hypothesis located at a crystal surface, multiplies the number of resonances associated with crystallite surfaces, and also thereby increases unreasonably the total intensity attributable to surface chains. e) The final conclusion based on Figure 12 is that the 'near-neighbor' spectra, while certainly becoming richer in the spectrum of the allomorph to which the perturbed carbon was thought to belong, still retain a significant contribution from the spectrum of the other allomorph. Part of the explanation for this lies in the slight non-ideality of the perturbation. However, judged by the pure I_{α} and I_{β} spectra of Figure 1, the ratios of I_{α} and I_{β} in the 'near-neighbor' spectra (Figures 12C, 12E, and 12G) do not agree particularly well with the apparent ratios deduced from the perturbation profiles (Figures 12B, 12D, and 12F). Thus, while crystalline polymorphism is strongly supported by the results, some details of the actual I_{α} and I_{β} spectra of Figure 1 are called into question. For example, the absence of a central component at C1 in the I_{β} spectrum is questioned. Also the absence of a weak downfield wing at C4 in the I_{β} spectrum and the absence of a weak C4 upfield wing in the I_{α} spectrum are questioned. Finally, the singlet character of C6 in the I_{α} spectrum is also questioned (see spectrum 12G). Admittedly, one of the original criteria we applied (1-3) in postulating the I_{α} and I_{β} spectra of Figure 1 was to minimize the number of magnetically inequivalent sites within the spectrum of each allomorph. In fact the results of both Figures 9 and 12 suggest that the unit cell of each allomorph may contain more than two magnetically inequivalent sites, hence, larger or less symmetric unit cells.

With regard to the question of whether the higher plant celluloses contain only one crystalline allomorph, namely, I_{β} , two ^{13}C spin exchange experiments were also carried out on hydrocellulose from cotton linters. Figure 13, which is in the same format as Figure 12, shows these results. For reasons of sensitivity, only a 50ms mixing time was used to generate the 'near-neighbor' spectra. This shorter mixing time reduces only slightly the spherical volume around the perturbed carbon probed by spin exchange. The two sites of perturbation are the central

resonance of C4 (spectra 13B and 13C) and the central resonance of C1 (spectra 13D and 13E). The central resonance of C4 is expected (see Figure 1) to belong equally to both the I_{α} and I_{β} allomorphs. Therefore, the corresponding 'near-neighbor' spectrum should give back both the I_{β} and any I_{α} contributions at C1. In spectrum 13C, there is no indication of a central feature at C1 although it is difficult to get sufficiently good signal-to-noise to eliminate a weak central component at C1. On the other hand, the 'near-neighbor' spectrum (13E) from the perturbation of the central C1 region consists of weaker resonances, compared with spectrum 13C; also the resonances seem rather broad and ill-defined. From Figure 9 we know that T_1^C in the central C1 region is shorter than for other crystalline resonances; therefore, spectrum 13E is weak. However, if there were an I_{α} component in the higher plant celluloses, then one might have expected some sharper resonance features associated with the I_{α} allomorph in spectrum 13E. Because of the rather poor signal-to-noise, sharper resonance features are difficult to identify. It is significant, however, that the 'near-neighbor' spectrum, 13E, contains some intensity in the regions of the crystalline C4 and C6 carbons. The results of Figure 13 together with those of Figure 9 leave open the distinct possibility that the higher plant celluloses represent a single crystalline allomorph whose crystalline spectrum is very much like that of Figures 9C or 13C. Then it would follow that the number of anhydroglucose units per unit cell is larger than four, (more than two chains per unit cell) judging by the intensities of the multiplet at C4. At the same time the presence of a small I_{α} fraction is still possible; however, it is doubtful that there is enough of the I_{α} present to account fully for the downfield wing of C4. Therefore, a unit cell with more than four inequivalent anhydroglucose units must be considered likely.

Finally, the question arises as to the true spectrum for each allomorph in native cellulose. Figure 14 shows candidate spectra for the I_{α} and I_{β} allomorphs based on linear combinations of the original and hydrolyzed *Cladophora* cellulose spectra of Figure 6A and 6E. These spectra are reproduced in spectra 14A and 14B. The latter spectrum strongly resembles the spectrum of the regenerated cellulose I which was originally used (1-3) as the I_{β} -rich spectrum for generating the I_{α} and I_{β} spectra. The spectrum of the regenerated cellulose I had inferior resolution compared with 14B, so it was not used. Figure 14C is the I_{α} spectrum and Figures 14D and 14E are two candidates for the I_{β} spectrum. Spectrum 14D is based on the original idea (1-3) that the I_{β} resonance at C1 is a doublet, whereas spectrum 14E considers the I_{β} spectrum to be that which duplicates the higher plant cellulose C4 and C1 crystalline resonances (see the discussions of Figures 9 and 13 above).

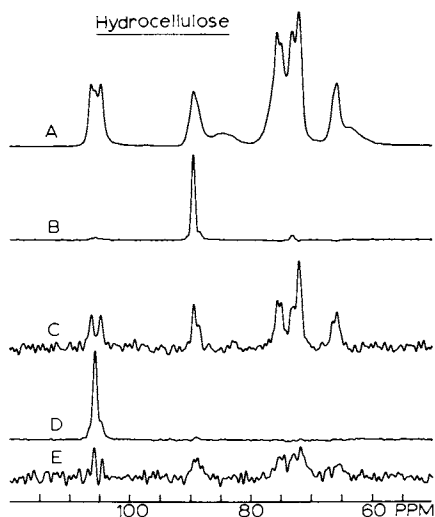


Figure 13. CP-MAS spectra of hydrocellulose from cotton linters associated with two 'near-neighbor' spectra obtained after 50s of spin exchange. The format is the same as in Figure 12.

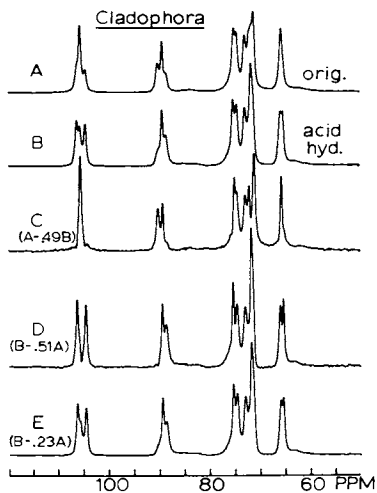


Figure 14. Candidates for I_{α} and I_{β} CP-MAS spectra based on the spectra of Cladophora (A) and acid hydrolyzed Cladophora (B) celluloses. Proportions of mixing for spectra C-E are indicated in the figures for the linear combination spectra, which are further renormalized to give the same total intensities as in A and B. Spectrum C is the I_{α} spectrum; spectrum D and E are two candidates for the I_{β} spectrum.

If spectra 14C and 14D are the true spectra of the I_{α} and I_{β} allomorphs, then, judging by the C4 and C6 resonances, each of the two unit cells contain only two equally-occupied magnetically inequivalent anhydroglucose sites. On the other hand, if spectrum 14E is the true I_{β} spectrum, then the intensity ratio at C4 implies a unit cell with at least three magnetically inequivalent sites in such a ratio as to require a unit cell with more than four anhydroglucose units. To entertain the notion of non-equivalent anhydroglucose units along any given chain (48-50) certainly seems appropriate in this context. The number of resonances in the C1 and C2,3,5 regions generally support the foregoing comments about magnetic inequivalence; these resonances, however, are less informative than the C4 and C6 resonances because the crystalline and the non-crystalline (or surface) carbon resonances at each site overlap strongly. One cannot easily improve the analysis for the C1 and C2,3,5 regions by isolating and subtracting the shape of the resonance which does not belong to the crystal. Evidence points to a variation from sample to sample in the shape of this resonance, presumably because the ratio of surface chains to chains in three-dimensionally disordered environments is sample dependent.

Summary

The hypothesis (1-3) that all native celluloses are a composite of two crystalline allomorphs, designated I_{α} and I_{β} , has been further tested using ^{13}C solid state NMR. In particular, two alternate origins of sharp resonance features were considered in addition to the usual origin, the crystalline unit cell. The first source is ordered layers on crystal surfaces; the second is possible anisotropic bulk magnetic susceptibility (ABMS) shifts associated with well defined fibril patterns (tertiary morphology).

A survey of several native celluloses reinforced the similarity of the higher plant celluloses to one another, although limits of resolution and questions of chemical purity in the cellulose chains make comparison difficult and less meaningful. A parallel survey of NMR spectra from the more chemically pure algal celluloses and the bacterial cellulose, *Acetobacter xylinum*, indicated a general uniformity, albeit these spectra were distinct from the spectra of the higher plant celluloses. These algal cellulose spectra, however, showed small variations, outside of experimental error, which were taken as evidence for crystalline polymorphy.

Exposure of cotton linters to acid hydrolysis did not alter the I_{α} to I_{β} ratios, judging by the C4 resonance profile. On the other hand, exposure of the algal cellulose from *Cladophora* to mechanical beating and/or strong acid hydrolysis caused changes in the NMR spectra, which, in the crystalline composite model, would be interpreted as enriching the I_{β} content of the spectra. Acid hydrolysis was more effective than beating in changing the apparent I_{α} to I_{β} ratio. Whether the enrichment of the I_{β} content by beating was accomplished via a differential mass recovery or an actual conversion of one allomorph to the other is not clear. The

acid hydrolysis, on the other hand, was harsh and material recovery was only 12-22%. Therefore, the differences in rates of hydrolysis between the I_{α} and I_{β} allomorphs may not be large. It is possible that differences in hydrolysis rates are related to morphology and the physical access of the acid to the crystallites rather than a greater inherent resistance to hydrolysis of the I_{β} allomorph. However, an important observation is that sonicated and dispersed individual crystallites from the extensively hydrolyzed cellulose did not show, by electron microscopy, any reduction in cross-sectional area compared to the original cellulose crystallites; therefore, spectral changes resulted from a selection process rather than from an alteration of the surface-to-volume ratio of crystallites. The NMR spectrum of the hydrolyzed algal cellulose strongly resembled the spectra of the higher plant celluloses, except for the much better resolution in the former spectrum. (The improved resolution is very consistent with a much greater lateral crystallite dimension.) The similarity, except for resolution, of the multiplet intensities in spectra of the hydrolyzed *Cladophora* (Figure 6E) and of the higher plant celluloses (Figure 7B) is strong evidence that ordered layers on crystal surfaces are not responsible for the multiplet intensity patterns, particularly at C4, in the higher plant cellulose spectra. Or, from a different perspective, the similarity of these spectra supports the existence of a crystal structure associated with the higher plant celluloses, i.e., the small crystallite width does not lead to a more statistical assembly of chains.

A set of experiments aimed at enhancing the core crystalline resonances over the crystalline surface chain resonances was also undertaken. The approaches, which utilized $T_{1\rho}^H$ and T_1^C relaxation behavior, were predicated on the existence of greater molecular mobility (enhanced relaxation rates) for chains at the crystal surface relative to the crystallite interior. Strong proton-proton spin exchange during $T_{1\rho}^H$ relaxation blurs somewhat the differences between surface chain and interior chain relaxation; nevertheless, this approach has the advantage that the ^{13}C CP spectra, taken as a function of the $T_{1\rho}^H$ decay, have undistorted intensities over dimensions of monomer units. On the other hand, T_1^C relaxation is much more a function of the individual carbons; ^{13}C - ^{13}C spin-exchange is weak. Therefore one has an excellent opportunity to see differential effects due to molecular mobility variations. In this case, it is not obvious that spectra should retain undistorted relative intensities. Fortunately, however, and probably due to a combination of weak ^{13}C - ^{13}C spin exchange and the relative rigidity of the pyranose ring, the resonance profiles of carbons C1-C5 seem to be undistorted, i.e. on average, the C1-C5 carbons in the same spatial region give identical contributions to the observed intensity during a T_1^C decay. The important conclusions of these relaxation experiments are the following: If crystal surface chains are more mobile than interior chains so that the nuclei on the former chains relax more efficiently than their interior-chain counterparts, then: a) the C4 crystalline resonance profile is

unchanged (except for a slight sharpening of the multiplet lines) as one enhances the relative resonance contribution from the crystalline core. Therefore, C4 is the best indicator of multiplicity related to the true crystalline unit cell(s), i.e. surface-chain resonances do not make a significant contribution to the multiplet intensities there. b) The higher plant celluloses are seen to possess only a minimal I_{α} content (15% or less). In fact, the I_{α} content may be zero. If so, the true unit cell inequivalences, which are best expressed by the multiplet intensities within the C4 resonance profile, lead to a unit cell containing more than four anhydroglucose residues. Even with a 15% contribution from the I_{α} form, it is doubtful that the intensity of the downfield multiplet component of C4 could be fully accounted for. Therefore, the likelihood that the I_{β} crystalline form, which dominates the higher plant celluloses, has more than four anhydroglucose residues per unit cell is very high. c) The algal celluloses display no discernible change in multiplet relative intensities in a T_1^C experiment, thus it is concluded that, within the assumption stated above, carbons in each polymorph have equal average proximity to the crystallite surface. Normally this would mean that the two polymorphs were either intimately mixed or that the average lateral dimensions of the crystallites were the same. The differential response to hydrolysis of *Cladophora* cellulose eliminates the intimate mixing hypothesis, leaving only the latter conclusion.

A ^{13}C - ^{13}C spin exchange experiment was conducted on both a highly crystalline algal cellulose (*Rhizoclonium*) and on hydrocellulose from cotton linters. This experiment probed the resonance profiles of ^{13}C nuclei within, roughly, a 0.7-1.0 nm sphere surrounding a properly chosen, single resonance within a given multiplet. Spin populations of lines belonging to either the I_{α} or I_{β} crystalline phase were selectively perturbed and the 'near-neighbor' spectra of those carbons involved in subsequent ^{13}C - ^{13}C spin-exchange events were monitored. Qualitatively, the I_{α} perturbations in the algal cellulose gave rise to I_{α} -rich 'near-neighbor' spectra, compared with the original spectrum. Similarly, I_{β} perturbations yielded 'near-neighbor' spectra which were ' I_{β} -rich'. In this way different environments within the algal celluloses were clearly identified, thereby, strongly supporting the thesis of crystalline polymorphy in the algal celluloses. Some details about the originally proposed spectra are called into question by these results; nevertheless, the existence of crystalline polymorphy in the algal celluloses seems abundantly clear. On the other hand, the spin exchange experiments performed on cotton hydrocellulose failed to detect the presence of any I_{α} crystalline form, but the signal-to-noise levels were not adequate for eliminating the possibility of a minor amount of the I_{α} form. These results differ considerably from the suggestions offered by Cael, et al (47), who, in an attempt to rationalize x-ray structural work and NMR spectra, identified two NMR component spectra based on a 2-chain or an

8-chain unit cell. They argued that algal celluloses consist of pure 8-chain unit cells, whereas higher plant celluloses, like ramie, are mixtures of 2-chain and 8-chain unit cells.

Finally, an attempt is made to isolate the true I_{α} and I_{β} spectra, based on the original and hydrolyzed samples of Cladophora cellulose. Whereas the I_{α} spectrum is nearly identical to that originally proposed (1-3), the I_{β} spectrum is ambiguous and two possible spectra are proposed.

In contrast to the polymorphic algal and bacterial celluloses, which contain large fractions of the I_{α} and I_{β} polymorphs, the higher plant celluloses are dominated by the I_{β} crystalline form with only a minor, if any, I_{α} component. The shape of the C4 resonance in the higher plant celluloses is evidence, especially if no I_{α} component exists, of a unit cell containing more than four anhydroglucose residues. In view of these findings, the crystal structures of native cellulose based on Valonia cellulose should be reexamined, and assumptions about symmetry in the unit cell of the higher plant celluloses should be reconsidered.

Acknowledgment

We wish to express our profound thanks to Dr. J.-F. Revol of the Pulp and Paper Research Institute of Canada for his interest, discussions, and his willingness to characterize the lateral dimensions of crystallites in certain of the algal cellulose preparations.

Literature Cited

1. VanderHart, D. L.; Atalla, R. H. Preprints of the International Dissolving and Specialty Pulps Conference: Boston, 1983, p. 207.
2. Atalla, R. H.; VanderHart, D. L. Science 1984, 223, 283.
3. VanderHart, D. L.; Atalla, R. H. Macromolecules 1984, 17, 1465.
4. Frey-Wyssling, A.; Muhlethaler, K. Makromol. Chem. 1963, 62, 25.
5. Manley, R. St. J. J. Polym. Sci. Part A-2 1971, 9, 1025.
6. Blackwell, J.; Kolpak, F. J. Macromolecules 1975, 8, 322.
7. Lazaro, R.; Chiverina, J. Cell. Chem. Technol. 1973, 7, 269.
8. Roche, E.; Chanzy, H. Int. J. Biol. Macromol. 1981, 3, 201.
9. Goto, T.; Harada, H.; Saiki, H. Mokuzai Gakkaishi 1973, 19, 463.
10. VanderHart, D. L. Deductions about the Morphology of Wet and Wet Beaten Celluloses from Solid State ^{13}C NMR, NBSIR 82-2534.
11. Dudley, R. L.; Fyfe, C. A.; Stephenson, P. J.; Deslandes, Y.; Hamer, G. R.; Marchessault, R. H. J. Am. Chem. Soc. 1983, 105, 2469.
12. Wellard, H. J. J. Polym. Sci. 1954, 13, 471.
13. Honjo, G.; Watanabe, M. Nature 1958, 181, 326.
14. Meyer, K. H.; Misch, L. Helv. Chim. Acta. 1937, 20, 232.

15. Ellis, K. C.; Warwicker, J. O. J. Polym. Sci. 1962, 56, 339.
16. Gardener, K. H.; Blackwell, J. Biopolymers 1975, 14, 1581.
17. Sarko, A.; Muggli, R. Macromolecules 1974, 7, 486.
18. French, A. D. Carbohydr. Res. 1978, 61, 67.
19. Marrinan, H. J.; Mann, J. J. Polym. Sci. 1956, 21, 301.
20. Revol., J.-F.; Goring, D. A. I. Polymer 1983, 24, 1547.
21. Revol., J.-F., personal communication.
22. VanderHart, D. L.; Earl, W. L.; Garroway, A. N. J. Magn. Res. 1981, 44, 361.
23. Earl, W. L.; VanderHart, D. L. Macromolecules 1981, 14, 570.
24. Hartmann, S. R.; Hahn, E. L. Phys. Rev. 1962, 128, 2042.
25. Pines, A.; Gibby, M. G.; Waugh, J. S. J. Chem. Phys. 1973, 59, 569.
26. Andrew, E. R.; Bradbury, A.; Eades, R. G. Nature (London) 1958, 182, 1659.
27. Lowe, I. J. Phys. Rev. Lett. 1959, 2, 285.
28. Bodenhausen, G.; Freeman, R.; Morris, G. A. J. Magn. Res. 1976, 23, 171.
29. Morris, G. A.; Freeman, R. J. Magn. Res. 1978, 29, 433.
30. Caravatti, P.; Bodenhausen, G.; Ernst, R. R. J. Magn. Res. 1983, 55, 88.
31. Torchia, D. A. J. Magn. Res. 1978, 30, 613.
32. VanderHart, D. L. J. Magn. Res., in press.
33. Browning, B. L. Methods of Wood Chemistry; Interscience Publishers: New York, 1967.
34. Atalla, R. H.; Gast, J. C.; Sindorf, D. W.; Bartuska, V. J.; Maciel, G. E. J. Am. Chem. Soc. 1980, 102, 3249.
35. Earl, W. L.; VanderHart, D. L. J. Am. Chem. Soc. 1980, 102, 3251.
36. Horii, F., Hirai, A.; Kitamaru, R. Polym. Bull. 1982, 8, 1963.
37. Haigler, C. H.; Brown, R. M., Jr.; Benjamin, M. Science, 1980, 210, 903.
38. Nelson, M. L.; Tripp, V. W. J. Polym. Sci. 1953, 10, 577.
39. Abragam, A. Principles of Nuclear Magnetism; Oxford University Press: London, 1961.
40. Douglass, D. C.; Jones, G. P. J. Chem. Phys. 1966, 45, 956.
41. Horii, F.; Hirai, A.; Kitamaru, R. J. Carbohydr. Chem. 1984, 3, 641.
42. Packer, K. J.; Pope, J. M.; Young, R. R.; Cudby, M. E. A., J. Polym. Sci. Polym. Phys. Ed. 1984, 22, 589.
43. Havens, J. R.; VanderHart, D. L. Macromolecules 1985, 18, 1663.
44. Vega, A. J.; Vaughan, R. W. J. Chem. Phys. 1978, 68, 1958.
45. Teeäär, R.; Lippmaa, E. Polym. Bull. 1984, 12, 315.
46. VanderHart, D. L.; Garroway, A. N. J. Chem. Phys. 1979, 71, 2773.
47. Cael, J. J.; Kwoh, D. L. W.; Bhattacharjee, S. S.; Patt, S. L. Macromolecules 1985, 18, 821.
48. Atalla, R. H. Adv. Chem. Ser. 1979, No. 181, p. 55.

49. Atalla, R. H. Proceedings at the International Symposium on Wood and Pulping Chemistry, Stockholm, June 1981.
50. Atalla, R. H. Proceedings at the 9th Cellulose Conference, May 1982.

RECEIVED March 20, 1987

Chapter 6

Cross-Polarization-Magic Angle Spinning Carbon-13 NMR Approach to the Structural Analysis of Cellulose

F. Horii, A. Hirai, and R. Kitamaru

Institute for Chemical Research, Kyoto University, Uji, Kyoto 611, Japan

CP/MAS ^{13}C NMR approach has been described to characterize molecular chain conformations and crystal structures of native and regenerated cellulose samples in the dry and hydrated states. First, ^{13}C isotropic chemical shifts in the solid state are correlated to torsion angles ϕ and ψ in the β -1,4-glycosidic linkage and χ about the exo-cyclic C5-C6 bond, respectively. On the other hand, the contributions of the crystalline and noncrystalline components to the CP/MAS ^{13}C NMR results are critically analyzed in terms of the differences in ^{13}C chemical shifts and spin-lattice relaxation times T_1 and spectra of the respective components are recorded separately. Finally, the crystal structure and molecular chain conformations characteristic for native and regenerated celluloses are discussed.

Cellulose is a macromolecule of D-glucoses which are joined by β -1,4-glycosidic linkages. Since each glucose residue adopts preferably the rigid $^4\text{C}_1$ conformation, the molecular chain conformation of cellulose is simply defined in terms of torsion angles ϕ and ψ about C1-O and O-C4 bonds in the β -1,4-glycosidic linkage (see Figure 5). In addition, the orientation of the side CH_2OH group depends on the torsion angle χ about the exo-cyclic C5-C6 bond. Therefore, if these torsion angles are known by an appropriate analyzing technique, we can directly describe the molecular chain conformation by using these parameters instead of average parameters such as radius of gyration.

This work is a new approach to determine the torsion angles by ^{13}C isotropic chemical shifts obtained by solid-state high-resolution ^{13}C NMR spectroscopy and to characterize the complicated chain conformation of cellulose in the crystalline and noncrystalline regions. However, the ^{13}C chemical shifts obtained in the solid state are also influenced by the interatomic contribution, so-called packing effect, as well as hydrogen bonding. Therefore, we first show the relationships between ^{13}C chemical shifts and torsion angles

0097-6156/87/0340-0119\$06.00/0
© 1987 American Chemical Society

in cases of monosaccharides and disaccharides relating to cellulose and also discuss the effects of the packing and hydrogen bonding on the chemical shifts. Next, we show that cross-polarization/magic angle spinning (CP/MAS) ^{13}C NMR spectra of dry and hydrated celluloses contain the contributions of the crystalline and noncrystalline components and that the spectra of both components can be separately recorded by using the difference in ^{13}C spin-lattice relaxation time T_1 . Finally, we discuss the molecular chain conformations and crystal structure of cellulose on the basis of these results.

Experimental

Samples. Celluloses, monosaccharides, and disaccharides used in this work were prepared by the methods described elsewhere(1-3). One part of each cellulose sample was well dried at 50°C under vacuum for 2-3 days before and after packing in a conventional MAS rotor. Another part of each dried sample was exposed to atmospheres of different relative humidities at 20°C for a week, packed in a MAS rotor with an O-ring seal which is shown below, and then allowed to equilibrate in the same atmospheres for a few more days(4). Some samples were soaked in deionized water at room temperature for 24 hr and then packed in the rotors.

CP/MAS ^{13}C NMR Measurements. CP/MAS ^{13}C NMR experiments were performed at room temperature by a JEOL JNM-FX200 spectrometer equipped with a CP/MAS unit operating at 4.7 T. The Hartmann-Hahn matched field strength $\gamma\text{B}_1/2\pi$ of 69 kHz was applied to ^{13}C and ^1H nuclei and the ^1H rf strength was reduced to 54 kHz during ^1H - ^{13}C dipolar decoupling. Pulse waiting time after the acquisition of an FID was 10-15 s, which was at least more than 5 times of the ^1H T_1 for each sample. Magic-angle spinning was carried out at a rate of 3.2-3.5 kHz for both dry and hydrated samples. In order to keep water in the rotor during sample spinning at such a high rate, we have developed a new rotor with an O-ring seal, which is shown in Figure 1, by modifying a conventional bullet-type rotor of poly(chlorotrifluoroethylene) (4,5). This type of rotor can be steadily rotated without practical loss of water for samples with any water content. Such high performance is so enough even for one-week measurements that ^{13}C T_1 values, which are normally of the order of 10-1000 s for crystalline components of polymers, are able to be obtained. ^{13}C chemical shifts relative to tetramethylsilane (Me_4Si) were determined using a narrow crystalline line at 33.6 ppm of a small chip of linear polyethylene inserted in each sample.

Results and Discussion

1. ^{13}C Chemical Shifts-Torsion Angles Relationships.

Figure 2 shows CP/MAS ^{13}C NMR spectra of α -D-glucose, α -D-glucose $\cdot\text{H}_2\text{O}$, and β -D-glucose crystals together with the spectrum of D 2 glucose in D $_2$ O(2). Since α - and β -anomers coexist in solution, many resonance lines corresponding to both anomers can be observed(6). On the other hand, each crystal spectrum contains a group of resonance lines corresponding to those of

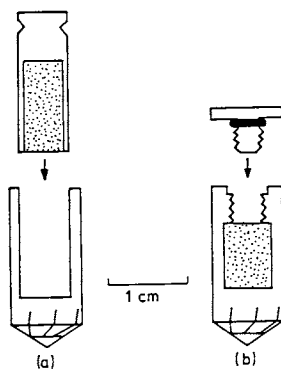


Figure 1 Schematic diagrams of MAS rotors. (a) conventional rotor; (b) newly developed rotor with an O-ring seal. (Reproduced from Ref.4. Copyright 1985 Academia Republicii Socialiste Romania.)

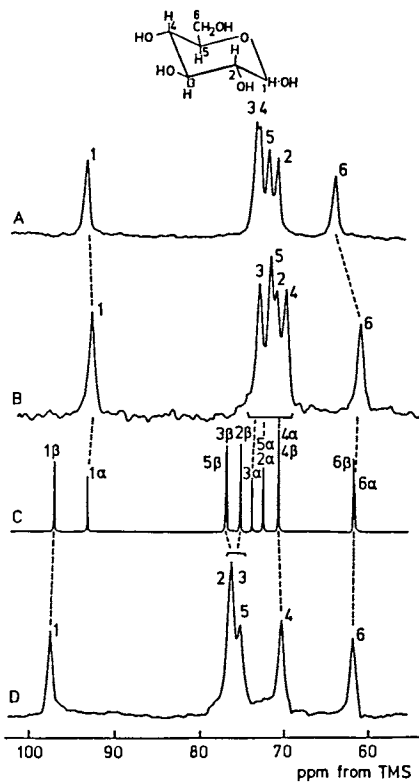


Figure 2 25 MHz CP/MAS and scalar-decoupled ^{13}C NMR spectra of D-glucoses. A: α -D-glucose crystal, B: α -D-glucose \cdot H_2O crystal, C: D-glucose in D_2O solution, D: β -D-glucose.

either anomer as shown by broken lines in Figure 2, where the respective lines of each crystal were assigned according to Pfeffer et al(7,8). It has therefore been found that each crystal is composed of either pure anomer.

The C6 line of the α -D-glucose crystal undergoes a large downfield shift of 2.4-2.9 ppm in comparison to C6 lines of the α -D-glucose \cdot H₂O as well as the β -D-glucose crystal and their solution. According to x-ray analyses(9-11), the conformations of the CH₂OH groups about the C5-C6 bond are gauche-trans for the α -D-glucose and gauche-gauche for the α -D-glucose \cdot H₂O and β -D-glucose, respectively. Here, for example, gauche-trans indicates that the C6-O6 bond is gauche to the C5-O5 bond and trans to the C4-C5 bond. It is, therefore, assumed that the large downfield shift appearing in the C6 line of the α -D-glucose crystal is correlated to the gauche-trans conformation, while the chemical shifts of the other crystals is correlated to the gauche-gauche conformation.

In order to verify this assumption, the chemical shifts of the C6 carbons of glucoses and glucose residues of different disaccharides are plotted in Figure 3(2,3,12) against torsion angles χ about the C5-C6 bonds which were obtained by x-ray crystal analyses(9-11). It is known from a recent survey(13) that the CH₂OH groups of low-molecular-weight glucosides preferably adopt two conformations of gauche-gauche and gauche-trans. The orientation of the trans-gauche must be sterically hindered due to the intramolecular interaction between two OH groups which are connected to the C4 and C6 carbons. Therefore, the result of cellulose I crystal which is described later is also plotted, because this is the only one case of the trans-gauche conformation. In native cellulose this conformation may be possible owing to hydrogen bonds associated with the CH₂OH group. As seen in Figure 3, the chemical shift for this unfavorable conformation is very large compared to the values for the other conformations. As a result, there seems to exist a simple linear relationship between the chemical shifts and torsion angles χ , although the chemical shift must be abruptly decreased for torsion angles close to 360°. According to these results, three preferred conformations, gauche-gauche, gauche-trans, and trans-gauche, are well correlated to the chemical shifts of 61-62 ppm, 62.7-64.5 ppm, and about 66 ppm, respectively.

Figure 4 shows similar relationships between ¹³C chemical shifts of C1 and C4 lines and torsion angles ϕ and ψ in different disaccharides containing β -1,4-glycosidic linkages, respectively(3,12). The chemical shifts of the crystalline components of cellulose samples which are shown later are also plotted against the corresponding ϕ and ψ values. In the celluloses two or three different chemical shifts obtained are plotted against the same ϕ and ψ values except for ramie, because the single values of ϕ and ψ have been reported by x-ray crystal analyses(14-17) irrespective of the observation of the multiple chemical shifts. Although the data are somewhat scattered, the chemical shifts of C1 and C4 carbons can be also well correlated to the torsion angles ϕ and ψ , respectively.

The origin of the scattering of the data seen in Figures 3 and 4 is not clear at present. However, as described in Introduction, ¹³C chemical shifts also depend on the effects of packing and hydrogen bonding. For example, the resonance line of central CH₂ carbons of triclinic n-C₂₀H₄₂ crystals is shifted about 1.3 ppm downfield

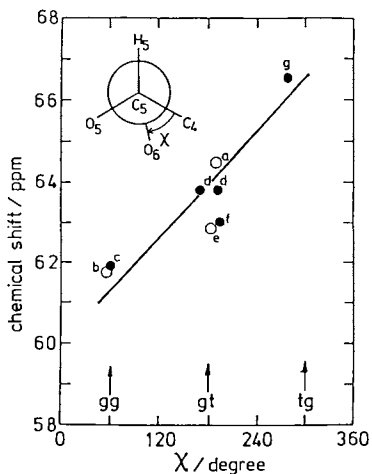


Figure 3 ^{13}C chemical shifts of C6 carbons vs. torsion angles χ . a: α -D-glucose, b: α -D-glucose $\cdot\text{H}_2\text{O}$, c: β -D-glucose, d: β -D-cellobiose, e: α -D-lactose $\cdot\text{H}_2\text{O}$, f: β -D-lactose, g: cellulose I. o : α -glucose and α -glucose residues, ● : β -glucose and β -glucose residues. (Reproduced from ref. 3. Copyright 1984 American Chemical Society)

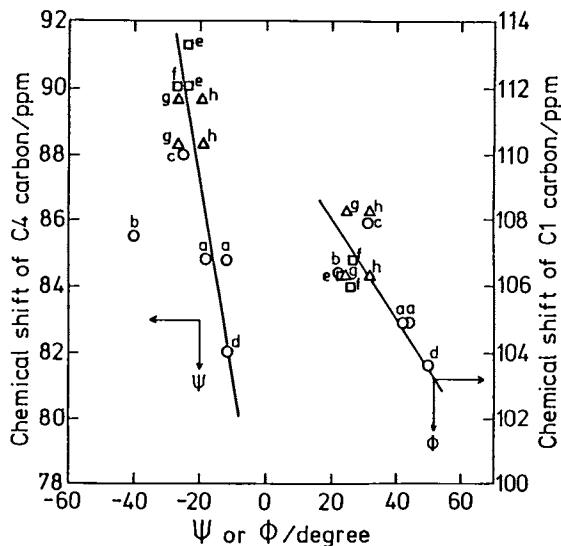


Figure 4 ^{13}C chemical shifts of C1 and C4 carbons vs. torsion angles ϕ and ψ . a: β -cellobiose, b: β -methyl cellobioside $\cdot\text{CH}_3\text{OH}$, c: α -lactose $\cdot\text{H}_2\text{O}$, d: β -lactose, e: cellulose I(Ref.14), f: cellulose I(Ref.16), g: cellulose II(Ref.15), h: cellulose II(Ref.17). (Reproduced from ref. 12. Copyright 1983 International Society of Magnetic Resonance.)

compared to the corresponding lines of n-paraffins with other crystal forms(18), although the molecular chain conformations are almost the same in these crystals. Moreover, significant downfield shifts can be observed for carbons chemically bonded to hydroxyl groups which are forming hydrogen bonds, when the O...O distance in the hydrogen bond is less than about 2.7 Å(19,20).

We have estimated these two effects in the case of cellulose by comparing the ^{13}C chemical shifts in the solid state and the corresponding values in solution for monosaccharides and disaccharides relating to cellulose (3). Here, no comparison was made for carbons having conformational freedom to neglect the effects of the differences in conformation between the two states. As a result, it has been found that the difference $\Delta\delta$ in chemical shift between the solid and dissolved states ranges from -1.51 ppm to 2.43 ppm, being independent on the O...O distance(3). Although such an extent of $\Delta\delta$ is thought as a result of the superposed effects of packing and hydrogen bonding, these effects can be estimated to produce a downfield or upfield shift less than at most 2.5 ppm in cellulose.

2. Contributions from Crystalline and Noncrystalline Regions.

It has been widely accepted that cellulose samples contain the noncrystalline component together with the crystalline component regardless of the source of the samples, although the fractions of the components determined by one method are not always in accord with those estimated by another technique. It is therefore very important to first examine the contributions from the two components to CP/MAS NMR results.

Figure 5 shows 50 MHz CP/MAS ^{13}C NMR spectra of cotton cellulose with different water contents. As previously described for the dry sample shown in Figure 5a(1,3), the respective resonance lines are assigned to C1, C4, and C6 carbons from the downfield side except for the cluster of resonances at 80-70 ppm which belong to C2, C3, and C5 carbons(21-23). Of these resonances the C4 and C6 split into two components, sharp downfield and broad upfield components. These sharp and broad components have been assigned to the crystalline and noncrystalline components, respectively, by comparing the fractions of the former component with the degrees of crystallinity determined by x-ray analysis for samples with widely different crystallinities(1,3). Although such two components cannot be explicitly observed in the C1 line, their existence will become clear later.

As seen in Figure 5(4), each resonance line evidently narrows with increasing water content, resulting in clearer splitting into the crystalline and noncrystalline components of the C4 carbon. A similar better splitting into the two components can be also recognized in the C6 line as a result of an upfield shift of the noncrystalline line. In addition, a fine splitting of the C1 resonance is more clearly observed with increasing water content, although this multiplicity arises from both crystalline and noncrystalline components as discussed later. Similar effects of water on CP/MAS ^{13}C spectra have also been found for cellulose(24), (1-3)- β -D-glucans(25), and amylose(5,26).

In order to know the contributions of the crystalline and noncrystalline regions in detail, we have measured ^{13}C T₁ values using a pulse sequence as developed by Torchia(27). As a result, it has been found that each resonance line contains two components with

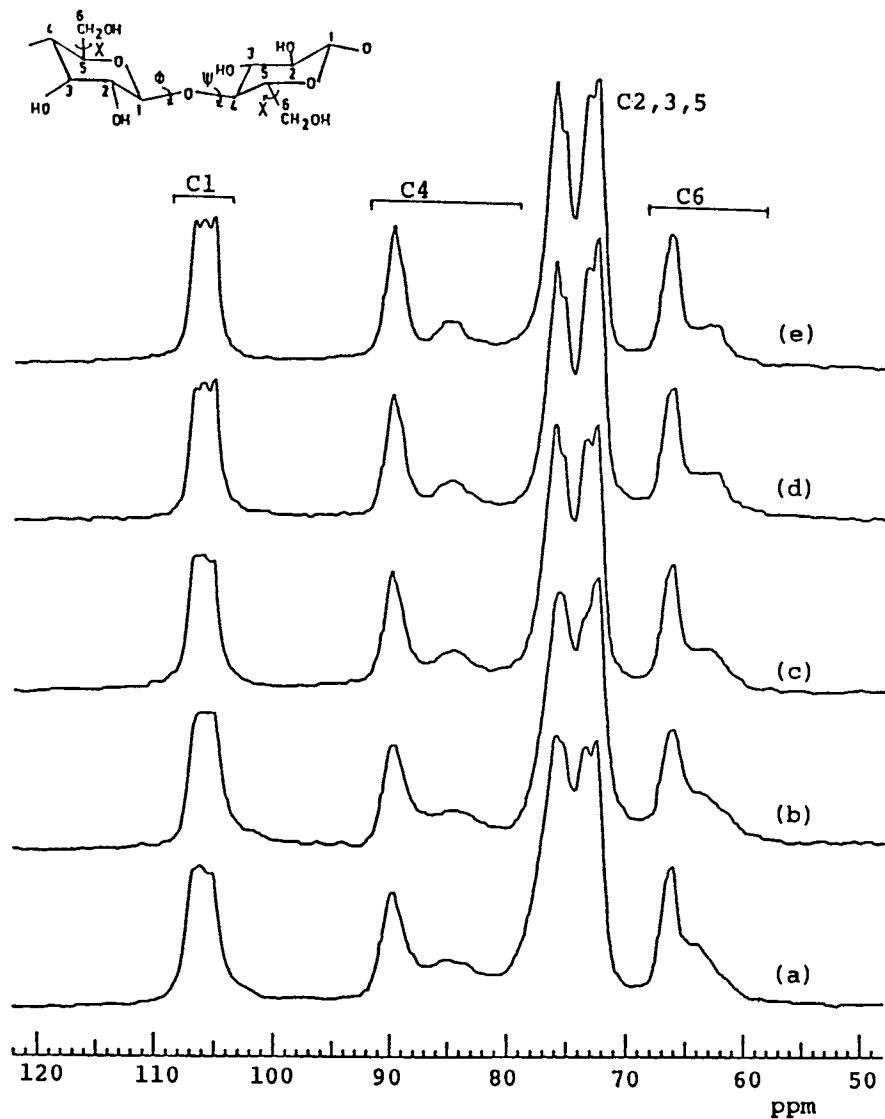


Figure 5 50 MHz CP/MAS ^{13}C NMR spectra of cotton cellulose with different water contents. (a) 0%; (b) 4.2%; (c) 8.4%; (d) 19.1%; (e) 161%. (Reproduced from Ref.4. Copyright 1985 Academia Republicii Socialiste Romania.)

T_1 's of 5-35 s and 109-131 s for the dry cotton and 7-18 s and 107-170 s for the cotton soaked in H_2O , which correspond to the noncrystalline and crystalline components, respectively (3,4,28). Two T_1 values have also been obtained for cellulose by Teeaar and Lippmää(29), although their T_1 values for the crystalline component are rather longer than ours. On the basis of these different T_1 values, we have recorded the spectra of the crystalline and noncrystalline components of cellulose separately(3,4,28).

Figure 6b shows the spectrum of the crystalline component of cotton soaked in H_2O (water content=161%), which was obtained by Torchia's pulse sequence(27,28). The delay time between two $\pi/2$ pulses in the pulse sequence was set to be 100 s. As is clearly seen, the spectrum shown in Figure 6b reflects the components corresponding to the downfield sharp lines of C4 and C6 carbons in the whole spectrum shown in Figure 6a. A similar crystalline spectrum was obtained by others(29) using almost the same technique. On the other hand, Figure 6c indicates the spectrum of the noncrystalline component of the cotton cellulose, which was obtained by subtracting the spectrum of the crystalline component shown in Figure 6b from the whole spectrum shown in Figure 6a. This spectrum evidently corresponds to the components associated with the upfield broad resonances of C4 and C6 carbons.

Similar recording of the respective spectra were possible for other native celluloses such as ramie, bacterial, and valonia celluloses as well as regenerated celluloses.

3. Crystal Structure and Molecular Chain Conformation

Figure 7 shows the spectra of the crystalline components of cotton celluloses with the water contents of 0% and 161%, which were obtained by the method described in the previous section(4). The multiplet of the C1 resonance is clearly seen in these spectra; in the dry state two nonequivalent lines seem to constitute this resonance but they split into one doublet and one small singlet centered at the doublet in the hydrated form. Moreover, C4 and C6 resonances tend to split into a triplet and a doublet, respectively. Almost the same spectra were obtained for ramie cellulose in both dry and hydrated forms.

The crystalline spectra of dry and hydrated bacterial celluloses are shown in Figure 8(30,31). In this case the effect of water is also prominent and both C1 and C4 resonances split into different types of triplets from those of cotton and ramie celluloses. Almost the same features of spectra including C1 and C4 fine splittings have also been observed for valonia cellulose. Although it is very difficult at present to determine whether such fine splittings within 1-2 ppm are due to the difference in torsion angles, packing, or hydrogen bonding, they are closely associated with crystallographical inequivalences of the glucose residues. It is therefore concluded that the crystal structure of cotton and ramie celluloses is different from that of bacterial and valonia celluloses, contrary to the claim(14,16) that all native celluloses have the same crystal structure, cellulose I.

Atalla and VanderHart(32,33) have proposed two crystalline forms for cellulose I, which they name I_α and I_β , to explain the multiplicities of C1 and C4 lines. Analogous to their work, Cael et al.(34) have concluded that the spectra of different native

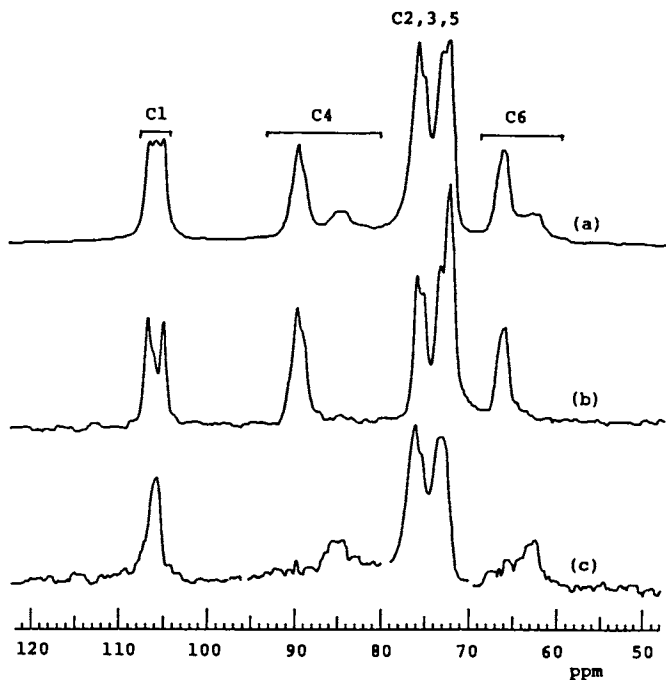


Figure 6 50 MHz CP/MAS ^{13}C NMR spectra of cotton cellulose with the water content of 161%. (a) whole spectrum, (b) crystalline component, (c) noncrystalline component.

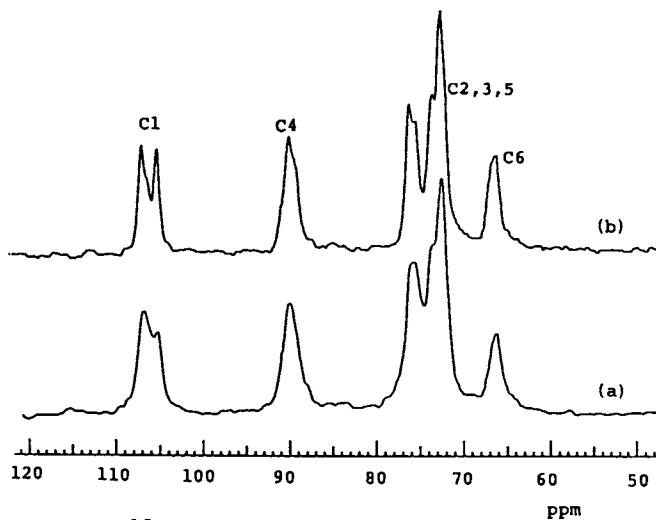


Figure 7 CP/MAS ^{13}C NMR spectra of the crystalline components of cotton cellulose with the water contents of 0% (a) and 161% (b). (Reproduced from Ref.4. Copyright 1985 Academia Republicii Socialiste Romania.)

celluloses are linear combinations of two spectra. In contrast to the view of Atalla and VanderHart, however, they have attributed these spectra to the resonances of the glucose residues in the two-chain and eight-chain unit cell regions of cellulose. According to their models, relative intensities in the multiplets of C1 and C4 lines can be calculated; for example, the predicted intensity ratios in the C1 triplet are $(1-f):2f:(1-f)$ for the two-crystal model and $(2-f'):2f':(2-f')$ for the two-unit-cell model, respectively. Here, f and f' denote the fractions of the I_{α} crystal and the eight-chain unit cell, respectively. In an attempt to examine the validity of these models, we estimated the integrated intensity ratios of the C1 and C4 lines by analyzing the multiplets in terms of three Lorentzian curves by a computer(30). In this analysis such Lorentzian assumptions were most reasonable. As a result, it has been found that in many cases the experimental ratios are not in accord with those predicted by either model. Thus, a new model to fit the experimental results should be constructed. It should be here emphasized that for the detailed analysis of the multiplets the contribution from the noncrystalline component must be removed precisely like our case; this contribution was not considered in the former two cases (32-34).

Analogous to different fine structures in C1 and C4 resonances, the crystalline lines of C6 carbons exhibit a doublet for cotton and ramie celluloses and a singlet for bacterial and valonia celluloses, respectively. However, since the spacing of the doublet is as small as 0.2 ppm, the chemical shifts of the C6 carbons are almost the same (about 66.4 ppm) for both groups of cellulose. Such high shift values seem to be well correlated to the trans-gauche conformation, which agrees with the results of x-ray crystal analyses(14,16).

Figure 9 shows the spectra of the crystalline components obtained from cupra rayon with water contents of 0% and 158%(4). In this case, although water also significantly narrows each resonance line, the features of the spectrum remain unchanged; the C1 and C4 resonances split into doublets with equivalent intensities. This result is in contrast to the case of native cellulose, reflecting that the crystal structure of regenerated cellulose is cellulose II(15-17). In addition, the chemical shifts of C6 carbons are 64.2 ppm in the dry and hydrated states, whose values correspond to the gauche-trans conformation as is seen in Figure 3. This conflicts with the result of x-ray crystal analyses(15,17): No line with a higher chemical shift corresponding to the trans-gauche conformation is observed, while both gauche-trans and trans-gauche are assumed in the x-ray analyses. Since the T_1 value of the C6 carbon has almost the same order as long T_1 values of the ring carbons(3,4,28), there is no possibility of the rapid exchange between gauche-trans and trans-gauche conformations. It is difficult at present to find the reason for the conflict.

Figure 10 shows the spectra of the noncrystalline components of cotton cellulose with water contents of 0% and 161%(4). These spectra were obtained by subtracting the spectra of the crystalline components from the corresponding whole spectra as shown in Figure 6. It is clearly seen that the linewidths of the C1 and C4 resonances become markedly narrower upon absorbing water, while holding the chemical shifts unchanged. For instance, the half-value widths of the C1 resonance lines are 60 Hz and 160 Hz, respectively. Such a

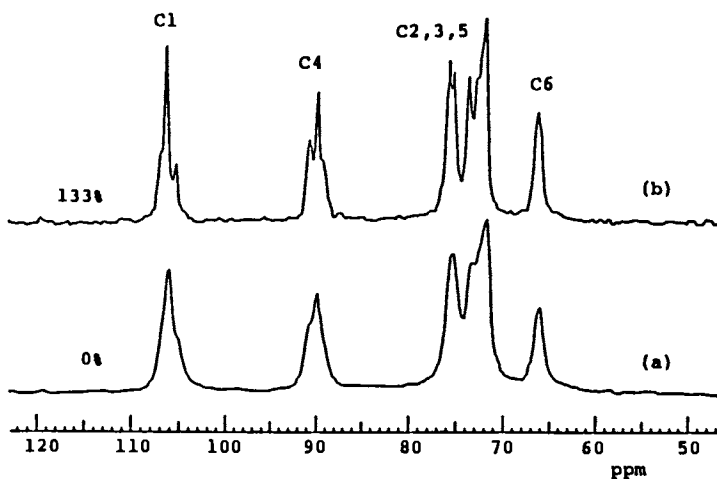


Figure 8 CP/MAS ^{13}C NMR spectra of the crystalline components of bacterial cellulose with the water contents of 0% (a) and 133% (b).

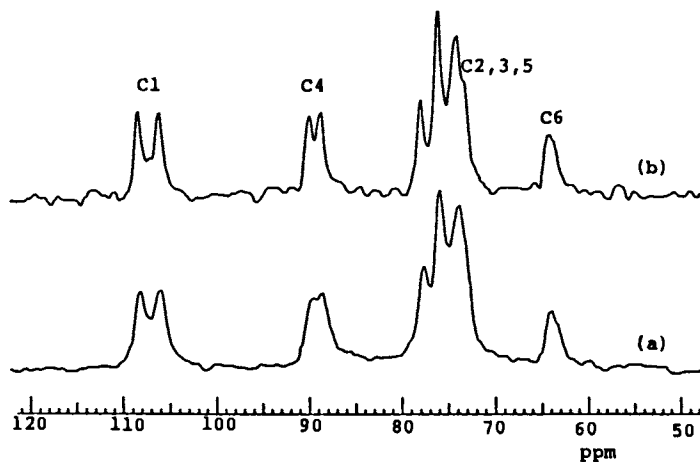


Figure 9 CP/MAS ^{13}C NMR spectra of the crystalline components of cupra rayon with the water contents of 0% (a) and 155% (b). (Reproduced from Ref.4. Copyright 1985 Academia Republicii Socialiste Romania.)

marked difference in linewidth cannot be primarily ascribed to the difference in molecular mobility of the two samples, because there is some evidence that water does not significantly enhance the mobility of the cellulose chains under these experimental conditions. One is that the ^{13}C T_1 values of the C1 and C4 carbons do not greatly decrease with increasing water content. Furthermore, the C6 resonance line also becomes narrow only slightly, though the C6 carbon involved in the methylol side group should be much more mobile than the backbone carbons if water greatly enhances the molecular mobility. Another strong evidence in favor of the low molecular mobility of cellulose chains in the hydrated state is obtained from the results of the measurements on rayon fibers as described below. Therefore, the origin of such narrowing of the C1 and C4 resonance lines has to be sought elsewhere.

The distributions in torsion angles ϕ and ψ about the β -1,4-glycosidic linkage provide the most likely explanation of these narrowings. We have already described that the ^{13}C chemical shifts of the C1, C4 and C6 carbons are primarily correlated on the torsion angles ϕ and ψ about the β -1,4-glycosidic linkage and χ about the C5-C6 bonds, respectively. On the basis of these results, we have concluded(3) that the distributions in the torsion angles ϕ and ψ are relatively narrow in the dry native cellulose, whereas they are broad in the dry regenerated cellulose. It is, therefore, plausible that such distributions are further narrowed by water in the hydrated cotton. Thus it can be assumed that the noncrystalline chains of cotton are in the relatively ordered state in the presence of water. However, the chains may undergo some distortion upon drying and as a result the torsion angles ϕ and ψ will be distributed somewhat broader in the dry sample.

Figure 11 shows the spectra of the noncrystalline components of rayon fibers with the water contents of 0% and 158%(4). In contrast to the case of cotton, the linewidths of the respective resonances do not remarkably decrease by the addition of water; for examples, the half-value width of the C1 resonance line is 205 Hz for the hydrated sample, whereas it is 256 Hz for the dry sample. As pointed out above, this fact implies that the molecular mobility of the noncrystalline chains does not greatly increase with the increase of water content. Moreover, the noncrystalline component of rayon does not undergo such a significant change of distributions in torsion angles ϕ and ψ as observed for cotton cellulose, possibly because the molecular conformation of this component is rather random in the dry state. In other words, such a disordered conformation may hardly allow marked distortion of the noncrystalline chains to be produced upon drying cupra rayon.

Figure 12 shows schematic structural models of native and regenerated cellulose samples, which have been proposed in an attempt to explain our observation(30,31). Haigler et al.(35) have recently found in the incubation of *Acetobacter xylinum* in the presence of a fluorescent brightener that the nascent fibril of bacterial cellulose is composed of bundles of chains in the tactoidal and noncrystalline phase. Furthermore, Kai(36) has reported using similar techniques that the cellulose chains are not oriented at random in the cross-section of the nascent fibril but are in the form of monomolecular layers corresponding to the (110) plane of cellulose I. On the basis of these results, it seems plausible to assume that

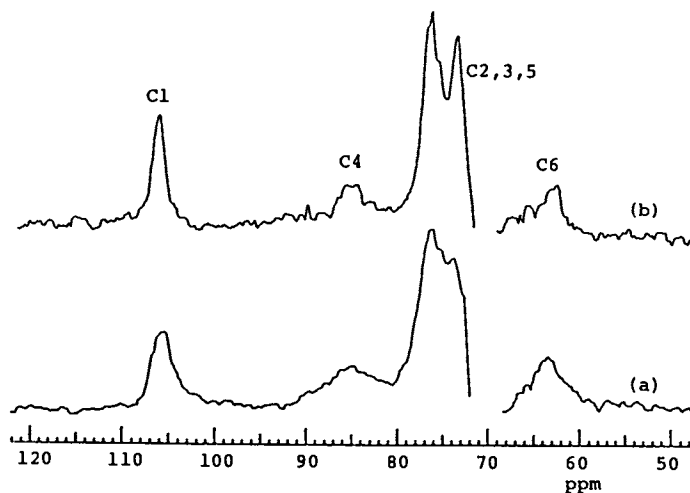


Figure 10 CP/MAS ^{13}C NMR spectra of the noncrystalline components of cotton cellulose with the water contents of 0% (a) and 161% (b). (Reproduced from Ref.4. Copyright 1985 Academia Republicii Socialiste Romania.)

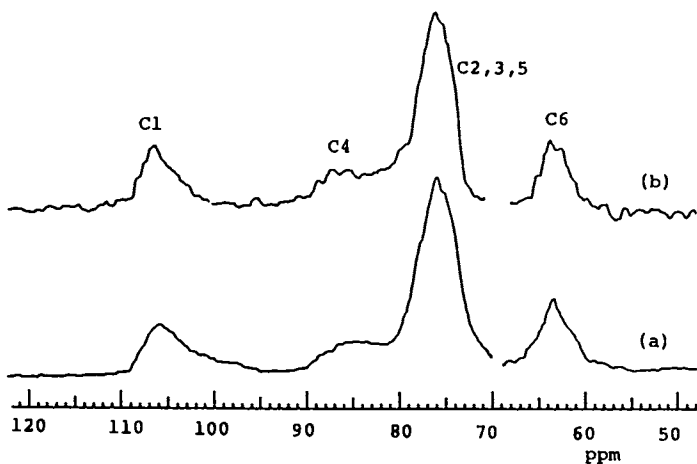


Figure 11 CP/MAS ^{13}C NMR spectra of the noncrystalline components of cupra rayon with the water contents of 0% (a) and 155% (b). (Reproduced from Ref.4. Copyright 1985 Academia Republicii Socialiste Romania.)

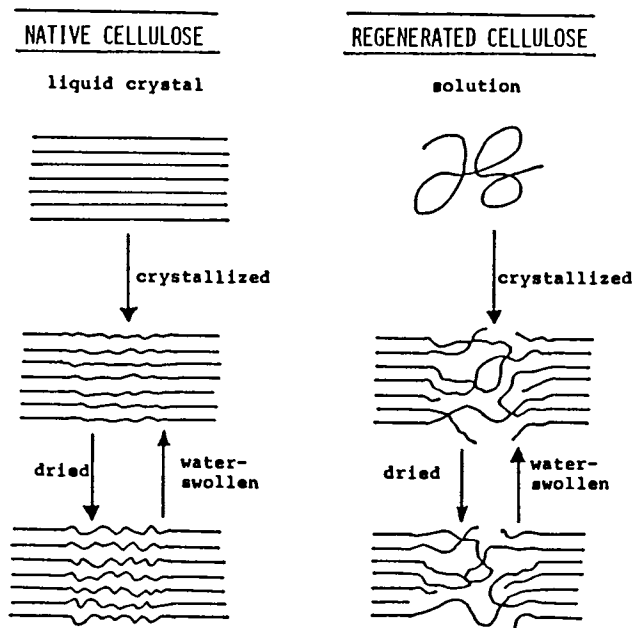


Figure 12 Schematic structural models of native and regenerated cellulose samples.

native celluloses including cotton and ramie are crystallized from the ordered state such as liquid crystal. In that case the chains which remain as noncrystalline portions after crystallization are also relatively ordered as shown in Figure 12. Such ordered noncrystalline chains will undergo some distortion upon drying but this kind of distortion must be relaxed by absorbing water again. This process is thought to induce such narrowing of resonance lines as shown in Figure 10. On the other hand, the noncrystalline chains in rayon fibers must be considerably disoriented because the fibers are spun and crystallized from the solution where chains adopt the almost random conformation. Therefore, the noncrystalline sequences hardly undergo any change in conformation when dried or hydrated as shown in Figure 12. Such a noncrystalline state is thought to be reflected on the small change in linewidth as seen Figure 11.

Literature Cited

1. Horii, F.; Hirai, A.; Kitamaru, R. Polym. Bull., 1982, 8, 163.
2. Horii, F.; Hirai, A.; Kitamaru, R. Polym. Bull., 1983, 10, 357.
3. Horii, F.; Hirai, A.; Kitamaru, R. "Polymers for Fibers and Elastomers", ACS Symp. Series, No.260, J. C. Arthur, Jr., Ed., Am. Chem. Soc., Washington, D.C., 1984, p.27.
4. Horii, F.; Hirai, A.; Kitamaru, R.; Sakurada, I. Cellulose Chem. Technol., 1985, 19, 513.
5. Horii, F.; Hirai, A.; Kitamaru, R. Macromolecules, 1986, 19, 930.
6. Pfeffer, P. E.; Valentine, K. M.; Parrish, F. W. J. Am. Chem. Soc., 1979, 101, 1265.
7. Pfeffer, P. E.; Hicks, K. B.; Frey, M. H.; Opella, S. J.; Earl, W. L. J. Magn. Reson., 1983, 55, 344.
8. Pfeffer, P. E.; Hicks, K. B.; Frey, M. H.; Opella, S. J. J. Carbohydr. Chem., 1984, 3, 197.
9. Brown, G. M.; Levy, H. A.; Science, 1965, 147, 1038.
10. Hough, E.; Neidle, S.; Rogers, D.; Throughton, P. G. H. Acta Cryst., 1973, B29, 365.
11. Chu, S. S. C.; Jeffrey, G. A. Acta Cryst., 1968, B24, 830.
12. Horii, F.; Hirai, A.; Kitamaru, R. Bull. Magn. Reson., 1983, 5, 233.
13. Perez, S.; S.-Pierre, J.; Marchessault, R. H. Can J. Chem., 1978, 56, 2866.
14. Gardner, K. H.; Blackwell, J. Biopolymers, 1974, 13, 1975.
15. Kolpak, K. J.; Blackwell, J. Macromolecules, 1976, 9, 273.
16. Woodcock, C.; Sarko, A. Macromolecules, 1980, 13, 1183.
17. Stipanovic, A. J.; Sarko, A. Macromolecules, 1976, 9, 851.
18. VanderHart, D. L. J. Magn. Reson., 1981, 44, 117.
19. Imashiro, F.; Maeda, S.; Takegoshi, K.; Terao, T.; Saika, A. Chem. Phys. Lett., 1982, 92, 642.
20. Imashiro, F.; Maeda, S.; Takegoshi, K.; Terao, T.; Saika, A. Chem. Phys. Lett., 1983, 99, 189.
21. Atalla, R. H.; Gast, J. C.; Sindorf, D. W.; Bartuska, V. J.; Maciel, G. E. J. Am. Chem. Soc., 1980, 102, 3249.
22. Earl, W. L.; VanderHart, D. L. J. Am. Chem. Soc. 1980, 102, 3251.

23. Earl, W. L.; VanderHart, D. L. Macromolecules, 1981, 14, 570.
24. VanderHart, D. L. NBS Report NBSIR, 82-2534.
25. Fyfe, C. A.; Stephenson, P. J.; Taylor, M. G.; Bluhm, T. L.; Deslandes, Y.; Marchessault, R. H. Macromolecules, 1984, 17, 501.
26. Veregin, R. P.; Fyfe, C. A.; Marchessault, R. H.; Taylor, M. G. Macromolecules, 1986, 19, 1030.
27. Torchia, D. A. J. Magn. Reson., 1978, 30, 613.
28. Horii, F.; Hirai, A.; Kitamaru, R. J. Carbohydr. Chem., 1984, 3, 641.
29. Teeaar, R.; Lippmaa, E. Polym. Bull, 1984, 12, 315.
30. Hirai, A.; Horii, F.; Kitamaru, R. Polym. Prepr., Japan, 1985, 34, 2473; to be published.
31. Horii, F.; Hirai, A.; Kitamaru, R. Ann. Rept. Res. Inst. Chem. Fibers, Japan, 1985, 42, 41.
32. Atalla, R. H.; VanderHart, D. L. Science, 1984, 223, 283.
33. VanderHart, D. L.; Atalla, R. H. Macromolecules, 1984, 17, 1465.
34. Cael, J. J.; Kwoh, D. L. W.; Bhattacharjee, S. S.; Patt, S. L. Macromolecules, 1985, 18, 821.
35. Haigler, C. H.; Brown, R. M.; Benziman, M. Science, 1980, 210, 903.
36. Kai, A. Makromol. Chem., Rapid Commun., 1984, 5, 307.

RECEIVED April 1, 1987

Chapter 7

Possible Cause of Structural Irreversibility Between Cellulose I and Cellulose II Families

Jisuke Hayashi¹, Hiroshi Kon¹, Mitsuo Takai¹, Masahiro Hatano²,
and Tsunenori Nozawa²

¹Department of Applied Chemistry, Faculty of Engineering, Hokkaido University,
Sapporo 060, Japan

²Chemical Research Institute of Nonaqueous Solution, Tohoku University, Katahira-cho,
Sendai, Japan

Transformations of allomorphs in the cellulose I family to allomorphs in the cellulose II family are generally thought to be irreversible. We propose that the conformations of chain skeletons are the same within each family but different between the families, and that the difference in stabilities (through relief of a short contact between H1' and H4) of the conformations results in the irreversibility. In contrast, Blackwell et al. and Sarko et al. have proposed that the crystal structures of allomorphs in the cellulose I and II families are based on parallel and antiparallel packing of chains, respectively, and the irreversibility results from the increase in entropy inherent in converting from parallel to antiparallel arrangements. IR and solid state ¹³C NMR spectra of the allomorphs were studied to investigate the proposals. In both spectral methods, the bands or signals that are related to chain conformation split into two peaks in the II family (II, II_{II}, IV_{II}). This indicated "bent and twisted" form chain conformations within the unit cell which we ascribe to asymmetry within chains rather than two different chains. In spectra from members of the I family (I, III_I, IV_I), the same peak showed little or no splitting, indicating a single, more symmetric chain conformation. Other bands that are related to chain packing could be similar between families but differed when the unit cell shapes were different.

The transformation from cellulose I to II occurs easily, but the reverse transformation is not readily accomplished. It had been thought that the irreversibility results from a large difference in thermodynamic stability between the crystal structures of cellulose I and II until quite recently.

In our previous papers (1, 2), we showed that the same irreversibility exists between allomorphs of the cellulose I family (I,

0097-6156/87/0340-0135\$06.00/0
© 1987 American Chemical Society

III_I and IV_I) and those of the cellulose II family (II, III_{II} and IV_{II}). The transformations among allomorphs within each family occurred reversibly, but transformations between families were irreversible. For example, IV_I could be made either directly from I or through III_I, and was transformed into I by hydrolysis. Also, IV_I can be converted into III_{II} and IV_{II} through cellulose II. When IV_{II}, derived from IV_I or other members of the cellulose I family, was transformed into II by hydrolysis, it could not be transformed back into a member of the cellulose I family. There is strong similarity between the x-ray patterns of III_I and III_{II} and between those of IV_I and IV_{II}, but the meridional intensities are quite different (3). The IR and ¹³C NMR spectra are clearly different and it is clear that III_I, III_{II}, IV_I and IV_{II} are distinct allomorphs.

When cellulose trinitrate I_I (TNC I_I) and triacetates I_I and II_I (TAC I_I and II_I) were prepared from allomorphs of the I family in the fibrous state under low-swelling conditions, they could be saponified into cellulose I. On the other hand, TNC I_{II}, TAC I_{II} and TAC II_{II} can be saponified into cellulose II (4-6). When the esters of the I family were recrystallized by heat treatment, they were transformed irreversibly into corresponded esters (for example, TAC I_I to TAC I_{II}). They crossed the barrier of irreversibility and were saponified into cellulose II.

The same phenomena were observed for soda celluloses. Na-cellulose I_I prepared from the I family under conditions of low swelling (high temperature or with stretching) could be converted to cellulose I with hot water. Na-cellulose I_{II} prepared from cellulose II under the same conditions was converted to cellulose II (7-10). In ordinary mercerization of native cellulose a mixture of Na-cellulose I_I and I_{II} was obtained; both decomposed to cellulose II with cold water. Na-cellulose I_I was transformed irreversibly into Na-cellulose I_{II}.

The allomorphs and derivatives prepared from cellulose I and II in solid state could be transformed into cellulose I and II, respectively. The memory phenomenon of the original crystal structure should be due to a structural characteristic (chain conformation, chain polarity or others) of an individual chain that is common within each family and kept through the change of crystal structure. There were direct irreversible conversions between corresponding cellulose esters, Na-cellulose and cellulose IV prepared from cellulose I and II just like that between I and II. Accordingly, the structural characteristic should be the cause of the structural irreversibility between the I and II families.

In the 1970's (3, 4), we proposed that the chains in the cellulose I family have a "bent" form, which has an approximate 2₁ screw axis. The chains in the cellulose II family were proposed to be "bent and twisted"; they deviate substantially from a 2₁ axis. By keeping the conformation of the original member in a family, the allomorphs and derivatives can return to the original crystal structures. In the "bent" form the non-bonded distance between H1' and H4 is about 1.8 Å for a wide range of rotations of glycosidic units about the O1-O4 virtual bond. (Figure 4). This is a short distance compared to the sum of the radii of two hydrogen atoms (2.4 Å). On the other hand, in the "bent and twisted" form, the distance can be increased by the twisting. When the intramolecular hydrogen bonds that fix the chain conformation are relaxed, the

twisting of the chain is caused by a small drop in energy and the "bent" form is changed to the "bent and twisted" form. In addition, the irreversibility between families should arise from the drop in energy that drives the twisting of the chains.

Atalla and Van der Hart (11, 12) concluded, based on their Raman and ^{13}C NMR spectra, that the molecules in cellulose I and II have different conformations. Based on x-ray analyses, Sarko et al. (13, 14) and Blackwell et al. (15, 16) both concluded that crystal structures of cellulose I and II were based on parallel and antiparallel packing, respectively, of chains that have similar backbone conformations. Sarko (17) concluded that the allomorphs in the I and II families were based on parallel and antiparallel chains, respectively. The irreversibility may arise from the increase in entropy when parallel packing is converted to antiparallel packing.

In the present work, we tried to determine which proposal is better using IR and solid state ^{13}C NMR. There are many papers on the spectra of cellulose I and II (12, 18-24), however, there are few on the other allomorphs. Mann and Marrinan (21) found differences in the OH stretching bands of IR spectra of III_I and III_II and of IV_I and IV_II . Chidambareswaran et al. (25) reported IR spectra for several allomorphs, but their spectra lacked enough resolution for detailed discussion of chain conformation. The ^{13}C NMR spectra of the other allomorphs have not been reported.

Experimental

Preparation of Cellulose Samples

Native cellulose. Celluloses from purified Valonia ventricosa, Acetobacter xylinum, ramie and cotton linters were used. Pellicles of bacterial cellulose were grown under the conditions described by Colvin (26) for 48-96 hours. The bacterial medium was thoroughly washed away with distilled water and 1% NaOH aqueous solution. A membrane of bacterial cellulose having uniaxial orientation was prepared from a young pellicle by stretching to about twice the initial length in a wet state and drying under tension.

Cellulose II. Fortisan, ordinary viscose rayon, mercerized ramie, mercerized bacterial cellulose, and saponified triacetate film were used. A film having uniaxial orientation was prepared from saponified triacetate film by stretching and drying under tension.

Cellulose III_I and III_II . Native cellulose and cellulose II, described above, were treated with liquid ammonia for about 2 hours at about -80°C . Gradual evaporation of ammonia was permitted in dry air at about -15°C .

Cellulose IV_I and IV_II . These allomorphs were prepared from III_I and III_II , respectively, by heating in glycerol at 260°C for 30 min.

Deuteration. The film samples were dried under vacuum in the presence of P_2O_5 for 2 days, deuterated in vapor of D_2O (99.75%) for 1 day, and then dried under vacuum in the presence of P_2O_5 for 1 day.

X-ray Diffraction

X-ray diffractograms were measured by reflection method with $\text{CuK}\alpha$. Samples of membrane were measured laying surface of membrane parallel to the reflection plane. Other samples were measured as powders smaller than 60 mesh.

IR Spectra

IR spectra of the allomorphs were obtained with an A 202 spectrometer manufactured by Japan Spectroscopic Co. The infrared radiation was polarized with an AgCl plate polarizer.

Solid-state ^{13}C NMR Spectra

Solid-state ^{13}C NMR spectra were observed using the cross-polarization/magic angle spinning technique on a Bruker CXP-300 spectrometer operating at 7 T. Contact time, repetition time and high power decoupling observation time were 2 ms, 2 s, and 20-30 ms, respectively. The magic-angle spinning frequency was in the range 3460-3800 Hz. The spectra were also obtained with a JEOL FX60 spectrometer operating at 59.8 MHz.

Results and Discussion

Infrared Spectra of Cellulose Allomorphs

In order to compare IR spectra of allomorphs in detail, especially in the $900\text{-}1500\text{ cm}^{-1}$ region, highly crystalline samples are needed. Such samples of III_I and IV_I were prepared from Valonia cellulose. Attempts to transform Valonia cellulose I to II were difficult in general and gave only samples of low crystallinity. Viscose and saponified films of cellulose esters had crystallinity that was too low to yield high-resolution spectra. Bacterial cellulose membranes of suitable thickness were mercerized under stretching, giving relative highly crystalline cellulose II. From this, sample of III_{II} and IV_{II} were made.

Figures 1 and 2 show x-ray diffractograms of members of the cellulose I and II families, respectively. Diffractograms of each were typical, and indicated complete transformation and uniplanar orientation of $(1\bar{1}0)$ relative to the membrane surface. It was remarkable to retain this orientation of the mercerized bacterial cellulose and of the III_{II} and IV_{II} prepared from it. The crystallinity of members of the cellulose II family were not high. But their IR spectra showed enough resolution for detailed discussion.

Figure 3 shows IR spectra of OH stretching bands of the allomorphs. Arrows show OH stretching bands having strong dichroism parallel to the chain axes and correspond to $03'\text{-}05$ intramolecular hydrogen bonds (27). The O-H stretching band in all allomorphs in the II family was split into two.

Figure 4 shows the chain conformations of cellulose I ("bent") and of cellulose II ("bent and twisted") proposed in our previous work (28) on the crystal structure of cellulose II. These models of cellulose I and II have one and two kinds of intrachain ($03'\text{-}05$) hydrogen bond, respectively. The number of O-H stretching peaks in

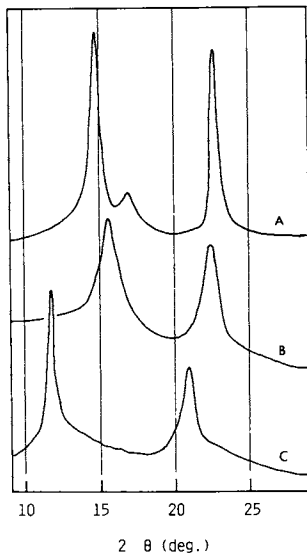


Fig. 1 X-ray diffractograms of the allomorphs in cellulose I family by the reflection method (the reflection plane is parallel to the membrane surface). A: I, valonia cellulose, B: IV_I prepared from A through III_I (C), C: III_I prepared from valonia.

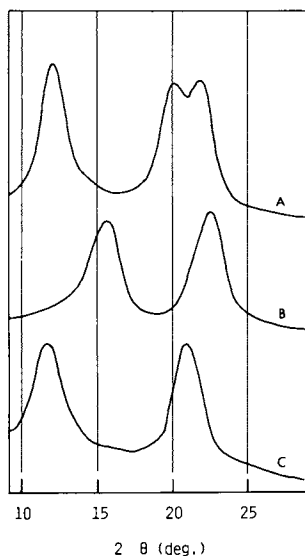


Fig. 2 X-ray diffractograms of the allomorphs in cellulose II family by the reflection method. A: II, mercerized bacterial cellulose, B: IV_{II} prepared from A through III_{II} (C), C: III_{II} prepared from A. The treatments were carried out under stretching.

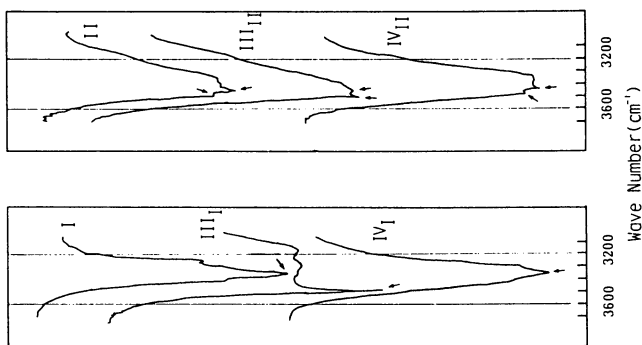


Fig. 3 IR spectra of the allomorphs in OH stretching region. The samples used for IR spectra are same to the samples in Fig. 1 and 2. Arrow shows OH stretching bands having parallel dichroism and assigned to intramolecular hydrogen bonds. There are one and two of the band in the I and II families, respectively.

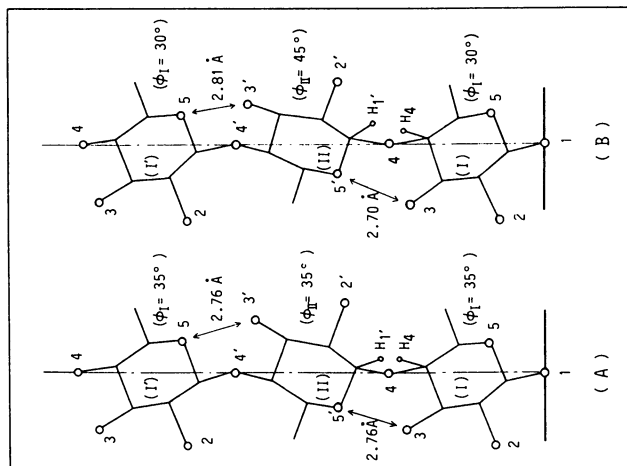


Fig. 4 Chain conformations of cellulose proposed by X-ray analysis (28). A: "bent form chain for cellulose I, B: "bent and twisted form chain deviated from 2_1 for cellulose II. There are two kinds of the distance of $O3' - O5'$. Internal rotation angle around glucosidic linkage is according to Jone's expression (32). $O1 - O1'$ distance is 5.16Å, C - C, C - O, and C - H bond length are 1.54, 1.34, and 1.09 Å respectively. Bond angle is 109.28° .

the IR spectra found with parallel polarization corresponds to the number of types of intrachain hydrogen bonds.

Table I. O-H Stretching with Parallel
of Cellulose Allomorphs

Allomorph	Frequency (cm ⁻¹)	
I	3345	
III _I	3475	
IV _I	3340	
II	3480	3440
III _{II}	3475	3440
IV _{II}	3475	3440

Mann and Marrinan (22) assigned the two bands of the OH stretching in II to the intrachain hydrogen bonds of O3'-O5 and O6'-O2. The results of Liang and Marchessault (23, 24) argued against O6'-O2 hydrogen bonds. They found that the dichroism of CH₂ symmetric and antisymmetric stretching bands indicated a position (gt) for O6 that is not suited for formation of this hydrogen bond. Instead, an intermolecular hydrogen bond from O6" to O3 was proposed. We observed the following CH₂ stretching bands.

Table II. Symmetric CH₂ Stretching (Parallel dichroism)
of Cellulose Allomorphs

Allomorph	Frequency (cm ⁻¹)	Allomorph	Frequency (cm ⁻¹)
I	2850	II	2850
III _I	2850	III _{II}	2850
IV _I	2850	IV _{II}	2860

Table III. Antisymmetric CH₂ Stretching (Perpendicular
dichroism) of Cellulose Allomorphs

Allomorph	Frequency (cm ⁻¹)	Allomorph	Frequency (cm ⁻¹)
I	2940	II	2930
III _I	2935	III _{II}	2925
IV _I	2940	IV _{II}	2935

These results are consistent with a gt position for O6 in all allomorphs, with little possibility of the O6'-O2 hydrogen bond.

There is a large difference between the dimensions of the ab plane of the unit cells of II and IV_{II}. Therefore, intermolecular hydrogen bonds should be fairly different between II and IV_{II}. However, OH stretching bands assigned to intrachain hydrogen bonds had almost the same frequency in II and IV_{II}. Liang and Marchessault's reliance on an inter-chain interaction to achieve a second kind of O3'-O5 bond is not consistent with this spectral information, but it can be explained by the two O3'-O5 distances arising from our "bent and twisted" conformation.

Sarko and Muggli (13) and Gardner and Blackwell (15) both concluded that cellulose I had two intrachain hydrogen bonds, O3'-O5 and O6'-O2. Stipanovic and Sarko (14) and Kolpak and Blackwell (16) proposed structures of II in which the corner chains in the unit cell had O3'-O5 and O6'-O2 bonds and the center chain had only O3'-O5 bonds. According to their crystal models, there are chains having two kind of hydrogen bonds, O3'-O5 and O6'-O2 in both of cellulose I and II. If the two kinds of bonds are the cause of the two parallel OH stretching bands, the two bands should be observed in cellulose I. But all allomorphs in the cellulose I family showed only one of the bands. There is the possibility that the splitting of the spectral bands might arise from two different chain conformations in the unit cell. But if the chain conformation changes depend on the crystal structure, the frequencies of the two parallel OH bands should change with crystal structures. The frequencies of allomorphs of the cellulose II family were almost the same in spite of their quite different crystal structure. If the chain conformation does not change with crystal structure, the question would arise whether the chain conformation of cellulose I can change into two kinds of chain conformation in equal amounts by mercerization or other transformation processes. This is a pending problem. At least, however, the OH stretching bands assigned to the intrachain bonds showed common characteristics among allomorphs in each family.

Marrinan and Mann (22) reported that there were two types of OH stretching bands in native cellulose; the difference appeared near 3250 cm^{-1} . However, no differences in the main bands of OH stretching are noticed now. Our IR spectra of valonia did not show essential differences with that of ramie shown by Liang through all range. It should not hinder the present discussion.

Figure 5 shows IR spectra in the OD stretching region. Only cellulose that is amorphous or on surfaces of crystallites is deuterated, so crystal packing should have slight influence on the OD band. In the I family, a main band of OD stretching was at 2480 cm^{-1} . The band showed dichroism parallel to the chain axis and was assigned to the intramolecular bond O3'(D)-O5. In all allomorphs of the II family, the main band was at 2545 cm^{-1} and exhibited parallel band dichroism. Another parallel band was at 2560 cm^{-1} in II and III_{II} although it was not clear in IV_{II}. The results of the OD bands suggested that the amorphous cellulose had conformations similar to the molecules in the crystallites.

The main band of III_I was at the same frequency as the main band in I or IV_I, despite the corresponding band of OH being at higher frequency than that in I or IV_I. It suggested that the shift to higher frequency of the OH band of III_I had been effected with molecular packing in the cellulose II type of unit cell.

Figure 6 shows the region from 900 to 1200 cm^{-1} . The spectra showed common characteristics within each family. Two bands were assigned to stretching of the glucose ring for allomorphs in the cellulose I family. The bands were sharp and showed a weak perpendicular dichroism.

The corresponding bands of the II family were split into two each although they were not well-separated. They also differed from those for the I family by showing strong parallel dichroism. One of the four bands was at 1090 - 1095 cm^{-1} and obscured separation of the

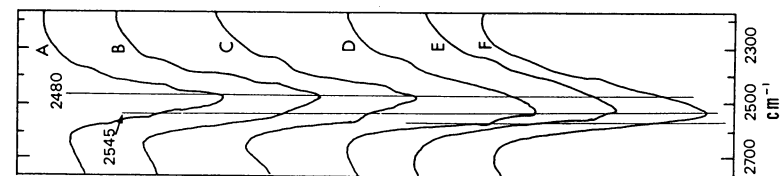


Fig. 5 IR spectra of the deuterated allomorphs in OD stretching region. A: I, valonia cellulose, B: IV_I prepared from III_I (C), C: III_I from A, D: II, cellulose from D, F: IV_I from E.

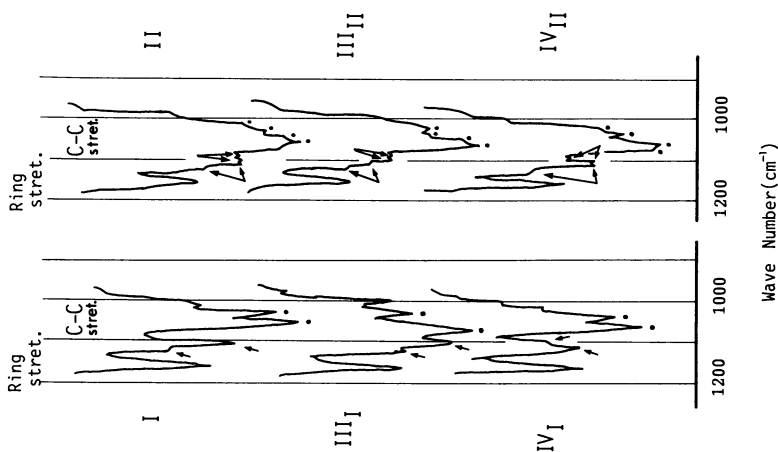


Fig. 6 IR spectra of the allomorphs in 900 to 1200 cm^{-1} region. Arrow shows bands assigned to ring stretching. Dot shows main bands assigned to C - C and C - O stretching. Samples are same to them in Fig. 4.

main band arising from ring stretching at about 1100 cm^{-1} and the main band of C-C stretching at about 1065 cm^{-1} .

Table IV. Glucose Ring Stretching of Allomorphs
in Cellulose I Family

Allomorph	Frequency (cm^{-1})	
I	1120	1110
III _I	1120	1105
IV _I	1115	1105

Table V. Glucose Ring Stretching of Allomorphs
in Cellulose II Family

Allomorph	Frequency (cm^{-1})			
II	1120	1115	1110	1090
III _{II}	1120	1115	1110	1090
IV _{II}	1120	1110	1105	1100

For each allomorph in the I family, there were two sharp bands in the region of $1020 - 1070\text{ cm}^{-1}$ assigned to C-O and C-C stretching.

Table VI. C-O and C-C Stretching of Allomorphs
in Cellulose I Family

Allomorph	Frequency (cm^{-1})	
I	1060	1035
III _I	1075	1030
IV _I	1060	1035

As before, the two corresponding bands were split into four bands for the II family.

Table VII. C-O and C-C Stretching of Allomorphs
in Cellulose II Family

Allomorph	Frequency (cm^{-1})			
II	1065	1060	1030	1020
III _{II}	1070	1065	1030	1020
IV _{II}	1065	1060	1035	1020

Figure 7 shows the region from 1200 to 1500 cm^{-1} for the allomorphs. The unit cells of IV_I and IV_{II} are similar to that of I, and those of III_I and III_{II} are similar that of to II. Especially in this spectral region, there were common characteristics within these groups based on similarities of the cell as well as membership in the same family. Accordingly, there were similarities between I and IV_I and between II and III_{II}, although there were distinguishable differences. The IR spectra of III_I, II and III_{II}

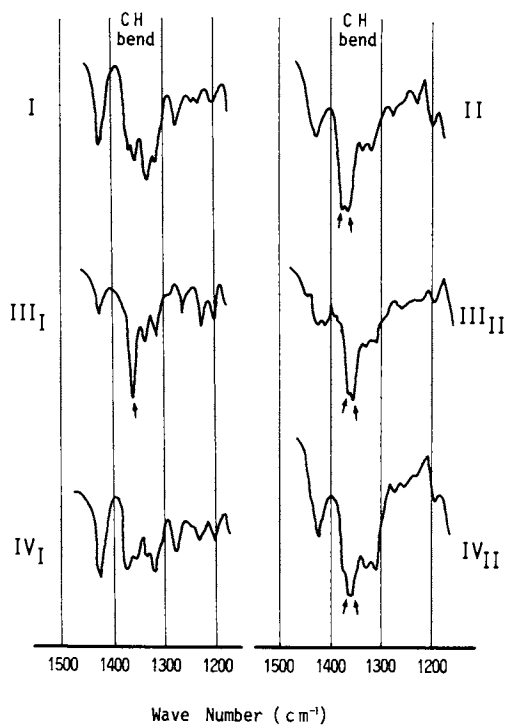


Fig. 7 IR spectra of the allomorphs in 1200 to 1500 cm^{-1} region. Arrow shows bands assigned to CH bending.

had a CH bending band at about 1370 cm^{-1} that showed strong absorption compared with neighboring bands. However, the band for III_I was single, while the band for III_{II} consisted of two bands. The IR spectra for IV_{II} showed some of the characteristics of I and IV_I , but its CH bending band was split, similar to II.

Generally, bands related to the chain conformation were singular in the cellulose I family and doublets in the cellulose II family. This is consistent with two chain conformations, ie. "bent" (I family) and "bent and twisted" (II family), that have one and two types of glycosidic linkage. If chain conformations were essentially the same in all allomorphs, the differing sets of characteristics common within the families would not be explicable. The differences in the IR spectra should result from differences in chain conformation and from chain packing. Even though the chain polarity is the same when the unit cell types are as different as I and III_I , the chain packing must be quite different. By the difference of the chain polarity between the families, the characteristics common within the families could not be also explicable.

The bands that showed common characteristics based on the unit cell types and gave important information on the intermolecular hydrogen bonds will be discussed in another paper.

High Resolution Solid-state ^{13}C NMR Spectra of the Allomorphs

Atalla et al. (12), Earl et al. (18) and Horii et al. (19) reported that the signals of C1 and C4 in solid-state ^{13}C NMR spectra consist of two, three or more peaks for cellulose I and II. The chemical shifts of C1 peaks were at 105.2 and 107.0 ppm for I and 106.0 and 108.3 ppm for II and the C4 peaks were 89.3 and 90.1 ppm for I and 88.7 and 89.9 ppm for II (12).

Figures 8 and 9 show solid state ^{13}C NMR spectra of the allomorphs in the I family prepared from ramie and those in the II family prepared from Fortisan. The signal of C1 for III_I and IV_I did not show enough resolution to split into peaks though there was a shoulder at about 105 ppm. For all allomorphs in the I family, the chemical shifts of the C1 signal ranged from 106.5 to 107.0 ppm and their half-widths were 250 Hz. The C1 signals for the II family were all split into two peaks at 106 and 108.5 ppm. The half-widths were 320, 330 and 290 Hz, for II, III_{II} and IV_{II} , respectively. Larger widths were observed for the cellulose II family. The values of the chemical shift and half-width were averages of values measured for the samples with the various origins, except for the Valonia and bacterial celluloses, which had substantially different values.

Recently, we have obtained better NMR data for the allomorphs with a Bruker instrument at 200 MHz for protons. The C1 signal of III_I seemed to be a singlet, but its profile was broadened unsymmetrically to the lower ppm side and suggested additional weak peaks. The half-width was almost the same as that of cellulose I. The common characteristics related to half-width of the C1 signal within each families were clearly evident.

The same phenomena were observed for signals from C4. The chemical shifts for the I family were 89.3 to 90.0 ppm, with half-widths of 180 (I), 200 (III_I) and 200 (IV_I). The chemical shifts of

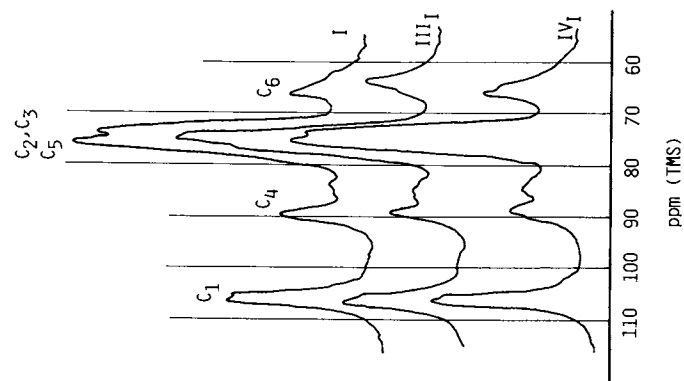


Fig. 9 Solid-state CP/MAS ^{13}C NMR spectra of the allomorphs in cellulose II family. II: Fortisan, III: prepared from Fortisan, IV: prepared from Fortisan through IIII.

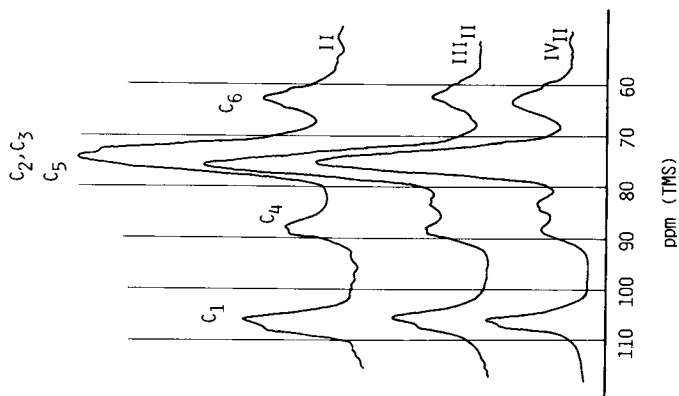


Fig. 8 Solid-state CP/MAS ^{13}C NMR spectra of the allomorphs in cellulose I family. I: ramie, III: prepared from ramie, IV: prepared from ramie through the III.

American Chemical Society
Library

1155 16th St., N.W.

In The Structures of Cellulose, Atlanta, R.;

Washington, D. C., 20036

C4 for the II family were 88.0 to 89.5 ppm with half-widths of 310 (II), 320 (III_{II}) and 320 (IV_{II}). The half-width was controlled basically by the degree of separation of the two peaks split in the C1 and C4 signals. The effect of the crystallinity of samples on the half-width was small. The uniformity of half-widths within the families suggests that the signals of C1 and C4 consist of two peaks even though they are observed as single peaks. The signals of C1 and C4 should reflect the symmetry at the glycosidic linkage. The splitting into two peaks agrees with the "bent and twisted" conformation proposed for cellulose II. The splitting for the I family suggested that the conformation is not the simple "bent" model in the strictest sense, but, referring to the IR spectra, the degree of twisting may not be as large as in the II family.

Dudley et al. (29) suggested the observed doublets of C1 and C4 in cellulose II were due to independent chains in the unit cell. Cael et al. (30) explained the ¹³C NMR spectrum of cellulose I with the eight-chain unit cell using Dudley's proposal. But the proposal could not explain the similarity of the C1 and C4 signals of the allomorphs in each of the families. They should show similarity between III_I and III_{II} or IV_I and IV_{II} because their chain packing should be similar to each other. When the high resolution NMR spectra of these are measured the problem will be more clear.

The chemical shift of the signal from C6 was influenced by the unit cell type as well as the family. This is because O6 plays an important part in intermolecular hydrogen bonding. The range was from 66.3 to 67 ppm for I and IV_I. Cellulose III_I is in the I family but its unit cell is the II type; the shift for O6 was 64.0 ppm. For II and III_{II}, the shift was 63.5 to 64.0 ppm. The shift of C6 in IV_{II}, which is in the cellulose II family but has a type I unit cell, has a value of 64.5 ppm, which is rather high for a member of the cellulose II family. The relation between chemical shift of the peak from C6 and the intermolecular hydrogen bonds will be further discussed in another paper.

The results were summarized in Table VIII.

Table VIII. Similarity of ¹³C NMR Spectra of the Allomorphs Based on the Families or the Unit Cell Types

Allomorph			Signal		
Family	Unit Cell type		Half-width (Hz)		Chemical shift (ppm)
			C1	C4	C6
I	I	I	250	180	67.0
III _I	I	II	250	200	64.0
IV _I	I	I	250	200	66.3
II	II	II	320	310	64.0
III _{II}	II	II	330	320	63.5
IV _{II}	II	I	290	320	64.5

By analogy with the IR spectra, the ¹³C NMR spectra showed that there were common differences based on the cellulose families at signals related to the chain conformation. The results were given a more reasonable interpretation through our hypothesis than the proposal of parallel and antiparallel chain systems.

Kai et al. (31) have reported that nascent microfibrils of bacterial cellulose were transformed into cellulose II with 10⁻³% NaOH aq. Solution or 86 vol % acetone aq. solution. They examined them with electron microscopy and diffraction. The microfibrils transformed into II with the acetone solution did not show any morphological change, retained the microfibrillar state of the original material, and had uniformly thin width and long lengths. The result is not consistent with a mechanism based on change from "parallel chain" to "antiparallel chains" during the transformation from I to II.

In conclusion, we think that the cause of structural irreversibility between the cellulose I and II families is an irreversible transformation between the skeletal chain conformations in the families. Although we expect that further studies of cellulose will provide clearer details of chain conformation, it is not likely that it will be possible to completely solve the structures on the basis of the limited amount of X-ray data available.

Acknowledgments

The authors are indebted to Dr. R. H. Marchessault, Xerox Research Centre of Canada, for valuable suggestions, and to Dr. T. Yoshida, Government Industrial Development Laboratory, Hokkaido, for his aid in obtaining some of the ¹³C NMR spectra. The preliminary study of the IR spectra by Dr. A. Sueoka provided valuable assistance in this work. The work was supported by a grant-in-Aid for Scientific Research from the Ministry of Education, Japan.

Literature Cited

1. Hayashi, J.; Sueoka, A.; Watanabe, S. Nippon Kagaku Kaishi, 153(1973).
2. Sueoka, A.; Hayashi, J.; Watanabe, S. Nippon Kagaku Kaishi, 594(1973), *ibid*, 1345(1973).
3. Hayashi, J.; Sueoka, A.; Watanabe, S. J. Polym. Sci., Polym. Letters., 13, 23(1975).
4. Watanabe, S.; Imai, K.; Hayashi, J. Kogyo Kagaku Zasshi 74, 1427(1971), 1470(1971).
5. Hayashi, J.; Sueoka, A.; Watanabe, S. Nippon Kagaku Kaishi, 160(1973).
6. Hayashi, J.; Imai, K.; Hamazaki, T.; Watanabe, S. Nippon Kagaku Kaishi, 1587(1973).
7. Hayashi, J.; Yamada, T.; Watanabe S. Sen-i Gakkaishi, 30, 190(1974).
8. Hayashi, J.; Yamada, T. Sen-i Gakkaishi, 31, 544(1975).
9. Hayashi, J.; Yamada, T.; Kimura, K.; Watanabe, S. Nippon Kagaku Kaishi, 1967(1974).
10. Hayashi, J.; Yamada, T.; Kimura K. J. Appl. Polym. Sci., Symposium 28, 713(1976).
11. Atalla, R.H. J. Appl. Polym. Sci., Symposium 28, 659(1976).
12. VanderHart, D.L.; Atalla, R.H. Macromolecules, 17, 1465(1984).
13. Sarko, A.; Muggli R. Macromolecules, 7, 486(1974).
14. Stipanovic, A.J.; Sarko A. Macromolecules, 9, 851(1976).
15. Gardner, K.H.; Blackwell, J. Biopolymers, 13, 1975(1974).

16. Kolpak, F.J.; Blackwell, J. Macromolecules, 9, 273(1976).
17. Sarko, A. Tappi, 61, 59(1978).
18. Atalla, R.H.; Gast, J.C.; Sindrot, D.W.; Bartuska, V.J.; Maciel, G.E. J. Am. Chem. Soc., 102, 3249(1980)
19. Earl, W.L.; VanderHart, D.L. Macromolecules, 14, 570(1981), J. Am. Chem. Soc., 102, 3249(1980).
20. Horii, F.; Hirai, A.; Kitamaru, R. Ploym. Bulletin, 8, 163(1982).
21. Marrinan, H.J.; Mann, J. J. Appl. Chem., 4, 204(1954), J. Polym. Sci., 21, 301(1956).
22. Mann, J.; Marrinan, H.J. Trans. Faraday Soc., 52, 177(1956), J. Polym. Sci., 32, 125, 357(1958).
23. Liang, C.Y.; Marchessault, R.H. J. Polym. Sci., 37, 358(1959), ibid, 39, 269(1959).
24. Marchessault, R.H.; Liang, C.Y. J. Polym. Sci., 43, 71(1960).
25. Chidambareswaran, P.K.; Srebnivasan; Patil, N.B. J. Appl. Polym. Sci., 27, (1982).
26. Colvin, J.R. Can. J. Microbiol., 11, 641(1965).
27. Hayashi, J.; Sueoka, A.; Watanabe, S. Nippon Kagaku Kaishi, 1320(1974).
28. Watanabe, S.; Hayashi, J. Kogyo Kagaku Zasshi, 73, 1890(1970).
29. Dudley, R.L.; Fyfe, C.A.; Stephenson, P.J.; Deslandes, Y.; Hamer, G.K.; Marchessault, R.H. J. Am. Chem. Soc., 105, 2469(1983)
30. Cael, J.J.; Kwoh, D.L.W.; Bhattacharjee, S.S. Macromolecules, 18, 819, (1985).
31. Kai, A.; Koseki, T. Bull. Chem. Soc., Japan, 57, 1437(1984), Chem. Lett., No. 5, 607(1985), Polym. preprint, Japan, No. 9, 2477(1985)
32. Jones, D.W. J. Polym. Sci., 32, 371(1958)

RECEIVED March 5, 1987

Chapter 8

Raman Spectra of Celluloses

James H. Wiley and Rajai H. Atalla

Institute of Paper Chemistry, Appleton, WI 54912

An investigation to study molecular orientation and polymorphy in cellulose fibers, and to further assign the bands in the vibrational spectrum of cellulose was conducted utilizing the Raman microprobe. The microprobe allows spectra to be recorded from domains as small as 1 micrometer and thereby greatly increases the potential of Raman spectroscopy as a tool for studying the structure of cellulose fibers. In the band assignment work, spectra were recorded from oriented fibers by varying the polarization of the incident light relative to the fiber axis. Analysis of the band intensities revealed new information about the directional character of the vibrational displacements. This information was used in conjunction with the spectra of deuterated celluloses and normal coordinate analyses of cellulose model compounds to make assignments.

Cellulose polymorphy was studied by comparing the spectra of Valonia, ramie, and mercerized ramie. It appears that the conformation of the cellulose backbone is the same in Valonia and ramie celluloses, but that the hydrogen bonding patterns are different. Mercerized cellulose and native celluloses differ in both their backbone conformations and hydrogen bonding patterns.

Cellulose orientation in the plane perpendicular to the chain axis was studied by recording spectra of ramie cross sections with different polarizations of the incident light relative to the cell wall surface. The intensities are consistent with random cellulose orientation. It appears, however, that the sample preparation techniques can influence the cellulose orientation. Therefore, further studies will be necessary to understand the molecular orientation in cellulose fibers.

Many questions about the molecular organization in plant cell walls remain unanswered. A new instrument, the Raman microprobe, has

0097-6156/87/0340-0151\$06.00/0
© 1987 American Chemical Society

provided a novel method for investigating plant cell wall structure. The objective in this work was to study the structure of the principal cell wall component, cellulose, using the Raman microprobe's unique capabilities. The investigation had two phases. In the first phase, the information made accessible by the microprobe was used to advance the assignment of the Raman spectrum of cellulose. In the second phase, the microprobe was used to study molecular orientation and polymorphy in cellulose fibers. The major results from both phases of this investigation will be discussed in this report.

Background

Raman Spectra of Cellulose. In laser excited Raman spectroscopy, a sample is exposed to monochromatic light, and the scattered light is analyzed. The frequency of a small fraction of the scattered light is shifted relative to the exciting light. The magnitude of the frequency shift corresponds to the vibrational frequencies of the molecules in the sample. Therefore, Raman spectroscopy provides information similar to that provided by infrared spectroscopy.

Both Raman and infrared spectroscopy yield information about chemical functionality, molecular conformation, and hydrogen bonding. Raman spectroscopy, however, has some important advantages. Highly polar bond systems, which result in intense infrared bands, have relatively low polarizabilities and, hence, weak Raman intensities. Water, therefore has very weak Raman bands and does not interfere with the spectrum of cellulose. In the Raman technique, control of the polarization of the exciting light coupled with analysis of the polarization of the scattered light can facilitate assignment of the spectra and provide information about molecular orientation. In infrared spectra, the attenuation of the incident beam is measured. This means that any processes other than absorption which cause attenuation of the incident beam are problematic. Since the refractive index of the sample will often go through large excursions in the neighborhood of absorption bands, the scattering losses will vary greatly with frequency over the infrared region. The variations in the refractive index can cause anomalous features in infrared spectra. In Raman spectroscopy, refractive index variations are not a problem, since the excitation frequency is far removed from any absorption bands. Therefore, it is easier to record Raman rather than infrared spectra from samples such as cellulose which scatter light strongly.

Raman Microprobe. A recent innovation in Raman spectroscopy was the development of the Raman microprobe. The microprobe is a specially designed optical microscope coupled with a conventional Raman spectrometer. The microscope performs two key functions. It focuses the exciting light on the sample down to a diameter of one micrometer; then it gathers the scattered light and transmits it to the entrance slit of the spectrometer. Since the microprobe acquires spectra from such small domains, the structural heterogeneity of the domains is greatly reduced relative to the domains examined in conventional Raman spectroscopy. The microprobe makes it possible to identify the morphological features from which

spectra are recorded so that orientation, composition, and structure can be studied as a function of morphology.

The special attributes of the microprobe make new information available. This investigation utilized the ability of the microprobe to record spectra from morphologically homogeneous domains, using polarized light to derive new information for assigning the Raman spectrum of cellulose. These assignments along with other spectral information obtained with the microprobe were then used to study polymorphy within the cellulose I family and cellulose orientation as a function of morphology.

Band Assignments. In order for Raman spectroscopy to provide structural information, the assignment of the spectra must be understood. The large number of vibrational degrees of freedom and low symmetry possessed by the cellulose molecule have made interpretation of the spectrum difficult. Given the complexity of the problem, a series of detailed normal coordinate analyses of model compounds were conducted in our laboratory to provide a basis for interpreting the vibrational spectrum of cellulose (1-8). The calculations showed that, except for the internal vibrations of the methylene groups, the modes below 1500 cm^{-1} are delocalized motions which are not adequately described by the group frequency approximation in which modes are assumed to be localized within certain chemical groups in the molecule.

Polymorphy. The two major allomorphs of cellulose, cellulose I and cellulose II, have been studied extensively. The question of polymorphy within the cellulose I (native cellulose) family has not received as much attention. Evidence has been reported, however, that the structure of native cellulose varies depending on the source. Early x-ray studies of cotton, ramie, linen, algal cellulose, and bacterial cellulose detected significant differences in the unit cell parameters (9). Based on electron diffractograms, Honjo and Watanabe (10) and others (11-13) concluded that the unit cell of algal cellulose is larger and has lower symmetry than the commonly accepted cell for cellulose I. Marrinan and Mann (14-15) and later Liang and Marchessault (16) observed that the infrared spectra of algal and bacterial cellulose differ from the spectra of ramie.

More recently, Atalla and VanderHart (17-18) have studied the solid-state ^{13}C NMR spectra of several forms of native cellulose. They concluded that native celluloses appear to be composites of two distinct crystalline forms of cellulose called I_{α} and I_{β} . The proportions of I_{α} and I_{β} in the composite varies depending on the source of the cellulose. In algal and bacterial cellulose, the I_{α} form dominates, whereas the I_{β} form dominates in ramie, cotton, and wood pulp. These results are consistent with the data from diffractometry and infrared spectroscopy in that algal and bacterial cellulose are similar to each other but different from other native celluloses.

The structural differences between I_{α} and I_{β} are not understood yet. Atalla (18) compared the Raman spectra of various native celluloses with different I_{α} to I_{β} ratios. He also compared the native cellulose spectra with the spectrum of cellulose II. The spectra of

the native celluloses are all similar to each other in the region most sensitive to cellulose conformation. The spectrum of cellulose II is quite different in this region. Therefore Atalla concluded that celluloses I_{α} and I_{β} have similar conformations but are packed in different lattices. In cellulose II, both the conformation and lattice are different from that of cellulose I.

Other workers (19-20) have interpreted these differences in the NMR spectra and other data in alternative ways. They believe that celluloses I and II have the same skeletal conformation but are packed in different lattices. In this theory, the differences within the cellulose I family are derived from the size of the unit cells. Valonia contains a larger 8 chain unit cell, whereas ramie contains a mixture of the 8 chain unit cell and the smaller Meyer and Misch unit cell. Therefore the interpretation of the NMR spectra remains controversial.

Orientation. The orientation of the cellulose chain axis in a number of different fibers has been studied in detail (21-22). Much less is known about the cellulose orientation in the plane perpendicular to the chain axis. The orientation in this plane is determined by the lateral arrangement of the microfibrils relative to each other. In algal celluloses, the evidence from x-ray and electron diffraction indicates that the microfibrils are arranged nonrandomly in the plane perpendicular to the chain axis (21-29). Preston (22) proposed the model shown in Figure 1 to explain his x-ray data. There are two different orientations of the microfibrils. The 002 planes in one set of microfibrils are approximately perpendicular to the 002 planes in the second set. In both sets of microfibrils, the 101 planes are oriented parallel to the cell wall surface (refer to Figure 1). Preston's model has been confirmed in more recent studies (29). In the remainder of this report, the type of orientation shown in Figure 1 will be referred to as alternating orientation.

Direct measurements of cellulose orientation in fibers have yielded conflicting results. Evidence from x-ray diffraction studies of wood samples suggested that the cellulose crystallites are arranged randomly in the plane perpendicular to the fiber axis (30-33). Raman spectroscopic studies of cotton fibers dried under tension, however, demonstrated that the methine C-H bonds are oriented preferentially perpendicular to the surface of the cell wall (34). Since the C-H bonds are perpendicular to the 002 plane, the orientation suggested by the Raman evidence differs from the alternating orientation in algal celluloses.

Overview of Experimental Method

In the spectra of nonrandomly oriented polymers, the intensity and polarization of the Raman scattered light are dependent on the polarization of the exciting light relative to the orientation of the molecules (35). If the orientation of the molecules is known, comparison of spectra recorded with different polarizations of the exciting light yields useful information about the directionality of the vibrational motions. Conversely, information about molecular orientation can be gained if the directionality of the vibrations is

known. In the present work, the major technique employed in the experiments was to compare spectra recorded with different polarizations of the incident laser beam relative to the morphology of the samples.

In all spectra recorded, precautions were taken to avoid complications associated with the dichroism inherent in the optics of the microscope and the monochromator. First, a polarization scrambler was inserted in the path of the Raman scattered light at the coupling between the microscope and the monochromator. Second, we did not change the polarization of the incident light directly but instead used a rotating stage to rotate the sample relative to the plane of polarization of the incident light.

Two classes of experiments were conducted. In both sets of experiments, fibers in which the cellulose chains are oriented parallel to the fiber axis were used. In the first class of experiments, the plane of polarization of the incident light was changed relative to the axis of the fibers by rotating the fibers around the optical axis of the microscope (see Figure 2a). The dependence of the band intensities on the polarization of the incident light was studied to determine the directional character of the vibrational motions. This information was used to advance the assignment of the Raman spectrum of cellulose. Spectra from *Valonia*, ramie, and mercerized ramie fibers, which have different allomorphic compositions, were compared to study the structural differences between the allomorphs.

In the second class of experiments, spectra were recorded from ramie fiber cross-sections. The plane of polarization of the incident light was changed relative to plane of the cell wall by rotating the cross-sections around the optical axis of the microscope axis (see Figure 2b). The information from these spectra was used to study the orientation of the cellulose in the plane perpendicular to the chain axis.

Results and Discussion

Assignment of the Vibrational Spectrum of Cellulose. Sets of spectra in which the orientation of the electric vector of the incident light was varied in 15 degree increments relative to the fiber axis were recorded. Figure 3 shows the set recorded from a fibrillar aggregate of *Valonia macrophysa* cellulose. Scanning electron micrographs showed that the aggregates are highly oriented bundles of fibrils. Therefore, the cellulose chains are parallel to the axis of the bundle. A set of spectra recorded from a ramie fiber is shown in Figure 4. In ramie, the cellulose chains are also approximately parallel to the fiber axis (21-22).

From the figures it is clear that the band intensities are strongly dependent on the polarization of the light. The intensities are related to the orientation of the electric vector by the following equation:

$$I = a + b (\cos^2\theta) + c (\cos^4\theta) \quad (1)$$

where a , b , and c are constants related to scattering activities, and θ is the angle between the electric vector of the incident light

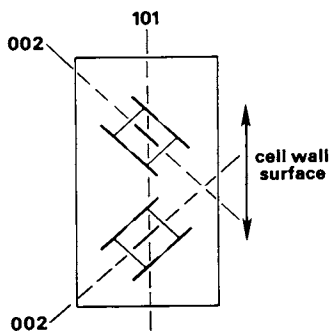


Figure 1. The cellulose orientation in the plane perpendicular to the chain axis found in algal celluloses.

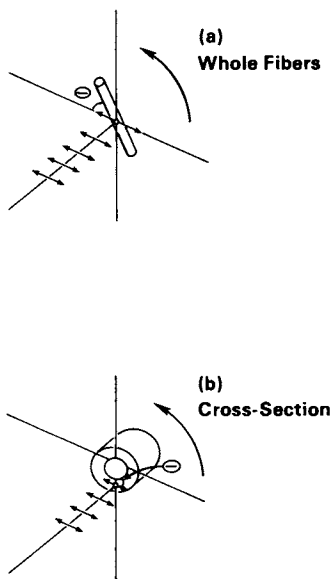


Figure 2. Microprobe experiments in which the polarization of the exciting light was varied relative to the geometry of the samples.

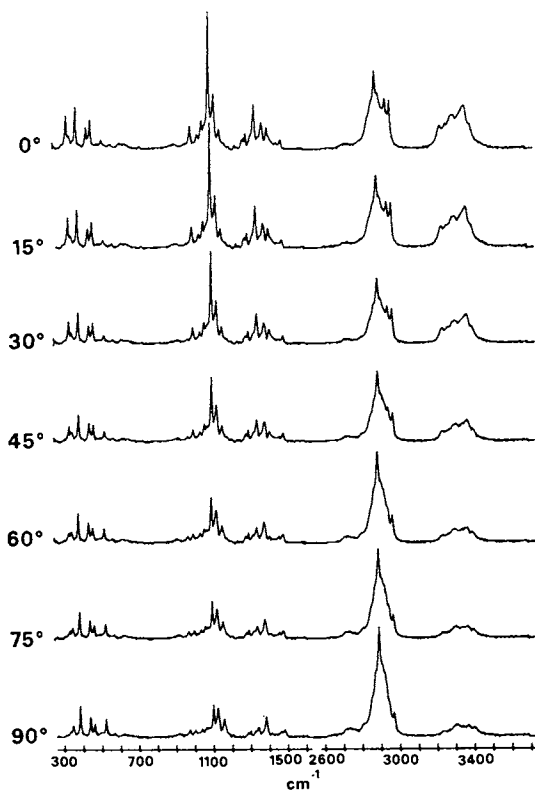


Figure 3. Polarized Raman spectra from a fibrillar aggregate of *Valonia* cellulose. The angle between the electric vector and the chain axis was varied from 0° to 90°.

and the fiber axis. Equation 1 was derived by following Snyder's treatment (35) and assuming that the cellulose chains are parallel to the fiber axis, and that the chains are oriented randomly around their axes. Equation 1 was fitted to the data in Figure 3 and 4 by a linear regression technique. Equation 1 adequately described the observed data for bands which were well resolved. An example of the fit which could be achieved by this analysis is shown in Figure 5, where the observed and predicted peak heights are plotted against θ for the intense band at 1095 cm^{-1} . Bands which were weak and/or poorly resolved could not be fitted as well.

Based on the number and location of the maxima and minima in the intensity vs. θ curves, the bands in the Raman spectrum of native cellulose were divided into four categories. Table 1 summarizes the band classifications for those bands which were resolved well enough to be analyzed. The classifications provide information about the directional character of the vibrations. The four categories are described as follows:

- 1) A_0 bands are most intense when the incident electric vector is parallel to the cellulose chain axis. Therefore, the maximum change in polarizability associated with the vibrations is parallel to the chain axis. The intensity vs. θ curves contain a single maximum and minimum.
- 2) A_{90} bands are most intense when the incident electric vector is perpendicular to the chain axis. The maximum change polarizability is perpendicular to the chain axis. These bands also exhibit a single maximum and minimum in the intensity vs. θ curves.
- 3) B_0 bands are most intense when the incident electric vector is parallel to the chain axis. As was the case with A_0 bands, the maximum change in polarizability is parallel to the chain axis. In the intensity vs. θ curves, however, these bands exhibit two maxima and a single minimum. The multiple maxima may result from accidentally degenerate modes which have maxima at 0 and 90° or from modes in which some of elements of the polarizability decrease during the vibration.
- 4) B_{90} bands are most intense when the incident electric vector is perpendicular to the chain axis. The maximum change in polarizability is perpendicular to the chain axis. These bands also exhibit two maxima and a single minima in the intensity vs. polarization curves.

As a supplement to the intensity work, the nature of the vibrations was also studied by recording spectra from deuterated celluloses. By comparing the spectrum of fully deuterated cellulose with that of normal cellulose, the vibrations involving the hydrogen atoms can be separated from the pure skeletal motions. Figure 6 is the spectrum of carbon-deuterated bacterial cellulose. This sample was kindly provided by Dr. H. L. Crespi. It was prepared by growing Acetobacter xylinum in deuterated growth media (36). The residual intensity in the O-H and C-H stretching regions indicates that the cellulose is not fully deuterated. We also recorded Raman spectra

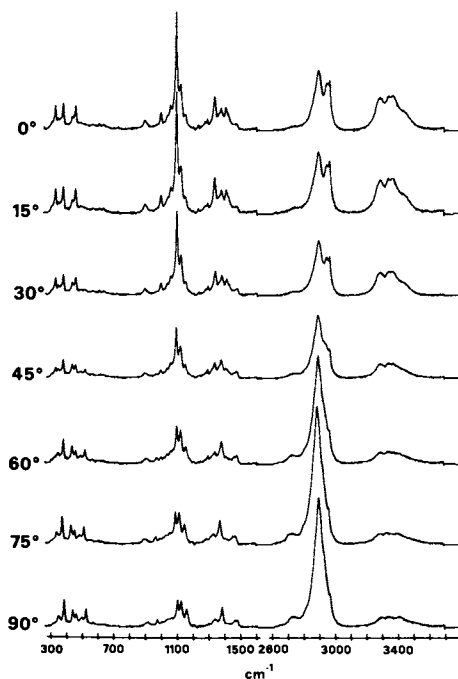


Figure 4. Polarized Raman spectra from a ramie fiber. The angle between the electric vector and the chain axis was varied from 0° to 90° .

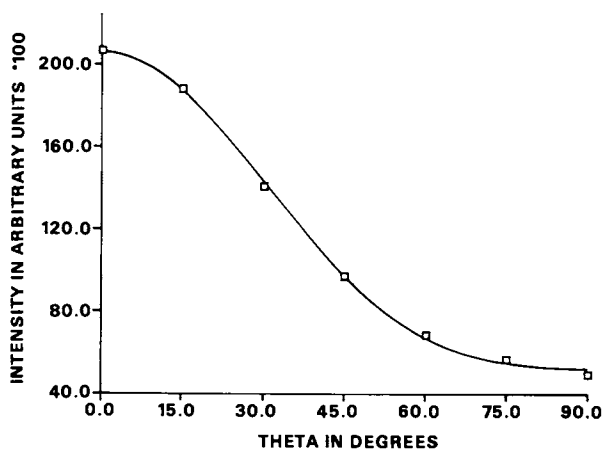


Figure 5. The dependence of intensity on the polarization of the incident light for the band at 1095 cm^{-1} in the spectra of Valonia.

Table 1. Summary of intensity maxima, deuteration sensitivities, and band assignments for the Raman spectra of Valonia and ramie

Band Frequency ^a (cm ⁻¹)		Intensity Classi- fication	Deuteration Sensitivity	Assignment
Valonia	Ramie			
331	331	A ₀	weak	heavy atom bending, some
344	344	B?	"	heavy atom stretching
381	380	B?	"	"
437	437	B?	"	"
459	458	B ₀	"	"
520	519	A _{g0}	"	"
913	910	B ₀	?	HCC and HCO bending at C6
968	969	B _{g0}	?	heavy atom (CC and CO)
997	995	A ₀	?	stretching
1034	1035	A ₀	?	"
1057	1057	A ₀	?	"
1095	1095	A ₀	weak	"
1118	1117	B ₀	"	"
1123	1121	A ₀	"	"
1152	1151	B?	?	heavy atom stretching plus HCC and HCO bending
1279	1275	A ₀	?	HCC and HCO bending
1292	1291	?	?	"
1334	1331	A ₀	strong	"
1337	1337	A ₀	"	HCC, HCO, and HOC bending
1378	1378	B?	"	"
1406	1407	A ₀	"	"
1455	1456	B _{g0}	"	HCH and HOC bending
1477	1475	A _{g0}	"	"
2868	2866	B _{g0}	"	C-H and CH ₂ stretching
2885	2889	B _{g0}	"	"
2941	2943	B?	"	"
2965	2963	B ₀	"	"
3291	3286	B ₀	"	O-H stretching
3334	3335	? ₀	"	"
3261	3363	? ₀	"	"
3395	3402	B ₀	"	"

^aOnly the bands resolved in both the Valonia and ramie are included in the table.

of oriented samples of partially deuterated cellulose with the electric vector both parallel and perpendicular to the chain axis. Based on these studies, the deuteration sensitivity for several of the bands was determined. This information is also listed in Table I.

Based on the intensity studies, deuterated cellulose spectra, and normal coordinate analyses of model compounds (7-8), the assignment of the bands in the vibrational spectrum of cellulose was advanced. The information is summarized in Table 1. A detailed discussion of the band assignments is beyond the scope of this report and will be given elsewhere (37). A brief overview of the assignments will be given here. The frequency region between 600 and 2500 cm^{-1} is dominated by bending motions of the cellulose skeleton. These are complex modes which are very delocalized and often involve motion at the glycosidic linkage. The frequencies, especially between 400 and 300 cm^{-1} , are sensitive to the conformation of the anhydroglucose residues about the linkage (8). In the modes between 900 and 1200 cm^{-1} , CC and CO stretching motions are dominant. This region contains very intense bands. The modes between 1200 and 1500 cm^{-1} involve methylene, methine, and hydroxyl bending motions. Although the modes in this region are generally delocalized motions, the HCH bending motion is isolated and behaves as a group mode. In the regions between 2700 and 3000 cm^{-1} and 3200 and 3500 cm^{-1} , the C-H and O-H stretching motions occur. These motions behave as pure group vibrations. Although the assignments do not provide a complete description of the vibrational motions, they serve to increase our understanding of the cellulose vibrational spectrum.

Polymorphy. Cellulose polymorphy within the cellulose I family was studied by comparing the Raman spectra of Valonia and ramie cellulose. Solid state NMR spectra indicate that the I_{α} form predominates in Valonia while the I_{β} form predominates in ramie (17-18). The cellulose I spectra were also compared with spectra of cellulose II recorded from a mercerized ramie fiber. Figures 7 and 8 show the Raman spectra of these three celluloses. Spectra were recorded with the electric vector of the incident light parallel and perpendicular to the chain axis. These spectra can be divided into two regions. The region below 1600 cm^{-1} (Figure 7) is most sensitive to the conformation of the cellulose backbone (especially below 700 cm^{-1}). The higher frequency region, above 2700 cm^{-1} (Figure 8), is more sensitive to hydrogen bonding.

In the low frequency region (Figure 7), there are only minor differences between the spectra of native ramie and Valonia. The peaks in the Valonia spectra are narrower and better resolved. The reason for this is probably the larger size of the crystallites in Valonia cellulose (38-39). When the crystallites are larger, the environment of the molecules is more homogeneous. Therefore, the vibrational energy of the molecules is more uniform, resulting in narrower bands.

The most significant difference between the two native cellulose spectra in the low frequency region is that the intensity of the peak at 913 cm^{-1} is greater in the ramie spectra. This peak is also more intense in the spectrum of bacterial cellulose than in the

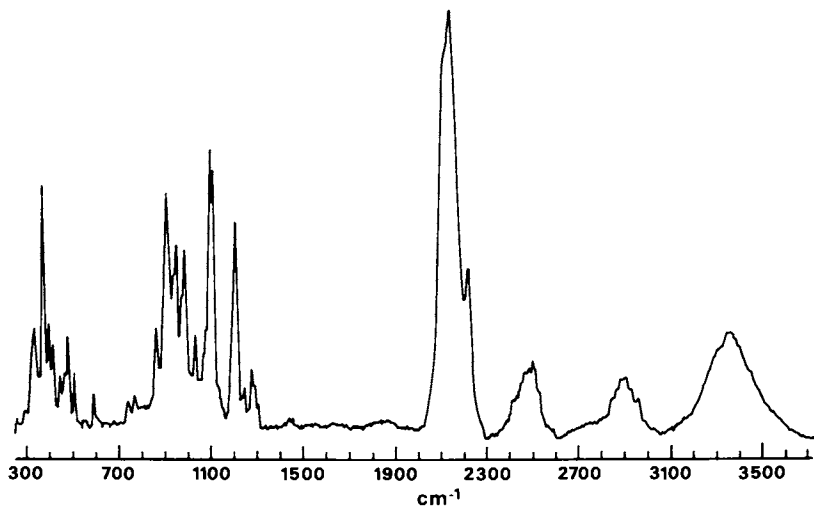


Figure 6. Raman spectrum of deuterated bacterial cellulose.

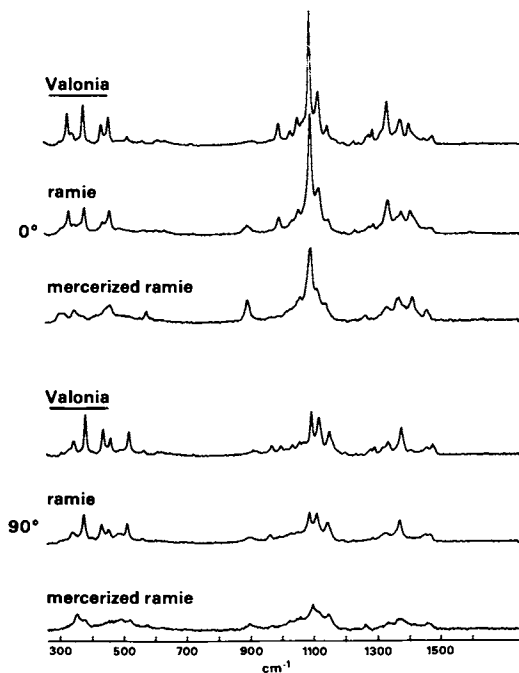


Figure 7. Comparison of the Raman spectra from Valonia, ramie, and mercerized ramie (low frequency region). Spectra were recorded with the electric vector at both 0° and 90° .

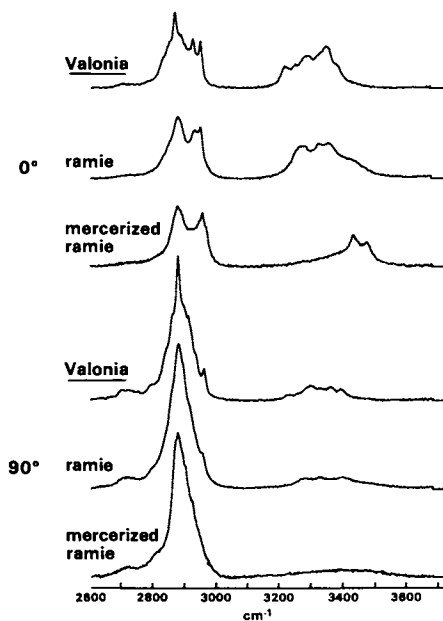


Figure 8. Comparison of the Raman spectra from Valonia, ramie, and mercerized ramie (high frequency region). Spectra were recorded with the electric vector at both 0° and 90° .

Valonia spectra. Since bacterial cellulose has approximately the same I_{α} to I_{β} ratio as Valonia (17-18), the intensity of this peak does not appear to be related to structural differences between I_{α} and I_{β} . Instead, the intensity of this peak appears to be inversely correlated with the size of the crystallites. It is very weak in the spectra of Valonia which has very large crystallites, but it is stronger in the spectra of ramie and bacterial cellulose which both have smaller crystallites (38-39).

The differences between the spectra of ramie and Valonia are quite small compared to the differences between native cellulose and cellulose II (see Figure 7). In the spectra of ramie and Valonia, the different peak widths and relative intensities can be attributed to the difference in the crystallite sizes. In the spectrum of cellulose II, however, the frequency and number of peaks is significantly different. In previous publications, the differences between the spectra of celluloses I and II have been interpreted as evidence for different conformations in celluloses I and II (40-41). The spectral differences which are indicative of conformational change are not observed in the spectra of ramie and Valonia. Since ramie and Valonia have different I_{α} to I_{β} ratios, it would appear that celluloses I_{α} and I_{β} must have similar molecular conformations.

In the C-H stretching region (Figure 8, 2700-3000 cm^{-1}), the primary difference between the spectra of ramie and Valonia is the broadness of the peaks. The peaks in the ramie spectra are broader as was the case in the low frequency region presumably due to the smaller crystallite size. In the spectra of mercerized ramie, the C-H stretching region differs slightly from that in the native celluloses but the differences are not as large as those in the low frequency region.

In the O-H stretching region (3200-3600 cm^{-1}), however, significant differences are observed between all three celluloses. These differences are most prominent in the spectra recorded with the electric vector parallel to the fiber axis (Figure 8a-c). The frequency as well as the broadness of the peaks varies in this region. The spectra of Valonia cellulose have a peak at 3231 cm^{-1} that is not observed in the ramie spectra. The spectra of native ramie on the other hand, have a peak at 3429 cm^{-1} that is not observed in Valonia. The spectrum of mercerized ramie recorded with the electric vector parallel has two sharp peaks at frequencies above those observed in the native celluloses. The differences in the O-H region between Valonia, ramie, and mercerized ramie suggest that the hydrogen bonding patterns are different in each of these celluloses. In summary, the Raman spectra indicate that celluloses I_{α} and I_{β} exhibit different hydrogen bonding patterns but have similar molecular conformations. Celluloses I and II have different molecular conformations as well as different hydrogen bonding patterns.

Cellulose Orientation. The orientation of the cellulose molecules in the plane perpendicular to the chain axis was studied by using the microprobe to record spectra of ramie fiber cross sections. Figure 9 shows spectra recorded with the electric vector of the exciting light tangential, perpendicular, and at 45° to the cell wall surface. If the cellulose orientation in the plane perpendicular to the fiber axis is anisotropic, then the intensities

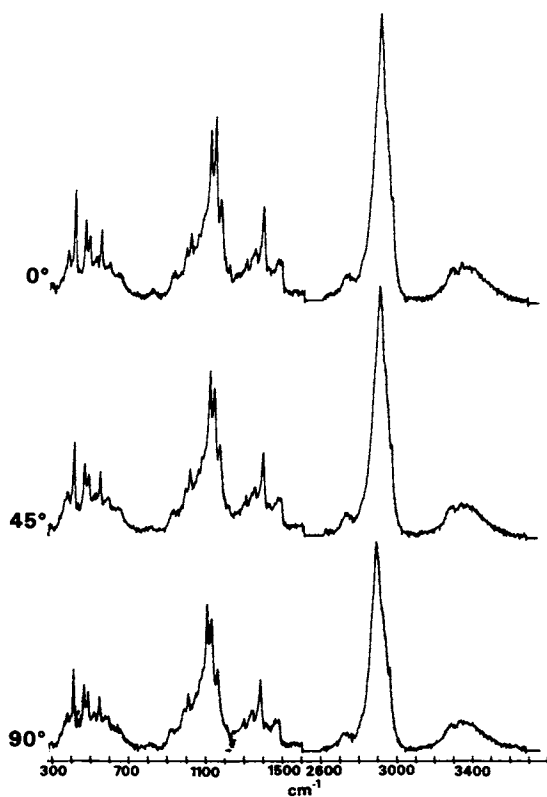


Figure 9. Polarized Raman spectra of a ramie cross section. The angle between the electric vector and the cell wall surface was varied from 0° to 90°.

should differ in the cross-section spectra recorded with different orientations of the incident electric vector. With the exception of the peaks at 1095 and 1123 cm^{-1} , the relative peak intensities in the cross-section spectra did not vary noticeably as the polarization of the incident light was changed (see Figure 9). The insensitivity of the majority of the bands to the orientation of incident electric vector is not consistent with either a preferential orientation of the methines perpendicular to the cell wall surface or the alternating type of orientation found in algal celluloses.

The variation in the relative intensities of the 1095 and 1123 cm^{-1} bands between the 0° and 45° spectra suggests anisotropy in the cellulose orientation. Table I shows that these peaks are skeletal stretching modes that are most intense when the electric vector of the incident light is parallel to the chain axis. Since the 1095 cm^{-1} peak is very sensitive to the orientation of the incident electric vector relative to the chain axis, the intensity variation suggests that the plane of sectioning was not exactly perpendicular to the cellulose chain axes so that the chains are tilted relative to the plane of sectioning.

If the cellulose is oriented randomly in the plane perpendicular to the chain axis, then the band intensities would be the same regardless of whether the incident electric vector was parallel, perpendicular, or 45° to the cell wall surface. The cross-section spectra, therefore, are consistent with random cellulose orientation in the plane perpendicular to the chain axis. These results conflict with our earlier spectra of tension dried cotton fibers (34) that indicated the methines were oriented preferentially perpendicular to the cell wall surface. More recent spectra of cotton fibers have shown that if the fibers are not dried under tension, the methine orientation is random in the plane perpendicular to the chain axis. Therefore, it appears the cellulose orientation can be influenced by the sample preparation methods. Since microtoming exerts large forces on the fibers, it is also possible that the cellulose orientation could have been disrupted during the preparation of the cross-sections. Further experiments will be necessary to understand the factors which influence the cellulose orientation.

Conclusions

Based on the number and location of the maxima and minima in the relationship between the band intensities and the polarization of the incident light relative to the chain axis, the bands in the Raman spectrum of cellulose could be divided into four groups. The about the direction of the vibrational motions in cellulose. The directions of the vibrations are such that the major change in polarizability associated with the motions is either parallel or perpendicular to the chain axis. Raman spectra recorded from deuterated celluloses allowed the vibrational modes involving C-H and O-H motions to be identified. These spectra demonstrated that most of the modes are complex coupled vibrations. Normal coordinate analyses of cellulose model compounds were done to determine the types of motion most likely to occur in each region of the spectrum. The calculations also suggested that the vibrational motions are very complex. The information from the normal coordinate calculations,

intensity studies, and spectra of deuterated celluloses was used to advance the assignment of the cellulose vibrational spectrum.

Comparison of the Raman spectra of Valonia, ramie, and mercerized ramie indicates that the conformation of the cellulose backbone is similar in Valonia and native ramie but different in mercerized ramie. The hydrogen bonding patterns, however, are different in Valonia and native ramie as well as in mercerized ramie.

Spectra recorded from ramie cross-sections suggest that the cellulose is oriented randomly in the plane perpendicular to the chain axis. It appears, however, that the sample preparation methods can influence the cellulose orientation. Therefore, further studies will be necessary to characterize the molecular orientation in cellulose fibers.

Acknowledgment

The authors wish to thank Dr. H. L. Crespi for furnishing the sample of deuterated bacterial cellulose and for his advice concerning the growth of algae in heavy water, and Dr. U. P. Agarwal for the many helpful discussions he contributed to this work. Portions of this work were used by J. H. Wiley as partial fulfillment of the requirements for the Ph.D. degree at The Institute of Paper Chemistry.

References

1. Pitzner, L. J. An investigation of the vibrational spectra of the 1,5-anhydropentitols. Doctoral Dissertation. Appleton, WI, The Institute of Paper Chemistry, Jan. 1973. 402 p.
2. Pitzner, L. J.; Atalla, R. H. Spectrochimica Acta 1975, 31A, 911-29.
3. Watson, G. M. An investigation of the vibrational spectra of the pentitols and erythritol. Doctoral Dissertation. Appleton, WI, The Institute of Paper Chemistry, June 1974. 178 p.
4. Edwards, S. L. An investigation of the vibrational spectra of the pentose sugars. Doctoral Dissertation. Appleton, WI, The Institute of Paper Chemistry, Jan. 1976. 245 p.
5. Williams, R. M. An investigation of the vibrational spectra of the inositols. Doctoral Dissertation. Appleton, WI, The Institute of Paper Chemistry, June 1977. 377 p.
6. Williams, R. M.; Atalla, R. H. J. Phys. Chem. 1984, 88, 508-19.
7. Wells, H. A. An investigation of the vibrational spectra of glucose, galactose, and mannose. Doctoral Dissertation. Appleton, WI, The Institute of Paper Chemistry, Jan. 1977. 431 p.
8. Carlson, K. P. An investigation of the vibrational spectra of the cellodextrins. Doctoral Dissertation. Appleton, WI, The Institute of Paper Chemistry, Nov. 1978. 153 p.
9. Wellard, H. J. J. Polym. Sci. 1954, 13, 471-6.
10. Honjo, G.; Watanabe, M. Nature 1958, 181, 326-8.
11. Fisher, D. G.; Mann, J. J. Polym. Sci. 1960, 42, 189-94.
12. Nieduszynski, I. A.; Atkins, E. D. T. Biochim. et Biophys. Acta 1970, 222, 109-18.
13. Hebert, J. J.; Muller, L. L. J. Appl. Polym. Sci. 1974, 18, 3373-7.

14. Marrinan, H. J.; Mann, J. J. Polym. Sci. 1956, 21, 301-11.
15. Mann, J.; Marrinan, H. J. J. Polym. Sci. 1958, 32, 357-70.
16. Liang, C. Y.; Marchessault, R. H. J. Polym. Sci. 1959, 37, 385-95.
17. VanderHart, D. L.; Atalla, R. H. Macromolecules 1984, 17, 1465-72.
18. Atalla, R. H. Polymorphy native in cellulose: recent developments. Function and Biosynthesis of Plant Cell Walls. W. M. Dugger; S. Bartnicki-Garcia, eds., Am. Soc. Plant Physiologists, Rockville, MD., 1984:381.
19. Dudley, R. L.; Fyfe, C. A.; Stephenson, P. J.; Deslandes, Y.; Hamer, G. K.; Marchessault, R. H. J. Am. Chem. Soc. 1983, 105, 2469-72.
20. Cael, J. J.; Kwoh, D. L. W.; Bhattacharjee, S. S.; Patt, S. L. Macromolecules 1985, 18, 819-21.
21. Frey-Wyssling, A. The Plant Cell Wall. Gebruder Borntraeger, Berlin, Stuttgart, 1976.
22. Preston, R. D. Physical Biology of Plant Cell Walls. Chapman and Hall, 1974.
23. Goto, T.; Harada, H.; Saiki, H. J. Japan Wood Res. Soc. 1973, 19(10), 463-8.
24. Revol, J.-F. Carbohyd. Polym. 1982, 2, 123-34.
25. Preston, R. D. Disc. Faraday Soc. 1951, 11, 165-70.
26. Schurz, J. Phyton 1955, 5(2), 53-66.
27. Tanaka, F.; Okamura, K. J. Polym. Sci. Polym. Phys. Ed. 1977, 15, 897-906.
28. Okamura, K. Memoirs of the College of Agriculture, Kyoto Univ. 1980, 115, 63-7.
29. Revol, J.-F.; Goring, D. A. I. Polymer 1973, 24, 1547-50.
30. Revol, J.-F.; Gancet, C.; Goring, D. A. I. Wood Sci. 1982, 14(3), 120-6.
31. Tanaka, F.; Takaki, T.; Okamura, K.; Koshijima, T. Wood Res. 1980, 66, 17-22.
32. Tanaka, F.; Koshijima, T. J. Japan Wood Res. Soc. 1983, 29(1), 1-7.
33. Tanaka, F.; Koshijima, T. Wood Sci. Technol. 1984, 18, 177-86.
34. Atalla, R. H.; Whitmore, R. E.; Heimbach, C. J. Macromolecules 1980, 13, 1717.
35. Snyder, R. G. J. Mol. Spect. 1971, 37, 353-65.
36. Crespi, H. L. Biosynthesis with deuterated microorganisms. Technical Committee Meeting on Modern Trends in the Biological Applications of Stable Isotopes., Leipzig, Germany., Dec. 6-10, 1976. p. 1-15.
37. Wiley, J. H.; Atalla, R. H. Carbohyd. Res. in press.
38. Nieduszynski, I.; Preston, R. D. Nature 1970, 225, 273-4.
39. Boylston, E. K.; Hebert, J. J. J. Appl. Polym. Sci. 1980, 25, 2105-7.
40. Atalla, R. H. Appl. Polym. Symp. 1976, 28, 659-69.
41. Atalla, R. H. Spectroscopic studies of polymorphy in cellulose: a new structural model. Proceedings of the International Symposium on Wood and Pulping Chemistry, Stockholm, June, 1981. SPCI Report, 1981, 38(1), 57.

RECEIVED March 5, 1987

Chapter 9

Crystalline Alkali-Cellulose Complexes as Intermediates During Mercerization

Anatole Sarko, Hisao Nishimura¹, and Takeshi Okano²

Department of Chemistry and Cellulose Research Institute, College of Environmental
Science and Forestry, State University of New York, Syracuse, NY 13210

During a controlled mercerization of ramie cellulose, the cellulose I crystal structure is irreversibly converted to cellulose II through several crystalline alkali-cellulose complexes. The crystal structures of three of the complexes -- Na-celluloses I, IIB, and IV -- are providing information on the characteristics of the interactions between cellulose and the Na⁺ ions, on the forces operating in the formation of these structures, and on the likely mechanism of the conversion. Although the formation of secondary bonds between Na⁺ ions and the hydroxyl groups of cellulose must be an important driving force in the formation of crystalline complexes, the hydrophobic attractions between cellulose chains appear to be at least as important. The transformation of the parallel-chain structure of cellulose I to an antiparallel one takes place already during the initial conversion step, from cellulose I to Na-cellulose I.

It was observed in earlier studies of controlled alkali-mercerization of ramie cellulose that the crystal structure of native cellulose is transformed to cellulose II through a series of crystalline alkali-cellulose complexes (1,2). The relationships between these "Na-celluloses" and their pathways of transformation are illustrated in Fig. 1. It has further been observed that all of the transformations are crystal-to-crystal phase changes, not involving intermediate amorphous phases. All of the experimental evidence has suggested

¹Current address: Research Center, Daicel Chemical Industries, Ltd., Himeji, Japan

²Current address: Department of Forest Products, Faculty of Agriculture,
University of Tokyo, Bunkyo, Tokyo, Japan

0097-6156/87/0340-0169\$06.00/0
© 1987 American Chemical Society

that the first conversion step -- from cellulose I to Na-cellulose I -- is apparently the step in which a transformation of the parallel-chain polarity to the antiparallel one takes place.

As shown by the x-ray diffraction diagrams reproduced in Fig. 2, the Na-celluloses exhibit a relatively high degree of crystallinity and excellent crystalline orientation. In view of this, further delineation of the transformations and the mechanism of mercerization were attempted through the crystal structure analysis of three of the complexes: Na-celluloses I, IIB, and IV. All analyses have now been nearly completed, and a preliminary account of the results is given below. The detailed descriptions of the crystal structures will be published separately after the completion of the studies.

Experimental

The methods of sample preparation, the characteristics and the probable composition of all of the complexes, and the procedures for obtaining x-ray fiber diffraction diagrams have been previously described in detail (1,2). The procedures of crystal structure analysis followed in these studies are identical to those used in previous analyses concerned with the structures of celluloses and other polysaccharides (cf., in particular, refs. 3-5). In all cases, both stereochemical and crystallographic structure refinements were carried out in parallel. The refinement of both the chain conformation and the chain packing were conducted with completely flexible chain models, using computational procedures that allow any desired structural parameter to be made a refinable variable (3). The positions of the solvent and the complexing molecules in the unit cell were explicitly considered, whenever warranted (5). Further details of the analysis and the refinement procedures will be given in reports dealing with the individual crystal structures.

Results

Na-cellulose I. The structure of the Na-cellulose I complex, although not as crystalline as that of cellulose I, obviously shows an equally good fibrous orientation (cf. Fig. 2A). The crystal structure is described by a large, four-chain unit cell, shown in Fig. 3. It contains 8 Na⁺ and OH⁻ pairs of ions and probably 16 molecules of water. The chain conformation is marked by features common to all crystalline cellulose polymorphs: an approximately 10.3 Å fiber repeat, a ribbon-like, twofold helical molecular shape, and the familiar O(3)--O(5') and O(6)--O(2') intramolecular hydrogen bonds. The characteristics of the chain packing are in accord with this chain conformation, showing a stacking into sheets along two directions. The presence of NaOH and water in the crystal structure, however, obviously contributes to considerable differences between the structures of Na-cellulose I and cellulose I.

The major difference between these two crystal structures resides in the chain packing polarity. As expected from the conversion studies and the irreversibility of the cellulose I to Na-cellulose I transformation, the crystal structure of Na-cellulose I is based on antiparallel chains (cf. Fig. 3). Because of the presence of Na⁺ ions, which apparently form secondary bonds with the cel-

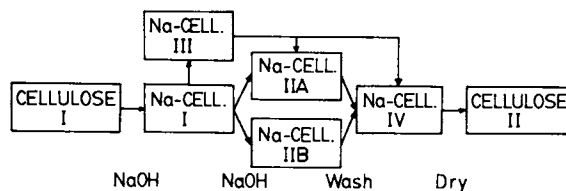


Fig. 1. Transformation pathways between cellulose and Na-cellulose crystal structures. (Reproduced with permission from ref. 1. Copyright 1986 John Wiley & Sons, Inc.)

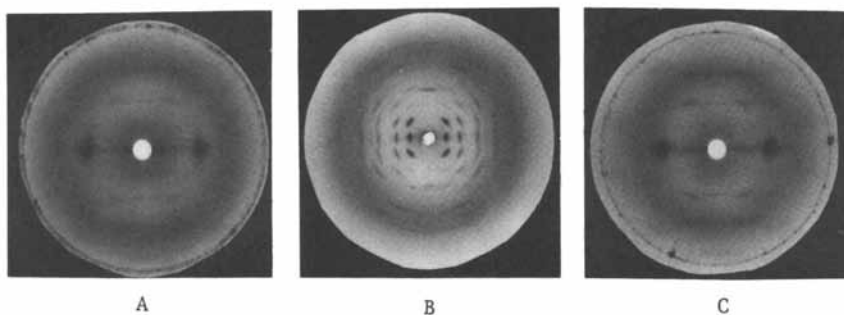


Fig. 2. X-ray fiber diffraction diagrams of: (A) Na-cellulose I, (B) Na-cellulose IIB, and (C) Na-cellulose IV. (Fiber axis is vertical).

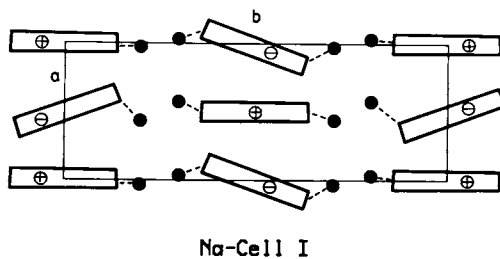


Fig. 3. The unit cell of Na-cellulose I in x - y projection: $a = 8.83$, $b = 25.28$, c (fiber axis) $= 10.29$ Å. The cellulose chains are shown in outline only, and filled circles indicate the positions of Na^+ ions. Secondary and hydrogen bonds are shown by dashed lines.

lulose hydroxyl groups, all of the interchain hydrogen bonds that ordinarily stabilize the cellulose I structure have been broken. As a result, distances between chains in the b direction of the unit cell have increased and intermolecular hydrogen bonds are not present. Nonetheless, the chains are still arranged in sheet-like structures, both along the a and b dimensions of the unit cell. It appears that these sheet-like formations result from the ribbonlike conformation of the cellulose molecule and, as discussed later, hydrophobic attractions.

Na-cellulose IIB. When Na-cellulose I is allowed to absorb more NaOH, a considerably different crystal structure results (cf. Fig. 4). The chain conformation departs from 2_1 symmetry and forms, instead, a threefold helix. The helices pack antiparallel in a hexagonal fashion, with a relatively large separation distance. The unit cell contains more than 60% of non-cellulose constituents -- NaOH and water -- surrounding each helix with a liquid-like structure. The presence of a large number of Na^+ ions quite likely results in the formation of many secondary bonds between the cellulose hydroxyls and the ions, forcing a scission of the remaining intramolecular hydrogen bonds that are present in the Na-cellulose I structure.

The threefold helices of cellulose are chiral, i.e., their left- and righthanded conformations are not identical. It is not yet known whether the structure of Na-cellulose IIB is characterized by one particular helix handedness, as both conformations are stable and of not very different conformational energy. The x-ray diffraction diagram (cf. Fig. 2B) is rich in detail and it should be possible to determine the handedness of the Na-cellulose IIB helix from a detailed x-ray refinement.

Na-cellulose IV. After all of the alkali has been washed from the Na-cellulose IIB complex, but prior to its drying, an x-ray diffraction diagram very similar to that of cellulose II is obtained (cf. Fig. 2C). The crystal structure of this intermediate -- Na-cellulose IV -- is based on a two-chain, monoclinic unit cell that is indeed very similar to that of cellulose II (cf. Fig. 5). The similarities extend to an antiparallel chain packing and a hydrogen-bonded sheet structure (6); the differences arise from the presence of two water molecules in the unit cell. The water molecules are situated in crystallographically defined positions, within the sheets composed of corner chains, i.e., between chains of like polarity. As a consequence, they participate in the hydrogen bonding linking the chains in the b direction of the unit cell. In so doing, they lengthen the b-axis relative to cellulose II. Although the overall pattern of hydrogen bonds in Na-cellulose IV differs little from that in cellulose II, there are some significant differences (6). For example, because the water molecules disrupt the O(3)--O(6) intermolecular hydrogen bonds between the corner chains, the normally tg conformation of the corner chain O(6) hydroxyls is changed to gt in Na-cellulose IV. This evidently allows the formation of a maximum number of hydrogen bonds, as each water molecule takes part in four hydrogen bonds. The center chains, not having any water molecules present within the sheet, retain the gt O(6) conformations and the

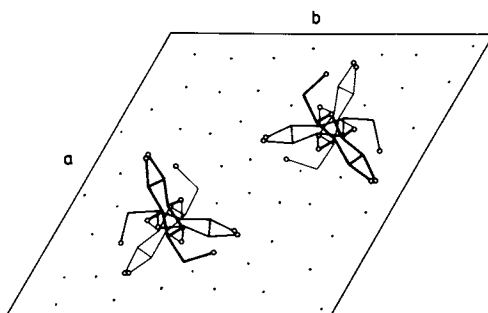


Fig. 4. The unit cell of Na-cellulose IIB in $\underline{x-y}$ projection: $\underline{a} = \underline{b} = 14.94$, \underline{c} (fiber axis) = 15.39 \AA , $\gamma = 120^\circ$. The unit cell is assumed to be filled with NaOH and water. (Also see caption of Fig. 3). (Reproduced with permission from ref. 13. Copyright 1985 Gordon & Breach.)

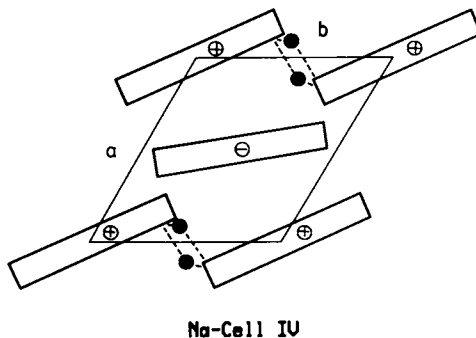


Fig. 5. The unit cell of Na-cellulose IV in $\underline{x-y}$ projection: $\underline{a} = 9.57$, $\underline{b} = 8.72$, \underline{c} (fiber axis) = 10.35 \AA , $\gamma = 122^\circ$. The positions of water molecules are indicated by filled circles. (Also see caption of Fig. 3).

intermolecular hydrogen bonds that are characteristic of cellulose II.

Discussion

From the point of view of the mechanism of mercerization, the features of these crystal structures and their interlinking transformations support our present understanding of the process. For example, it is known from previous studies that the conversion of cellulose I to Na-cellulose I begins in amorphous regions of the former, and proceeds initially by converting both such regions as well as the small crystallites (7,8). The amorphous or poorly crystalline regions of cellulose I are of the order of 30-40 Å in lateral dimensions, as indicated by crystallite size measurements (7). Therefore, a considerable amount of cellulose I material can be converted to Na-cellulose I before the larger crystallites are attacked. The conversion thus proceeds for the most part in the presence of crystallites of cellulose I that may exert a directing influence toward the product that forms. The threefold helical Na-cellulose IIB is likely to be a more stable structure relative to Na-cellulose I, but it apparently is not formed in the presence of unconverted cellulose I. The initial conversion to an alkali-complexed cellulose may, consequently, be controlled by some features of the sheet-oriented crystalline celluloses.

The antiparallel structure of Na-cellulose I is also not surprising. It is now well understood that a cellulose fiber is composed of a large number of microfibrils that are essentially single crystals in cross section. The microfibrils of cellulose I are parallel-chain single crystals whose formation is directed by biological processes (9). The aggregation of microfibrils into a fiber, however, is most likely a statistically random process, resulting in a fiber morphology that is marked by roughly equal numbers of "up" and "down" pointing microfibrils. The majority of the non-crystalline or amorphous regions in a cellulose I fiber may, therefore, be thought of as interfacial regions between microfibrils that are randomly pointing in two directions (cf. Fig. 4 in ref. 2). A supply of antiparallel-oriented chains is thus readily available, leading to an antiparallel-chain crystal structure with little effort in lateral rearrangement of chains. The presence of hydrogen-bond breaking NaOH in considerable quantity certainly facilitates lateral segmental motion and the resulting transformation to Na-cellulose I. These processes and the above-described fiber morphology are schematically illustrated in Fig. 6.

Once all vestiges of an interchain hydrogen-bonded cellulose structure have disappeared and the NaOH supply is sufficiently large, the more stable threefold helical Na-cellulose IIB structure forms quickly and easily. As reference to any conformational energy map of cellulose shows (cf., for example, Fig. 2 of ref. 10), both left- and righthanded threefold helical conformations of an isolated cellulose chain are within the allowed region of cellulose conformations. They are not within the minimum energy regions surrounding the twofold helical chain because of the absence of intramolecular hydrogen bonds. By providing a field of electrostatic attraction from the surrounding Na^+ ions and the probable formation of many secondary

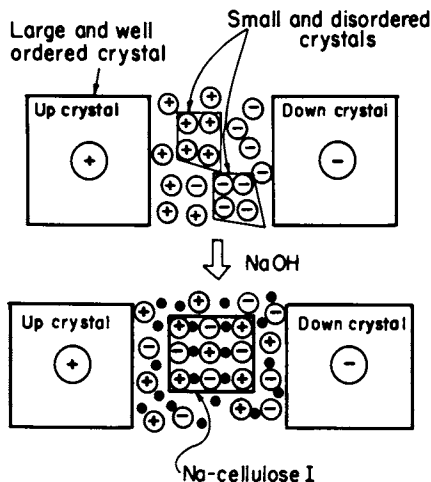


Fig. 6. Probable conversion of the cellulose I crystal structure to that of Na-cellulose I by the action of NaOH. Crystallites are indicated by boxed-in areas and chains by circles; + indicates "up" and - indicates "down" chain directions. The Na⁺ ions are denoted by filled circles. (Reproduced by permission from ref. 8. Copyright 1987 John Wiley & Sons, Inc.)

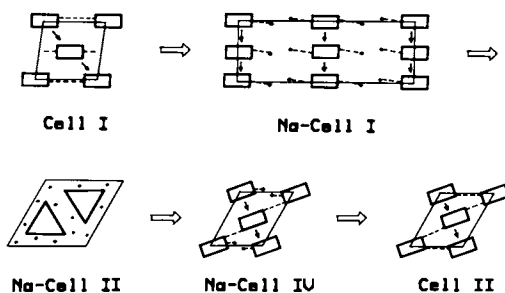


Fig. 7. A comparison of the unit cells of celluloses I and II, and Na-celluloses I, IIB, and IV, drawn roughly to scale. Arrows indicate the probable directions of hydrophobic attractions. Filled circles indicate the positions of Na⁺ ions or water molecules. Secondary and hydrogen bonds are shown by dashed lines.

bonds between the latter and the hydroxyl groups of each glucose residue, such a conformation could become a very stable one. Its stability is probably not decreased significantly by the liquid-like surroundings of the cellulose helix in Na-cellulose IIB relative to a structure in which all Na^+ ions would be in crystallographically defined positions.

Removing the NaOH from the structure through washing with water removes the energy-lowering electrostatic field. This results in a conversion of the structure to the only energy-lowering one that is available to it -- a twofold helical, interchain hydrogen-bonded sheet structure. Because cellulose II is the most stable cellulose polymorph (10), it is not surprising that the conversion product of Na-cellulose IIB approaches it after washing. It is somewhat surprising that a hydrated structure forms at all, as it is unstable and converts readily to cellulose II upon drying. Nonetheless, it does form and its structural features suggest the presence of hydrophobic attractions that may have a bearing on all twofold helical cellulose structures.

For example, interchain hydrogen bonds could be thought of as the single dominant force in the crystallization of celluloses and Na-celluloses. Therefore, it might be expected that in Na-celluloses I and IV the Na^+ ions and the water molecules, respectively, would occupy positions between the hydrogen-bonded sheets. Instead, they disrupt the hydrogen bonds within the sheets, leaving inter-sheet contacts along the 020 (and 110 , respectively) directions unchanged. Because there are no hydrogen bonds present in these planes, it is very probable that hydrophobic attractions operate along these directions, between the hydrogen-bonded sheets. Comparing the structures of celluloses I and II, and Na-celluloses I and IV, as shown in Fig. 7, reveals a common form of stacking of chains in all of these structures -- strongly suggestive of hydrophobic attractions. Other cellulose polymorphs, e.g., celluloses III_I, IV_I, and IV_{II} (not shown here), also conform to such chain stacking (11,12). Therefore, it is very probable that the aggregation of cellulose chains into various crystalline structures may primarily be governed by hydrophobic attractive forces. The only exception seems to be Na-cellulose IIB where the strong interaction between cellulose and the Na^+ ions appears to override any other forces, with the consequence that the cellulose chain adopts an unusual conformation.

Acknowledgment

The studies reported herein have been supported by the National Science Foundation, under grants CHE7727749, CHE8107534, and PCM8320548.

Literature Cited

1. Okano, T.; Sarko, A. J. Appl. Polym. Sci. 1984, 29, 4175.
2. Okano, T.; Sarko, A. J. Appl. Polym. Sci. 1985, 30, 325.
3. Zugenmaier, P.; Sarko, A. In Fiber Diffraction Methods; French, A. D.; Gardner, K. H., Eds.; ACS Symposium Series No. 141; American Chemical Society: Washington, DC, 1980; p 225.
4. Woodcock, C.; Sarko, A. Macromolecules 1980, 13, 1183.
5. Sarko, A.; Biloski, A. Carbohydr. Res. 1980, 79, 11.
6. Stipanovic, A. J.; Sarko, A. Macromolecules 1976, 9, 851.

7. Nishimura, H.; Sarko, A. J. Appl. Polym. Sci. 1987, 29, (in press).
8. Nishimura, H.; Sarko, A. J. Appl. Polym. Sci. 1987, 29, (in press).
9. Haigler, C. H.; Brown, R. M., Jr.; Benziman, M. Science 1980, 210, 903.
10. Sarko, A. Appl. Polym. Symp. 1976, 28, 729.
11. Sarko, A.; Southwick, J.; Hayashi, J. Macromolecules 1976, 9, 857.
12. Gardiner, E. S.; Sarko, A. Can. J. Chem. 1985, 63, 173.
13. Sarko, A. In *New Developments in Industrial Polysaccharides*; Crescenzi, V.; Dea, I. C. M.; Stivala, S. S., Eds.; Gordon & Breach: New York, 1985; p 100.

RECEIVED March 5, 1987

Chapter 10

Solid-State Carbon-13 NMR and Wide-Angle X-ray Scattering Study of Cellulose Disordering by Alkali Treatment

B. Philipp, J. Kunze, and H.-P. Fink

Academy of Sciences of the German Democratic Republic, Institute of Polymer Chemistry "Erich Correns," 1530 Teltow-Seehof, German Democratic Republic

High resolution solid state ^{13}C NMR spectroscopy supplemented by WAXS measurements proved to be a useful tool in elucidating structural changes of cellulose due to chemical transformations and phase transitions (1). The ^{13}C -CP/MAS-NMR spectra are sensitive to changes in chain conformation and packing density as well as to specific changes in the chemical environment of the different OH-groups of the anhydroglucose units. In our previous work in this field we discussed ^{13}C solid state NMR spectra of alkali cellulose and its dependence on NaOH concentration, experimentally obtained by us for the first time (2). Furthermore, we discussed the spectra of various samples of regenerated cellulose differing in supermolecular order (3). Quite recently, Kamide (4,5) in a more detailed ^{13}C NMR study on cellulose and its alkalization process correlated the changes in the ^{13}C NMR spectrum to a selective weakening or even destruction of the H-bonds in the cellulose moiety.

The following contribution summarizes some ^{13}C NMR and WAXS results of a still preliminary kind comparing the "disordering effects" obtained by aqueous and ethanolic NaOH solutions, and by aqueous guanidonium hydroxide to that achieved by ball-milling of cellulose samples.

Experimental

As starting materials we mainly used an acetate grade scoured and bleached cotton linters (DP in cuprammonium solution ~ 1500) and a cellulose powder prepared from linters by hydrolysis to DP ~ 150 and a subsequent mechanical disintegration. In the experiments with guanidonium hydroxide these samples were also employed after previous mercerization with 18% by weight aqueous NaOH. For comparison also linters and viscose staple fibre before and after ball-milling as well as a linters sample decrystallized by N_2O_4 -treatment according to (6) were included in our work.

Alkaline treatment was performed with an excess of steeping lye at room temperature, employing aqueous as well as ethanolic (ethanol:water = 70:30% by weight) solutions of NaOH up to 30% by weight. Treatment with guanidonium hydroxide was accomplished in

0097-6156/87/0340-0178\$06.00/0
© 1987 American Chemical Society

all experiments with an aqueous solution of about 50% by weight. After filtering off the excess of lye, samples were neutralized with aqueous or ethanolic acetic acid, washed with water or ethanol and dried at 25°C. In some series the lye was washed out with water or ethanol without addition of acetic acid. The procedure applied in each series is indicated in the tables or in the captions to figures.

The ^{13}C -CP/MAS-NMR-spectra of the NaOH-treated and of all the regenerated samples were registered at room temperature with a home-built spectrometer at 15.087 MHz and with a field of 1.5 mT for dipolar decoupling (7). Frequency for sample rotation was about 2 kHz, the repeat time 2 s (with backflip pulse) and the duration of cross-polarization 1.5 ms. The assignment of the signals to the different C-atoms of the anhydroglucose unit was based on experience of our own and on relevant data published in (8). The MAS technique proved to be applicable to the rather highly swollen samples of Na-cellulose without serious problems (2), while the gel-like structure of guanidonium cellulose could not be investigated employing this method. With regard to the influence of CP-impulse length we relied on the rather numerous and reliable data already published [comp. (18)] indicating that no significant differences between regions of different physical structure are to be expected. Generally the spectra were taken with about 5000 scans. With several samples alkalinized in the ethanol system only 2000 scans could be performed resulting in a lower signal to noise ratio still sufficient for deriving reliably the information subsequently discussed.

WAXS patterns of the alkalinized and the regenerated samples were obtained by the technique described in (9). Evaluation was performed with regard to lattice type, in some cases also with regard to degree of crystallinity and average lateral crystal dimensions (10).

Results

In Figure 1 the ^{13}C spectra of linters and viscose staple fibre are shown in the original state, after decrystallization by ball-milling, and after subsequently boiling the milled samples in water. Significant changes in the spectrum due to decrystallization are visible mainly in the C-1 and C-6 regions at ~ 105 ppm and 60 ppm, respectively, and in the C-4 region at ~ 85 ppm. In the first two regions mentioned a signal broadening occurs, while at 85 ppm lines present in the spectrum of the original sample disappear or are smeared out to a broad signal of low amplitude after milling. By boiling the decrystallized samples in water, these changes in the ^{13}C spectrum are only partially reversed. These results are generally confirmed by our experiments employing viscose staple fibre (Figure 1b). As also indicated in Figure 1b the spectrum of the N_2O_4 pretreated staple fibre resembles closely that decrystallized by ball-milling. In a visual evaluation of the WAXS patterns no indication of persisting crystalline peaks could be recognized after our ball-milling procedure (13).

Figure 2 gives a comparison of the NMR spectra of alkali-treated samples after steeping with aqueous NaOH (Spectra 2a) (2), or ethanolic NaOH (ethanol:water = 70:30% by weight) (Spectra 2b) prior

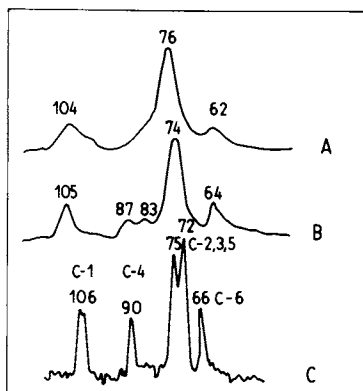


Figure 1a. CP/MAS- ^{13}C -NMR-spectra of cotton linters after various treatments (chemical shifts in ppm relative to TMS = 0).

- A - ball milled
- B - ball milled and boiled in water
- C - original state (original sample without treatment for comparison)

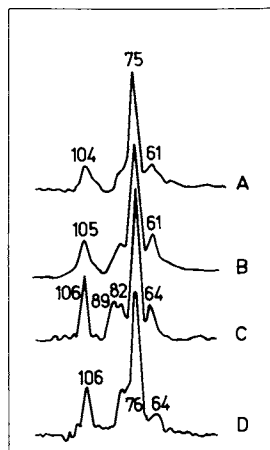


Figure 1b. CP/MAS- ^{13}C -NMR-spectra of viscose staple fibre after various treatments.

- A - ball milled
- B - ball milled and boiled in water
- C - original state (original sample without treatment for comparison)
- D - treated with N_2O_4

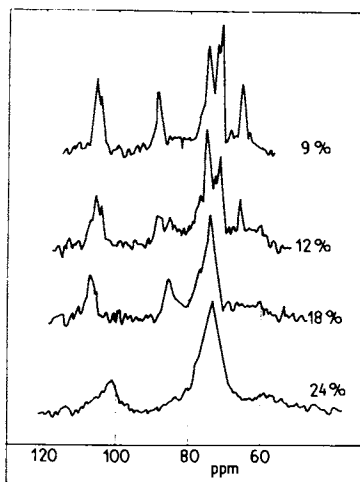


Figure 2a. CP/MAS-¹³C-NMR-spectra of cotton linters after treatment with aqueous NaOH.

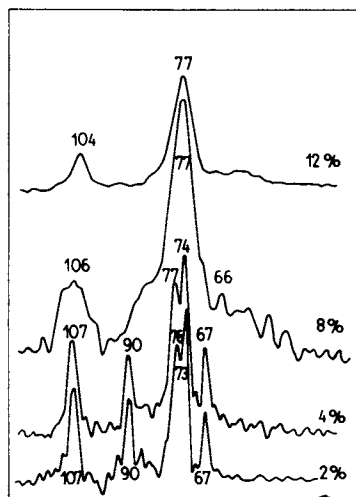


Figure 2b. CP/MAS-¹³C-NMR-spectra of hydrolyzed cotton linters powder after treatment with ethanolic NaOH.

to regeneration. As a general tendency, a broadening and flattening out of all the lines as well as a shifting of the signals (Table I) can be observed at a sufficiently high lye concentration. Also a significant influence of the reaction medium becomes clearly visible from these spectra: The line-shifting and the broadening of the C-1, C-4 and C-6 lines begin at a much lower NaOH concentration with the NaOH-solution in ethanol as compared to the aqueous system. The spectrum recorded after steeping with 12% by weight ethanolic lye is very similar to that obtained after action of a 24% by weight aqueous lye.

Table I. Line Positions of Cellulose After Alkali Treatment (ppm relative to TMS = 0)

Aqueous medium					
9%	NaOH	105	88	75/72	66
12%	by	106	89/86	75/72	66/60
15%	weight	106	85	76/74	62
Ethanolic medium					
4%	NaOH	107	90	77/74	67
8%	by	106	--	77	(66)
12%	weight	104	--	77	--

At lower NaOH-concentration the line shifting in the C-1, C-4 and the C-6 region due to interaction with NaOH are different and even opposite in direction after treatment with aqueous and with ethanolic lye, respectively.

With respect to changes in the WAXS pattern it can be concluded from our previous work (11) that in an aqueous system the cellulose I pattern of linters cellulose is persisting up to 10% NaOH in the lye, and lattice transformation to Na-cellulose is completed at about 15% NaOH in the steeping lye, with a rather high degree of crystalline order prevailing during the transition. In the ethanolic system, on the other hand, the cellulose I diffraction pattern could be detected in the concentration range up to 8% NaOH only (comp. Table II), and even at a steeping lye concentration in the range between 4 and 8% NaOH a decrease of order was indicated in the X-ray diffractogram. At still higher alkali concentration the diffractogram mostly revealed a poor state of order, some samples showing a faint pattern of alkali cellulose.

The ^{13}C NMR-spectra of linters cellulose regenerated after treatment with ethanolic solutions of NaOH are reproduced in Figure 3 and compared to that of a sample steeped with 12% aqueous NaOH and subsequently regenerated. The corresponding spectra of samples treated with 12% ethanolic and with aqueous NaOH show large differences, especially in the C-4 region. Even a NaOH concentration as low as 2% in the ethanolic system leads to significant differences between the line positions of the original, the alkali-treated

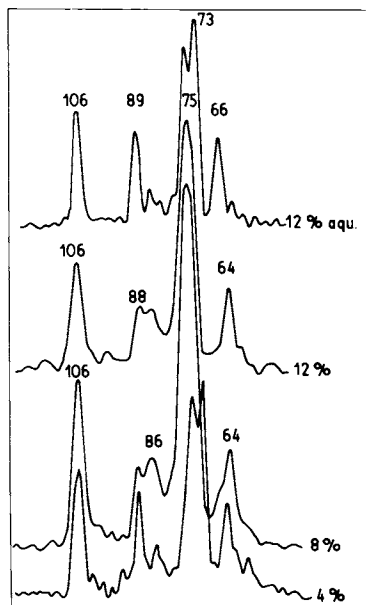


Figure 3. CP/MAS- ^{13}C -NMR-spectra of hydrolyzed cotton linters powder after alkali treatment and neutralization, resp., regeneration to cellulose.

4, 8, and 12% - treatment with ethanolic solution of NaOH

12% aqu. - treatment with aqueous solution of NaOH for comparison

and the regenerated sample, pointing to a structural changes, although the WAXS pattern in all three cases clearly indicated a cellulose I lattice without a significant difference in supermolecular order. Samples regenerated after treatment with ethanolic NaOH solutions of higher concentration consisted of a more or less well ordered cellulose II, the qualitative evaluation of the WAXS patterns being summarized in Table II. Comparing the ^{13}C NMR spectra of the two regenerated samples previously treated with 16% ethanolic and 18% aqueous NaOH, respectively, we find the general features of the cellulose II spectrum in both cases with minor differences in the C-4 and C-2, 3, 5 region.

Table II. Summary of WAXS-Results on Cellulose Samples Treated with a NaOH/Ethanol/Water System

NaOH-Conc. by Weight	Alkalized Samples, wet state	Samples Regenerated with Ethanol, dry state	Samples Regenerated with water, dry state
2	Cell. I	Cell. I	Cell. I
4	Cell. I	Cell. I	Cell. I
8	Low order, two broad interferences	Low order, two broad interferences	Cell. II
12	Low order, two broad interferences	Liquid like low order	Cell. II
16	Low order, two broad interferences	Low order, two broad interferences	Cell. II

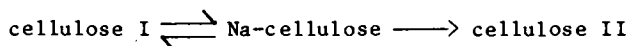
Our results obtained on structural changes of hydrolyzed cotton linters powder by treatment with aqueous guanidonium hydroxide are reported in detail in (12) and therefore shall be only briefly summarized here. The WAXS patterns of all the alkalyzed and the regenerated samples closely resemble the diffractogram of an amorphous cellulose by visual inspection, although a radial electron density distribution derived from X-ray scattering according to (13) still reveals some residual supermolecular order.

The ^{13}C NMR spectra of the guanidonium hydroxide treated with subsequently regenerated samples are different from those of the starting material predominantly in the C-1, C-4, and C-6 region, especially with regard to the narrow part in the C-4 region at 88 ppm (Figure 4). The intensity of this narrow line nearly disappears after guanidonium hydroxide treatment, but is recovered after recrystallization by boiling of the regenerated sample in water. Structural differences between the original and the mercerized

linters cellulose powder are obviously persisting during the guanidonium hydroxide treatment and the subsequent procedure of regeneration, as to be seen from intensity and line width of the different samples in the C-4 region (comp. Figure 4a with 4b).

Discussion and Conclusions

As already discussed in our previous work (14) on the basis of model consideration of Atalla (15) and of Hayashi (16), conformational changes at the glycosidic linkage between C-1 and C-4 of the cellulose chain can be assumed to be the predominant cause of structural changes in the transition



of native linters cellulose, the first step being partially reversible at an alkali concentration within the transition range. Besides this, selective interactions of the different OH-groups with NaOH and H₂O have to be taken into account, involving a disturbance or break down of the H-bonds of the cellulose moiety. Based on this general reasoning and on model ¹³C NMR-spectra recently calculated by Kamide (5) the following qualitative interpretation of our ¹³C NMR and WAXS results presented here may be proposed: As revealed by the total or partial disappearance of the narrow part of the line at 89 ppm, the signal broadening in the C-1, C-4, and C-6 region and the changes in the WAXS pattern, the interaction between cellulose and NaOH (in aqueous as well as in ethanolic solution) and also with aqueous guanidonium hydroxide results in a lowering of supermolecular order due to less dense packing of the chains and/or coexistence of different conformational stages. On regeneration, this decrease of supermolecular order is only partially reversed, depending on kind of alkali treatment and procedure of regeneration. The supermolecular order of the regenerated samples can be increased by boiling in water, as shown especially for cellulose treated with guanidonium hydroxide.

Comparing the two reaction media H₂O and EtOH, NMR and X-ray data reveal an onset of this effect of disordering at a much lower NaOH concentration in the case of EtOH as compared to H₂O. According to the NMR spectra, the structure of the alkalinized samples "12% NaOH in EtOH," "24% NaOH in H₂O" and an amorphous sample obtained by ball-milling are very similar. In the concentration range up to 8% NaOH in EtOH only a partial disordering occurs as shown by the still rather small and distinct NMR lines. With the aqueous system, on the other hand, no structural changes at all are detectable from the ¹³C spectra in this range of NaOH concentration. This different effect of NaOH on cellulose at a given lye concentration in an aqueous medium at one hand, in an ethanolic one at the other may be connected with a difference in component distribution as shown recently in (17) for the system cellulose/NaOH/isopropanol/H₂O. Referring to the model NMR spectra of cellulose calculated by Kamide (4), a preferential persistence of the O₃H...O'⁵H-bond might be assumed from a comparison of the line positions for C-1 and C-4 for the NaOH/EtOH/H₂O-system up to 8% by weight NaOH. Some information on the site of the NaOH-coordination in the abovementioned system may

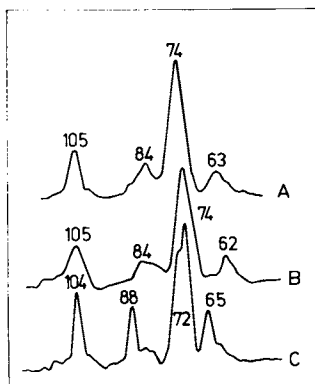


Figure 4a. CP/MAS- ^{13}C -NMR-spectra of hydrolyzed cotton linters powder after treatment with guanidonium hydroxide and neutralization, resp., regeneration.

- A - regenerated
- B - regenerated and boiled in water
- C - original state (original sample without treatment for comparison)

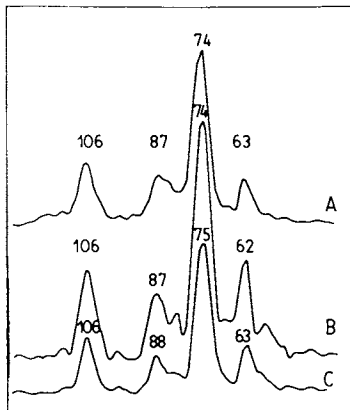


Figure 4b. CP/MAS- ^{13}C -NMR spectra of mercerized hydrolyzed cotton linters powder after treatment with guanidonium hydroxide and neutralization, resp., regeneration.

- A - regenerated
- B - regenerated and boiled in water
- C - original state (original sample without treatment for comparison)

be derived from a comparison of our experimental ^{13}C data with calculated spectra (5) of alkali cellulose. From the position of the C-6 signal a preferential coordination of Na^+ at OH-6 might be concluded.

Finally, from a methodological point of view it may be stressed that the combination of ^{13}C -CP/MAS-NMR-spectrometry and WAXS again proved to be a very useful tool in elucidating solid state structural changes in cellulose. Both methods are supplementing each other insofar, as WAXS provides information on the integral static supermolecular structure of the sample, while ^{13}C solid state NMR spectroscopy reveals details of structural changes at specific sites and additionally can provide information of structural dynamics by relaxation measurements. So far, this combination has been applied to the crystalline part of the cellulose structure mainly, but - as shown by this contribution and by some of our work now in progress - it also offers good chances to gain a deeper insight into the amorphous part of the structure and its relevance for macroscopic properties of cellulose.

Acknowledgment

The cooperation of Dr. Ho. Dautzenberg, Dr. F. Loth, and Dr. W. Wagenknecht in supplying the samples and of Dr. Sc. G. Scheler, Friedrich-Schiller-Universität Jena, in measuring the ^{13}C NMR-spectra is gratefully acknowledged.

References

1. Philipp, B.; Fink, H.-P.; Kunze, J.; Frigge, K. Annalen der Physik Leipzig 1985, 42, 507-23.
2. Kunze, J.; Ebert, A.; Schröter, B.; Frigge, K.; Philipp, B. Polymer Bulletin 1981, 5, 399.
3. Kunze, J.; Scheler, G.; Schröter, B.; Philipp, B. Polymer Bulletin 1983, 10, 56.
4. Kamide, K.; Okajima, K.; Kowsaka, K.; Matsui, T. Polymer J. 1985, 17, 701.
5. Kamide, K.; Kowsaka, K.; Okajima, K. Polymer J. 1985, 17, 707.
6. Makarenko, M. V.; Gert, E. V.; Kapuckij, F. N. Z. Prikl. Chim. 1982, 55, 2542.
7. Schröter, B. Dissertation A, Friedrich-Schiller-Universität Jena, 1982.
8. Atalla, R. H.; Gast, J. C.; Sindorf, D. W.; Bartuska, V. J.; Maciel, G. E. J. Amer. Chem. Soc. 1980, 102, 3249.
9. Purz, H. J.; Fink, H.-P. Acta Polymerica 1983, 34, 546.
10. Fink, H.-P.; Fanter, D.; Philipp, B. Acta Polymerica 1985, 36, 1.
11. Fink, H.-P.; Fanter, D.; Loth, F. Acta Polymerica 1982, 33, 241.
12. Kunze, J.; Scheler, G.; Sternberg, U.; Philipp, B. Acta Polymerica in press.
13. Fink, H.-P.; Philipp, B.; Serimaa, R.; Paakkari, T. Publication in preparation.
14. Fink, H.-P.; Philipp, B. J. Appl. Polymer Sci. 1985, 30, 3779.

15. Atalla, R. H. J. Appl. Polymer Sci., Appl. Polymer Symposium 1983, 37, 295.
16. Hayashi, J. Sen-i Gakkaishi 1976, 32, 37.
17. Yokota, H. J. Appl. Polymer Sci. 1985, 30, 263.
18. Lindberg, J.; Hortling, B. Advances in Polymer Science 66, 2-10, Springer Verlag Berlin-Heidelberg, 1985.

RECEIVED March 5, 1987

Chapter 11

Polymorphic and Morphological Aspects of Recrystallized Cellulose as a Function of Molecular Weight

I. Quenin and H. Chanzy

Centre de Recherches sur les Macromolécules Végétales, Centre National de la Recherche Scientifique, B.P. 68, 38402 Saint Martin d'Hères Cedex, France

The polymorphism and morphology of cellulose precipitated from solutions in amine oxide by the slow diffusion of water vapors, was investigated, as functions of the temperature of recrystallization and the degree of polymerization (DP) of the material to be recrystallized. At temperatures around 90°C, low DP cellulose crystallized almost exclusively as cellulose IV_{II}, whereas higher DP material was found in the form of cellulose II. Substantial differences were also found in the morphologies of the various samples: with cellulose II, rod-like crystals were obtained with low DP material while a crystalline fibrillar gel precipitated when high DP samples were recrystallized. In all cases, cellulose IV_{II} was obtained as a granular precipitate.

The crystallization behaviour of polysaccharides is influenced not only by their chain conformation but also by the multiple possibilities of inter and intra molecular hydrogen bonding (1,2). This multiplicity, in particular, explains why several polymorphic forms can be obtained when different crystallization conditions are selected for a given specimen.

A survey of the various parameters which have a role in directing the crystallization of a given polysaccharide toward one or another polymorph, presents the temperature of crystallization as being the most influential: polysaccharides such as cellulose (3), mannan (4), dextran (5,6), etc. are particularly sensitive to changes in crystallization temperatures as they yield completely different crystals at low or high temperature.

In other instances, it is the solvent of crystallization which plays a decisive role in orienting the crystallization toward one or the other polymorph. Such solvent dependant crystallization is well documented in the case of amylose (7) where minute changes in solvent/precipitant ratio have a dramatic effect on shifting the recrystallized amylose among three polymorphs: amylose A, B and V.

0097-6156/87/0340-0189\$06.00/0
© 1987 American Chemical Society

A final and unexpected polymorphism parameter is found in the molecular weight of the sample to be crystallized. This is in particular described in the case of mannan and glucomannan polymers (4,8) where crystals of mannan I are usually obtained with low degree of polymerization (DP) material, whereas only mannan II is found when higher DP are recrystallized.

The present study deals with the polymorphism of cellulose recrystallized from solution. In particular, the interest is focussed on the various parameters which are capable of orienting the crystallization toward cellulose II or cellulose IV_{II}, the so-called low and high temperature cellulose polymorphs. These two polymorphs have not only a different crystalline arrangement but also a different morphology as cellulose II occurs as a gel-like precipitate whereas cellulose IV_{II} is rather more granular. Recrystallized cellulose is of great industrial interest. For this reason, it seems important to know whether other parameters, such as the molecular weight of the crystallizing cellulose, may also play a role in directing the crystallization toward cellulose II or cellulose IV_{II} at a given crystallization temperature. With this goal in mind, a series of cellulose samples of various molecular weights were crystallized from solution at different temperatures. The morphology and structure of the crystalline precipitate were investigated by X-ray diffraction, electron microscopy and electron diffraction.

Experimental

Cellulose Samples. 4 different cellulose samples were selected for the experiments : a) bleached Egyptian Menoufi cotton (DP 2000), kindly provided by Dr. R. Hagège, Institut Textile de France, b) Cotton linters (DP 600), c) microcrystalline cellulose Avicel pH 101 (DP 120), d) microcrystalline cellulose from rayon (DP 34), a gift from Dr. G. Raynor, FMC corp.

Solutions Preparation. An amine oxide-based cellulose solvent which was still liquid at room temperature was selected. As described earlier (9), it consisted in a mixture of 22 % N-Methyl morpholine N-oxide (MMNO), 65 % N-N-dimethyl ethanolamine N-oxide (DMEAO) and 13 % H₂O (W/W). 5 mgs of cellulose to which were added 5 mgs of n-propyl gallate, a cellulose stabilizer (10) were dissolved in 10cc of cellulose solvent at 120°C with stirring. Dissolution took place in 15 minutes, following which the solutions were allowed to cool. They were then stored in a dessicator.

Cellulose Crystallization. For crystallization below 100°C, the solutions were poured into petri dishes and positioned inside a closed vessel containing an excess of water. The vessel was then fitted into a temperature controlled oil bath and brought to the crystallization temperature. Crystallization of cellulose resulted from the diffusion of water into the solution. Crystallization was complete within a few minutes at 90°C whereas several days were necessary at room temperature. For crystallization between 100°C and 120°C, a similar principle was used except that a thick-wall sealed glass vessel was used to prevent water vapor from escaping.

Sample Preparation. After crystallization, the solutions were cooled and the flocculent crystals were washed and recovered by successive centrifugation and redispersion in water and finally in ethanol.

Part of the crystals were allowed to dry and were then inserted into thin wall capillaries for X-ray diffraction studies which were made using a Waurus flat-film camera mounted on a Siemens Kristalloflex X-ray generator.

For electron microscopy, drops of crystal suspended in ethanol were allowed to dry on carbon coated electron microscopy grids. The grids were either used as such for electron diffraction or after W/Ta shadowing for imaging. The electron microscopy and electron diffraction experiments were performed with a Philips EM 400 T electron microscope operated at 80 KV for imaging and 120 KV for diffraction.

Results

When the various crystalline precipitates were examined by X-ray analysis, it became evident that the ratio of cellulose IV_{II}/cellulose II could be correlated not only with the temperature of crystallization, but also with the molecular weight of the starting material. This is particularly well illustrated in Figure 1 by comparing the X-ray diagram of two different specimens prepared at 90°C. In Figure 1A, corresponding to the cotton cellulose solution, the precipitate has a well defined diffraction line at 0.72 nm (cellulose II) but only a very weak one at 0.56 nm (cellulose IV_{II}). On the other hand, as seen in Figure 1B, when microcrystalline cellulose from rayon is recrystallized under identical conditions, the precipitate displays a large excess of cellulose IV_{II} and only a minor cellulose II component.

From the work of Stipanovic and Sarko on cellulose II (11) and that of Gardiner and Sarko (12) on cellulose IV, it can be deduced that the intensity of the lines at 0.72nm for cellulose II is between 1/2 to 1/3 of that at 0.56 nm for cellulose IV_{II}. By taking this into account, an estimate of the percentage of cellulose II and cellulose IV_{II} can be evaluated by recording a radial tracing of the X-ray patterns and comparing the correct intensities of the lines at 0.56nm and 0.72 nm. Such estimated cellulose II/cellulose IV_{II} compositions are summarized in Table I, as a function of the temperature of crystallization and for the 4 investigated samples. These results indicate a clear-cut tendency for low DP cellulose to yield a substantial amount of cellulose IV_{II} even at temperatures as low as 50°C. For cellulose of higher DP, this is not the case and, it is only at 90°C and above that cellulose IV_{II} can be detected.

At the ultrastructural level, substantial differences can be recorded when comparing the samples of various molecular weight. As seen in Table I, when temperatures of crystallization below 50°C were used, all the samples crystallized as the pure cellulose II polymorph. An examination with the electron microscope reveals that the low DP material occurred as an assembly of rod-like elements, each rod having a length between a micron and half micron and a width of the order of 100 nm. With higher DP samples, a gel-like

Table I. Polymorph Composition as Function of Cellulose DP and Temperature of Crystallization

Temperature of crystallization	DP 34	DP 120	DP 600	DP 1200
22°C	100% cell II	100% cell II	100% cell II	100% cell II
50°C	90% cell II 10% cell IV _{II}	100% cell II	100% cell II	100% cell II
90°C	25% cell II 75% cell IV _{II}	70% cell II 30% cell IV _{II}	90% cell II 10% cell IV _{II}	90% cell II 10% cell IV _{II}
120°C	20% cell II 80% cell IV _{II}	40% cell II 60% cell IV _{II}	40% cell II 60% cell IV _{II}	50% cell II 50% cell IV _{II}

precipitate consisting in endless and narrow intertwined fibrils, was obtained. These two morphologies are shown in Figures 2A and 2B which are printed at the same magnification for comparison.

With X-ray analysis, it is not possible to differentiate between the samples in Figures 2A and 2B. This is seen in the insert in 2C which could correspond to either sample. With the electron diffraction technique, however, a substantial difference is found when the diffraction diagrams are analyzed in term of their orientation with respect to oriented fragments of the precipitate. This point is illustrated by comparing Figures 3A and 3B. In Figure 3A, a selected assembly of parallel rod-like elements, yields an oriented electron diffractogram where the (110) reflection of cellulose II is aligned with the axes of the rods. Other features of the diagram indicate that the (110) interference is directed perpendicular with respect to the rod direction while (020) is at a slight angle off the (110) reflection. Such orientations indicate that in the rods, the chain axes are perpendicular to the rod axis and the rods consist in elongated cellulose crystals with (110) as the growth plane as observed before in a connected study (14). In Figure 3B the orientation is decisively different as a bundle of oriented gel gives a cellulose II fiber diagram with the cellulose chain axis aligned with the axis of the strands constituting the oriented structure.

When the samples crystallized at higher temperature are examined, the presence of cellulose IV_{II} can be visualized as it occurs in the form of a granular material mixed or not with the cellulose II precipitate. This is well illustrated in Figure 4A, corresponding to the specimen of dissolved Avicel, recrystallized at 90°C. In this Figure, the inserted X-ray diagram denotes the presence of about 30% of cellulose IV_{II}, located in several aggregates (see arrows), whereas the main part of the precipitate is made of intertwined rod-like cellulose II crystals similar to what was seen in Figure 2A.

* The indices refer to the unit cell of cellulose II, as defined by Kolpak and Blackwell (13).

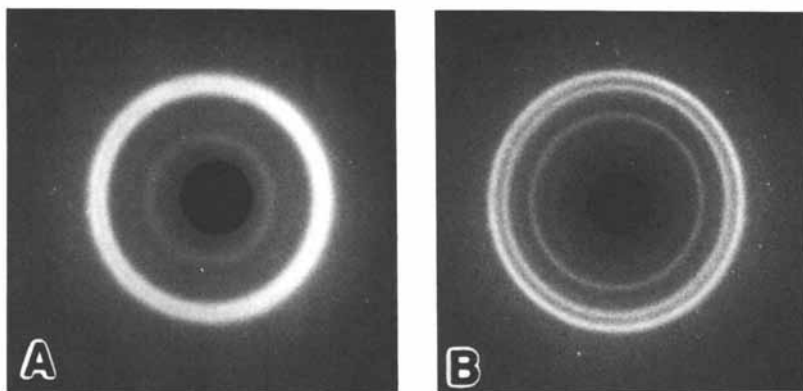


Figure 1. X-ray diagram of cellulose crystals recrystallized at 90°C. 1A from cotton cellulose (DP 2000) solution. 1B from microcrystalline cellulose (DP 34) solution.

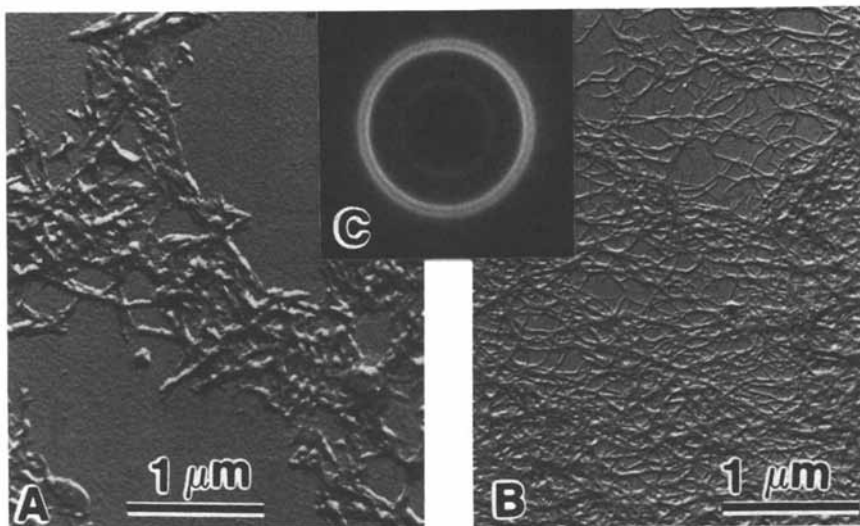


Figure 2. Electron micrographs of crystals of cellulose II prepared at 50°C, after shadowing with W/Ta. 2A Sample from microcrystalline cellulose (DP 34) solution. 2B Sample from cotton cellulose (DP 2000) solution. 2C X-ray diagram, identical for either samples.

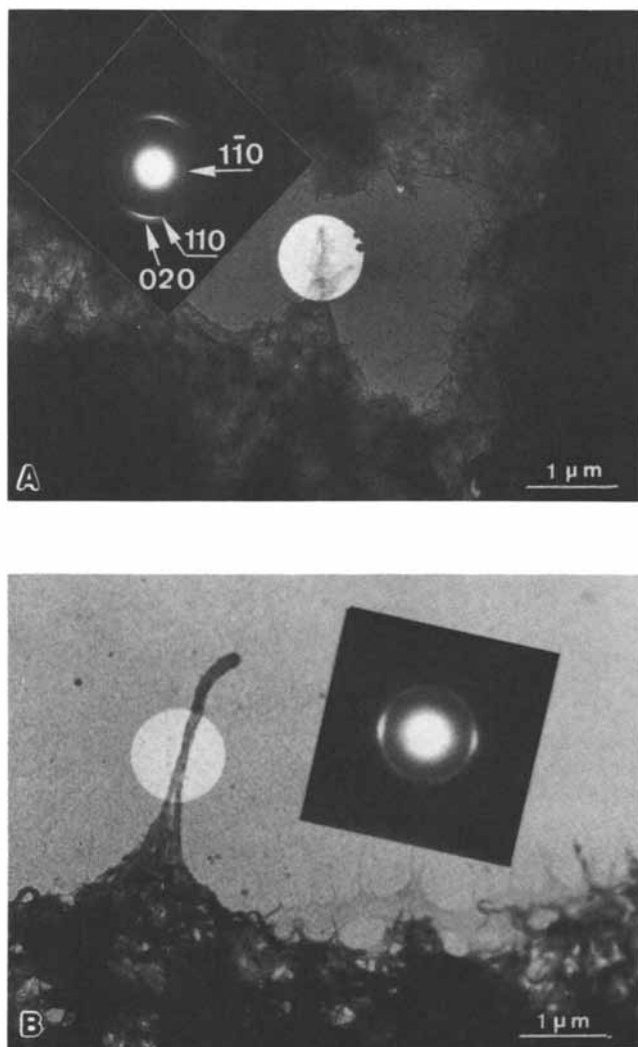


Figure 3. Low dose electron micrographs and selected area electron diffraction diagram of 3A samples as in Figure 2A. 3B sample as in Figure 2B. In both Figures, the diffraction diagrams are printed with correct orientation with respect to the images.

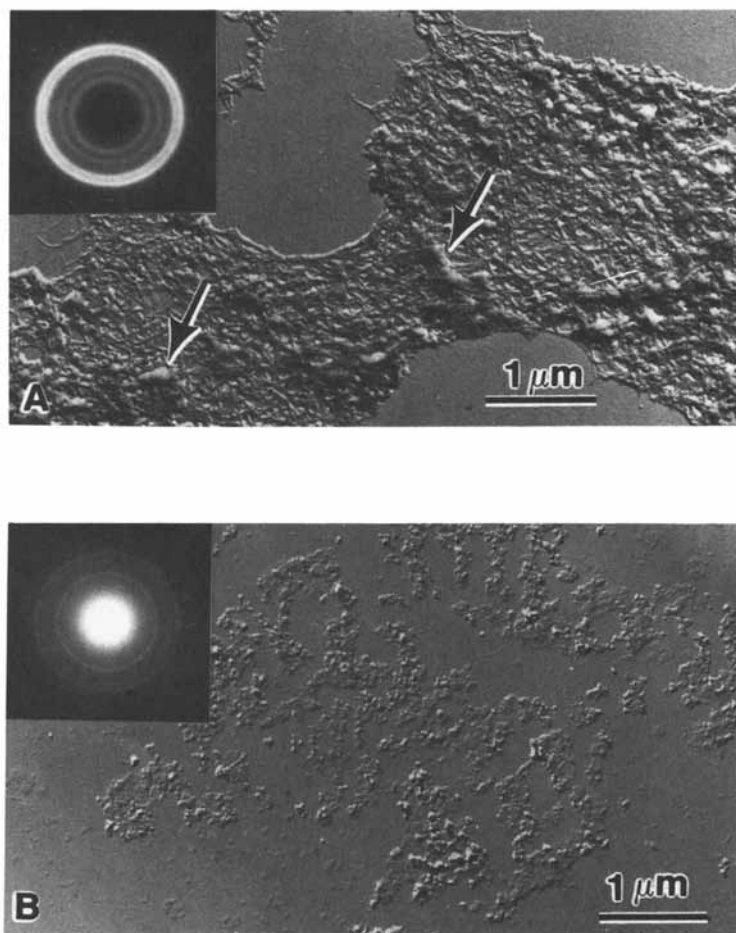


Figure 4. Electron micrographs of crystals of cellulose prepared at 90°C after shadowing with W/Ta. 4A from Avicel (DP 120) cellulose solution: the structure consists of rod-like elements together with granular aggregates (arrows). Insert: corresponding X-ray diagram. 4B from microcrystalline cellulose (DP 34) solution. Insert: corresponding electron diffraction diagram.

In Figure 4B, obtained from DP 34 material crystallized also at 90°C, the amount of cellulose IV_{II} is much larger as described above in Table I. In fact the electron microscopy study reveals large areas where only a granular precipitate is present. These areas consist exclusively of cellulose IV_{II}, as denoted by the inserted electron diffraction diagram in Figure 4B.

Discussion

This study presents several aspects of interest regarding the morphology of recrystallized cellulose and its recrystallized form. First, in agreement with earlier reports by Atalla et al. (15, 16), it is confirmed that the crystalline polymorphism of cellulose may be influenced by the molecular weight of the recrystallized sample. This is particularly well demonstrated in this system when temperatures of recrystallization around 100°C are selected. At those temperatures, the ratio of cellulose IV_{II} to cellulose II appears to be inversely related to the molecular weight of the cellulose samples under investigation. At present, it is difficult to come forward with a conclusive explanation for such behavior. It was shown by Maeda et al. (17) that chain aggregates formed in solution prior to crystallization when cellulose crystallized in the form of cellulose II. The stability of such a pre-associated structure depends on the number of hydrogen bonds connecting the cellulose chains together. This is why, in our opinion, such aggregates are more stable when higher molecular weights are used. On the other hand, when the temperature of crystallization is high or when low DP material is chosen, the pre-associated aggregates are less tightly interlocked and consequently less stable. This should lead to a different crystallization pattern, where individual chains instead of aggregated bundles, would enter the growing crystals in the cellulose IV_{II} mode. Such a concept, which needs to be further substantiated, could well explain the occurrence of cellulose IV_{II} or that of cellulose II when the crystallization parameters are varied.

A similarity can be established between the polymorphism of mannan and that of cellulose, as with both polysaccharides, one observes a molecular weight influence on the polymorphism, even though this influence is more pronounced in the case of mannan than in the case of cellulose. It was shown that with mannan and glucomannan polymers, the mannan I structure was obtained more easily with low molecular weight material, whereas mannan II corresponded to higher molecular weight (4,8). A close resemblance exists thus between the crystallization of cellulose IV_{II} and mannan I as with both polymers, the crystallization phenomena appear to be directed by related parameters. Similarly, the crystallization behavior of mannan II and cellulose II appear to be also correlated.

The resemblance between cellulose and mannan crystals is not limited to their susceptibility toward molecular weight or crystallization temperature modifications. Even morphological features are similar: mannan I and cellulose IV_{II} occur either as platelet crystals (18,19) when fractionated polymers are used, or

granular material with unfractionated polymer (see Figure 4B and ref 4); mannan II and cellulose II take the shape of either a fibrillar gel or elongated rod-like crystals, depending also on their molecular weight (Figure 2B and ref. 4). For both polymers, such a difference in morphology reflects certainly the dynamics of the organization of the inter-chain hydrogen bonds outside or within the growing crystals. With mannan or cellulose, the details and the kinetics of their crystal formation are at present unknown. It should however deserve further attention as the aforementioned shift from granular to fibrillar gel-like structures can have a dramatic importance for mannan or cellulose-based products.

A final interesting aspect of the present study is the change in morphology occurring with cellulose II when one goes from low to high DP material. With low molecular weight cellulose, the crystals occur as rod-like elements, where the cellulose chains are at 90° with respect to the rod axis. On the other hand, with high molecular weight, the cellulose II crystals are fibrillar in nature as they are elongated along the cellulose chain axis. Such changes in morphology, associated with a change in molecular weight, is remarkable and must certainly be connected with the impossibility for cellulose to crystallize as regular chain folded crystals (20). In an earlier study on cellulose II crystals (14), it was shown that the growth habit for low DP cellulose crystals was in the form of long flat ribbons when the crystallization conditions were optimized. In normal cases, low DP cellulose gave needle-like or rod like crystalline elements. The present study confirms this behavior which seems to be persistent with all cellulose crystallization systems. The case of high DP cellulose crystallization yielding a fibrillar gel-like precipitate is not new as it was reported earlier by Manley (21). Here however, our electron diffraction results prove that the chain axes of cellulose are indeed oriented along the fibrillar axis of the precipitate.

If one attempts to rationalize such drastic changes in the growth habit of cellulose II crystals, when the molecular weight is increased, it is possible to bring forward the following arguments : in all cases, it seems that the crystallization parameters in cellulose are governed by the semi rigidity of the cellulose chain and the strong influence played by the intermolecular hydrogen bonds. In particular, the fact that the cellulose chains are semi rigid is likely to hinder the formation of regular chain folded crystals (22). The growth of the cellulose crystals is envisaged as being a two step phenomenon (17). In the first step, a bundle of cellulose chain is formed with the chains associated in a parallel fashion through multiple hydrogen bonds leading to the crystallization nucleus. If only short chains are used, the next step is to incorporate similar elements in a lateral fashion, leading to ribbon or rod-like morphology growing perpendicular to the chain direction in a typical polymer single crystal fashion. When higher DP cellulose is used, the bundle of chains constituting the primary crystallization nucleus will tend to associate further as they are kept in close vicinity, due to the inherent semi rigidity of the cellulose chains. This leads to a second step where the growth is longitudinal instead of lateral. The structure becomes fibrillar and is based on long and narrow elements having

roughly the diameter of the initial nucleus. Such crystals are typical polymer fibrillar crystals, extended along the chain axis and narrow in a perpendicular direction. At present, the occurrence or not of chain folding in these fibrillar crystals remains to be demonstrated.

Acknowledgments

The authors acknowledge the assistance of Mr R. Vuong for his help with the electron microscopy.

Literature Cited

1. Marchessault, R. H.; Sarko, A. Advances in Carbohydrate Chemistry 1967, 22, 421.
2. Walton A.G. ; Blackwell, J. In Biopolymers , Academic Press New York, 1973 , p 464.
3. Jones, D. J. In Cellulose and Cellulose Derivatives, Bikales, N.; Segal, L. Edit., Wiley-Interscience, New-York, 1971; Vol IV, page 117.
4. Chanzy, H.; Grosrenaud, A.; Vuong R.; Mackie, W. Planta ,1984, 161, 320.
5. Chanzy, H.; Guizard, C; Sarko, A. Int. J. of Biol. Macromolecules , 1980, 2, 149 .
6. Chanzy, H.; Excoffier, G.; Guizard C. Carbohydrate Polymers, 1981, 67, 1.
7. Buléon, A.; Duprat, F.; Booy, F.; Chanzy, H. Carbohydrate Polymers, 1984, 4,161.
8. Chanzy, H.; Grosrenaud, A.; Joseleau, J.P.; Dubé M.; Marchessault, R.H. Biopolymers, 1982, 21, 301.
9. Chanzy, H.; Noé, P.; Paillet, M.; Smith, P. J. Applied Polym. Sci., Applied Polym. Symp., 1983, 37 , 239.
10. Brandner, A.; Zengel, H.G. Eur. Pat. Appl. E.P. 47,929 ,1982.
11. Stipanovic, A.; Sarko, A. Macromolecules, 1976, 9, 851.
12. Gardiner, E. S.; Sarko, A. Can. J.Chem. 1985, 63, 174.
13. Kolpak, F.J.; Blackwell, J. Macromolecules 1976, 9, 273.
14. Buléon, A.; Chanzy, H. J. Polymer Sci., Phys. Ed. 1978, 16, 833.
15. Atalla, R. H.; Ellis, J. D.; Schroeder, L. R. J.Wood Chem. and Tech. 1984, 4, 465.
16. Atalla, R. H.; Dimick, B. E.; Nagel, S. C. In Cellulose Chemistry and Technology ACS Symposium Series N°48, Arthur J.C. Edit, 1977; Chapter 3.
17. Maeda, H.; Kawada, H.; Kawai, T. Makromol.Chem. 1970, 131, 169.
18. Chanzy, H.; Dubé, M.; Marchessault, R.H.; Revol, J.F. Biopolymers, 1979, 8, 887.
19. Buléon, A.; Chanzy, H. J. Polym. Sci., Phys. Ed. 1980, 18, 1209.
20. Buléon, A.; Chanzy H.; Froment, P. J. Polym. Sci., Phys. Ed., 1982, 20, 1081.
21. St.John Manley, R. J.Polymer Sci., Phys.Ed. 1971, 9, 1025.
22. Kamide, K; Saiko, M.; Suzuki, H. Makromol. Chem. Rapid Comm. 1983, 4, 33.

RECEIVED March 5, 1987

Chapter 12

X-ray Studies of the Structure of Cellulose Complexes

John Blackwell, David Kurz, Mao-Yao Su, and David M. Lee

Department of Macromolecular Science, Case Western Reserve University,
Cleveland, OH 44106-2699

X-ray methods have been used to investigate the structures of crystalline complexes of cellulose I and II with diamines. The structures of three complexes: ramie cellulose I complexed with ethylenediamine and 1,3-diaminopropane, and cellulose II complexed with hydrazine, have been refined by linked atom least squares methods. Interaction with the low molecular weight specimens disrupts both the hydrogen bonding and hydrophobic forces between the cellulose chains. The results show that in all three cases the cellulose chains rearrange from quarter stagger to zero staggered (in register) packing. The complexes consist of a series of sheets of chains separated by hydrogen bonded complexing molecules. The parallel-I - antiparallel-II chain polarity is maintained in the complexes of the two forms of cellulose.

The existence of crystalline complexes of cellulose and certain low molecular weight compounds has been known since the 1930's, and several studies of their structures by X-ray methods have been reported since that time (1-6). These structures are of current relevance in view of the renewed interest in organic solvents for cellulose: in the last 15 years several new solvent systems have been reported, including dimethylsulfoxide-paraformaldehyde (7), N-methylmorpholine-N-oxide (8), hydrazine at elevated temperature and pressure (9), and lithium chloride-dimethylacetamide (10). Analysis of the structure of cellulose solvent complexes provides a detailed molecule model for the polymer solvent interaction. This paper describes our analyses of the structures of cellulose complexed with ethylenediamine, hydrazine, and 1,3-propylenediamine.

0097-6156/87/0340-0199\$06.00/0
© 1987 American Chemical Society

Our present investigations of the structure of cellulose complexes has been made possible by the increased knowledge of the structures of the uncomplexed forms in the last ten years. Figure 1 shows the refined structure of cellulose I derived by Gardner and Blackwell (11), based on the X-ray intensity data for fibers drawn from the cell wall of the sea alga *Valonia ventricosa*. This material has a monoclinic unit cell with dimensions $a = 16.34\text{\AA}$, $b = 15.72\text{\AA}$, $c = 10.38\text{\AA}$ (fiber axis), and $\gamma = 97.0^\circ$, containing disaccharide sections of eight chains (as first proposed by Honjo and Watanabe (12)). However, only a few weak reflections are seen with odd h and/or k indices (the rest are absent) and hence a two chain unit cell with the a and b dimensions reduced by half can be used as an adequate approximation to the full structure. This two chain unit cell is the Meyer and Misch (13) unit cell observed for other native celluloses, and it seems likely that the extra reflections (with odd h and/or k) are not seen for these due to the lower crystallinity and crystallite size. For *Valonia* cellulose, odd order 001 reflections are absent and the space group is $P2_1$, pointing to a 2_1 helical conformation for the chain in the crystalline regions.

In the analysis of the structure of cellulose I, the most important feature to be determined was the polarity of adjacent chains, i.e. do the chains in the two chain cell have the same (parallel) or opposite (antiparallel) sense? Both kinds of model were set up and refined using the linked atom least squares (LALS) routines (14) to obtain the best agreement between the observed and calculated X-ray intensities. The best model for cellulose I was found to be an array of parallel chains, as can be seen in Figure 1: the best antiparallel model could be rejected at a significance level of 0.005%, i.e., the parallel model is preferred by 200 to 1. The two chains have the same basic conformation, right down to the tg orientations of the pendant- CH_2OH groups, and are staggered by $0.265c$, consistent with the approximate quarter stagger first proposed by Meyer and Mark (15). Each glucose residue is involved in two intramolecular hydrogen bonds: $03'-H \cdots 05$, as first proposed by Hermans et al. (16) from study of space filling models and $02-H \cdots 06'$, which was suggested to account for the dichroism of the O-H stretching modes in the polarized infrared spectra (17, 18). The cellulose chain inevitably has a relatively stiff extended conformation due to the β -(1,4)- linkages, and these intramolecular bonds on both sides of the glycosidic linkage further stabilize the conformation. The chains are linked in sheets by $06-H \cdots 03$ intermolecular bonds along the b axis. However, there is no intermolecular bonding along the ab diagonals nor along the a axis, and the structure must be stabilized in these directions by hydrophobic forces, e.g. between the faces of the glucose rings. Figure 2 shows the structure of cellulose II, which was determined in a similar manner based on the intensity data for Fortisan rayon (19). The unit cell is monoclinic with dimensions $a = 8.01\text{\AA}$, $b = 9.04\text{\AA}$, $c = 10.36\text{\AA}$ (fiber axis), and $\gamma = 117.1^\circ$; the space group is approximately $P2_1$ and the cell contains disaccharide repeats of two chains. In this case the best agreement between observed and calculated X-ray intensities was

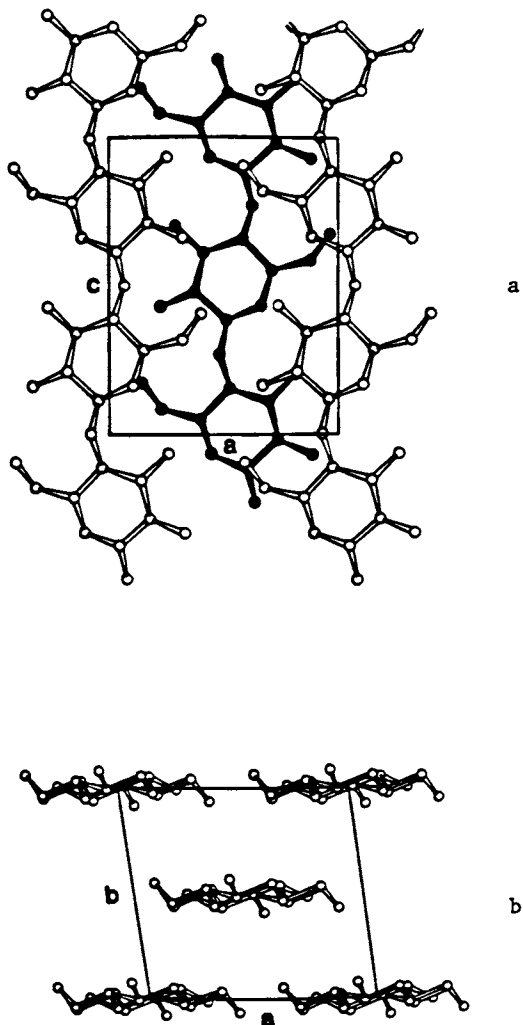


Figure 1. Structure of cellulose I [11]: (a) *ac* projection; (b) *ab* projection.

(Reprinted with permission from ref. 11. Copyright 1974 John Wiley & Sons.)

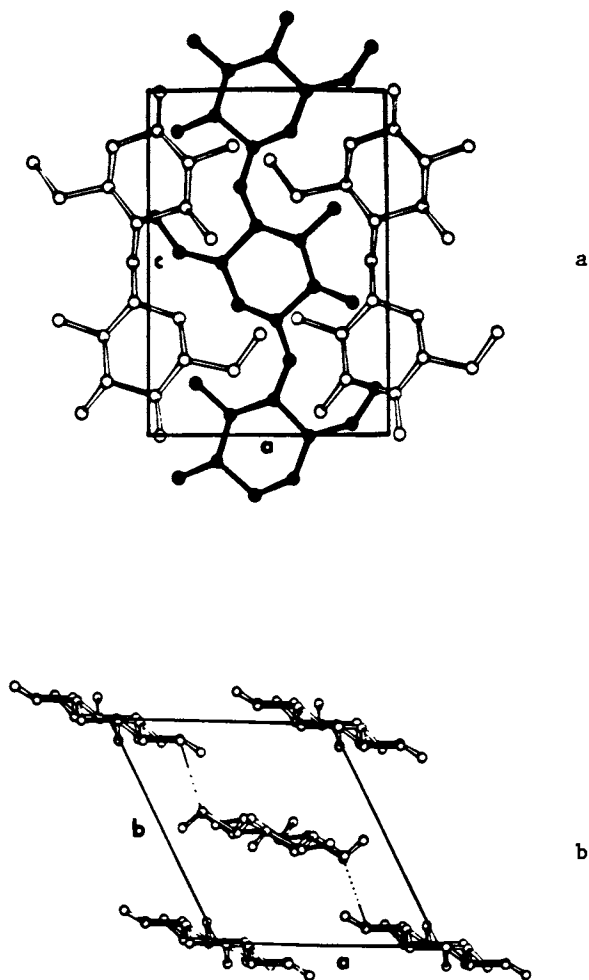


Figure 2. Structure of cellulose II [19]: (a) *ac* projection;
(b) *ab* projection.

(Reprinted with permission from ref. 19. Copyright 1976 American Chemical Society.)

obtained for an antiparallel chain model. The best contending models with parallel chains gave inferior agreement and were also found to be stereochemically unacceptable; constraining the models to avoid such "bad contacts" took them further out of consideration. In the structure as shown in Figure 2b, the corner chains have a conformation similar to that in cellulose I, with two intramolecular hydrogen bonds ($03'-H\cdots 05$ and $02-H\cdots 06'$) and linked along the b axis by an $06-H\cdots 03'$ intermolecular bond. The center chains have opposite sense and are staggered relative to the corner chains by $0.18c$ (the c axis separation of the glycosidic oxygens). These chains have the $03'-H\cdots 05$ intramolecular bond, but the $-CH_2OH$ group is in the *gt* conformation so that the second intramolecular bond is not possible. In this case, the $-CH_2OH$ groups are bonded $06-H\cdots 02$ along the b axis, and the $02-H$ groups form a further intermolecular bond $02-H\cdots 02'$ along the long ab diagonal. This extra intermolecular bond may account for the higher stability of cellulose II as compared to cellulose I. The parallel-I-antiparallel-II conclusion was also obtained in independent work by Sarko and co-workers (20,21).

The above results have obvious implications for the biosynthesis of cellulose microfibrils. The parallel chain structure of cellulose I rules out any kind of regularly folded chain structure, and reveals the microfibrils to be extended chain polymer single crystals, which leads to optimum tensile properties. Work by Brown and co-workers (22) on the mechanism of biosynthesis points to synthesis of arrays of cellulose chains from banks of enzyme complexes on the cell wall. These complexes produce a bundle of chains with the same sense, which crystallize almost immediately afterwards to form cellulose I microfibrils; there is no opportunity to rearrange to form a more stable antiparallel cellulose II structure. Electron microscopy by Hieta et al. (23) confirms the parallel sense of cellulose chains within the individual microfibrils: stains reactive at the reducing end of the cellulose molecule stain only one end of the microfibril.

The perceived difficulty with the parallel-I:antiparallel-II model concerns the I \rightarrow II conversion by Mercerization. Reversal of chain polarity is relatively easy to understand during regeneration via complete dissolution, but less so where cellulose I is simply swollen in caustic soda. One possible mechanism would involve regular chain folding, but this is inconsistent with the mechanical properties of Mercerized cotton. It is important to note however that the swelling involves fibrils which themselves are bundles of many microfibrils. The chains within an individual microfibril will have the same sense, but the cotton macrofibril probably consists of a 50/50 mixture of up and down microfibrils. Electron microscopy by Willison and Brown (24) on the cell walls of Glaucozystis show a winding of microfibrils around the cell. A similar mechanism for cotton would lead to equal numbers of up and down chains that are packaged into microfibrils in which all the chains have the same sense. Hence the mechanism for Mercerization probably involves rearrangement of extended chains. On swelling, the chains are separated and lose track of their previous neighbors. Then on removal of the swelling agent the chains are more likely to reunite with antiparallel neighbors due to the higher stability of cellulose II.

At this point the major features of the structures of cellulose I and II can be considered to be solved. Nevertheless, questions remain, especially as regards the differences between the infrared, Raman, and solid state NMR spectra obtained for different native celluloses, all of which appear to have the crystal structures shown in Figure 1. This has been a further motivation for our analyses of the structures of cellulose solvent complexes, which are described below.

Experimental

Materials. Delignified native ramie fibers were obtained from Dr. R.V. Allison of U.S.D.A., Belle Glade, FL. Mercerized specimens were prepared by repeated soakings in 22% aqueous sodium hydroxide solutions separated by thorough washings in water until no more than a trace of residual cellulose I could be detected in the X-ray pattern. Fortisan rayon fibers were the gift of Dr. L. Lanieve of Celanese Corporation. Reagent grades of ethylenediamine and hydrazine were purchased from Eastman Kodak Co., 1,2- and 1,3- propylenediamine from Fisher Scientific Co. These reagents were dried using molecular sieves.

Complex Formation

Cellulose complexes were prepared by soaking the taut fibers in the individual liquid complexing agents for 1 - 36 hours followed by vacuum drying. The soaking time was that necessary to remove all traces of the uncomplexed cellulose in the X-ray pattern. Ethylene and propylenediamine contents were determined by electrical analyses performed by Galbraith Laboratories, Knoxville, TN. Hydrazine contents were determined by addition of the specimen to 0.1N hydrochloric acid followed by potentiometric titration against 0.1N sodium hydroxide solution.

X-ray Diffraction

Wide angle X-ray diffraction patterns were recorded on Kodak No Screen X-ray film using nickel filtered $\text{CuK}\alpha$ radiation and a Searle toroidal focusing camera. The d-spacings were calibrated with sodium fluoride. The intensities of the X-ray reflections were determined from an x-y grid of optical density obtained using a scanning optical densitometer. These data were corrected for background and for the Lorentz and polarization effects. Overlapped intensities were apportioned in the ratio of the calculated intensities. Unobserved reflections, i.e. predicted reflections too weak to be detected, were assigned an intensity of one-half the background (threshold) but included in the data only when the calculated intensity exceeded the background. The atomic coordinates for the cellulose chain were based on those used by Kolpak and Blackwell (19) in their refinement of the structure of cellulose II, with minor adjustments in the glycosidic torsion angles to fit the slightly different fiber repeats. The N-N bond length in hydrazine was set at 1.44Å as in the crystal structure determined by Collin and Lipscomb (25); the

bond lengths and angles in theylenediamine were those used by Yokozuki and Kushita (26) for gas diffraction studies; the structure of 1,3 diaminopropane was based on that for trimethylene diamonium hydrochloride due to Hirokawa *et al.* (27).

Results and Discussion

The unit cells determined in this and other laboratories for cellulose I and II complexes with ethylenediamine and hydrazine are listed in tables 1 and 2. Table 3 shows our unit cells for the 1,2- and 1,3- diaminopropane complexes for which there have been no previous proposals.

As can be seen in table 2, a number of unit cells have been proposed for cellulose I-hydrazine complexes over the years. Some of this diversity is almost certainly due to poor quality data, which can be indexed in different ways. Nevertheless, visual comparison shows that our patterns are significantly different from those published previously, which probably reflects the fact that we used hydrazine containing no more than 3% water, as compared to up to 40% in earlier work. So far we have prepared three different cellulose II-hydrazine complexes, two for Fortisan (designated A and B) and one for Mercerized ramie. There may be some rationale for this: complex A has only been obtained using anhydrous hydrazine, and the Fortisan and Mercerized ramie have different morphologies. However, it seems likely that all three complexes can be formed by both specimens once the preparation conditions are better understood.

We are investigating the structures of these complexes using the refinement methods applied to celluloses I and II, as described above. In the next sections we describe the results of these analyses for three complexes: ramie cellulose I-ethylenediamine (28), ramie cellulose I-1,3-propanediamine (29), and Fortisan cellulose II-hydrazine A, which are the most crystalline complexes prepared to date.

Ramie Cellulose I-Ethylenediamine

Some 39 independent reflections are observed in the fiber diagram of ramie cellulose I-ethylenediamine complex, and there are a further 36 that are predicted within the range of these data, but which are too weak to detect. Elemental analysis indicates the presence of one ethylenediamine per glucose residue and density considerations require disaccharide units of two chains per unit cell.

The major features of the intensity data are determined by the cellulose chains themselves. Refinements omitting the complexing molecules show that the structure consists of stacks of chains along the *b* axis, and that these are "in register", i.e. there is zero stagger. This is also apparent from the fact that very few reflections with odd *h* indices are detected, indicating that we are dealing with essentially a one chain structure, i.e. the two chains along the *b* axis, together with their associated ethylenediamines, have approximately the same structure.

Table 1

Proposed Unit Cells for Cellulose Ethylenediamine Complexes

	a (Å)	b (Å)	c (Å)	γ°	Ref.
Cellulose I (Ramie)	12.16	13.1	10.3	135.2*	1
Cellulose I (Cotton)	12.2	12.3	10.3	137.0*	6
Cellulose I (Ramie)	12.37	9.52	10.35	117.8	28
Cellulose II (Regenerated)	12.81	18.27	10.34	118.0	28
Cellulose II (Mercerized)	13.42	8.41	10.34	119.1	28

* Acute angle used in the original paper.

Table 2

Proposed Unit Cells for Cellulose Hydrazine Complexes

	a (Å)	b (Å)	c (Å)	γ°	Ref.
Cellulose I (Ramie)	10.9	10.9	10.3	127.7*	1
Cellulose I (Ramie)	9.1	8.1	10.38	114.7	3
Cellulose I (Cotton)	9.68	9.96	10.3	125.2*	6
Cellulose I (Ramie)	9.19	16.39	10.37	97.4	30
Cellulose II A (Fortisan)	9.37	19.88	10.39	120.0	30
Cellulose II B (Fortisan)	8.84	23.76	10.38	120.0	30
Cellulose II (Mercerized Ramie)	9.48	15.39	10.37	96.4	30

* Acute angle used in the original paper.

Table 3

Proposed Unit Cells for Cellulose Diaminopropane Complexes

	a (Å)	b (Å)	c (Å)	γ°
Ramie 1,2- diaminopropane	4.72	11.55	10.38	92.8
Ramie 1,3- diaminopropane	4.54	12.22	10.38	90.0
Fortisan 1,2- diaminopropane	4.61	22.95	10.38	90.7
Fortisan 1,3- diaminopropane	4.57	23.90	10.38	93.1

The ethylenediamine molecules must be hydrogen bonded to the cellulose chains (why else would the complexes form and be stable?). Since all N-H and O-H groups are required to form donor bonds, it is clear from the stereochemistry of any possible model that each hydroxyl of the glucose residue must be linked to a nitrogen via a donor or acceptor bond. For convenience we attached the ethylenediamine molecule at O3-H by a hydrogen bond with an O...N distance of 2.8Å, and proceeded by treating this as a flexible side chain. Models were set up in which the ethylene diamine had three possible conformations, corresponding to *trans*, *gauche* and *gauche* for the central torsion angle. For completeness, we also considered both parallel and antiparallel packing of the two chains in the unit cell.

The antiparallel models gave significantly worse agreement with the observed intensity data than did the parallel chain models and hence could be rejected. The (native) cellulose I structure has parallel chains and the complex can be restored to the original form simply by washing in water. It seems unlikely therefore that complex conformation involves a reversal of chain polarity. Similarly, models with different conformations for the ethylenediamine could also be ruled out. Beyond this, the refinement led to four models that could not be distinguished on the basis of X-ray agreement, but of these, only one model had all the O-H and N-H groups hydrogen bonded, and this is selected as the final structure.

The refined structure for ramie cellulose I-ethylenediamine complex is shown in Figure 3 and had a crystallographic residual of $R'' = 0.189$. As can be seen in the *ac* projection (Figure 3b) the two ethylenediamine molecules have slightly different positions and conformations, which accounts for the two chain unit cell. Constraining the refinement to give a structure with identical conformations for the complexing molecules led to $R'' = 0.223$, and such a model can be rejected at the 0.005% significant level.

Comparison of the structure of this complex with that of the original cellulose I shows the extent of the rearrangement that has occurred. The chains have shifted from a quarter staggered arrangement to form stacks in register, i.e. with zero stagger. Thus the interaction with ethylenediamine not only breaks the hydrogen bonding network in the original structure but also affects the hydrophobic forces between the "surfaces" of the ribbonlike chains. The structure of the complex is very similar to that of chitin in which the chains are also stacked in register to form sheets. Within each stack the chains have approximately the same separation of 4.7Å and have a similar inclination to the stacking plane. In β -chitin, all the chains have the same sense, and the sheets can be separated to include water, leading to the formation of crystalline hydrates that are analogous to the present cellulose I-ethylenediamine complex. In the latter structure, the ethylenediamine molecules fit in channels between the molecules that exist in a zero staggered structure but not in the case of quarter stagger.

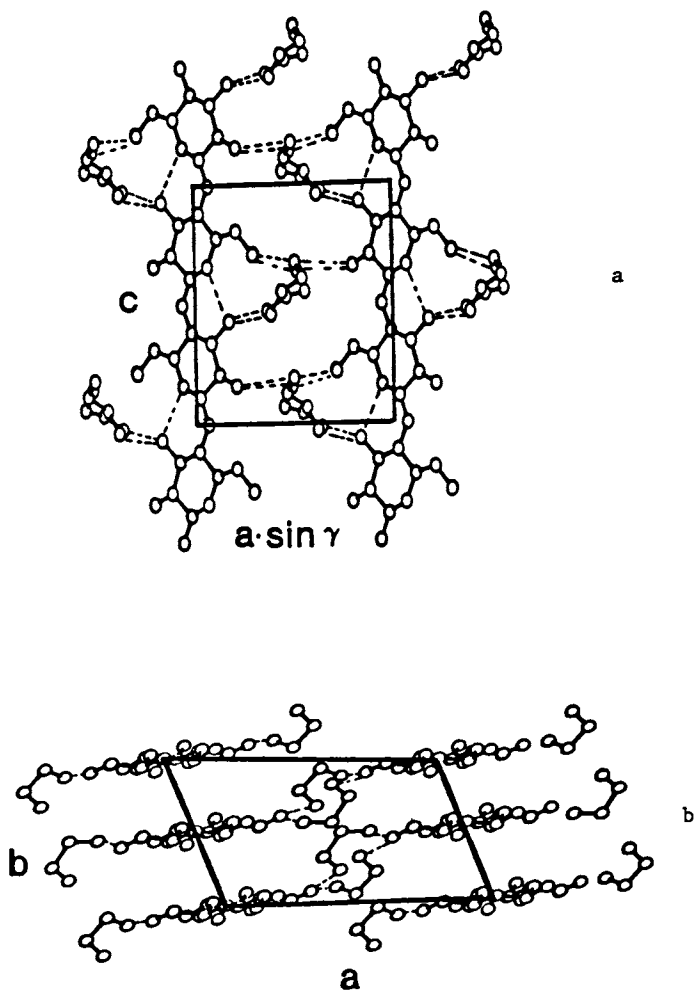


Figure 3. Structure of Ramie cellulose I - ethylenediamine complex [30]: (a) 010 projection; (b) ab projection.

(Reprinted with permission from ref. 30. Copyright 1984 John Wiley & Sons.)

Ramie Cellulose I-1,3-diaminopropane Complex

The ramie cellulose I-1,3-diaminopropane complex structure is the most crystalline of the diaminopropane complexes so far examined, and has a (metrically) orthorhombic unit cell that can contain only one chain which dictates a parallel chain structure. Elemental analysis and density measurements point to one molecule of 1,3-diaminopropane per glucose residue. Refinement proceeded in a manner similar to that described above for the ethylenediamine complex, based on intensity data for 24 observed and 12 unobserved reflections.

If the cellulose chain is assumed to have the same backbone conformation as in the ethylenediamine complex, then the structure is defined by nine potentially refinable parameters. The approximate chain orientation was refined first before the ethylenediamines were added. Thereafter C-N sections were attached by hydrogen bonds at two of the three hydroxyls (i.e. 1,3-diaminopropane omitting the central CH₂ group). This eliminated the possibility of a "bent" complexing molecule that is hydrogen bonded to hydroxyl on the same chain, and pointed to a structure in which the 1,3-diaminopropanes are bonded between chains, either along the b axis or the ab diagonals.

Twelve different possible packing models were refined separately, leading to structures with R" values between 0.147 and 0.194. These were not statistically distinguishable, nor were any of them completely hydrogen bonded. Note that the requirement that all the O-H and N-H groups must be hydrogen bonded becomes more severe as the size of the diamine molecule is increased. Of the 12 models, the one which came closest to being completely hydrogen bonded was that with the lowest R", for which the only defect was that O6-H did not form a donor bond. However, the -CH₂OH orientation was not far from the original tg position in the parent native cellulose, and incorporation of a constraint to require the formation of an O6-H...O2 hydrogen bond led to an acceptable hydrogen bonding network. This final structure is shown in Figure 4.

The one-chain unit cell prescribes an unstaggered array of parallel chains and thus the rearrangement from the original cellulose I structure that has occurred is very similar to that which occurs on formation of the ethylenediamine complex. A one chain unit cell is also seen for the 1,2-diaminopropane complex, and this structure appears to be similar, except for minor modifications of the a and b dimensions.

Fortisan Cellulose II-Hydrazine Complex A

This structure presents more difficult problems than those treated above. Some 26 reflections are observed, but these are indexed by a four-chain unit cell, and this is insufficient data to allow for refinement of the number of parameters necessary to define such a structure. However, 22 of these reflections can be indexed by a two-chain cell and we opted to work with this as an approximation to the full structure. Titration showed that the hydrazine content was close to one molecule per glucose residue.

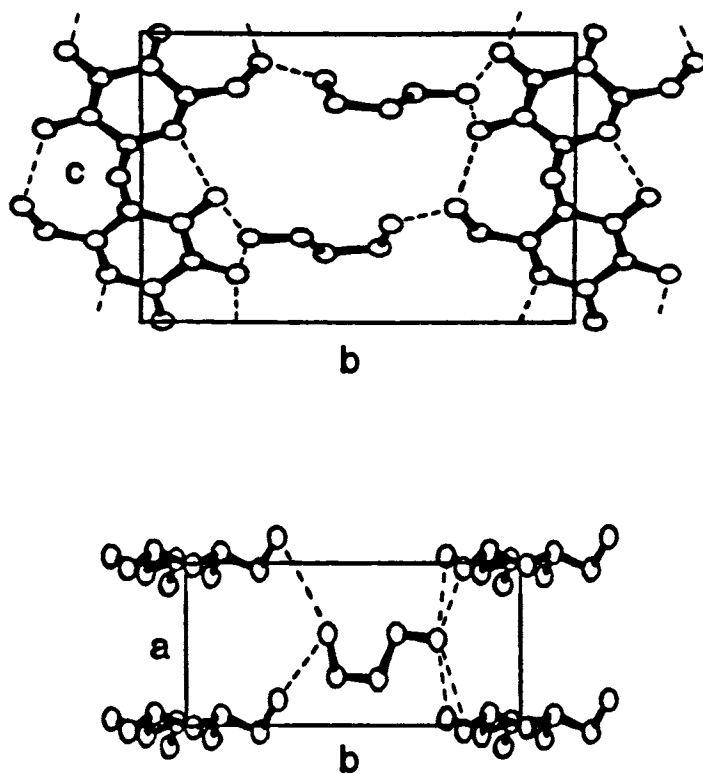


Figure 4. Structure of Ramie cellulose I-1,3-diaminopropane complex: (a) bc projection; (b) ab projection showing only half a repeat.

This being a complex of cellulose II, one would expect these two chains to be antiparallel. We did consider parallel chain models but these always gave inferior agreement with the intensity data and could be ruled out.

Intensity calculations quickly showed that the axes of the two chains pass through the origin and 0.0,0.5 in the *ab* projection. The hydrazines (N-N) were attached by hydrogen bonds at O2 and their position and the -CH₂OH orientations were refined, starting with the latter groups in combinations of three staggered positions (gt, tg and gg). Of the resulting nine models, all but four were rejected in that they were unable to form hydrogen bonds for all the O-H and N-H groups. The remaining four, however, were statistically undistinguishable in terms of their X-ray agreement. The model with the lowest residual, $R^* = 0.207$, is shown in Figure 5. The major features of the structure are the same as in the other acceptable models. It can be seen that the chains are arranged in stacks with the same sense, and successive stacks are antiparallel. The "up" and "down" stacks are not identical, but both are similar to those for the two cellulose I complexes described above. The glycosidic oxygens of the antiparallel chains are also approximately in register and this has the effect that the CH₂OH groups on adjacent chains are opposite each other. Thus there is a channel between the chains (between O2 and O3 on adjacent residues) and this is occupied by the hydrazine molecules. This cellulose II complex has a very similar structure to that of α -chitin, which also has antiparallel chains. In the latter the chains are in register along both the *a* and *b* axes, and the "channels" are occupied by the -NHCOCH₃ substituent groups.

Conclusions

For all three complexes described above, the effect of the complexing agent is to break the intermolecular hydrogen bonds and to rearrange the chains from quarter stagger to in register packing. These major features can be determined relatively easily from the X-ray intensity data, which depend largely on the chains themselves. Thereafter the positions of the complexing molecules are more difficult to determine. In each case we have found what appears to be reasonable structure in terms of X-ray agreement, stereochemical constraints, and the requirement that all of the O-H and N-H groups should be hydrogen bonded. Nevertheless, some competing arrangements cannot be ruled out, especially for the Fortisan cellulose II-hydrazine complex A. This ambiguity may reflect the fact that there may be some variety in the positions of the complexing molecules in the bulk complex, and also there are complications due to absorption of water molecules.

Acknowledgments

This work is being supported by National Science Foundation, grant No. DMR84-17525 from the Polymer Program.

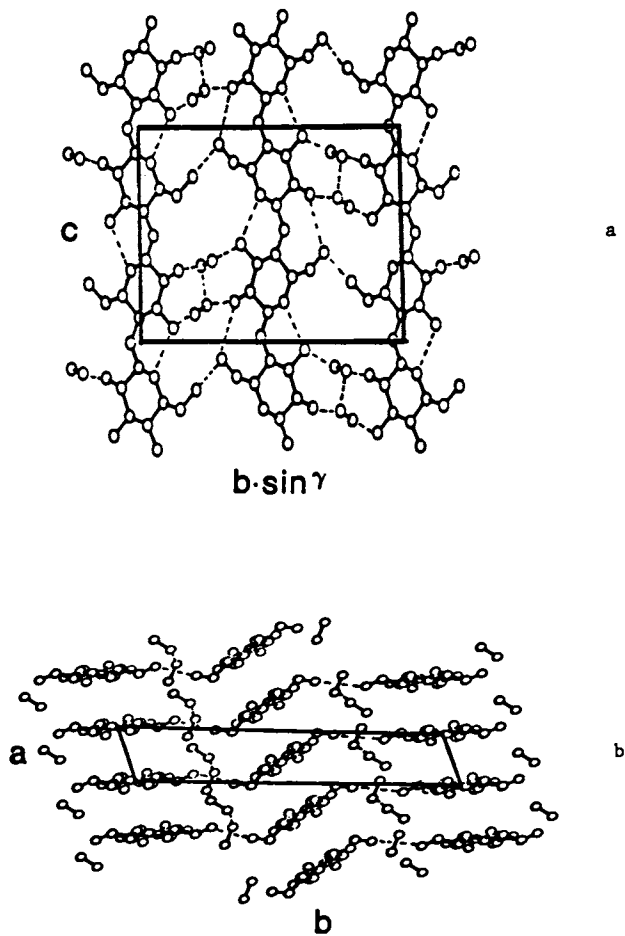


Figure 5. Structure of Fortisan cellulose II - hydrazine complex A [28]: (a) 100 projection; (b) ab projection. (Reprinted with permission from ref. 28. Copyright 1983 John Wiley & Sons.)

References

1. Halle, E. Kolloid-Zt. 1934, 69, 324.
2. Trogus, C.; Hess, K. Z. Phys. Chem. (Leipzig) 1931, B14, 387.
3. Sakurada, I.; Hutino, K. Kolloid-Zt. 1936, 77, 346.
4. Sakurada, I.; Okamura, S. Kolloid-Zt. 1937, 81, 199.
5. Centola, G. Gass. Chem. Ital. 1938, 68, 825.
6. Creely, J.J.; Segal; L., Loeb, L. J. Polym. Sci. 1959, 36, 205.
7. Johnson, D.L. U.S. Pat. 2 371 359, 1970.
8. Johnson, D.L. Br. Pat. 1 144 048, 1969.
9. Litt, M.H.; Kumar, G. U.S. Pat. 4,028,132, 1977.
10. Turbak, A.F.; El-Kafrawy, A.; Snyder, F.W.; Averbach, A.B. U.S. Pat. 4 302 252, 1981.
11. Gardner, K.H.; Blackwell, J. Biopolymers 1974, 13, 1975.
12. Honjo, G.; Watanabe, M. Nature, 1958, 326-328.
13. Meyer, K.H.; Misch, L. Helv. Chim. Acta, 1937, 20, 232.
14. Arnott, S.; Wonacott, A. Polymer 1966, 7, 157.
15. Meyer, K.H.; Mark, H. Ber. Dsch. Chem. Ges. 1928, 61B, 593.
16. Hermans, P.H.; de Booy, J.; Maan, C. Kolloid Zt. 1943, 102, 169.
17. Marrinan, H.J.; Mann, J. J. Polym. Sci. 1956, 21, 301.
18. Jones, D.W. J. Polym. Sci. 1958, 32, 371.
19. Kolpak, F.J.; Blackwell, J. Macromolecules 1976, 9, 273.
20. Sarko, A.; Muggli, R. Macromolecules 1974, 7, 486.
21. Stipanovic, A.J.; Sarko, A. Macromolecules 1976, 9, 851.
22. Brown, R.M.; Willison, J.H.M.; Richardson, C.L. Proc. Nat. Acad. Sci. U.S.A. 1976, 73, 4565.
23. Hieta, K.; Kuga, S.; Usuda, M. Biopolymers 1984, 23, 1807.
24. Willison, J.H.M.; Brown, R.M. J. Cell Biol. 1978, 77, 103.
25. Collin, R.N.; Lipscomb, W.N. Acta Cryst. 1951, 4, 10.
26. Yokozuki, A.; Kushita, K. Bull. Chem. Soc. Jpn. 1971, 44, 2926.
27. Hirokawa, S. et al. Org. Com. Structure Reports 1968, V33B, 26-27.
28. Lee, D.M.; Blackwell, J.; Litt, M.H. Biopolymers 1983, 22, 1383.
29. Kurz, D.; Su, M.-Y.; Blackwell, J. (in preparation).
30. Lee, D.M.; Burnfield, K.E.; Blackwell, J. Biopolymers 1984, 23, 111.

RECEIVED April 9, 1987

Chapter 13

Cellulose Textile Materials Studied by Using Fourier Transform Infrared Photoacoustic Spectroscopy

Charles Q. Yang¹, Randall R. Bresee², William G. Fateley¹, and Theresa A. Perenich³

¹Department of Chemistry, Kansas State University, Manhattan, KS 66506

²Department of Clothing, Textile, and Interior Design, Kansas State University, Manhattan, KS 66506

³Department of Clothing, Textile, Furnishing and Interiors, University of Georgia, Athens, GA 30602

A variety of cellulose textile materials, including sized cotton yarns and chemically treated cotton fabrics were studied with fourier transform infrared photoacoustic spectroscopy (FT-IR/PAS) in our laboratory. The distribution of chemical additives into cotton yarns and fabrics was determined using FT-IR/PAS. It is concluded that FT-IR/PAS is a non-destructive and information-rich analytical technique which is uniquely suitable to the near-surface characterization of a variety of cellulose textile materials. The fundamentals of FT-IR/PAS are also reviewed.

Infrared spectroscopy is probably one of the most widely used instrumental methods by cellulose chemists for investigating physical and chemical properties. The first infrared absorption spectrum of cotton cellulose was published by Rowen et. al. in 1947 [1]. During the following decade, infrared spectroscopy was extensively applied to the analysis of cellulose textiles using sampling techniques such as mineral oil mulls [2-5] or films cast on glass plates [6-7]. For many years, dispersive infrared spectroscopy has been applied to study characteristics of cellulose textile materials such as the cellulose molecular orientation, hydrogen bonding, degradation and decomposition processes, and chemical modification of cotton cellulose [8-10]. The most commonly used sampling technique for obtaining infrared absorption spectra of cellulose textile materials is the potassium bromide (KBr) pellet method. This technique first was introduced to cellulose analysis in 1957 [11], modified later [12], and has become a routine and versatile procedure for obtaining infrared spectra of textiles for both qualitative and quantitative analysis purposes [13]. Attenuated total reflectance (ATR) also has been used to obtain infrared absorption spectra of cellulose textile materials [14]. Even though the ATR technique can be used to study the surface chemistry of textile materials, this technique often suffers from the poor contact between samples and reflection crystals [15]. An alternative approach of sample preparation for infrared

0097-6156/87/0340-0214\$06.00/0

© 1987 American Chemical Society

transmission measurements of cellulose was also reported [16]. Other sampling techniques such as preparing a thin layer of parallel fibers sandwiched between two plates of window materials also have been used to obtain infrared spectra of textile materials [17-19], but these techniques usually require a high degree of skill and patience to obtain spectra of high quality.

Fourier transform infrared spectroscopy (FT-IR) has been developing rapidly and has become more important in the field of analytical spectroscopy during the past decade. It recently has been introduced to cellulose research for the identification and quantitative analysis of finishing agents on cellulose textiles [20,21]. With the assistance of a large capacity data system, FT-IR spectrometers have various advantages over dispersive infrared spectrometers. The multiplexing advantage makes it possible to measure all frequencies simultaneously, so infrared spectra can be collected at a much faster speed and the signal-to-noise (S/N) ratio for a given resolution can be improved by increasing the number of scan. The throughput advantage of FT-IR allows a large amount of energy to reach the detector, so a significant improvement in the S/N ratio results. Also, the use of a He-Ne laser interferometer to reference the position of a moving mirror greatly increases the accuracy of frequency determination, allowing spectral subtraction to become practical for identifying chemical species in a mixture [22].

Although ultraviolet and visible photoacoustic spectroscopy has been used by analytical chemists to investigate solid samples for many years, the photoacoustic technique was applied to the infrared region only when photoacoustic detection was combined with an interferometer and a large capacity data system in the late 1970s. Since then, FT-IR/PAS has attracted considerable interest due to its many advantages [23-25]. The high optical throughput and the multiplexing characteristics made FT-IR/PAS a routine analytical technique for qualitative analysis with a desirable S/N ratio.

A typical FT-IR/PAS experiment is illustrated in Figures 1 and 2. IR radiation passing through an interferometer is modulated by a moving mirror. The modulated IR beam is then focused onto a sample which is sealed inside a small volume cell (Figure 1). This PAS sample cell has an optical window for transmitting IR radiation in the region of interest, e.g., a KBr window for mid-infrared radiation or a polyethylene window for far-infrared radiation (Figure 2). The PAS cell also contains a sensitive microphone for photoacoustic signal detection (Figure 2). An infrared transparent gas such as helium is used to fill the PAS cell to carry photoacoustic signals. The IR radiation absorbed by the sample is converted to heat by a radiationless transfer process. When the heat propagates to the sample surface and transfers at the sample-gas interface into the surrounding gas, pressure variations of the gas are generated because the intensity of the IR radiation is modulated by the interferometer at an audio frequency region. This photoacoustic signal is detected by the microphone, and preamplified in the PAS sample cell unit (Figure 2). The electric signal is subsequently Fourier-transformed by the data system to yield a single beam FT-IR/PAS spectrum (Figure 1). Carbon black is normally used as a reference material because all IR radiation can be absorbed by carbon black and converted to photoacoustic signals.

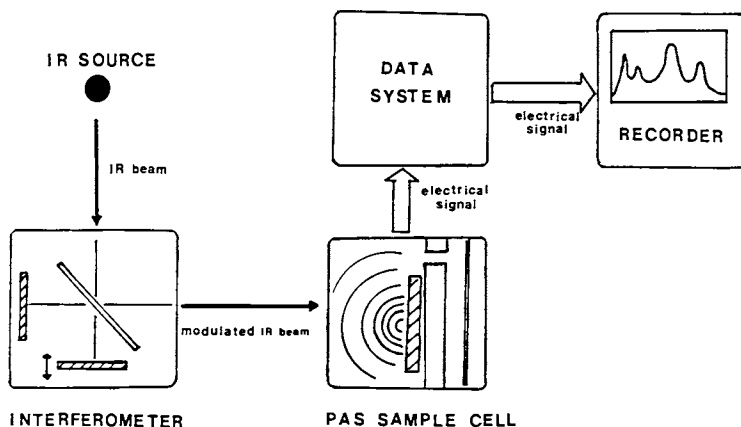


Figure 1. Schematic of a Fourier transform infrared spectrometer.

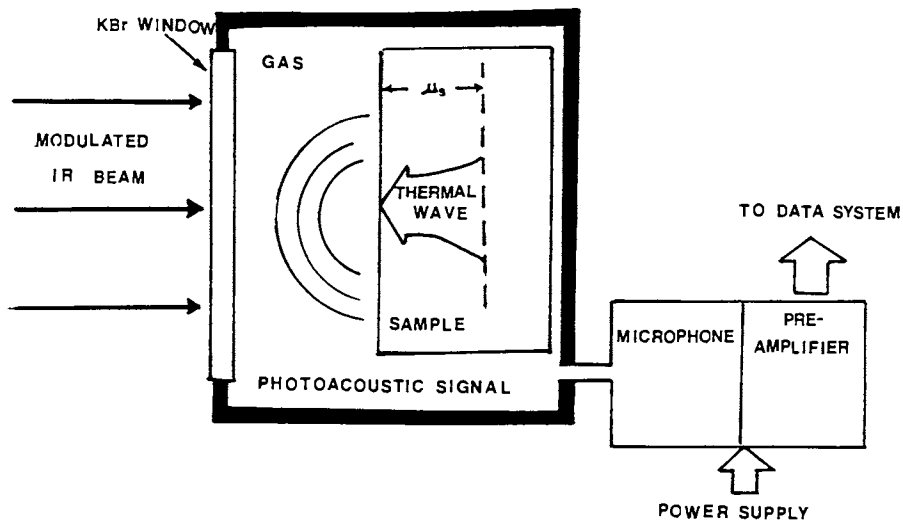


Figure 2. Schematic of a photoacoustic sample cell unit.

From the above PAS signal generation sequence, it can be seen that opaque materials or highly scattering samples can be measured using FT-IR/PAS without sample preparation and the sample integrity is maintained during the experiment. This is impossible for conventional infrared sampling techniques. Difficulties due to poor contact between samples and reflection elements common to ATR experiments is no longer a problem for FT-IR/PAS because photoacoustic signals are directly detected by a microphone without using any reflection elements and photodetector. For thermally thick samples, i.e., when sample thickness is greater than thermal diffusion length, only the heat generated within the first thermal diffusion length can propagate to the heat transfer surface and cause photoacoustic signals. Consequently, FT-IR/PAS can be used to study the chemistry of solid surface layers. This is another major advantage of FT-IR/PAS over conventional infrared techniques. The thermal diffusion length (μ_s) in cm can be calculated as follows [26];

$$\mu_s = \left(\frac{2k}{\rho c \omega} \right)^{1/2} \quad (1)$$

Where k is the sample's thermal conductivity in $\text{cal} \cdot \text{cm}^{-1} \cdot \text{s}^{-1} \cdot ^\circ\text{C}^{-1}$, ρ is the sample's density in $\text{g} \cdot \text{cm}^{-3}$, c is the sample's specific heat in $\text{cal} \cdot \text{g}^{-1} \cdot ^\circ\text{C}^{-1}$ and ω is the angular modulation frequency in $\text{radian} \cdot \text{s}^{-1}$. The angular modulation frequency ω can be calculated from the modulation frequency f in Hertz, as the following:

$$\omega = 2\pi f \quad (2)$$

$$f = \text{vel} \cdot \tilde{\nu} \quad (3)$$

where vel is the optical velocity of an interferometer in $\text{cm} \cdot \text{s}^{-1}$ and $\tilde{\nu}$ is the frequency of IR radiation in wavenumbers (cm^{-1}). In a Genzel design interferometer, which was used in our experiments, the optical velocity is equivalent to four times the mirror velocity.

By combining Equations 1-3, it can be seen that thermal diffusion length is inversely proportional to the square root of the product of optical velocity and wavenumber of IR radiation. Therefore, thermal diffusion length can be varied by changing the optical velocity of the interferometer. For optically opaque and thermally thick samples, i.e., when both optical penetration length and thermal diffusion length are smaller than the sample thickness, the PAS effective sampling depth can be changed by applying different mirror velocities if the optical penetration length is greater than the thermal diffusion length. Therefore, sample surface layers with different thicknesses can be examined by PAS, and the penetration of chemical additives in the surface layers of cellulose textile materials can be investigated by this depth profiling technique [27]. This information is of interest in textile research, but it is difficult to obtain by other non-destructive analytical techniques.

A variety of cellulose textile materials were studied using FT-IR/PAS in our laboratory. The distribution of sizing agents and finishing agents in cotton yarns and fabrics was determined. The results of these investigations are presented here.

Experimental

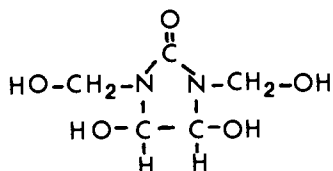
An IBM IR-98 spectrometer was used for all FT-IR/PAS measurements. The photoacoustic cell used was built at Ames Laboratory. Resolution for all PAS measurements was 8 cm^{-1} , and no smoothing function was used. Helium passing through a liquid nitrogen trap was used to purge the sample chamber and as conducting gas inside the PAS cell. Carbon black was used as a reference material. Optical velocities corresponding to various mirror velocities of the interferometer are presented in Table I.

Table I. Scan Velocity of IBM IR-98 FT-IR Spectrometer

Velocity	Mirror Velocity ($\text{cm}\cdot\text{s}^{-1}$)	Optical Velocity ($\text{cm}\cdot\text{s}^{-1}$)	Velocity	Mirror Velocity ($\text{cm}\cdot\text{s}^{-1}$)	Optical Velocity ($\text{cm}\cdot\text{s}^{-1}$)
0	0.059	0.235	5	0.140	0.559
1	0.070	0.280	6	0.166	0.665
2	0.083	0.333	7	0.198	0.791
3	0.099	0.396	8	0.236	0.941
4	0.118	0.470	9	0.280	1.119

The cotton yarns sized with various polymeric sizing agents were provided by Southern Regional Research Center, U.S. Department of Agriculture. These yarns had been sized on a laboratory single-end-slasher. Portions of the sized yarns also had been subjected to a desizing process involving a boil-off with 0.5% sodium hydroxide.

The cotton fabrics were treated using conventional padding and foam-finishing techniques by United Merchants and Manufacturers. The two finishing agents used have the tradenames of Valrez 248 and Valrez ULF. Valrez 248 is dimethyloldihydroxyethyleneurea (DMDHEU) with the following structure:



The hydroxymethyl groups in DMDHEU were methylated to form Valrez ULF.

Fibers with a cellulose triacetate core and a cellulose skin were prepared by partially saponifying cellulose triacetate fibers following a conventional procedure by the use of a hot, strong sodium hydroxide solution [28]. To determine the thicknesses of the skin and the core, the fibers were dyed with C. I. Direct Green 26 so cellulose was dyed more deeply than triacetate. Thickness of the cellulose skin was measured by optical microscopy after fiber cross

sections were prepared from the dyed fibers. The fibers were found to have diameter of approximately 18 μm and skin thicknesses of approximately 2 μm .

Results and Discussion

Near Surface Analysis. A cellulose fiber, a cellulose triacetate fiber and a fiber with a cellulose skin and a triacetate core were studied using FT-IR/PAS (Figure 3). The spectral characteristics of both the cellulose and the cellulose triacetate fibers (Figures 3A and 3B) are revealed in the spectrum of the cellulose skin-cellulose triacetate core fiber (Figure 3C), where the strong hydrogen-bonded OH stretching peak around 3300 cm^{-1} is due to the cellulose skin, and the strong carbonyl stretching peak at 1730 cm^{-1} is due to the cellulose triacetate underneath the skin. Since the thermal diffusion length of cellulose at scan velocity 0 is approximately 4-12 μm in the mid infrared frequency range (4000-400 cm^{-1}), which is larger than the skin thickness (2 μm), both the cellulose skin and the cellulose triacetate core can be detected by FT-IR/PAS. However, the intensity of the carbonyl peak at 1730 cm^{-1} relative to the intensity of the strongest peak at 1045 cm^{-1} in the spectrum of the skin-core sample (Figure 3C) is lower than that in the spectrum of pure cellulose triacetate (Figure 3B), because less cellulose triacetate was detected by PAS in the skin-core sample.

In the textile industry, sizing agents are generally applied to warp yarns to increase their abrasion resistance during weaving. After weaving is completed, sizing agents are removed through a desizing process to obtain desired yarn properties. In our research, a pure cotton yarn and a cotton yarn sized with a polyurethane were examined by PAS at velocity 0 (Figures 4A and 4B). An intense peak at 1730 cm^{-1} observed in Figure 4B was due to the carbonyl stretching of the polyurethane sizing agent. The sized cotton yarn was then ground into a powder to pass a 40-mesh screen and re-examined by FT-IR/PAS at velocity 0 (Figure 4C). It can be seen that the intensity of the carbonyl peak of the powder sample (Figure 4C) was greatly reduced compared with that of the whole yarn sample (Figure 4B). Since photoacoustic signals are generated only from the substances within one thermal diffusion length thickness, the infrared spectrum of the sized yarn (Figure 4B) provides information of the chemical composition of the substances within a few microns surface layer. Upon grinding the sample, however, the surface layer and the bulk were mixed and averaged. Because the diameter of the cotton yarn is approximately 350 μm , the amount of substances within a few microns surface layer is very small compared to the amount of substances in the bulk; therefore, the infrared spectrum of the powder sample (Figure 4C) represents mainly the chemical composition of the bulk. The observation that the carbonyl peak for the yarn sample in Figure 4B was much more intense than the same peak for the powder sample in Figure 4C demonstrates a higher concentration of the polyurethane sizing agent in the surface layer of the yarn than in the bulk. This suggests that the sizing process did not result in uniform distribution of the polyurethane sizing agent into the yarn bulk. Since the weaving performance of sized yarns is greatly affected by size penetration, FT-IR/PAS appears to be a valuable tool for studying sizing processes.

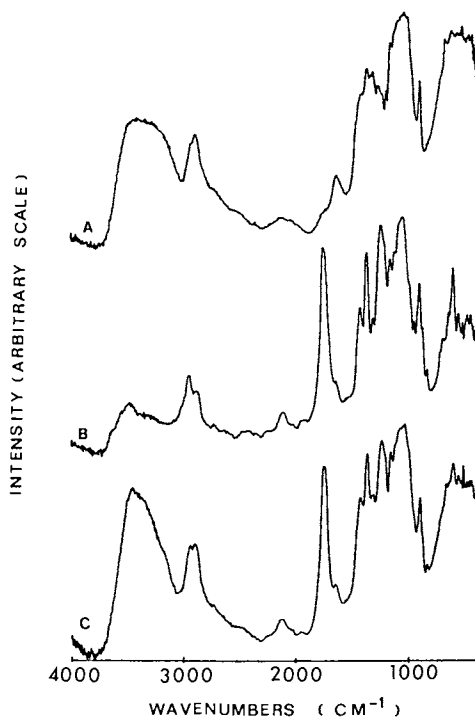


Figure 3. The photoacoustic infrared spectra of (A) a cellulose fiber; (B) a cellulose triacetate fiber; (C) a fiber with cellulose skin and cellulose triacetate core.

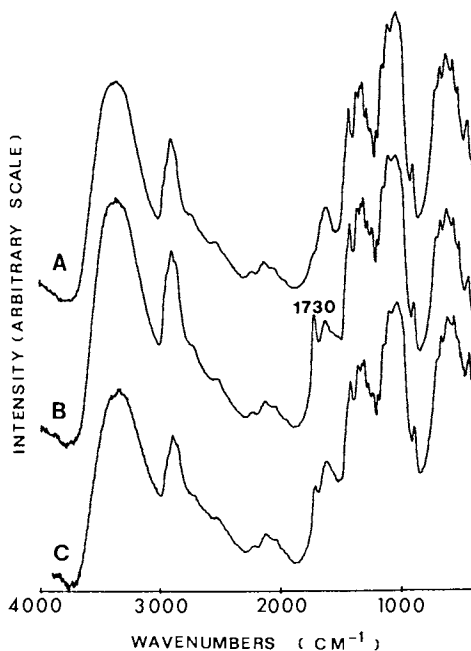


Figure 4. The photoacoustic infrared spectra of (A) a cotton yarn; (B) a cotton yarn sized with a polyurethane; (C) the corresponding powder from the sized yarn.

After a portion of the sized cotton yarn underwent a desizing process, the desized yarn and a corresponding powder sample were examined by FT-IR/PAS (Figure 5). Compared with the infrared spectrum of the sized yarn (Figure 4B), the carbonyl peak intensity in the spectrum of the desized yarn (Figure 5A) was greatly reduced as a result of the desizing process, indicating that most of the sizing agent was removed from the surface layer of the yarn. However, the concentration of the sizing agent in the bulk of the desized yarn is still relatively high as demonstrated by a relatively intense carbonyl peak in the spectrum of the powder sample (Figure 5B). This indicates that the sizing agent in the surface layer of the sized yarn was removed through the desizing process, but most of the sizing agent in the yarn interior still remained. Since incomplete sizing agent removal during desizing results in many problems such as nonuniform dyeing, FT-IR/PAS appears to be suitable for studying the effectiveness of desizing processes.

Infrared spectroscopy traditionally has been applied to study textile samples by grinding samples and preparing KBr pellets. Upon grinding, the surface layer is mixed with the bulk so the KBr approach cannot be used to investigate the chemistry of the near-surface of textile materials. The capability of near surface characterization is considered to be one of the major advantages of FT-IR/PAS over the traditional transmission technique.

Applications of the Spectral Subtraction Technique. Based on the advantage of precision wavenumber measurement provided by computerized FT-IR instrumentation, the absorbance-subtraction technique has become a practical method in analysis of multicomponent mixtures [22]. It was also found in this research that difference photoacoustic spectroscopy can be used to distinguish small differences between two samples. By comparing the PAS spectra of treated and untreated materials, the common spectral features can be cancelled out. The remaining bands can be interpreted in terms of the near-surface chemical species due to the treatment.

For example, when the PAS spectrum of an untreated cotton yarn (Figure 6B) was subtracted from the spectrum of the polyurethane-sized cotton yarn (Figure 6A), most of the spectral features of the polyurethane sizing agent appeared in the difference spectrum (Figure 6C). Even though no obvious differences between these two spectra (Figures 6A and 6B) could be observed in the CH stretching region, two bands at 2940 cm^{-1} and 2872 cm^{-1} due to the polyurethane sizing agent are revealed in the difference spectrum (Figure 6C). This example demonstrates that the near-surface analysis sensitivity using FT-IR/PAS can be improved significantly by applying the spectral subtraction technique. The molecular species in the surface layer of the chemically treated cellulose textiles can be identified by this technique even though no major differences are observed between the spectra of treated and untreated samples.

Determination of the Uniformity of Chemical Additives in Cellulose. An intense peak at 1730 cm^{-1} was also observed in the infrared spectrum of a cotton yarn sized with a polyacrylate sizing agent. This peak was due to the carbonyl groups of the polyacrylate. It was also observed that the carbonyl peak intensity in the spectrum of the powder sample was lower than that in the spectrum of the yarn sample,



Figure 5. The photoacoustic infrared spectra of (A) a sized cotton yarn with the polyurethane as a sizing agent; (B) the corresponding powder from the sized yarn.



Figure 6. The photoacoustic infrared spectra of (A) the cotton yarn sized with the polyurethane; (B) an untreated cotton yarn; (C) difference spectrum, A-B; (D) the polyurethane sizing agent.

indicating a higher concentration of the polyacrylate in the surface layer of the sized yarn than in the bulk.

The intensities of the carbonyl peak (1730 cm^{-1}) of the polyurethane-sized yarn and the polyacrylate-sized yarn and the corresponding powder samples are summarized in Table II. The carbonyl peak intensity was normalized against the peak intensity at 1430 cm^{-1} . The carbonyl peak intensity ratio of the yarn sample to the corresponding powder sample is used as a semiquantitative measurement of the degree of penetration of the sizing agent, since better penetration would result in smaller differences in concentration of the sizing agent between the surface layer and the bulk so that the intensity ratio would be closer to unity. It can be seen from Table II that the polyurethane sizing agent was more concentrated in the surface layer with a greater carbonyl peak intensity ratio (1.48), while the polyacrylate sizing agent is more homogeneously distributed between the surface and the interior which resulted in a smaller carbonyl peak intensity ratio (1.14).

Table II. The Carbonyl Peak (1730 cm^{-1}) Intensities of the Sized Cotton Yarns and the Corresponding Powders

Sizing Agent Applied	Carbonyl Peak Intensity (Arbitrary Unit)		Intensity Ratio (yarn/powder)
	Yarn	Powder	
Polyurethane	0.87	0.59	1.48
Polyacrylate	1.27	1.11	1.14

The amount of sizing agents removed by desizing can also be measured semiquantitatively using FT-IR/PAS. The carbonyl peak intensities of the sized and desized yarns and the corresponding powder samples are presented in Table III. The carbonyl peak intensity ratio (desized/sized) for the polyurethane-sized yarn is 0.25. This indicates that most of the polyurethane sizing agent was removed from the yarn near-surface by desizing. More polyacrylate sizing agent remained in the yarn surface layer after desizing as demonstrated by a greater carbonyl peak intensity ratio (desized/sized) of 0.50. It could also be concluded that the desizing process removed more sizing agents from the surface layer than from the bulk, because the carbonyl peak intensity ratio (desized/sized) for the powder samples is 0.76 for both desized yarns. This indicates that most of the sizing agents still remained in the interior after the desizing process. It should be pointed out that it is reasonable to perform semiquantitative measurements of the amount of the sizing agents removed through desizing by comparing the carbonyl peak intensities of the sized and the desized yarns, because the sized and desized yarns have similar yarn diameters and surface morphologies and the possible effect on photoacoustic signal amplitude due to differences in their surface morphologies and yarn diameters is very small.

Table III. Carbonyl Peak Intensities of the Sized Cotton Yarns

Sizing Agent	Sample Type	Carbonyl Peak Intensity (Arbitrary Unit)		Intensity Ratio (desized/sized)
		Sized	Desized	
Polyurethane	yarn	0.87	0.22	0.25
Polyurethane	powder	0.59	0.45	0.76
Polyacrylate	yarn	1.27	0.64	0.50
Polyacrylate	powder	1.11	0.84	0.76

The distribution of the finishing agents applied to cotton fabrics using conventional padding and foam finishing techniques (FFT) was also investigated with FT-IR/PAS. The foam-finishing technique was developed in the 1970s for the purpose of reducing energy cost [29]. The essential feature of FFT is the use of air instead of water as the primary finish diluent [30]. With a foam system, up to 75% of the water in the finishing formulation is replaced by air, thereby eliminating 75% of the energy needed to remove the water in the final evaporation process. It was also found that wrinkle recovery of the treated cotton fabric was improved as a result of FFT [31,32].

Two types of finishing agents (Valrez 248 and Valrez ULF) were used to treat cotton fabrics with conventional padding and foam finishing techniques. An intense carbonyl peak at 1720 cm^{-1} observed in the infrared spectrum of the Valrez 248-treated cotton fabric (Figure 7B) is due to the finishing agent. This carbonyl peak intensity was used to measure the amount of finishing agents applied to the fabrics. The cotton fabrics treated with Valrez 248 using conventional padding and foam-finishing techniques and the corresponding powder samples were examined by FT-IR/PAS (Figures 8 and 9). It can be seen that the carbonyl peak intensity was reduced more dramatically upon grinding the conventionally finished cotton fabric than the foam-finished fabric. This indicates that the finishing agent (Valrez 248) was more uniformly distributed in the foam-finished cotton fabric than in the conventionally finished fabric. The carbonyl peak (1720 cm^{-1}) intensity of various finished cotton fabrics and the corresponding powder samples are summarized in Table IV. The carbonyl peak intensity was normalized against the peak intensity at 1430 cm^{-1} , which represents the CH_2 bending in cellulose molecules. The carbonyl peak intensity ratio (powder/fabric) is used as a semiquantitative measurement of the uniformity of the finishing agents in the fabrics, because better uniformity of a finishing agent would result in a carbonyl peak intensity ratio closer to unity. It can be observed from the data presented in Table IV that the FFT treatment of cotton fabrics with both Valrez 248 and Valrez ULF gave better uniformity of the finishing agent with the carbonyl peak intensity ratios of 0.92 and 0.91 respectively. The cotton fabrics treated with a conventional padding technique show poor uniformity for both finish agents with the carbonyl peak intensity ratios of 0.57 and 0.58 respectively. This FT-IR/PAS examination explains the observation that wrinkle recovery angle was generally higher for the foam-finished cotton

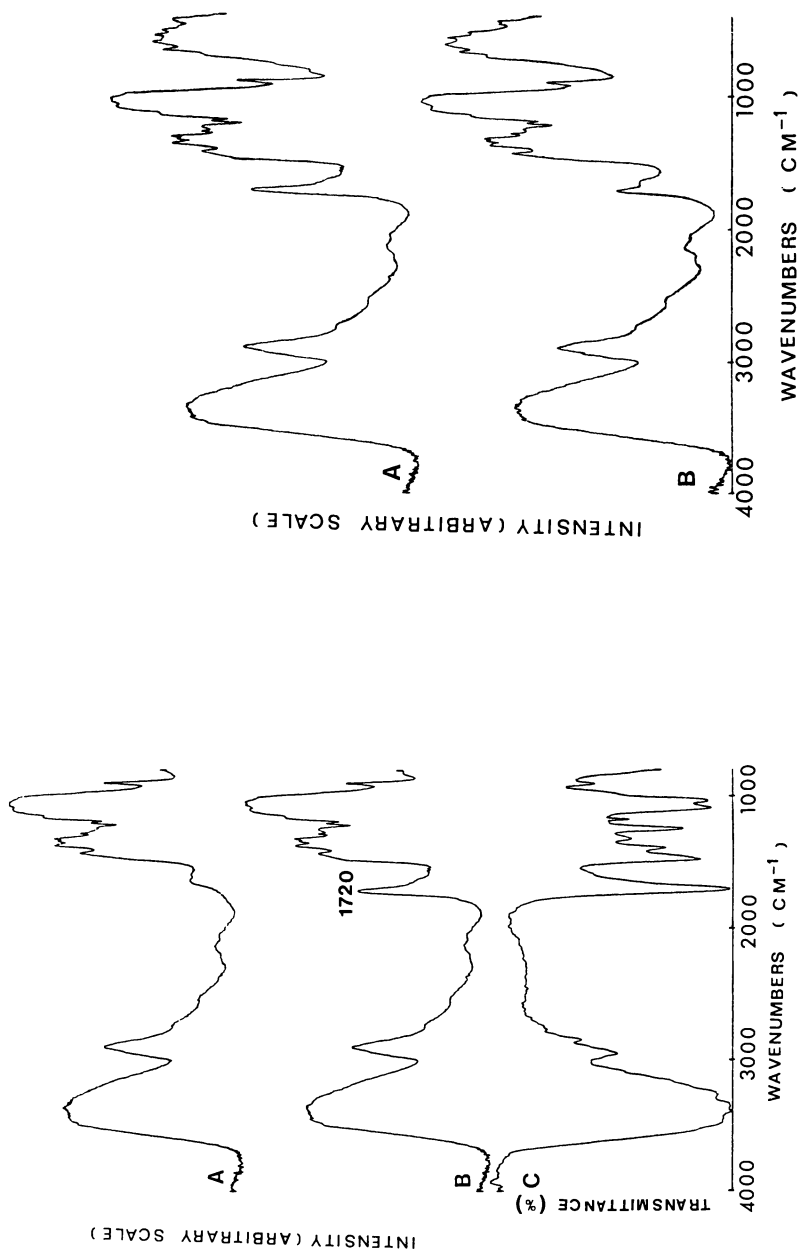


Figure 7. The photoacoustic infrared spectra of (A) a cotton fabric and (B) a Velrez 248-treated cotton fabric by conventional padding; (C) Infrared absorption spectrum of the finish (Velrez 248).

Figure 8. The photoacoustic infrared spectra of (A) the cotton fabric treated by a conventional padding technique; (B) the corresponding powder sample.

fabrics than for the conventional finished fabrics [29,32,33], because a better uniformity of the finishing agents throughout the cotton fabrics would allow more fibers to be crosslinked, thereby improving the wrinkle recovery properties.

Table IV. Carbonyl Peak Intensities of the Treated Cotton Fabrics

Finishing Agent	Finishing Technique	Carbonyl Peak Intensity (Arbitrary Unit)		Carbonyl Peak Intensity Ratio (Powder/Fabric)
		Fabric	Powder	
Valrez 248	conventional padding	1.14	0.65	0.57
Valrez 248	foam finishing	1.06	0.98	0.92
Valrez ULF	conventional padding	1.11	0.64	0.58
Valrez ULF	foam finishing	0.80	0.88	0.91

With the extensive use of chemical additives on textile materials, the identification and characterization of chemical additives such as sizing agents and finishing agents are of great importance in determining the properties of textile materials. Various analytical techniques such as solvent extraction of the finishing agent from textile materials followed by a ATR infrared spectroscopy measurement [33], and infrared transmission measurement using ground material pressed in a KBr pellet [34] have been developed to identify the chemical additives in textile materials. These techniques are bulk-analysis methods and cannot be used to examine the distribution of chemical additives in textiles. However, the results of our study show that FT-IR photoacoustic spectroscopy provides a convenient technique to determine the penetration and uniformity of sizing agents and finishing agents in textile materials. This has been accomplished by measuring the PAS spectra of the textile materials and the corresponding powder samples.

FT-IR/PAS Depth Profiling. The penetration of chemical additives in cellulose textile materials can also be investigated using a FT-IR/PAS depth profiling technique by applying different optical velocities. As discussed above, thermal diffusion length is inversely proportional to the square root of the product of optical velocity and wavenumber of IR radiation, so PAS sampling depth varies as interferometer scan velocity changes. Since most cellulose textile materials are optically opaque and thermally thick, and in most cases the optical penetration length is greater than the thermal diffusion length, the PAS sampling depth can be varied by changing

the interferometer mirror velocity. Therefore, sample surface layers with different thicknesses can be examined.

The polyurethane-sized cotton yarns discussed above were examined with FT-IR/PAS using different mirror velocities. The ratio of the peak intensity at 1730 cm^{-1} to the peak intensity at 1430 cm^{-1} , $(I_{1730\text{ cm}^{-1}})/(I_{1430\text{ cm}^{-1}})$, is plotted against optical velocity (Figure 10). The peak at 1430 cm^{-1} is regarded as a reference peak since it represents the C-H bending of the cellulose in cotton yarn. The peak intensity ratio, $(I_{1730\text{ cm}^{-1}})/(I_{1430\text{ cm}^{-1}})$, is considered to be a semi-quantitative measurement of the amount of polyurethane sizing agent compared to the amount of cellulose within the PAS sampling depth. It can be observed from Figure 10 that the intensity ratio, $(I_{1730\text{ cm}^{-1}})/(I_{1430\text{ cm}^{-1}})$, increases as the optical velocity is increased. The thermal diffusion length of cotton at 1730 cm^{-1} for the optical velocities applied is presented in Table V. It shows that when the optical velocity is increased from $0.235\text{ cm}\cdot\text{s}^{-1}$ to $1.119\text{ cm}\cdot\text{s}^{-1}$, the thermal diffusion length is decreased from $6.1\text{ }\mu\text{m}$ to $2.8\text{ }\mu\text{m}$. An increase in the peak intensity ratio $(I_{1730\text{ cm}^{-1}})/(I_{1430\text{ cm}^{-1}})$ in Figure 10 demonstrates that more concentrated polyurethane sizing agent was detected in a thinner surface layer.

Table V. Thermal Diffusion Length of Cotton at 1730 cm^{-1}

Velocity	Optical Velocity ($\text{cm}\cdot\text{s}^{-1}$)	Thermal Diffusion Length (μm)
0	0.235	6.1
3	0.396	4.7
6	0.665	3.6
9	1.119	2.8

It can be seen from the spectrum of the polyurethane sizing agent (Figure 6D) that the peak at 1246 cm^{-1} is the second most intense peak in the spectra. By comparing of the spectra of the sized yarn (Figure 6A) and the pure cotton yarn (Figure 6B), one observes that a weak peak at 1246 cm^{-1} in the spectrum of the sized yarn (Figure 6A) is due to the polyurethane sizing agent. The infrared spectra of the polyurethane-sized cotton yarn collected at velocities 0, 3, 6 and 9 are shown in Figure 11. The peak at 1246 cm^{-1} is almost invisible in the spectrum collected at velocity 0 (Figure 11A); however, its intensity increases as the optical velocity is increased from velocity 0 to velocity 9 (Figures 11A-11D). This result is consistent with the observation that the peak intensity ratio, $(I_{1730\text{ cm}^{-1}})/(I_{1430\text{ cm}^{-1}})$, was increased by increasing the optical velocity. Both observations indicate a higher concentration of the polyurethane sizing agent on the near-surface of the yarn than in its interior.

The polyacrylate-sized cotton yarn was also examined using different optical velocities, and the peak intensity ratio, $(I_{1730\text{ cm}^{-1}})/(I_{1430\text{ cm}^{-1}})$, is plotted against optical velocity

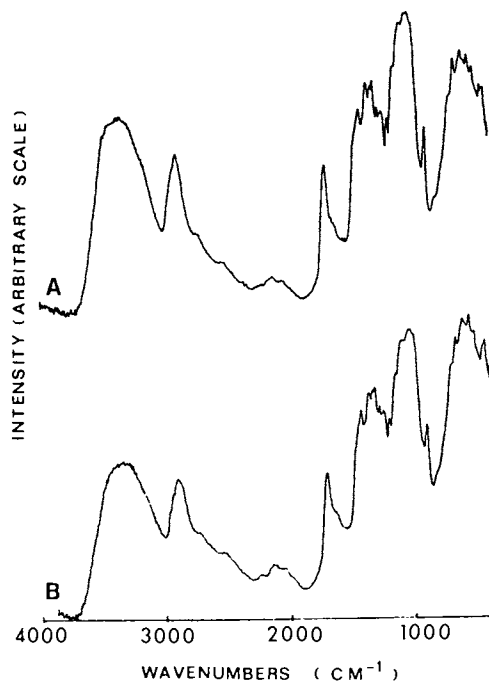


Figure 9. The photoacoustic infrared spectra of (A) the cotton fabrics treated by FFT; (B) the corresponding powder sample.

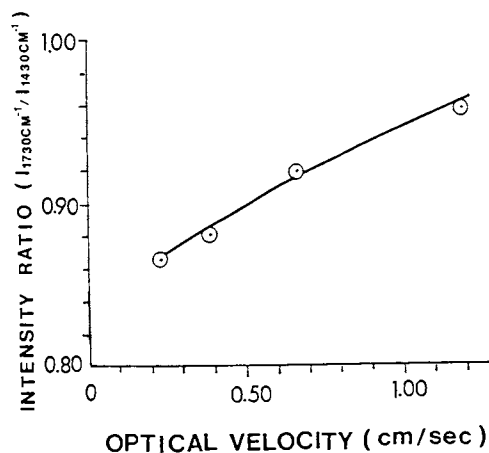


Figure 10. The photoacoustic infrared peak intensity ratio, $(I_{1730\text{ cm}^{-1}})/(I_{1430\text{ cm}^{-1}})$, of the polyurethane-sized cotton yarn vs. optical velocity of the interferometer.

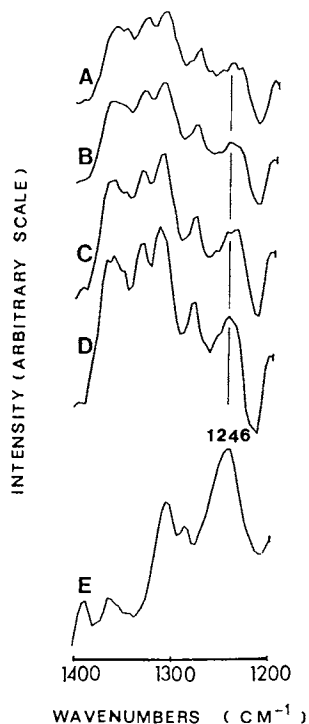


Figure 11. The photoacoustic infrared spectra of the polyurethane-sized cotton yarn collected at (A) velocity 0; (B) velocity 3; (C) velocity 6; (D) velocity 9; (E) FT-IR/PAS spectrum of the polyurethane sizing agent.

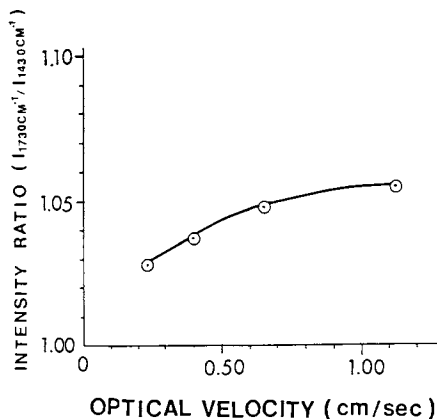


Figure 12. The photoacoustic infrared peak intensity ratio, $(I_{1730\text{ cm}^{-1}})/(I_{1430\text{ cm}^{-1}})$, of the polyacrylate-sized cotton yarn vs. optical velocity of the interferometer.

(Figure 12). It is also found that the peak intensity ratio increases when optical velocity is increased. However, the slope of the curve in Figure 12 is much smaller than that for the polyurathane-sized yarn (Figure 10), indicating that the difference in concentration of the polyacrylate sizing agent between the near-surface and the interior is smaller than that of the polyurethane-sized yarn. This observation is consistent with the observation that the polyacrylate sizing agent had better penetration than the polyurethane sizing agent.

The above examples demonstrate that FT-IR/PAS depth profiling provides a non-destructive and convenient method to investigate differences in concentration of chemical additives between the near-surface and the interior of cellulose textile materials so that the penetration and uniformity of these chemical additives can be elucidated. This is considered to be another advantage of FT-IR/PAS over conventional infrared sampling techniques. Even though variable angle ATR was successfully used to depth profile deformable samples [35], FT-IR/PAS detects a thicker surface layer than ATR [36] and also eliminates problems caused by the poor contact between samples and reflection crystals, which is common in ATR experiments.

In summary, the applications of FT-IR/PAS to studies of cellulose textile materials discussed above demonstrate that FT-IR/PAS has various advantages over the conventional transmission techniques. Some disadvantages of FT-IR/PAS should also be mentioned, however. Due to the high noise level in PAS experiments, a slow scan velocity and a large number of scans usually are necessary to obtain desirable S/N ratio. Consequently, a PAS experiment is more time-consuming than conventional transmission techniques. Water vapor in the PAS cell gives intense water bands which might seriously interfere with spectral observation. Therefore, samples must be kept dry and the helium used as a carrier should be pre-dried. Since sample morphology and possibly fiber diameter may affect photoacoustic signal amplitude, quantitative analysis using FT-IR is still difficult when dealing with samples with different surface morphology or diameter. In spite of these difficulties, however, FT-IR photoacoustic spectroscopy appears to have great potential to become an important instrumental technique for examining textile materials.

Acknowledgments

This paper was prepared with the support of U.S. Department of Energy, Grant No. DE-FG03-85ER13347. Special thanks are extended to Jerry Moreau of the U.S.D.A. Southern Regional Research Center for providing numerous samples.

References

1. Rowen, J.W.; Hunt, C.M.; Plyler, E.K. J. Res. Nat. Bur. Std. 1947, 39, 133.
2. Forziati, F.H.; Stone, W.K.; Rowen, J.W.; Appel, W.D. J. Res. Nat. Bur. Std. 1950, 45, 109.
3. Higgins, H.G. Australian J. Chem. 1957, 10, 496.
4. Hurtubise, F. Can. Textile J. 1959, 76, 53.

5. O'Conner, R.T.; Dupre, E.F.; Mitcham, D. Textile Res. J. 1958, 28, 382.
6. Marrinan, H.J.; Mann, J. J. Appl. Chem. (London) 1954, 4, 204.
7. Brown, L.; Holliday, P.; Trotter, I.F. J. Chem. Soc. 1951, 1532.
8. Liang, C. Y. in "Instrumental Analysis of Cotton Cellulose and Modified Cotton Cellulose"; O'Connor, R.T., Ed.; Marcell Dekker: New York, 1972; p 59-82.
9. Chatterjee, P. K.; Schwenker, R. J., Jr. *ibid*; p. 223-325.
10. O'Connor, R. T. *ibid*; p. 402-446.
11. O'Connor, R.T.; DuPre, E.F.; McCall, E.R. Anal. Chem. 1957, 29, 998-1005.
12. McCall, E.R.; Miles, S.H.; O'Connor, R.T. Am. Dyestuff Rep. 1967, 56, 13.
13. Berni, R.J.; Morris, N.M. in "Analytical Methods for a Textile Laboratory" 3rd; Weaver, J.W. Ed.; American Association of Textile Chemist and Colorists: Research Triangle Park, N.C., 1985; p. 267-269.
14. McCall, E.R.; Miles, S.H.; O'Connor, R.T. Am. Dyestuff Rep. 1966, 55, 400.
15. Krentz, V. Melliland Textilberichte 1969, 50, 557.
16. Zhbakov, R.G.; "Infrared Spectra of Cellulose and its Derivatives", Consultants Bureau: New York, 1966; Chap. 1.
17. Roussell, M.A.; Nelson, M.L. Textile Res. J. 1971, 41, 599.
18. Knight, J.A.; Smoak, M.P.; Porter, R.A.; Kirkland, W.E. Textile Res. J. 1967, 37, 924.
19. Knight, J.A.; Hicks, H.L.; Stephens, K.W. Textile Res. J. 1969, 39, 324.
20. Berni, R.T.; Morris, N.M. in "Analytical Methods for a Textile Laboratory", 3rd Ed.; Weaver, J.W. Ed; American Association of Textile Chemists and Colorists: Research Triangle Park, N.C., 1985; p. 287.
21. Morris, N.M.; Berni, R.J. in "Polymers for Fiber and Fabrics;" Arthur, J. C., Ed.; ACS Symposium Series No. 260; American Chemical Society: Washington, D.C., 1983; p. 61-74.
22. Krishnan, K.; Ferraro, J.R. in "Fourier Transform Infrared Spectroscopy"; Ferraro, J. R.; Basile, L. J., Eds.; Academic Press: New York, 1982; Volume II, p. 187-207.
23. Graham, J.A.; Grimm III, W.M.; Fateley, W.G. in "Fourier Transform Infrared Spectroscopy"; Ferraro, J. R.; Basile, L. J., Eds.; Academic Press: New York, 1985; Volume IV, p. 345.
24. Griffiths, P.R.; Fuller, M.P. in "Advances in Infrared and Raman Spectroscopy"; Clark, R.J.H.; Hester, R.E. Ed.; John Wiley and Sons: Chichester, 1982; Vol. IX, p. 346-392.
25. Gerson, R.J.; Wong, J.S.; Casper, T.M. Am. Lab. 1984, 69.
26. Rosenswaig, A. "Photoacoustic and Photoacoustic Spectroscopy" John Wiley and Sons: New York, 1980; p. 94-98.
27. Yang, C.Q.; Bresee, R.R.; Fateley, W.G. "Near Surface Analysis and Depth Profiling with FT-IR Photoacoustic Spectroscopy"; Appl. Spectrosc., in press.
28. Moncrieff, R.W. Man-Made Fibers, 6th ed.; Wenner-Butterworths: London, 1975; p. 259.
29. Perenich, T.A., Textile Chemist & Colorist 1984, 16, 241.
30. Nambodri, C.G.; Duke, M.W. Textile Research Journal 1979, 49, 156-162.

31. Gregorian, R.S.; Namboodri, C.G. Textile Chemist & Colorist 1981, 13, 28-31.
32. Goldstein, H.B.; Smith, H.W. Textile Chemist & Colorist 1980, 12, 27-32.
33. AATCC, Rhode Island Section, Textile Chemist & Colorist, 1973, 5, 279.
34. McCall, E.R.; Miles, S.H.; O'Connor, R.T. American Dyestuff Rep., 1967, 56, 13.
35. Willis, H.A.; Zichy, V.J.I. in "Polymer Surfaces"; Clark, D.T.; Feast, W.J. Ed.; John Wiley & Sons: Chichester, 1978, p 289-307.
36. Saucy, D.A.; Simko, S.J.; Linton, R.W. Anal. Chem. 1985, 57, 871.

RECEIVED March 5, 1987

Chapter 14

Fractal Analysis of Cotton Cellulose as Characterized by Small-Angle X-ray Scattering

J. S. Lin¹, Ming-Ya Tang², and John F. Fellers²

¹National Center for Small Angle Scattering Research, Oak Ridge National Laboratory, Oak Ridge, TN 37830

²Materials Science & Engineering, University of Tennessee, Knoxville, TN 37996-2200

Complete small-angle x-ray scattering (SAXS) curves are reported and analyzed by conventional and fractal theories in this study of Valonia and eleven cotton cellulose samples. The scattering source is identified as voids in a solid matrix. The void volume fraction ranges from 0.7% to 3.4% in the various cotton samples and is 17% in Valonia. Modifications such as dewaxing, scouring, and bleaching improve the packing efficiency within aggregates, and additionally increase the void fraction. NaOH mercerization and NH₃ treatment destroy the packing efficiency slightly and decrease the void fraction. Two types of power-law decay were observed for the SAXS intensity $I(s)$. Hydrocellulose II and Valonia follow Porod's inverse fourth power law. Conventional SAXS analysis then determines the average pore sizes to be 8.5 nm and 12.5 nm, and specific inner surfaces of 15.3 and 45.2 m²/cm³, respectively. The other ten cotton samples follow a power law decay with the exponent ranging from -2.7 to -2.1. The non-integer exponent is referred to as the Hausdorff dimension and suggests a fractal structure for the microcrystallites constituting the cellulose. The compliance of Hydrocellulose II and Valonia to Porod's law carries with it a model structure of a three dimensional void bounded by a smooth two dimensional surface. The other samples that have their fractal or Hausdorff dimension less than the Euclidian dimension implies there is a unit of measure small enough to sense discontinuities of the structure. The Hausdorff dimensions measured here suggest that native cellulose is a cluster aggregate of microcrystallites modified by

0097-6156/87/0340-0233\$06.25/0
© 1987 American Chemical Society

subsequent rearrangement. Such speculations may stimulate some new insight to the growth mechanism of cotton.

Structure

In the last sixty years, the morphology of cellulose has received much attention but has remaining unresolved features. Cellulose is a linear polymer composed of anhydroglucose units joined by 1-4 β -Glycosidic bonds. It forms the principal constituent of plant cell walls where it occurs as thin threads of indefinite length called microfibrils. In width, microfibrils vary from 7 to 30 nm, depending upon the source of the cellulose (1). It is generally agreed that cotton cellulose is arranged in thin fibrils forming the rather irregular outer or primary cell wall, and the highly ordered inner or secondary wall of the hollow tubular structure of the cotton fiber (2).

The existence of an ordered structure in cellulose is shown conclusively by wide-angle x-ray diffraction (WAXD) and electron diffraction studies (3). The diffraction patterns exhibit reasonably well-defined reflections for which unit cells have been defined. There are four basic recognized crystalline modifications, namely, cellulose I, II, III and IV. By the WAXD method as proposed by Hermans (4,5) it has been found that native celluloses of different biological origin vary in crystallinity over wide limits, from 40% in bacterial cellulose to 60% in cotton cellulose and 70% in Valonia cellulose.

The fine structure of cellulose is generally interpreted in terms of a two-phase crystalline-amorphous model (6). According to this concept cellulose microfibrils are regarded as assemblies of crystalline and amorphous regions. However, in contrast to most synthetic semicrystalline polymers, native or regenerated cellulose fibers do not show a meridional small-angle x-ray or neutron reflection (7-27), although in some special cases a very weak long spacing reflection could be detected for regenerated cellulose (12,13,24,27). This observation is explained by the assumption (13,25) that the difference of electron density between the "amorphous" and "crystalline" regions is too weak to give rise to a discrete small-angle reflection, but the distinction in chain order is real in the sense that it is the basis for selectivity with respect to chemical degradation.

Meanwhile the diffuse small-angle x-ray scattering of cotton has been interpreted as either due to microfibrils having negligible interparticular interference (7-10, 22,25,26) or due to a "dilute" system of microvoids or pores in a dense system (12, 14-19). The first view is apparently supported by the observation of Haase et al. (21,22) and Heyn (7-10, 26) that the smallest dimension revealed from the diffuse scattering agrees with the results of the line width analysis of WAXD and that of electron microscopy studies. However this analysis is dependent on the range of scattering angles (2θ), i.e. a different s ($s = 4\pi \sin\theta/\lambda$, λ = wavelength) range will lead to a different value of fibril diameters. The second view is supported by Statton

(12,18,19), Hermans et al. (14-16), and Kratky and Sekora (17) who found that the mass density can be satisfactorily correlated with the scattering invariant measurement. Here again the determination of void size is dependent on the range of scattering angles. Thus one has to extend the range of scattering angles as far as possible. This controversy can be partially overcome by applying the technique called contrast variation (28). Contrast variation can be obtained by changing the electron density of one of the phases since SAXS intensity is proportional to the square of the difference between the mean scattering density (number of electrons per unit volume) of each phase in the scattering system.

Implications of Structure from the Growth Process

Considering the cotton growth process may help dispel ambiguity about the structure of cotton. The growth of cotton can be considered as a deposition or aggregation of cellulose subunits. Many objects grow by random addition of subunits to form large clusters, including soot and smoke (29), droplet nucleation and growth (30), and colloids. The resultant structures are characterized by their tenuous, chainlike structure. However, only recently has it been realized that there is a geometric feature which characterizes many objects generated by irreversible growth: they seem to be scale-invariant fractals. The subject of fractals is treated in considerable detail in the literature (31,32). Fractal objects are characterized by the scale dependence of their total mass when a characteristic length scale is used to examine the fractal. That is

$$[\text{Mass}]_{\text{Total}} \sim (\text{Length})^D, \quad (1)$$

where D , the fractal or Hausdorff dimension is less than d , the Euclidian dimension of space, and is usually non-integral. Also the point to point density correlation function $c(x)$ within a fractal material has a power-law behavior:

$$c(x) = \langle \rho_m(r) \cdot r \rho_m(r+x) \rangle \sim 1/r^{d-D} \quad (2)$$

Thus, changing all length scales multiplies $c(x)$ by a constant; this means (33) the object "looks" the same on any length scale.

The idea that disorderly growth can lead to scale invariance was first pointed out by Witten and Sander (33) who were attempting to explain earlier observations of Forrest and Witten (34) of smoke aggregates. Computer simulations (33, 35-38) have also suggested that the resultant structures exhibit scale invariance and can be described as fractals. Two general classes of irreversible aggregation have emerged from the simulations. The first of these classes involves cluster formation by the successive addition of single randomly walking (diffusion) particles onto a seed particle representing a nucleation center at a fixed point (33,35) (diffusion-limited aggregation, DLA) and the resultant structure has $D \approx 1.7$ ($d = 2$) and 2.5 ($d = 3$).

Certain real systems seem to be described by DLA, notably electrodeposition on a sharp point (39) and dielectric breakdown (33,40). The second class involves cluster formation by the homogeneous aggregation of a collection of two clusters of comparable size (37,38) (cluster-cluster aggregation, CA) and the resultant aggregate has a more open structure and lower fractal dimension, $D \approx 1.4$ ($d = 2$) and 1.8 ($d = 3$). Real smoke (34) and colloids (41) seem to have $D = 1.8$; this is a satisfying verification of the model. A process that has not, however, been included in the simulations is rearrangement within the clusters. This would lead to denser structures with higher Hausdorff dimensions (42).

More recently, scattering techniques (SAXS, Small Angle Neutron Scattering (SANS) and light scattering) were employed to characterize the fractal structure of aggregates of silica particles (42-44) and gold colloids (45). They reported a power law decay of the scattering intensity $I(s)$ over some range of scattering vector, s :

$$I(s) \sim s^{-D}. \quad (3)$$

Schaefer et al. (42, 43) reported that the fractal dimension of silica aggregates is 2.12 ± 0.05 , independent of the stage of aggregation except at the early phase of growth. Sinha et al. (44) reported that the fractal dimension of resuspended Cab-o-sil aggregates was 2.52 ± 0.05 for samples pressed into different densities ranging from 0.05 gm/cm^3 to 0.2 gm/cm^3 . Weitz and Huang (45) reported a fractal dimension of 1.75 for aqueous gold colloids. Thus the application of fractal concepts involving aggregation growth processes may provide some new insight into cotton structure.

In the present paper we extend the range of scattering angles as far as five degrees and combine SAXS measurement with wide-angle x-ray diffraction measurements. We report what we believe to be the first complete SAXS curves for cotton and Valonia cellulose. We also demonstrate how the fractal concept can be applied to explain the microcrystallite structure in cellulose.

Materials

Eleven cotton celluloses and one of Valonia were studied. Among the twelve samples, the first nine cotton samples are in a randomly oriented fibril state (cotton sliver), EHC I and Hydrocellulose II are powders, and Valonia is in membrane pieces. They are listed and described below.

Cotton Cellulose. Three classes of cotton cellulose were studied. They are

Greige Cotton Series:	Greige Cotton
	Dewaxed Greige Cotton
	Scoured Greige Cotton
	Scoured and Bleached Greige Cotton

- Absorbent Cotton Series:** Absorbent Cotton
NaOH Mercerized Absorbent Cotton
NH₃ Treated Absorbent Cotton, NH₃
removed at room temperature
NH₃ Treated Absorbent Cotton, NH₃
removed at 95°C
NH₃ Treated Absorbent Cotton,
sample immediately immersed in
H₂O after NH₃ treatment
- Hydrolyzed Cotton Series:** EHC I, cotton cellulose
Hydrolyzed in HCl until the
optimal crystallinity was
obtained
Hydrocellulose II, cotton treated
with NaOH for mercerization and
then hydrolyzed with HCl to
provide a highly crystalline
cellulose II powder

Valonia Ventricosa Cellulose. This is a unicellular alga, the vesicles of which may reach a volume as large as 30 cc. *Valonia ventricosa* was gathered off the eastern coast of Florida. Before use it was stored in ice-cold, original sea water for 11 months, after which it was cleaned and scoured in boiling 2% NaOH with 0.5% Prechem 70 under Argon for 1 hour. It was kept refrigerated in water, with a small amount of chloroform added to prevent growth of bacteria. It was air-dried at 100°C for 3 hours.

SAXS Sample Preparation

The samples were vacuum dried at room temperature for 12 hours before SAXS measurement. Iodine embedded cotton was prepared according to the iodine sorption test procedure proposed by Nelson et al. (46). Soaking with glycerine was carried out at room temperature for 24 hours.

Small-Angle X-Ray Scattering

Small-angle x-ray scattering experiments were performed on the 10 meter SAXS facility at the National Center for Small Angle Scattering Research at the Oak Ridge National Laboratory (47). This instrument consists of a rotating anode x-ray source, pinhole collimation, a two dimensional position-sensitive proportional counter (48), and a mini-computer system for data acquisition and analysis. The system was constructed in such a way that a change in the angular range can be achieved by lengthening or shortening the aluminum beam path between the sample chamber and the detector. Three sample to detector distances, namely 5 meters (long geometry, $2\theta = 1$ to 20 mrad), 2 meters (short geometry, $2\theta = 3$ to 45 mrad) and 1 meter (ultra short geometry, $2\theta = 5$ to 90 mrad) were used and it was found the combination of 5 meter and 1 meter beam paths was sufficient to obtain the complete SAXS intensity distribution curve. All

measurements were carried out at room temperature under vacuum ($< 15 \mu\text{m Hg}$). $\text{CuK}\alpha$ radiation ($\lambda = 0.54 \text{ nm}$) was used.

The raw scattering data were first corrected for instrumental background and dark current counts and then corrected for non-uniform detector efficiency at each detector channel element. Then the sensitivity corrected data were plotted as a two-dimensional contour plot with contour levels increasing by a factor of 2 from the outermost one. Lupolen 23/7 was used as a calibration standard to determine the absolute SAXS intensity (49,50).

Wide-Angle X-Ray Diffraction

Wide-angle x-ray diffraction (WAXD) measurements were performed with a Rigaku x-ray diffractometer in the transmission mode. $\text{CuK}\alpha$ radiation was obtained by using a Ni-filter and detected by a scintillation counter and a pulse height discriminator. For the scan over $2\theta = 5^\circ$ to 13° , the background of the empty beam was subtracted from the measured intensity.

Results

SAXS from Cotton Samples

The two-dimensional iso-intensity contour plots of the native Greige cotton, Hydrocellulose II and Valonia ventricosa are shown in Figures 1,2 and 3 respectively. The spherically symmetrical patterns are the result of randomly oriented fibrils or powder samples. By converting the radially averaged intensity values into absolute units (namely, electron units, eu/nm^3), the intensity (I) data obtained from different sample to detector distances L can be superimposed, as shown in Figure 4 for native Greige cotton. Figure 5 plots the $\log I$ versus $\log s$ for native Greige cotton, Hydrocellulose II, and Valonia and Figure 6 is a Guinier plot (51) of the three samples. The scattering intensity curves of all of the cotton samples and EHC I are qualitatively similar to that of Greige cotton.

SAXS from Glycerine Soaked and Iodine Embedded Samples

The electron density contrast in cotton was varied by two ways: decreasing it by filling the pores and voids with glycerine and increasing it by putting iodine into the solid phase. The resulting two-dimensional iso-intensity contour plots are shown in Figure 7. The $\log I$ versus $\log s$ plots for glycerine soaked, scoured, and bleached Greige cotton and for iodine embedded cotton are shown in Figures 8 and 9, respectively.

WAXD from Cotton Samples

The scattering intensity curves in the 2θ range of 5° to 13° for some of the cotton samples are shown in Figure 10. The order of the curves in Figure 10 does not correspond to the order of the

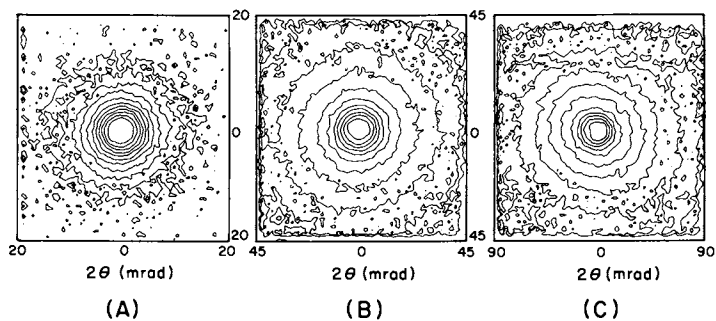


Figure 1. Two dimensional isointensity contour plots of Greige cotton.

- | | |
|-----|---|
| (A) | $L = 5 \text{ m}, P_0 = 1.8 \times 10^6 \text{ cps};$ |
| (B) | $L = 2 \text{ m}, P_0 = 2.5 \times 10^6 \text{ cps};$ |
| (C) | $L = 1 \text{ m}, P_0 = 2.5 \times 10^6 \text{ cps}.$ |

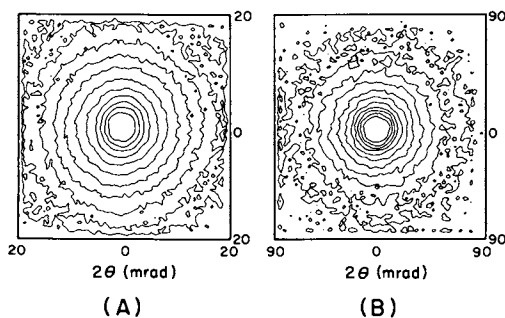


Figure 2. Two dimensional isointensity contour plots of Hydrocellulose II powder.

- | | |
|-----|---|
| (A) | $L = 5 \text{ m}, P_0 = 1.8 \times 10^6 \text{ cps};$ |
| (B) | $L = 1 \text{ m}, P_0 = 2.5 \times 10^6 \text{ cps}.$ |

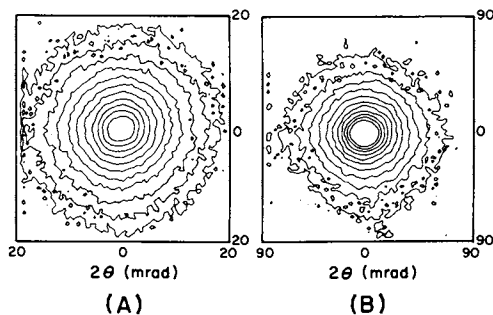


Figure 3. Two dimensional isointensity contour plots of Valonia.
 (A) $L = 5 \text{ m}$, $P_0 = 1.8 \times 10^6 \text{ cps}$;
 (B) $L = 1 \text{ m}$, $P_0 = 2.5 \times 10^6 \text{ cps}$.

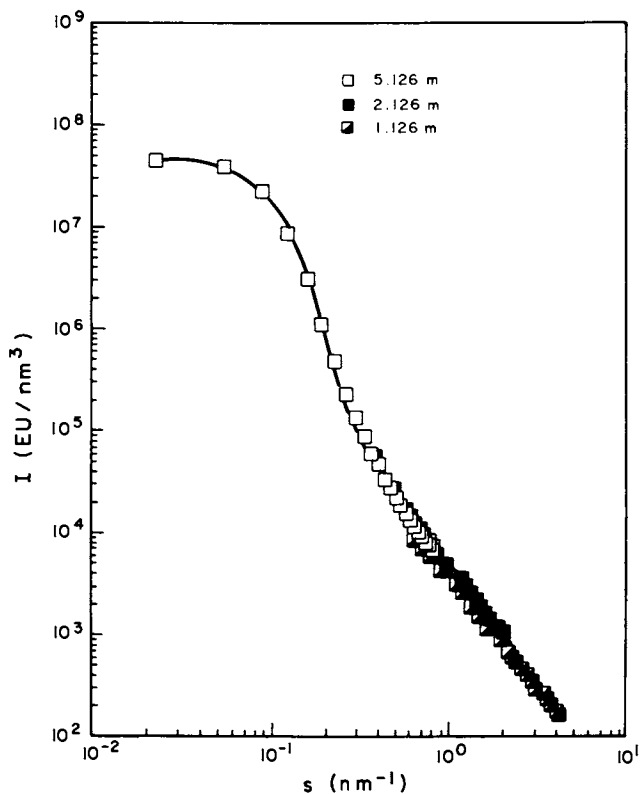


Figure 4. Superposition of scattering intensity data of native Greige cotton obtained at different sample to detector distances.

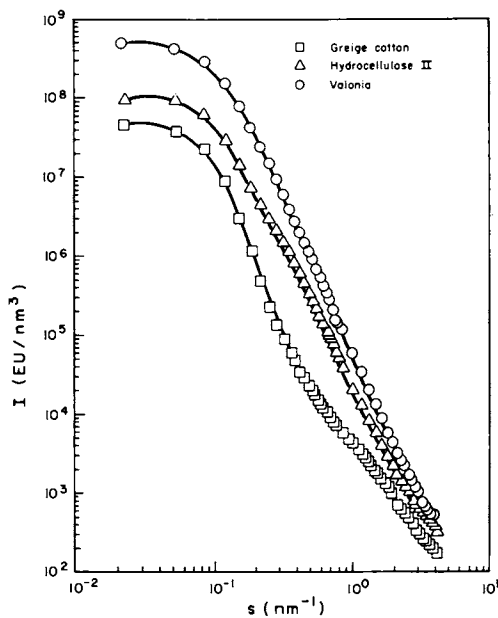


Figure 5. Log I (s) versus log s plots for native Greige cotton, Hydrocellulose II, and Valonia.

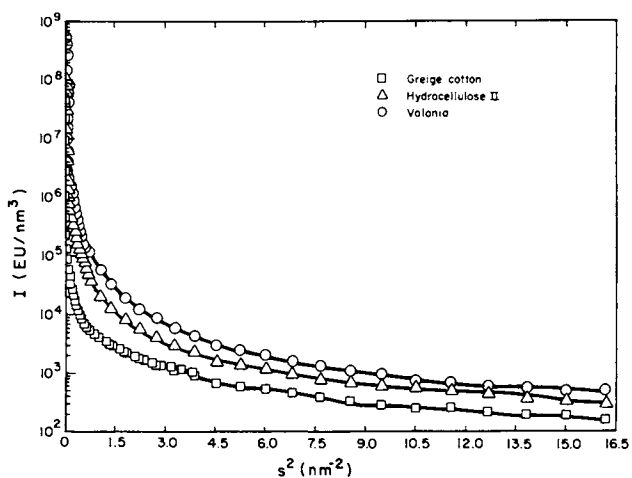


Figure 6. Guinier plots for native Greige cotton, Hydrocellulose II, and Valonia.

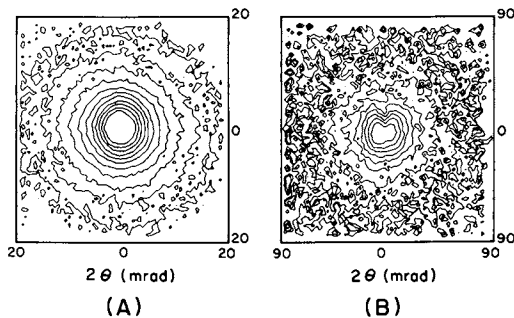


Figure 7. Two dimensional isointensity contour plots of (A) iodine embedded cotton (NH_3 treated absorbent cotton with NH_3 removal at 95°C), and (B) glycerine soaked, scoured and bleached Gerige cotton.

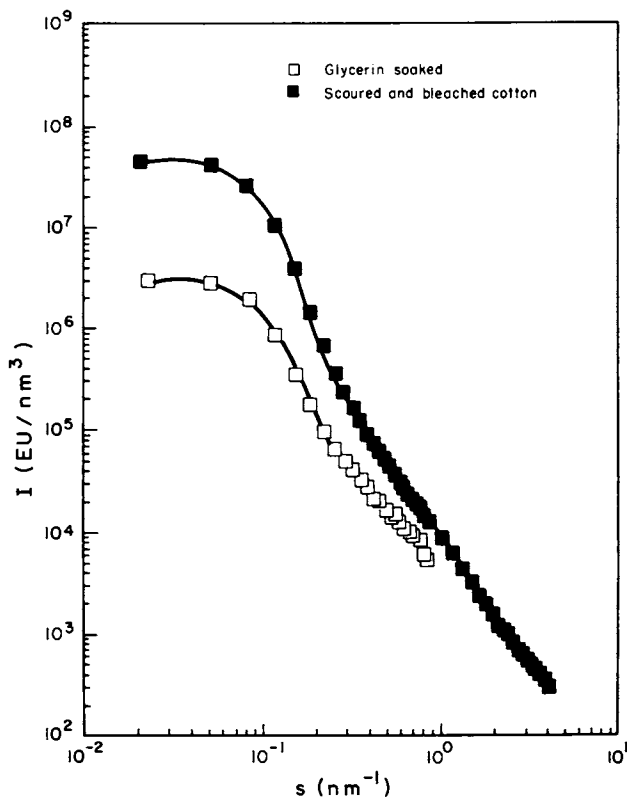


Figure 8. Comparison of the scattering intensity of original and glycerine soaked, scoured and bleached Greige cotton.

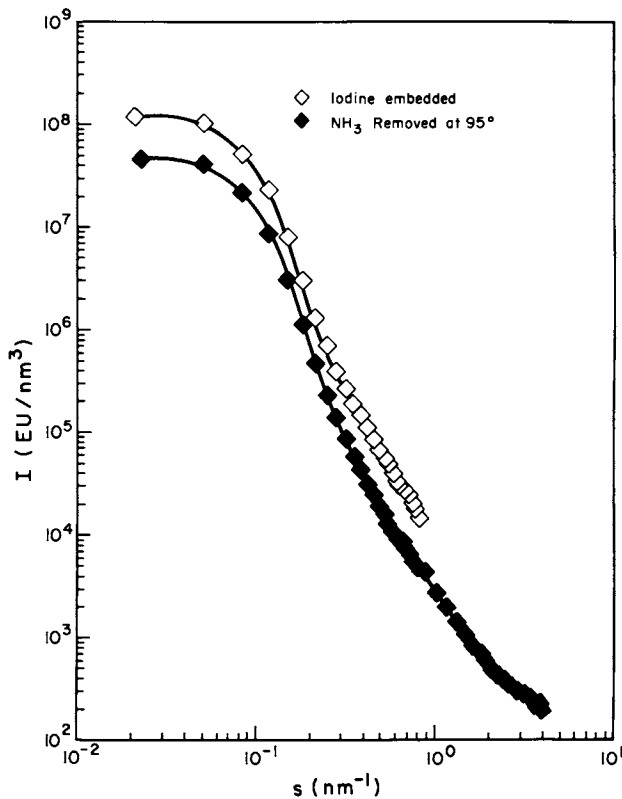


Figure 9. Comparison of the scattering intensity of original and iodine embedded cotton (NH₃ treated absorbent cotton with NH₃ removal at 95°C)

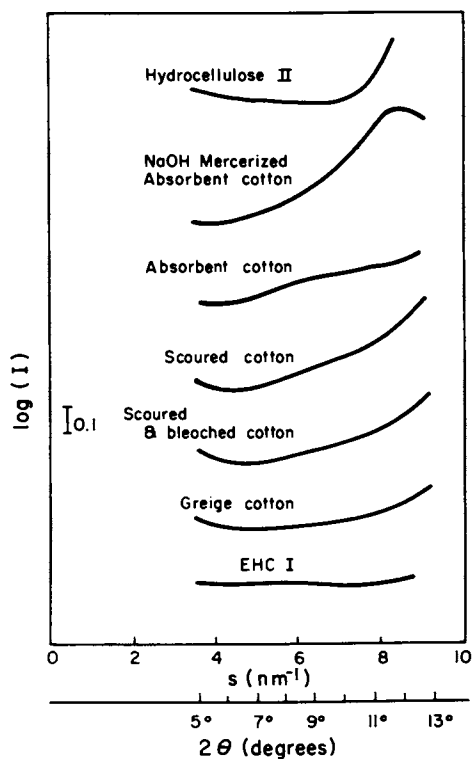


Figure 10. WAXD data of cotton samples in the 2θ range of 5° to 13° .

magnitude of the real scattering intensity. ECH I and Hydrocellulose II are put on this plot as the two extremes for comparing the effect of cellulose crystalline forms on the shape of the intensity curves.

Discussion

Scattering Source

The question of whether SAXS arises from the microfibrillar structure (7-10,22,25-26) of cotton or from microvoids (12,14-19) dispersed through the cotton is approached here by the use of scattering contrast experiments. Wadsworth and Cuculo (52) indicated that iodine penetrates both the amorphous and crystalline regions of cellulose. By comparing the scattering intensity of cotton and iodine embedded cotton (see Figure 9), it is clear that the scattering is caused by the contrast between the solid phase in cotton and the voids. While the entire curve of the former shifts up at a constant ratio on the log I versus log s plot, the slight discrepancy at the tail part may be due to the swelling of the cellulose caused by iodine sorption (53).

The scattering behavior of glycerine soaked cotton is relatively more difficult to explain. By theoretical calculation, if the glycerine fills the voids completely then the intensity should drop to 1/14.5 of that of the unfilled cotton. However, this is true only for the first two data points. Three reasons are proposed for this observation: (i) only big pores, whose sizes exceed the lower resolution limit of the SAXS instrument, are filled with glycerine; (ii) some pores may be isolated and therefore are not accessible to glycerine; (iii) glycerine acts as a swelling agent to cellulose and causes a change in microstructure. Nonetheless, combining the results from the iodine embedded sample and the glycerine soaked sample, the conclusion that the scattering arises from contrast in the electron density between cellulose and dispersed microvoids in the cellulose is strongly supported.

Power Law Behavior

It is observed in Figures 5 and 10 that the scattering intensity curves of the cellulose samples continuously decrease from $2\theta = 0^\circ$ to about 60° . The short-range atomic structure in the sample becomes significant when 2θ is greater than about 40° . In most samples the intensity first falls and is then nearly constant between $2\theta = 60^\circ$ and 70° . When 2θ is greater than 90° , the intensity starts to increase again and the change of its shape with crystalline form can be clearly seen.

Two types of power law behavior are observed. For Hydrocellulose II and Valonia, $I(s)$ is proportional to s according to Porod's inverse fourth power law (54) for a wide interval of s . For the other ten cotton samples, the intensity is proportional to s with exponents less negative than -4. These two cases will be discussed separately.

Porod's Inverse Fourth Power Law. The theory of small-angle scattering by isotropic two-phase systems with well defined smooth phase boundaries predicts a decrease of the intensity proportional to s^{-4} at large values of s . This is known as Porod's law (54),

$$\lim_{s \rightarrow \infty} I(s) = k_p / s^4 \quad (4)$$

where k_p is known as the Porod constant.

By a least-squares fit it is found that for Hydrocellulose II the intensity I is proportional to $s^{-(3.93 \pm 0.02)}$ over $s = 0.4$ to 1.1 nm^{-1} and for Valonia I is proportional to $s^{-(4.07 \pm 0.02)}$ over $s = 0.26$ to 2.2 nm^{-1} . The slight deviation of the exponent from -4 may be the result of a density transition of finite width between the phases and density fluctuations within the phases (55), or of the scattering from spherical pores with a power-law dimension distribution (56), or simply due to experimental errors. Atomic-scale density fluctuations can account for the large deviation from Porod's law at the outer part of the scattering curve. Values for the Porod constant of Hydrocellulose II and Valonia are given in Table I.

Table I. Estimated Structural Parameters for Hydrocellulose II and Valonia

Sample	k_p	R_{\min}^*	Q^{**}	S/V_2
	(eu/nm ²)	(nm)	(nm)	(m ² /cm ³)
Hydrocellulose II	22800 ± 200	8.8	8.5	15.3
Valonia	67400 ± 800	13.5	12.5	45.2

$$^*R_{\min} = 3.5/s_{\min}$$

$$^{**}Q = 8\pi Q/k_p$$

Deviation From Porod's Law. Except for Valonia and Hydrocellulose II the intensity of the other ten cotton samples decreases with s with a non-integer exponent. Values of the exponent for the various samples are given in Table II. Note they range from -2.7 to -2.1 .

Non-integer exponential behavior has been observed by Perret and Ruland (57,58) for carbon fibers. By preparing a plot of $I \cdot s^3$ versus s^2 (slit collimation system), they obtained a linear relation

$$I(s) = k_p \cdot s^{-3} + b \cdot s^{-1} \quad (5)$$

and suggested the $b \cdot s^{-1}$ term is directly related to the fluctuation in the electron density in the 00ℓ direction of the carbonaceous material. In another paper (55), Ruland suggested

Table II. Power Law Parameters for Cellulose Samples

Sample	Power Law Exponent	s Range for Power Law Fit (nm ⁻¹)	Slope of I·s ⁴ vs. s ² plot (eu/nm ⁴)
Greige Cotton	-2.13 ± 0.02	0.54 to 2.0	
Dewaxed Greige Cotton	-2.24 ± 0.02	0.50 to 3.2	
Scoured Greige Cotton	-2.48 ± 0.02	0.47 to 3.1	
Sco & Ble Greige Cotton	-2.52 ± 0.01	0.40 to 3.2	
Absorbent Cotton	-2.72 ± 0.03	0.60 to 2.8	2950 ± 50
NaOH Mercerized	-2.24 ± 0.02	0.47 to 3.1	3080 ± 90
NH ₃ removed at R.T.	-2.73 ± 0.03	0.70 to 2.5	890 ± 30
NH ₃ removed at 90°C	-2.54 ± 0.03	0.60 to 2.5	2270 ± 60
H ₂ O immersed	-2.50 ± 0.03	0.57 to 2.8	2760 ± 90
EHC I	-2.48 ± 0.02	0.67 to 2.9	
Hydrocellulose II	-3.93 ± 0.02	0.40 to 1.1	
Valonia	-4.07 ± 0.02	0.26 to 2.2	

that density fluctuations within the phases produce positive deviations from Porod's law and can be detected by $I \cdot s^4$ versus s^2 plots. Such a plot is shown in Figure 11 for the absorbent cotton series and the slopes determined from this plot are given in Table II. If Ruland's proposal (55) is true in the case of cotton cellulose, then we should observe a correlation between the value of the slope of the $I \cdot s^4$ versus s^2 plot and the degree of disorder of cotton; that is, the higher the disorder, the higher the value of the slope. It is well known that NaOH mercerization and the liquid ammonia treatment increase the degree of disorder in cotton (3,59). However, the variation of slopes with these samples does not follow the correlation that Ruland proposed (55,57,58). Thus, fluctuations in the dense phase cannot explain the deviation from Porod's law satisfactorily. A different model will be proposed in a later section to explain this deviation.

Invariant and Void Fraction

The general theory developed by Porod (54) as well as by Debye and Buche (60) starts from the fact that the small angle scattering depends only on variations of the electron density. The intensity is determined by the mean scattering power of the system which is given the designation η^2 or mean square electron density fluctuation. For a two-phase system of volume V with volume fractions x_1 and x_2 and with the respective electron densities ρ_1 and ρ_2 , it can be shown that

**American Chemical Society
Library**

1155 16th St., N.W.

Washington, D.C. 20036

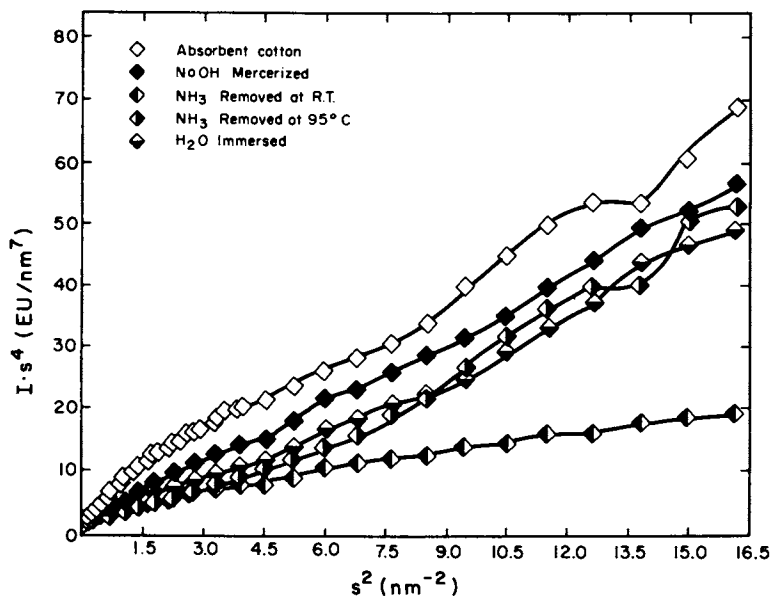


Figure 11. $I \cdot s^4$ versus s^2 plots for absorbent cotton series.

$$\eta^2 V = (\rho_1 - \rho_2)^2 \cdot x_1 \cdot x_2 \quad (6)$$

Additionally, Porod (54) derived an integral over all scattering space, the so-called invariant, which is directly related to the mean square fluctuation of electron density, irrespective of the geometrical features of the structure,

$$\int_0^\infty [I(s) dV s] / (2\pi)^3 = \eta^2 V \quad (7)$$

For an isotropic scattering system, Eq. (6) reduces to

$$\int_0^\infty [4\pi s^2 \cdot I(s) ds] / (2\pi)^3 = \eta^2 V \quad (8)$$

The invariant values together with the volume fraction of pores for cellulose samples are listed in Table III. For the Greige cotton series, dewaxing followed by scouring and bleaching, increases the pore volume fraction at each step, but has no significant influence on the shape of the SAXS curve. For the absorbent cotton series, mercerization treatment with either sodium hydroxide or liquid ammonia decreases the pore volume fraction to a similar level. The conditions for ammonia removal essentially do not affect the pore volume fraction. However, hydrolyzed cotton cellulose has a much higher pore volume fraction than the other cotton samples. The effects due to the chemical process of hydrolyzing need further study.

Table III. Invariant and Pore Volume Fraction in Cellulose Samples

Sample	Invariant (eu/nm ⁶)	Pore Vol. Frac. (%)
Greige Cotton	1790	0.76
Dewaxed Greige Cotton	1960	0.83
Scoured Greige Cotton	2490	1.06
Sco & Gle Greige Cotton	2530	1.12
Absorbent Cotton	2620	1.12
NaOH Mercerized	1780	0.76
NH ₃ Removed at R. T.	1790	0.76
NH ₃ Removed at 95°C	1620	0.69
H ₂ O Immersed	1900	0.81
EHCI	3680	1.58
Hydrocellulose II	7730	3.37
Valonia	33490	17.02

The estimated uncertainty in the determination of the invariant is about five percent. The error involves the

estimation of sample thickness, determination of incident x-ray power, density, and statistical error in detector counts. Also since some of the pore sizes are bigger than can be measured with the ORNL 10m SAXS instrument, the invariant and the void volume fraction are considered to be underestimated.

Pore Size

Two methods are employed to evaluate the size of pores in samples which follow Porod's law. The first is a rough estimate of the average pore dimension R obtained from s_{\min} , the smallest value of s at which Porod's law scattering is observed. Usually one expects $s_{\min} \cdot R \gg 1$. As a conservative estimate, $s_{\min} \cdot R > 3.5$ can be assumed (54, 61). The average dimension of the pores must then be at least $3.5/s_{\min}$.

The second method involves the calculation of the so called average chord length $\bar{\lambda}$ (62),

$$\bar{\lambda} = 8 \pi Q / k_p \quad (9)$$

This $\bar{\lambda}$ is a measure of the size of the inhomogeneities. Q is the invariant and k_p is Porod's constant. Due to the resolution limit, the calculated invariant Q is underestimated and thus $\bar{\lambda}$ is underestimated in this study. Table I compares the pore dimensions in Hydrocellulose II and Valonia. It appears that the sizes determined by the two methods are comparable. The pores in Valonia are much bigger than those in Hydrocellulose II. It is reasonable to postulate that the pores in the other cotton samples are about the same as those in Hydrocellulose.

Specific Inner Surface

The specific inner surface is defined as the ratio of the area of the phase interface S to the volume occupied by the disperse phase V_2 . When it can be verified experimentally that the intensity of a two-phase scattering system follows the inverse fourth power law, the specific inner surface can be obtained (54,62):

$$S/V_2 = 4 x_1 \cdot x_2 / \bar{\lambda} \quad (10)$$

The values for Hydrocellulose II and Valonia are listed in Table I. Since Q is underestimated, the calculated specific inner surface tends to be overestimated. The typical surface area of cotton determined by sorption of nitrogen and argon ranges between 0.3 to 1.9 m^2/g (3). The value determined by SAXS is five to ten time greater than the latter. This is reasonable since SAXS can detect the inaccessible pore surface too.

Aggregate Fractals in Cotton

The property of scale-invariance implies the power-law form for the density-density correlation function:

$$c(x) = \langle \rho_m(r) \cdot r \rho_m(r+x) \rangle \sim 1/r^{d-D} \quad (2)$$

The electron density-electron density correlation function should have a similar form:

$$\rho_{el}^2(r) \sim 1/r^{d-D} \quad (11)$$

and leads to a power-law dependence for the scattering intensity which is the Fourier transform of $\rho_{el}^2(r)$:

$$\begin{aligned} I(s) &= \int \rho_{el}^2(r) \exp(-r \cdot s) \, dV_s \\ &\sim \int r^{D-d} e^{-r \cdot s} \, dV_s \\ &\sim s^{-D} \end{aligned} \quad (12)$$

The log I versus log s curves of the Greige cotton series, absorbent cotton series, and EHC I have the same overall shape as the scattering curve shown in Figure 4. The values of the exponents are between -2.12 ± 0.02 to -2.73 ± 0.03 over the range $0.5 \text{ nm}^{-1} < s < 3 \text{ nm}^{-1}$. Below $s = 0.5 \text{ nm}^{-1}$, the slope becomes more negative. This region characterizes the pore structure and approaches Porod's law $I(s) \sim s^{-4}$ rather than Guinier's approximation. The Guinier treatment in Figure 6 clearly indicates there is no simple straight line relationship, and reveals there is no simple characteristic length scale deducible from the data. Scattering curves of this kind have traditionally been analyzed as scattering from particles with a distribution of sizes. This approach can be used to represent the present data, but the parameters derived in this fashion depend on the range of scattering angles and their relationship to the physical structure is dubious. Instead, we argue that the power law behavior for $I(s)$ is an indication of the fractal structure of cellulose microcrystalline aggregates. The power-law decay of the SAXS intensity over the range $0.5 \text{ nm}^{-1} < s < 3 \text{ nm}^{-1}$ suggests the scatters are fractals over $0.3 \text{ nm} > s^{-1} > 2 \text{ nm}$. 0.3 nm is about the size of one cellulose monomer, 2 nm is the size of microcrystallites as measured by line width analysis of WAXD (21,22) and electron microscopy (26). We interpret the behavior in this range to mean that while cellulose monomer units form microcrystallites with their usual 3 dimensional order, the microcrystallites form aggregated fractals of Hausdorff dimension < 3 .

Computer simulations which may mimic aggregation processes in 3 d space yield values of $D \approx 2.5$ for DLA and $D \approx 1.8$ for CA (33, 35-38). Clearly neither the DLA or CA model describes the cotton cellulose system. A possibility that so far has not been included in the simulations is that the aggregates might restructure after formation. Schaefer et al. (42,43) suggested that additional attachments will lead to an increased D so

restructuring may explain $D > 1.8$ for CA in 3 d space. Another view has been expressed by Vicsek and Family (63). They explore the properties of a cluster size distribution function and discuss the relationship between D and the moments of the distribution function. The mechanisms of aggregation processes will continue to be of interest to those studying a variety of physical processes.

The fundamental assertion we make here regarding the fractal nature of cellulose microcrystalline aggregates is speculative. We view the well established microporous and microfibrillar character of cellulose cotton fibers to support our fractal interpretation. The behavior of the SAXS scattering function is consistent with this fractal interpretation and does not conform to the usual Guinier and Porod methods of analysis. We hope the approach used in this study is sufficiently provocative to stimulate the thinking of other researchers regarding the growth process of cotton cellulose, whether it be via aggregation of microcrystallites followed by some rearrangement or another process.

Acknowledgments

This work was performed as part of Specific Cooperative Agreement No. 58-7B30-3-560 between the United States Department of Agriculture and The University of Tennessee. Portions of this work were performed at the National Center for Small Angle Scattering Research at Oak Ridge National Laboratory which is supported by NSF Grant No. DMR-77-24458 through interagency agreement No. 40-637-77 with the Department of Energy.

Literature Cited

1. Manley, R. St. J. J. Polym. Science 1971, A2, 9, 1025.
2. Peterlin, A.; Ingram, P. Textile Res. J. 1970, 40, 345.
3. Warwicker, J. O.; Jeffries, R.; Colbran, R. L.; Robinson, R. N. A Review of the Literature on the Effect of Caustic Soda and Other Swelling Agents on the Fine Structure of Cotton; Shirley, Institute, Didsbury, Manchester, England 1966.
4. Hermans, P. H. J. Chem. Phys. 1947, 44, 135.
5. Hermans, P. H.; Weidinger, A. J. Appl. Phys. 1948, 19, 491.
6. Scallan, A. M. Textile Res. J. 1971, 41, 647.
7. Heyn, A.N.J. J. Am. Chem. Soc. 1948, 70, 3138.
8. Heyn, A.N.J. Nature (London) 1953, 172, 1000.
9. Heyn, A.N.J. J. Appl. Phys. 1955, 26, 519.
10. Heyn, A.N.J. J. Appl. Phys. 1955, 216, 1113.
11. Stern, F. Trans. Far. Soc. 1955, 51, 430.
12. Statton, W. O. J. Polym. Sci. 1956, 22, 385.
13. Kiessig, H. Kolloid - Z. 1957, 152, 62.
14. Hermans, P. H.; Heikens, D.; Weidinger, A. J. Polym. Sci. 1959, 35, 145.

15. Heikens, D. J. Polym. Sci. 1959, 35, 139.
16. Hermans, P. H.; Weidinger, A. Makromol. Chem. 1960, 39, 67.
17. Kratky, O.; Sekora, A. Pure and Applied Chem. 1966, 12, 483.
18. Statton, W. O. J. Polym. Sci. 1962, 58, 205.
19. Statton, W. O. In Newer Methods of Polymer Characterization; ed. by B. Ke, Interscience, New York, 1964; Chapter 6.
20. Ratho, T.; Sahu, N. C. J. Colloid and Interface Sci. 1971, 37, 115.
21. Haase, J.; Hosemann, R.; Renwanz, B. Kolloid Z. Polym. 1973, 251, 871.
22. Haase, J.; Hosemann, R.; Renwanz, B. Colloid Polym. Sci. 1974, 252, 712.
23. Ratho, T.; Patel, A.; Signal, O. P. J. Polym. Sci. Polym. Chem. Ed., 1974, 12, 2595.
24. Schurz, J.; John, K. Cellul. Chem. Technol. 1975, 9, 493.
25. Haase, J.; Hosemann, R.; Renwanz, B. Colloid Polym. Sci. 1976, 254, 199.
26. Heyn, A.N.J. J. Appl. Cryst. 1979, 12, 395.
27. Fischer, E. W.; Herchenroder, P.; Manley, R. St. J.; Stamm, M. Macromolecules 1978, 11, 213.
28. Stuhmann, H. B. In Small Angle X-ray Scattering; ed. by O. Glatter and O. Kratky, Academic Press, New York, 1982.
29. Freidlander, S. K. Smoke, Dust and Haze: Fundamentals of Aerosol Behavior; Cornell Univ. Press, Ithaca, 1953.
30. Goldberg, W. I.; Huang J. S. In Fluctuation Instabilities and Phase Transitions; ed. by T. Riste, Plenum Press, New York, 1975.
31. Mandelbrot, B. B. The Fractal Geometry of Nature; Freeman, San Francisco, 1982.
32. Proceedings of the International Topical Conference on Kinetics of Aggregation and Gelation, April 1984, ed. by F. Family and D. P. Landau, North-Holland, New York, 1984.
33. Witten, T. A., Jr.; Sander, L. M. Phys. Rev. Lett. 1981, 47, 1400; Phys. Rev., 1983, B27, 5686.
34. Forrest, S. R.; Witten, T. A., Jr. J. Phys. 1979, A12, L109.
35. Meakin, P. Phys. Rev. 1983, A27, 604; 1983, A27, 1495.
36. Sander, L. M.; Cheng, Z. M.; Richter, R. Phys. Rev. 1983, B28, 6394.
37. Meakin, P. Phys. Rev. Lett. 1983, 51, 1119.
38. Kolb, M.; Botet, R.; Jullien, R. Phys. Rev. Lett. 1983, 51, 1123.
39. Ball, R. Bull. Am. Phys. Soc. 1984, 29, 457.
40. Niemeyer, L.; Pietronero, L.; Wiesmann, H. J. Phys. Rev. Letters 1984, 52, 1033.
41. Weitz, D. A.; Oliveira, M. Phys. Rev. Lett. 1984, 52, 1433.
42. Schaefer, D. W.; Martin, J. E.; Wiltzius, P.; Cannell, D. S. Phys. Rev. Lett. 1984, 52, 2371.
43. Schaefer, D. W.; Martin, J. E.; Wiltzius, P.; Cannell, D. S. In Proceedings of the International Topical Conference on Kinetics of Aggregation and Gelation, April 1984, ed. by F. Family and D. P. Landau, North-Holland, New York, 1984.

44. Sinha, S. K.; Freltoft, T.; Kems, J. In Proceedings of the International Topical Conference on Kinetics of Aggregation and Gelation, April 1984, ed. by F. Family and D. P. Landau, North-Holland, New York, 1984.
45. Weitz, D. A.; Huang, J. S. In Proceedings of the International Topical Conference on Kinetics of Aggregation and Gelation, April 1984, ed. by F. Family and D. P. Landau, North-Holland, New York, 1984.
46. Nelson, M. L.; Rousselle, M. A.; Cangemi, S. J.; Trouard, P. Textile Res. J. 1970, 40, 872.
47. Hendricks, R. W. J. Appl. Cryst. 1978 11, 15.
48. Borkowski, C. J.; Kopp, M. K. IEEE Trans. Nucl. Sci. 1972 NS19, 161.
49. Kratky, O.; Pilz, I.; Schmitz, P. J. J. Colloid and Interface Sci. 1966, 21, 24.
50. Tang, M. Y. Ph.D. Dissertation, University of Tennessee, Knoxville, March, 1984.
51. Guinier, A. Ann. Phys. 1939, 12, 161; Guinier, A.; Fournet, G. Small-Angle Scattering of X-rays; Wiley, New York, 1955.
52. Wadsworth, L. C.; Cuculo, J. A. In Modified Cellulosics; ed. by R. M. Rowell and R. A. Young, Academic Press, New York, 1978.
53. Minhas, P. S.; Robertson, A. A. Textile Res. J. 1969, 37, 400.
54. Porod, G. Kolloid Z. 1951, 124, 83; ibid., 1951, 125, 51.
55. Ruland, W. J. Appl. Cryst. 1971, 4, 70.
56. Schmidt, P. W. J. Appl. Cryst. 1982, 15, 567.
57. Perret, R.; Ruland, W. J. Appl. Cryst. 1968, 1, 308.
58. Perret, R.; Ruland, W. J. Appl. Cryst. 1970, 3, 525.
59. Rousselle, M. A.; Nelson, M. L.; Hassenboehler, C. B., Jr.; Legendre, D. C. Textile Res. J. 1976, 46, 304.
60. Debye, P.; Bueche, A. M. J. Appl. Phys. 1949, 20, 518.
61. Bale, H. D.; Schmidt, P. W. Phys. Rev. Letts. 1984, 53, 596.
62. Kahovec, L.; Porod, G.; Ruck, H. Kolloid Z. 1953, 133, 16.
63. Vicsek, T.; Family, F. Proceedings of the International Topical Conference on Kinetics of Aggregation and Gelation, April 1984, ed. by F. Family and D. P. Landau, North-Holland, New York, p. 111, 1984.

RECEIVED March 5, 1987

Chapter 15

Chemical Characterization of Cellulose

Noelie R. Bertoniere¹ and S. Haig Zeronian²

¹Southern Regional Research Center, P.O. Box 19687, New Orleans, LA 70179

²University of California—Davis, Davis, CA 95616

Crystallinity, accessibility, and the nature of microstructural features of cellulose have long been targets for clarification because they hold the key to understanding the course of chemical reactions that occur in textile finishing, paper making, preparation of regenerated cellulose and appreciation of the details of physical performance of the products of such processes. Crystallinity and accessibility measurements are generally based on assessments of opposites: (a) high degrees of order in arrangement and hydrogen bonding of cellulose molecules and (b) incomplete or lack of order in molecular arrangement and hydrogen bonding. It is the precise relationship of crystalline order to accessibility (disorder) that raises questions concerning the interface between the two. Studies in this area and the development and application of new methods of measurement of microstructural detail constitute the promise for greater appreciation and understanding of the structure of cellulose and the basis for development of improvements and new products based on cellulose chemistry.

Crystallinity Determinations

Many methods have been developed for studying the degree of crystallinity, or order, of cellulose. The most useful chemical techniques for estimating them are based on chemical reaction and sorption. Warwicker and co-workers (1,2) have assembled the results of workers who used various techniques for determining the crystallinity of different celluloses. Some of the data is presented in Table I. In this table, the "chemical non-swelling" data, also reported by Warwicker and co-workers, are omitted since they do not appear to measure the internal disordered structure of the fibers. When reviewing the table it should be remembered that the various techniques do not measure the same type or level of disorder. The chemical reaction and sorption methods determine the fraction of the cellulose which is not readily accessible to the reagents. In some instances, the surface of the crystalline or ordered regions is included as part of the disordered fraction;

0097-6156/87/0340-0255\$06.00/0

© 1987 American Chemical Society

especially in the case of the great majority of sorption techniques.

Table I. Average Ordered Fraction Present in Celluloses Determined by Various Techniques^a

Technique	Cotton	Mercerized Cotton	Wood Pulp	Regenerated Cellulose
<u>Physical</u>				
X-ray diffraction	0.73	0.51	0.60	0.35
Density	0.64	0.36	0.50	0.35
<u>Chemical Reaction</u>				
Acid Hydrolysis	0.90	0.80	0.86	0.72
Formylation	0.79	0.65	0.69	0.37
Periodate Oxidation	0.92	0.90	0.92	0.80
CMA ^b	0.73			
<u>Sorption</u>				
Deuteration	0.58	0.41	0.45	0.28
Moisture Regain				
Sorption Ratio	0.58	0.38	0.51	0.23
Hailwood Horrobin	0.67	0.50	0.55	0.35
Iodine Sorption	0.87	0.68	0.73	0.48

^a Approximate average values from published literature (1,2).

^b CMA = Chemical Microstructural Analysis; based on availability of O(3)H (5).

It will be observed that the moisture regain and deuteration determinations yield lower values for degree of order than the chemical reaction techniques. As will be discussed later Zeronian et al. (3) have demonstrated it is feasible to use the moisture regain technique in a manner which will permit differentiation between sorption on crystallite surfaces and sorption in the disordered regions of the cellulose. When allowance was made for the sorption on the crystallite surfaces they found the degree of order for cotton and mercerized cotton was similar to those found by the acid hydrolysis technique.

In most celluloses the crystallites are neither perfect nor large, thus their degree of crystallinity may be underestimated by physical methods. It is feasible that in some regenerated celluloses there are some very small crystallites present which are not being measured by the x-ray or density methods. This may be in part the reason that the discrepancy between the physical

and chemical estimates of crystallinity are larger for regenerated cellulose than for native cellulose. The low value for the degree of order of regenerated cellulose by the formylation method will be discussed below.

It should be noted that average values are given in Table I. Especially in the case of x-ray determinations, estimates of crystallinity will depend strongly on the calculation methods which have been reviewed by Tripp (4). Thus using Warwicker's data, the standard error and coefficient of variation (%) for crystallinity of cotton by x-ray determinations are 2.5 and 15, respectively, and by acid hydrolysis are only 1.1 and 5.9, respectively. The various chemical reaction and sorption techniques will now be discussed in more detail.

Chemical Reaction

These techniques are based on the premise that some reactions occur preferentially in the disordered regions of the cellulose. Thus, initially, it is thought, reaction occurs in the disordered regions and extends later to the ordered regions.

Acid Hydrolysis. This procedure has been used heavily. The sample is hydrolyzed at elevated temperatures using aqueous mineral acids. Chain cleavage occurs and the products of this heterogeneous reaction are glucose, soluble oligosaccharides and an insoluble residue termed hydrocellulose. The weight of the hydrocellulose is plotted against reaction time. The plot can be resolved into two components (Figure 1). Extrapolation of the data at the slower rate to zero time permits an estimate to be made of the ordered fraction of the sample.

The estimates of degree of order by this technique may be high for two reasons. It is feasible that crystallization occurs in the disordered regions due to chain cleavage permitting realignment of the cellulose chains. Also, the assumption that hydrolysis of the crystallites proceeds at the same rate during the early stages of hydrolysis, when disordered material is present, may be incorrect. From the work of Sharples (7) it appears the acid hydrolysis of the crystallites occurs at their ends rather than their lateral surfaces. Consequently, the degradation of the crystallites may not start until the disordered material is eliminated. Rowland and Roberts (8) estimated that the amount of disordered regions in desized, scoured, and bleached cotton fibers before hydrolysis was 1.6 times the values measured in the conventional manner.

Formylation. The formylation method is based on the determination of the ratio of the extent of esterification of cellulose by formic acid after a given length of time, to that of soluble starch for the same length of time. It is assumed that the starch is completely accessible to the reagent; thus a measure of the accessible fraction of the cellulose can be calculated (9,10). By extrapolating the plot of this ratio against time to zero time, the initial accessible fraction of the sample can be determined (9). The complement of this value is the ordered fraction. Other workers have arbitrarily measured accessibilities after 16 hrs

esterification (10-12). However, much closer agreement with the acid hydrolysis values is obtained if the initial ordered fraction is obtained. Nickerson's estimates of the initial non-accessible fractions of cotton, mercerized cotton and viscose rayon are 0.91-0.92, 0.85-0.86, and 0.70-0.72, respectively (9). Advantages of this method are: the reaction is auto catalytic; the formic acid molecule is small, polar and water miscible; the reagent is a relatively strong swelling agent for cellulose but does not penetrate the ordered regions (9). A disadvantage is some chain scission may occur (10) and result in crystallization.

Periodate Oxidation. This method is based on the preferential oxidation of the disordered regions of cellulose by sodium metaperiodate (12,13). Conditions are selected so that the reaction is confined as far as possible to the Malaprade course resulting in the formation of 2,3 dialdehyde units. The course of the reaction is followed by measuring oxidant consumption from the amount of periodate consumed. From plots of log oxidant consumption against time, a measure of the fraction of ordered material can be calculated in a manner analogous to that used with the acid hydrolysis method.

Chemical Microstructural Analysis (CMA). This chemical technique provides information concerning hydrogen bonding of hydroxyl groups on accessible surfaces in the microstructure of cellulose. A chemical agent from a simple reaction leaves a tag on accessible hydroxyl groups and the tag is identified and located through a series of chemical operations and gas-liquid chromatography (14-17). To be tagged the hydroxyl group must lie on a surface accessible to the reagent and it must be available for reaction, i.e., it must be free of involvement in a donor hydrogen bond.

CMA involves five steps (14,16,18): a) reaction of cellulose with N, N-diethylaziridinium chloride (DAC, Figure 2), b) total hydrolysis of the DEAE-cellulose to glucose and DEAE-glucoses, c) fermentation to remove the unmodified glucose, d) silylation of the DEAE-glucoses, and e) gas-liquid chromatographic analysis. The chemical analyses identify the locations of the DEAE tags in the glucose units (19) and the locations of the DEAE-glucoses in the cellulose chains (20). A typical chromatogram for a sample of mature cotton from a capillary column is illustrated in Figure 3. Quantitation involves the sum of alpha- and beta-anomers of DEAE-glucoses to be recorded as mg of DEAE-glucose per g of initial DEAE-cellulosic substrate.

CMA is conducted under controlled conditions of reaction for which the following rate expressions are applicable:

$$dS_2/dt = k_2 [O(2)H]_a [R] \quad (1)$$

$$dS_3/dt = k_3 [O(3)H]_a [R] \quad (2)$$

$$dS_6/dt = k_6 [O(6)H]_a [R] \quad (3)$$

The rate of substitution (S) at a particular hydroxyl group (indicated by subscripts) is a function of the rate constant (k) for that hydroxyl group, the activity of the reagent (R), and the activity of the available hydroxyl group.

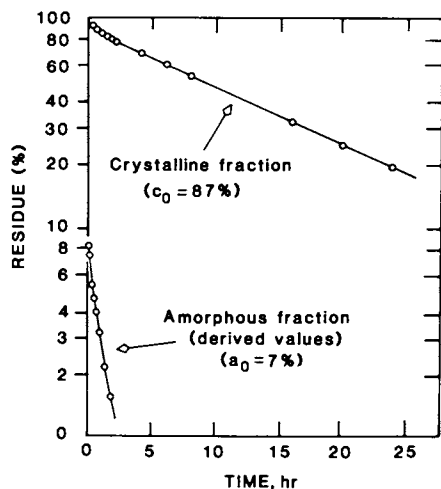


Figure 1. Relation between residue weight and time of hydrolysis at 100°C with 6 M HCl for cotton linters (5,6).

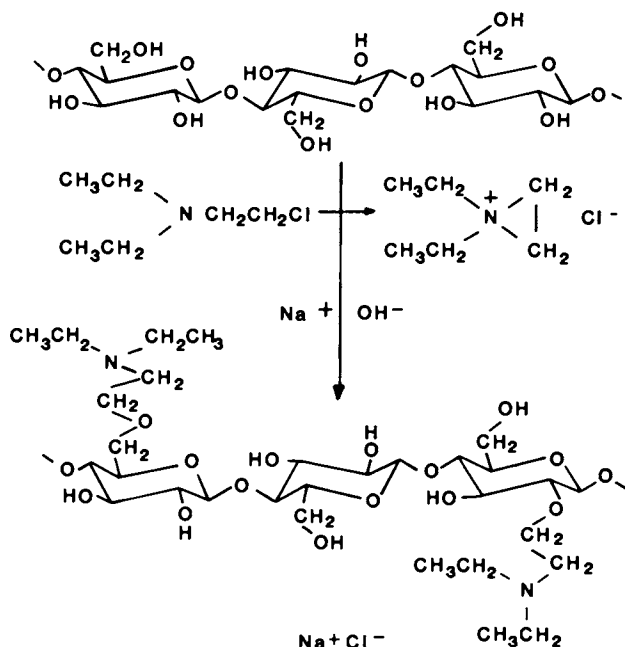


Figure 2. Reaction of cellulose to low degree of substitution of *N,N*-diethylaminoethyl groups occurs in aqueous solution of *N,N*-diethylaziridinium chloride generated from 2-chloroethyldiethylamine.

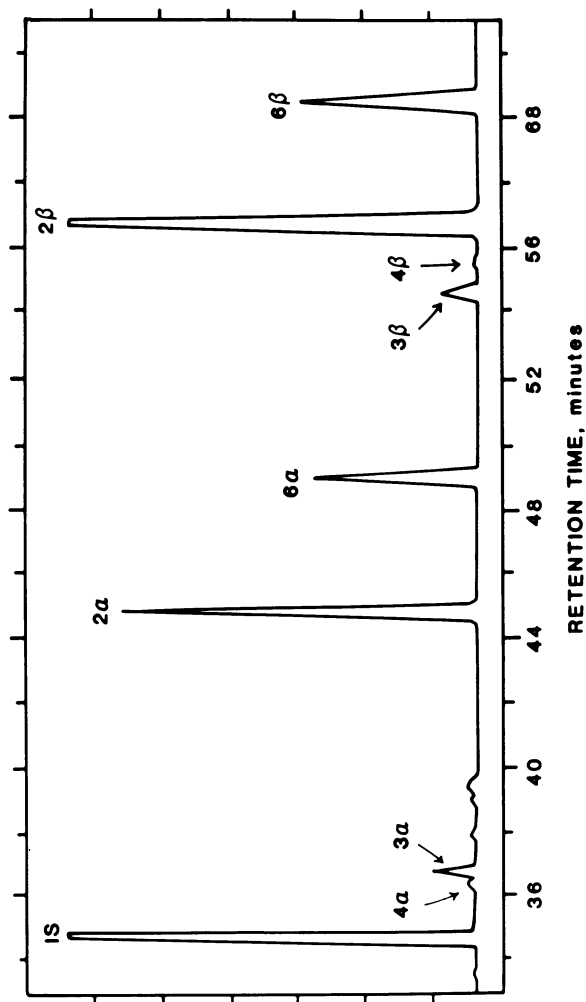


Figure 3. Typical chromatogram of DEAE-glucoses in CMA of a sample of mature cotton cellulose. The peaks are identified as inositol (IS, internal standard) and alpha and beta anomers of 2-0-, 3-0- and 6-0-DEAE-glucoses together with traces of 4-0-DEAE-glucose from presence of a 1,3-glucan in the cellulose.

Equations 2 and 3 are divided by equation 1 to generate expressions that state the relationships of rates as follows:

$$\frac{dS_3/dS_2}{dS_6/dS_2} = k_3 [O(3)H]_a / k_2 [O(2)H]_a \quad (4)$$

$$= k_6 [O(6)H]_a / k_2 [O(2)H]_a \quad (5)$$

When accessibilities to the reagent and availabilities for reaction with the reagent of the three hydroxyl groups are equal as is the case for a completely disordered sample of cellulose, the activity expressions in equations 4 and 5 cancel out to yield new expressions,

$$dS_3/dS_2 = k_3/k_2 \quad (6)$$

$$dS_6/dS_2 = k_6/k_2 \quad (7)$$

which state that the ratio of substitution at hydroxyl groups is a measure of the relative rate constants for the hydroxyl groups.

The relative rate constants for O(2)H, O(3)H and O(6)H are determined by measurements of the distribution of substituents in a sample of completely disordered cellulose (21). The resulting rate constants characterize available hydroxyl groups in any solid crystalline cellulose for which the reaction is conducted under identical conditions.

Equations 4 and 5 are rearranged as follows:

$$[O(3)H]_a / [O(2)H]_a = k_2 (dS_3) / k_3 (dS_2) \quad (8)$$

$$[O(6)H]_a / [O(2)H]_a = k_2 (dS_6) / k_6 (dS_2) \quad (9)$$

Equations 8 and 9 define the relative availabilities of the designated hydroxyl groups. The sole additional data required to determine relative availabilities of the hydroxyl groups of an "unknown" sample of cellulose are the distributions of substituents ($dS_2/dS_3/dS_6$) resulting from the reaction of DAC with that sample of cellulose.

Because relative availabilities of O(2)H are always highest in native cellulose and because x-ray diffraction data are interpreted to indicate that an O(2)H on an accessible surface is free of encumbering donor hydrogen bonds (15), availabilities of O(3)H and O(6)H are stated relative to that of O(2)H (i.e., as in expressions 8 and 9). Selected data are presented in Table II. In actual CMA studies of the relative availabilities of O(2)H, O(3)H and O(6)H, there has been no evidence of the restriction of reactivity of O(2)H by involvement in a hydrogen bond. The measured availability of O(2)H serves, therefore, as a suitable basis for indexing availabilities of O(3)H and O(6)H. From actual measurements on crystalline celluloses, relative availabilities of O(3)H have ranged downwards from 0.9 to as low as 0.05(20,22), suggesting a limiting value of zero for this availability on a perfectly ordered crystalline surface.

In preceding studies, (15,16,17,20) the measured relative availability of O(6)H to O(2)H decreased from about 0.8 to 0.55 as crystallinity increased, suggesting a limiting ratio of 0.50, that is, half of the O(6)H are restrained in hydrogen bonds. Accepting 0.00 and 0.50 as the lower limiting values of availabilities of

Table II. Relative Availabilities of Hydroxyl Groups in Selected Celluloses (5)

Cellulose Substrate	$[O(3)H]_a/[O(2)H]_a$	$[O(6)H]_a/[O(2)H]_a$
Native cotton	0.27	0.82
Mercerized cotton	0.79	0.86
EHC-I ^a	0.28	0.55
EHC-II ^a	0.23 ^b	0.74 ^b
Disordered cellulose	1.00 ^b	1.00 ^b

^a Exemplar hydrocelluloses, selected for their uniquely highly ordered structures.

^b By definition.

O(3)H and O(6)H, respectively, data from relative availabilities of O(3)H and O(6)H may be converted to percentage of disruption of perfection of hydrogen bonding in cellulose I with the following expressions:

$$\text{Disruption of O(3)H bonding} = [O(3)H]_a/[O(2)H]_a \cdot 100 \quad (10)$$

$$\text{Disruption of O(6)H bonding} = \frac{\{[O(6)H]_a/[O(2)H]_a - 0.5\} \cdot 100}{0.5} \quad (11)$$

In recent studies (18,23) CMA was applied to the cotton fiber during its period of development in the cotton boll. Results show the formation of a highly ordered structure of cellulose during deposition of the secondary wall and the disruption of the high degree of order at the time of boll opening and desiccation and collapse of the fiber.

The methodology of CMA is straightforward and superficially simple but requirements for control of a multitude of chemical steps in the analysis impose severe demands for precision and reproducibility of results. Nevertheless, there is at present no alternate measurement or series of measurements that provide detailed information concerning the sites of chemical reactions, the types of accessible surfaces, and the order of hydrogen bonding that characterize the cotton fiber and are pertinent to the chemical modification and finishing of cotton cellulose.

Sorption

Deuteration. When cellulose is treated with saturated deuterium oxide vapor at room temperature, the easily accessible hydroxyl groups exchange rapidly, and a less accessible component exchanges more slowly. Other hydroxyl groups do not exchange. The easily accessible hydroxyl groups have been equated with the amorphous

fraction of cellulose and include hydroxyl groups on crystallite surfaces. The extent of deuteration and therefore crystallinity, has been estimated by infrared methods (24) and gravimetrically (25).

Moisture Regain. The advantage of this method is that water vapor normally does not penetrate well-defined crystallites of cellulose (26). Thus the amount of moisture adsorbed by a sample after conditioning at a specific relative vapor pressure and temperature can be used to estimate its accessibility and degree of order. In one method using water sorption (27), the fraction of amorphous material (F_{am}) has been calculated from the sorption ratio (SR) of the sample using the equation

$$F_{am} = SR/2.60 \quad (12)$$

SR is defined as the moisture regain of the sample (g per 100 g dry cellulose) at a given relative vapor pressure (RVP) and temperature divided by the moisture regain of cotton under the same conditions. The SR for cellulose tends to be independent of the temperature and RVP over a wide range of conditions. Equation 12 was derived by Valentine (27) by correlating the fraction of amorphous material for a series of cellulose samples, as measured by Mann and Marrinan (24), using their deuteration technique, with the sorption ratios of the fibers. An objection to the use of this equation for estimations of crystallinity is that the surface of the crystalline regions is accessible to H₂O and D₂O vapor. Thus, the estimates of F_{am} include the surface of the crystallites as part of the amorphous regions of the samples.

Jeffries (25) made a similar study. He defined crystalline regions as those regions which are hydrogen bonded in a manner sufficiently regular and ordered to give an infrared hydroxyl-stretching band containing well defined characteristic peaks. Amorphous regions were defined as those in which the hydrogen-bonding is not regular and gives a broad featureless hydroxyl stretching band. He noted that by this definition the amorphous regions contain a certain amount of material that is crystalline to x-ray diffraction and may be the cellulose lying in the surfaces of crystallites. Jeffries related the percent amorphous fraction (A) to the percent moisture regain (S) at 60% RVP and 30°C by equation 13.

$$A = 5.795 + 5.416 S \quad (13)$$

Zeronian and co-workers (3) proposed that a better estimate of the fraction of amorphous material (F) in a cellulose sample can be obtained from its moisture regain (M_s) if the moisture regain of the microcrystalline cellulose produced from hydrolysis (M_c) and the moisture regain of amorphous cellulose (M_a) are taken into consideration by using equation 14. The preparation of the microcrystalline cellulose is critical in order for it to be used as a reasonable facsimile of the crystalline regions present in the fiber (3).

$$F = (M_s - M_c)/(M_a - M_c) \quad (14)$$

The regains are all measured at the same RVP and temperature. From F a measure of the disordered cellulose can be obtained which does not include crystalline surfaces. The accessibility of the sample (A_s) is given by the following equation:

$$A_s = M_s/M_a \quad (15)$$

Comparison of the values for F and A_s for a cellulosic sample then will yield an estimate of the contribution of the disordered (or amorphous) regions relative to that of crystallite surfaces towards the accessibility of the sample. The fraction of crystalline material (X) is given in equation 16.

$$X = 1 - F \quad (16)$$

Zeronian and co-workers obtained X values for cotton and mercerized cotton (Table III) which agree well with the values for fraction of ordered material obtained by the acid hydrolysis method (Table I). F and A_s values are also given in Table III.

Table III. Fraction of Amorphous Material (F), Fraction of Crystalline Material (X) and Accessibility (A_s) of Cotton and Mercerized Cotton Calculated from Water Sorption Data (3)

Sample	F^a	X^b	A_s^c
Cotton	0.090	0.91	0.37
Mercerized cotton	0.21	0.79	0.52

^a $F = (M_s - M_c)/(M_a - M_c)$

where M_s , M_c , and M_a are the monomolecular moisture regains of the sample, its microcrystalline counterpart, and amorphous cellulose, respectively.

^b $X = 1 - F$

^c $A_s = M_s/M_a$

Hailwood and Horrobin (28) developed an equation for water sorption of cellulose based on a solution theory. It permits the calculation of the fraction of the sample inaccessible to water vapor. However, Hailwood and Horrobin assumed in the development of their equation that an ideal solid solution of polymer, hydrated polymer and water is formed. This assumption has been questioned in the general discussion following the presentation of their paper and also by McLaren and Rowen (29).

Iodine Sorption. In this technique the amount of iodine absorbed by the sample from an iodine/potassium iodide solution is measured. The method has been questioned by several researchers. For example, as the sample weight increases the equilibrium concentration of iodine in the solution falls and so does the amount of iodine absorbed by the sample (12). Other problems with the methods have been reviewed by Wadsworth and Cuculo (30).

Bromine Sorption. The measurement of accessibility by sorption of bromine from bromine water has been suggested (31). Bromine sorption appears to be Langmuirian. By measuring the number of moles of anhydroglucose units per mole of bromine at saturation the percent accessibility of the sample can be calculated. The non-accessible fractions of the Paymaster, Amsark, Pima, Heath, Bradley and Moores cotton fibers were determined to be 0.78, 0.73, 0.80, 0.77 and 0.46, respectively.

Leveling-off Degree of Polymerization

When cellulose is hydrolyzed at elevated temperatures with aqueous mineral acid not only does it lose weight but the degree of polymerization (DP) of the residue falls rapidly initially and then attains a relatively constant value which is called the leveling-off degree of polymerization (LODP) (Figure 4).

Battista (33) has provided a comprehensive review of early work in this area. The LODP can be multiplied by the length of an anhydroglucose unit to give a measure of the length of the crystallites present in the cellulose (34-36). However, it has been suggested that during hydrolysis of cotton, crystallization of the cellulose can take place (36,37). Thus it is possible that crystallite lengths determined from the LODP measurements cannot be used as absolute values. Nevertheless, they remain of value for placing celluloses of differing crystallite length in relative order and can yield insights into the effect of various treatments on the fine structure and lateral order distribution of celluloses (1,10,38). The dissolving pulp industry uses LODP determinations to establish whether pulp mercerization has occurred during purification processes.

LODP can be determined by subjecting a sample to a 15 minute hydrolysis at the boil in 2.5 M HCl and measuring the DP of the residue. Any intracrystalline swelling of a cellulose appears to result in a lowering of its LODP. For example, after cotton has been treated with 5M LiOH, NaOH and KOH at 21°C or 0°C, the KOH-treated sample has a lower LODP than either the LiOH- or NaOH-treated material (39,40). The LODP values of the samples are lowered more by the treatments at 0°C than at 21°C.

The effect of the swelling depends not only on the reagent but on the cellulose. For example, the LODP of Pima S-5 cotton before and after mercerization is 168 and 87, respectively whereas the LODP of Deltapine Smooth Leaf cotton before and after mercerization is 153 and 62, respectively (41). The large fall in LODP after mercerization is noteworthy and needs to be borne in mind when attempts are made to elucidate the supramolecular structure of celluloses.

It has been suggested that the order in cellulose can best be represented by a distribution curve (42). The lateral order distribution (LOD) of the ordered regions of a cellulose can be determined by studying the effect of progressively increasing the concentration or temperature of a swelling agent, such as aqueous sodium hydroxide, on a property of the cellulose such as its LODP. The transition range can be determined in terms of other properties such as moisture regain and formylation accessibility as well (9). The LOD is obtained by plotting the slope of the curve, relating the cellulose property to the alkali concentration, against alkali concentration. The greater the perfection of the crystalline material in the fiber the higher will be the alkali concentration at the peak of the LOD curve. Also, the broader the range of degree of perfection of the ordered fraction in the sample, the wider will be the LOD curve.

Pore Structure

In early investigations Aggebrandt and Samuelson (43) effectively used solute exclusion of a series of polyethylene glycols to obtain accessibilities for cotton and rayon fibers. Stone and Scallan (44) and Stone et al. (45) conducted static measurements with oligomeric sugars and series of dextrans to characterize the distributions of pore sizes in wood pulps and celluloses. A column chromatographic technique based on size exclusion was subsequently developed by Martin and Rowland (46,47). Columns have been prepared from amorphous (48), chopped (49) and whole fiber (50,51) cottons. The solutes that have been used as "molecular probes" are series of sugars (glucose, maltose, raffinose, and stachyose), ethylene glycols (degree of polymerization = 1 through 6), and glymes (degree of polymerization 1 through 4). Chromatographic results are obtained in terms of elution volume for each specific solute V_e , total void volume for the column V_0 (elution volume of a high molecular weight solute such as Dextran T-40, molecular weight 40,000, which is totally excluded from the internal pore structure), the total column volume V_t , and the weight (dry basis) of material in the column W . Calculated results are expressed as accessible internal volume V_i (ml/g), specific gel volume V_g (ml/g) and total internal water V_w (ml/g). These terms (per g dry cellulose) were defined by the following equations (52).

$$V_i = (V_e - V_0)/W \quad (17)$$

$$V_g = (V_e - V_0)/W \quad (18)$$

$$V_w = V_g - 0.629 \quad (19)$$

The specific volume occupied by the solid cellulose in the water-wet fiber (required to calculate V_w , Equation 19) was taken as 0.629 ml/g which corresponds to a density of 1.59 g/ml (53,54). The relationship between V_i and molecular weight is linear for the sugars but curvilinear for both the ethylene glycols and the glymes (50). Within a homologous series molecular weight is an indicator of relative molecular size. When comparing different series it is desirable to do so on a molecular size basis. A plot

of V_i versus molecular diameter (55,56) for purified and caustic mercerized cotton batting is presented in Figure 5 for each series of molecular probes. Each series of solutes should provide similar, but not identical, information on the pore structure of the treated cottons. From such plots the internal volume accessible to molecules of specified molecular size can be calculated. An estimate of internal volume that is accessible to the water molecule (V_2) was obtained from the extrapolated value of V_i at 2 Å. Extrapolation of these least squares lines to $V_i = 0$ gives an estimate of the permeability limit (M_x), which is defined as the minimum size of solute that will be completely excluded from permeating the gel structure. Changes in V_2 reflect the changes occurring in the small pores whereas changes in M_x provide a sensitive measure of the extent to which the large pores in the cellulosic composition have been expanded or contracted. Data are assembled in Table IV from Figure 5 for the cotton and mercerized cotton purified battings.

Table IV. Internal Volume Accessible to Water (V_2) and Permeability Limits (M_x) of Cotton and Mercerized Cotton (50)

Sample	Sugars	Ethylene Glycols	Glymes
		V_2 , ml/g	
Cotton	0.305	0.290	0.248
Mercerized Cotton	0.575	0.535	0.490
		M_x , Å	
Cotton	35.9	34.6	38.9
Mercerized Cotton	34.7	31.6	39.9

Differences among the results for the three series of solutes reflect differences in the abilities of these different molecular probes to discriminate among the various pores. The sugars are relatively stiff and bulky molecules which are similar to cellulose itself in hydrophilicity. In contrast the ethylene glycols are more flexible, slender molecules containing ether oxygens along with hydroxyl groups. While these molecules might be expected to have greater penetrating power because of their flexibility and capability of tighter coiling, they would compete less successfully for internal bound water and would find a smaller fraction of the internal water available as solvent. The glymes contain only ether structures.

The principal value of this measurement is its ability to provide information on the distribution of accessible pores in

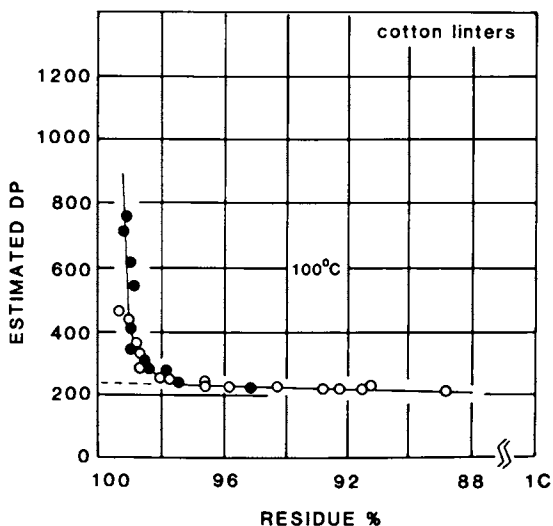


Figure 4. Relation between degree of polymerization (DP) of hydrocellulose and residual weight after hydrolysis at 100°C with HCl of concentrations ranging from 0.01 to 2.5M (5,32).

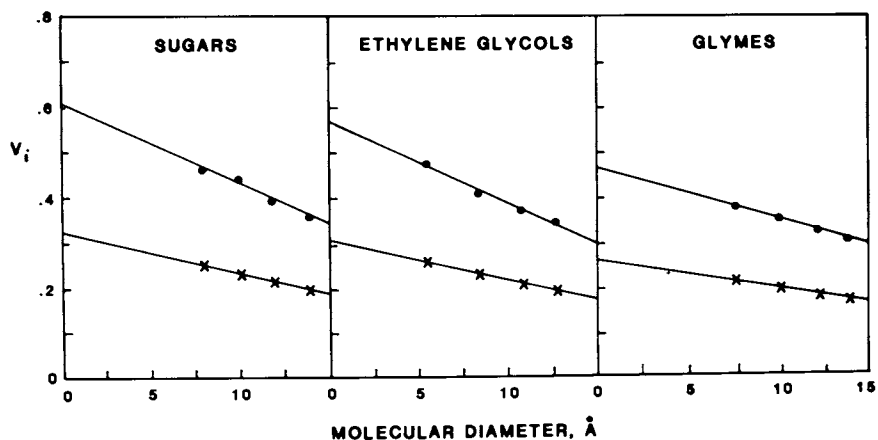


Figure 5. Internal water (V_i) that is accessible to a solute as a function of molecular weight. Column packings were cotton (x) and mercerized cotton (●).

water swollen cellulosic fibers over a critical size range. The technique is limited by the lack of availability of a wide variety of series of water soluble solutes for use as molecular probes. Like CMA, the technique demands precision and reproducibility but provides information that is pertinent to the chemical modification of cotton.

Acknowledgment

The authors express their appreciation to Stanley P. Rowland for assistance in preparing the section of the manuscript relating to Chemical Microstructural Analysis.

Literature Cited

1. Warwicker, J. O., Jeffries, R., Colbran, R. L., and Robinson, R. N. "A Review of the Literature on the Effect of Caustic Soda and Other Swelling Agents on the Fine Structure of Cotton.", Shirley Institute Pamphlet No. 93. The Cotton Silk and Man-Made Fibers Research Association, Manchester, England, 1966.
2. Jeffries, R., Jones, D. M., Roberts, J. G., Selby, K., Simmens, S. C., and Warwicker, J. O., Cell. Chem. Technol., 1969, 3, 255.
3. Zeronian, S. H., Coole, M. L., Alger, K. W. and Chandler, J. M. J. Appl. Poly. Sci., Appl. Polym. Symp., 1983, 37, 1053.
4. Tripp, V. W. in "Cellulose and Cellulose Derivatives," Bikales, N. M., and Segal, L., editors. Part 4, pg 305 et seq. (High Polymers Vol. 5) 2nd Edition Wiley Interscience, New York, 1971.
5. Rowland, S. P. and Bertoniere, N. R. in "Cellulose Chemistry and its Applications." Nevell, T. P. and Zeronian, S. H., editors, pg. 118. Ellis Horwood Ltd, Chichester, England; Halsted Press, John Wiley and Sons, New York, 1985.
6. Nelson, M. L. J. Polym. Sci., 1960, 43, 351.
7. Sharples, A. Trans. Faraday. Soc., 1957, 53 1003.
8. Rowland, S. P. and Roberts, E. J. J. Polym. Sci., Part A-1, 1972, 10 2447.
9. Nickerson, R. F. Text. Res. J., 1951, 21 195.
10. Marchessault, R. H. and Howsmon, J. A. Text. Res. J., 1957, 27 30.
11. Rowland, S. P. and Pittman, P. F. Text. Res. J., 1965, 35, 421.
12. Jeffries, R., Roberts, J. G. and Robinson, R. N. Text. Res. J., 1968, 38. 234.
13. Cousins, E. R., Bullock, A. L., Mack, C. H., and Rowland, S. P. Text. Res. J., 1964, 34, 953.
14. Rowland, S. P., Roberts, E. J. and Wade, C. P. Text. Res. J., 1969, 39, 530.
15. Rowland, S. P. in Modified Cellulosics, eds. R. M. Rowell and R. A. Young, Academic Press, New York, 1978, p. 147.
16. Rowland, S. P., Roberts, E. J. and Bose, J. L. J. Polym. Sci., Part A-1, 1971, 9, 1431.
17. Rowland, S. P., Roberts, E. J., Bose, J. L. and Wade, C. P. J. Polym. Sci., 1971, 9, 1623.

18. Rowland, S. P., Howley, P. S. and Anthony, W. S. Planta, 1984, 161, 281.
19. Roberts, E. J. and Rowland, S. P. Can. J. Chem., 1967, 45, 261.
20. Rowland S. P. and Roberts, E. J., J. Polym. Sci., Part A-1, 1972, 10, 2447.
21. Roberts, E. J. and Rowland, S. P. Carbohydr. Res., 1971, 21, 357.
22. Rowland S. P. and Wade, C. P. J. Polym. Sci. Polym. Chem. Ed., 1980, [18] 2577.
23. Rowland S. P. and Howley, S. P. J. Polym. Sci. Polym. Chem. Ed., 1985, 23, 183.
24. Mann, J. and Marrinan, H. J. Trans. Faraday Soc., 1956 52, 481, 487, 492.
25. Jeffries, R. J. Appl. Polym. Sci., 1964, 8, 1213.
26. Valentine, L. J. Polymer. Sci., 1958, 27, 313.
27. Valentine, L. Chem. Ind. (London), 1956, 1279.
28. Hailwood, A. J. and Horrobin, S. Trans. Faraday Soc., 1946, 42B, 84.
29. McLaren, A. D. and Rowen, J. W. J. Polym. Sci., 1951, 7, 289.
30. Wadsworth, L. C. and Cuculo, J. A. in "Modified Cellulosics" Rowell, R. M. and Young, R. A., Editors, pg 117 et seq. Academic Press, New York, 1978.
31. Lewin, M., Guttman, H., and Saar, N. Appl. Polym. Symp., 1976, 28, 791.
32. Nelson, M. L. and Tripp, V. W. J. Polym. Sci., 1953, 10, 577.
33. Battista, O. A. Ind. Eng. Chem., 1950, 42, 502.
34. Nickerson, R. F. and Habrle, J. A. Ind. Eng. Chem., 1947, 39, 1507.
35. Battista, O. A., Coppick, S., Howsmon, J. A. Morehead, F. F., and Sisson, W. A. Ind. Eng. Chem., 1956, 48, 333.
36. Immergut, E. A. and Rånby, B. G. Ind. Eng. Chem., 1956, 48, 1183.
37. Sharples, A. J. Polym. Sci., 1954, 13, 393.
38. Zeronian, S. H. J. Appl. Polym. Sci., 1971, 15, 955.
39. Zeronian, S. H. and Cabradilla, K. E. J. Appl. Polym. Sci., 1972, 16, 113.
40. Zeronian, S. H. and Cabradilla, K. E. J. Appl. Polym. Sci., 1973, 17, 539.
41. Aboul-Fadl, S. M. , Zeronian, S. H., Kamal, M.M., Kim, M. S., and Ellison, M. S. Text. Res. J., 1985, 55, 461.
42. Howsmon, J. S. and Sisson, W. A. in "Cellulose and Cellulose Derivatives," Ott, E., Spurlin, H. M. and Grafflin, M. W.; Editors. pp. 251-155 (High Polymers Vol 5) 2nd ed. Interscience Publishers, New York, 1954.
43. Aggebrandt, L. and Samuelson, O. J. Appl. Polym. Sci., 1964, 8, 2801.
44. Stone, J. E. and Scallan, A. M. Pulp. Pap. Mag. Can., 1968, 69, 69.
45. Stone, J. E., Treiber, E. and Abrahamson, TAPPI, 1969, 52, 108.
46. Martin, L. F. and Rowland, S. P., J. of Chromatog., 1967, 28, 139.

47. Martin, L. F. and Rowland, S. P. J. of Polym. Sci: Part A-1, 1967, 5, 2563.
48. Martin, L. F., Bertoniere, N. R., Blouin, F. A., Brannan, M. A. and Rowland, S. P. Text. Res. J., 1970, 40, 8.
49. Blouin, F. A., Martin, L. F., and Rowland, S. P. Text. Res. J., 1970, 40, 1970.
50. Rowland, S. P., Wade, C. P. and Bertoniere, N. R. J. Appl. Polym. Sci., 1984, 29, 3349.
51. Bertoniere, N. R., King, W. D., and Rowland, S. P. J. Appl. Polym. Sci., 1986, 31, 2769.
52. Rowland, S. P. and Bertoniere, N. R., Textile Res. J., 1976, 46, 770.
53. Hermans, P. H. "Physics and Chemistry of Cellulose Fibers with Particular Reference to Rayon", Elsevier, New York, 1949, pg. 20.
54. Martin, L. F., Blouin, F. A., and Rowland, S. P., Sep. Sci., 1971, 6, 287.
55. Stone, J. E. and Scallan, A. M. Cell Chem. Technol., 1968, 2, 343.
56. Nelson, R. and Oliver, D. W. J. Polym. Sci., Part C, 1971, 36, 305.

RECEIVED March 5, 1987

Chapter 16

Physical Structure and Alkaline Degradation of Hydrocellulose

Victor M. Gentile, Leland R. Schroeder, and Rajai H. Atalla

Institute of Paper Chemistry, Appleton, WI 54912

Degradations of fibrous cotton hydrocellulose and an amorphous hydrocellulose were conducted in oxygen-free 1.0M NaOH at 60 and 80°C. The physical structure of the fibrous hydrocellulose was not significantly altered, while the amorphous hydrocellulose underwent partial recrystallization into the cellulose II form and some loss of amorphous material through degradation. Endwise depolymerization (peeling) and formation of stable carboxylic acid endgroups (chemical stopping) were more rapid and extensive with the amorphous substrate. Both peeling and chemical stopping were inhibited by the more highly ordered physical structure of the fibrous hydrocellulose and the majority of degrading molecules terminated to stable inaccessible reducing endgroups, that is, by physical stopping. In contrast, chemical stopping was the dominant stabilization mechanism in the amorphous hydrocellulose. The rate of chemical stopping relative to peeling increased with temperature for both substrates. In addition, random chain cleavage, normally believed to be important only at much higher temperatures, was detected in the amorphous hydrocellulose.

Alkaline degradation of cellulose occurs by random cleavage of glycosidic linkages and by stepwise elimination of monomer units from the reducing end (peeling) (1,2). These reactions occur in competition with another reaction which stabilizes cellulose against alkaline degradation by converting the reducing endgroup to an alkali-stable, carboxylic acid endgroup (chemical stopping).

Though the major alkaline reactions of cellulose have been relatively well defined, the role of cellulose physical structure in those reactions has not been clearly established. Cellulose molecules have been reported to undergo physical stopping of the peeling reaction when a molecule is peeled back to a crystalline region in the cellulose structure, with the result that the reducing endgroup

0097-6156/87/0340-0272\$06.00/0
© 1987 American Chemical Society

becomes inaccessible to the alkaline medium (3-5). It is also reported that for native cellulose the rate of peeling relative to chemical stopping is higher than for mercerized cellulose (3,6-8). Furthermore, random chain cleavage occurs more rapidly in mercerized cellulose than in native cellulose (6). These findings suggest that both molecular accessibility and conformation (i.e., cellulose I or II) influence the susceptibility of cellulose molecules to alkaline reactions. However, separating the different effects of physical structure from the inherent reactivity of the cellulose molecule (in an alkaline environment) is made difficult by its limited solubility in alkaline solutions.

In the present study, the role of cellulose physical structure in alkaline reactions was investigated by comparing the alkaline degradation of highly crystalline (cellulose I) fibrous hydrocellulose with that of amorphous (noncrystalline) hydrocellulose. The amorphous substrate was taken as a cellulose model the reactivity of which would most closely approximate that of alkali-soluble cellulose. The availability of such an approximation to the inherent reactivity of cellulose allowed evaluation of the effects of the more highly ordered structure of the fibrous hydrocellulose.

Results and Discussion

Experimental Approach. The experimental study was a comparison of the alkaline degradations of fibrous and amorphous hydrocelluloses in oxygen-free 1.0M NaOH, at 60 and 80°C. The fibrous hydrocellulose was predominantly crystalline (cellulose I) and therefore served as a substrate which would undergo alkaline reactions with significant physical structure effects. In contrast, the amorphous hydrocellulose was noncrystalline (9,10). Thus, it was a substrate which would experience substantially less structural constraint during its alkaline reactions.

The fibrous hydrocellulose was prepared by mild acid hydrolysis of cotton fibers to provide sufficient numbers of reducing endgroups for peeling and stopping to occur at measurable rates. The amorphous hydrocellulose was prepared by dissolving the fibrous hydrocellulose in the dimethylsulfoxide-paraformaldehyde (DMSO-PF) solvent (9-12) and then regenerating the hydrocellulose with a sodium methoxide-isopropoxide solution (9,10). Both hydrocelluloses were freeze-dried during preparation and after degradation to minimize drying-induced structural changes. Thus, structural changes caused by the alkaline medium and the degradation reactions could be detected more readily.

Data on endgroup contents and number-average degrees of polymerization (\overline{DP}_n) for the hydrocellulose substrates are presented in Table I. The hydrocelluloses have similar numbers of carboxylic acid endgroups formed during purification of the cotton fibers. But only the amorphous hydrocellulose contained no inaccessible reducing endgroups, demonstrating the capacity of the dissolution/regeneration process to enhance accessibility (9,10). On the other hand, the total reducing endgroup content of the amorphous hydrocellulose was greater than that of the fibrous hydrocellulose. This, together with the lower \overline{DP}_n of the amorphous substrate, indicates that some chain cleavage occurred during regeneration. The chain cleavage was

apparently related to the scale-up of the process, since no cleavage was detected when relatively small samples (< 2 g) were regenerated (9). For this reason, in comparisons of the peeling and stopping reactions of the two substrates, reaction rates were corrected for the different accessible (reactive) reducing endgroup contents.

Table I. Endgroup^a and \overline{DP}_n ^b Data for Hydrocellulose Substrates

	Fibrous Hydrocellulose	Amorphous Hydrocellulose
Carboxylic acid endgroups	1.09×10^{-3}	1.02×10^{-3}
Accessible reducing endgroups	1.13×10^{-3}	3.42×10^{-3}
Inaccessible reducing endgroups	0.15×10^{-3}	0
Total reducing endgroups	1.28×10^{-3}	3.42×10^{-3}
\overline{DP}_n	422	225

^aEndgroup values expressed as mole fractions of total monomer units.

^bCalculated from the total endgroups content⁻¹.

During the course of the alkaline degradations, both physical and chemical structures of the hydrocelluloses were monitored. Hydroxyl accessibility (13) was determined as a practical measure of the fraction of molecules accessible to the alkaline medium. The crystalline structure was characterized by x-ray diffraction (14). In addition, Raman (15) and solid-state carbon-13 nuclear magnetic resonance (¹³C-NMR) (16,17) spectra were utilized to assess conformational changes. Yield loss was determined gravimetrically and taken as a measure of anhydroglucose units lost due to peeling. The chemical stopping reaction was monitored by measuring carboxylic acid endgroup formation, using methylene blue absorption values (10). The reactive species for both peeling and stopping, that is, the accessible reducing endgroups, were detected by selective reduction with tritium-labeled sodium borohydride (9,10). Inaccessible (nonreactive) reducing endgroups were also detected by reduction with sodium borohydride-³H after they were made accessible via the previously discussed regeneration technique (9). It was therefore possible to detect the so-called "physical stopping" of the peeling reaction as evidenced in the formation of inaccessible or unreactive reducing endgroups.

The physical structure data together with the alkaline reaction data permitted evaluation of the effects of physical structure on alkaline degradation of cellulose.

Alkaline Degradations - Change in Physical Structure. The hydroxyl accessibility of the fibrous hydrocellulose was initially $51.4 \pm 0.8\%$. In contrast, the amorphous substrate had an accessibility of $99.2 \pm 1.0\%$. Exposure of the fibrous hydrocellulose to the alkaline media caused the accessibility to decrease slightly to $50.7 \pm 1.0\%$ and $49.1 \pm 1.2\%$ at 60 and 80°C, respectively, but accessibility did not change significantly during the reaction periods (0-168 hr).

The accessibility of the amorphous hydrocellulose, however, did decline, both upon exposure to the alkaline media and during the reaction periods (Figure 1). This indicates both recrystallization and selective removal of amorphous material.

X-ray diffractograms of the fibrous hydrocellulose (Figure 2) exhibit the characteristic 002, 101, and $10\bar{1}$ reflections of the cellulose I crystalline lattice (14,18). The sharply defined peaks indicate a high degree of crystallinity. Although there appears to be a slight increase in peak intensity in the diffractogram of the zero-time sample relative to that of the initial substrate, no further change is evident in the diffractogram of the 48-hour sample. Thus, x-ray diffraction confirms that the fibrous hydrocellulose does not undergo significant change in physical structure during degradation.

The diffuse diffractogram of the initial amorphous substrate (Figure 3) is indicative of noncrystalline cellulose (19). The diffractogram of the zero-time sample exhibits a set of weak reflections corresponding to the 002, 101, and $10\bar{1}$ planes of the cellulose II crystalline lattice (14,18). The poorly defined peaks indicate a relatively low degree of crystallinity. Since the diffractogram of the 48-hour sample displays slightly more intense reflections, a small increase in the cellulose II content occurred during the reaction period. This is consistent with the hydroxyl accessibility data.

Raman spectra of the fibrous hydrocellulose in the conformation sensitive 250 to 650 cm^{-1} region have relatively intense cellulose I bands (Figure 4), indicating that the molecules are predominantly in the cellulose I conformation (15). This is best demonstrated by the intense band at 378 cm^{-1} . The lack of significant differences in the spectra of the initial substrate, zero-time sample, and 48-hour sample confirm that no significant changes in physical structure occurred during degradation.

In contrast, the same region in the Raman spectrum of the initial amorphous substrate exhibits broad bands (Figure 5) indicative of irregular sequences of conformations along the cellulose chains (15). The emergence of a band at 355 cm^{-1} in the spectrum of the zero-time sample indicates the presence of the cellulose II allomorph. The additional, small increase in band intensity in the spectrum of the 48-hour sample again demonstrates a further slight increase in cellulose II content during degradation.

The solid-state ^{13}C -NMR spectra of the fibrous hydrocellulose also demonstrate the predominance of the cellulose I allomorph (Figure 6). All three spectra contain the sharp resonances associated with the cellulose I conformation and the broader C-4 and C-6 resonances indicative of regions of three-dimensional disorder and crystallite surfaces (16,17). The relative intensities of the sharp and broad resonances of the three spectra are similar, again demonstrating the lack of change in physical structure during degradation.

In comparison, the ^{13}C -NMR spectrum of the initial amorphous substrate exhibits only broad resonances (Figure 7) characteristic of regions of three-dimensional disorder (16,17). The progressive appearance of sharper resonances in the spectra of the zero-time and 48-hour samples indicates increasing conformational order.

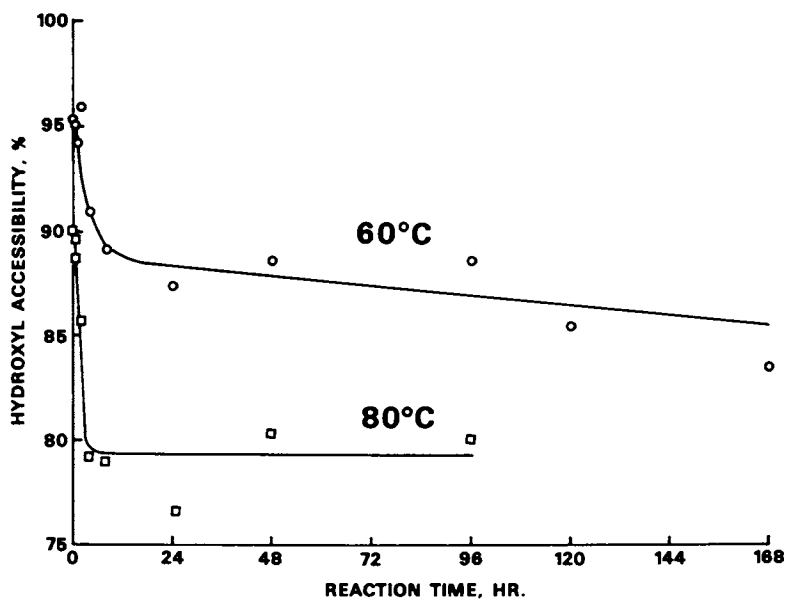


Figure 1. Hydroxyl accessibility of the amorphous hydrocellulose during degradation in 1.0M NaOH.

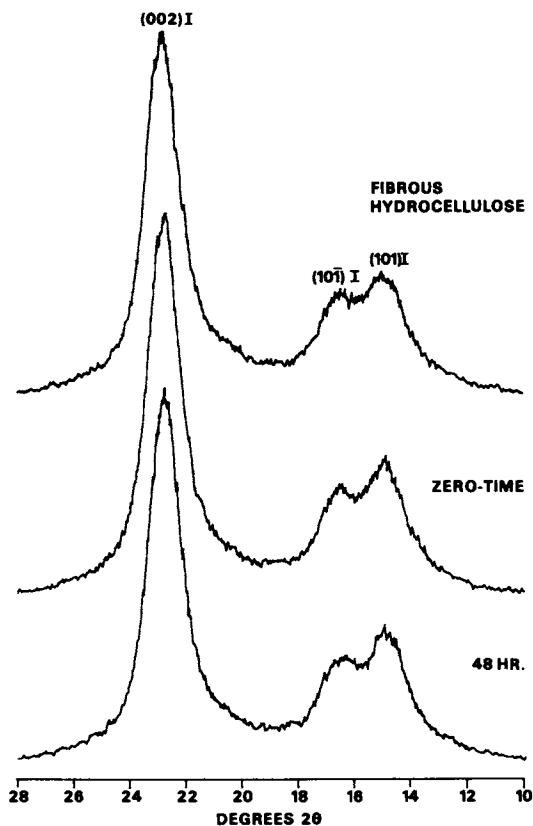


Figure 2. X-ray diffractograms of the fibrous hydrocellulose during degradation in 1.0M NaOH at 80°C.

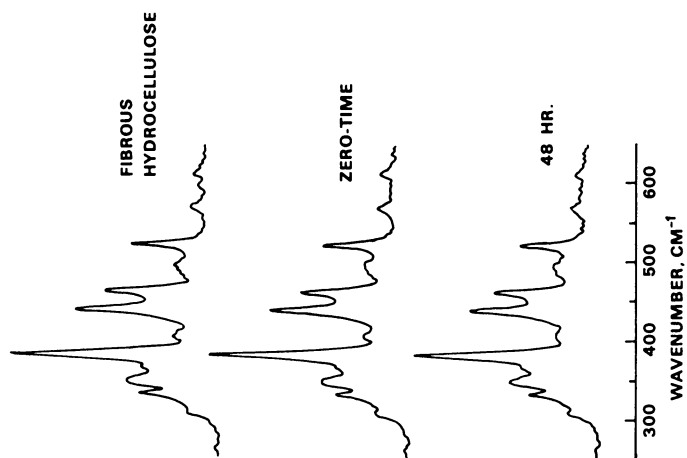


Figure 4. Raman spectra of the fibrous hydrocellulose during degradation in 1.0M NaOH at 80°C.

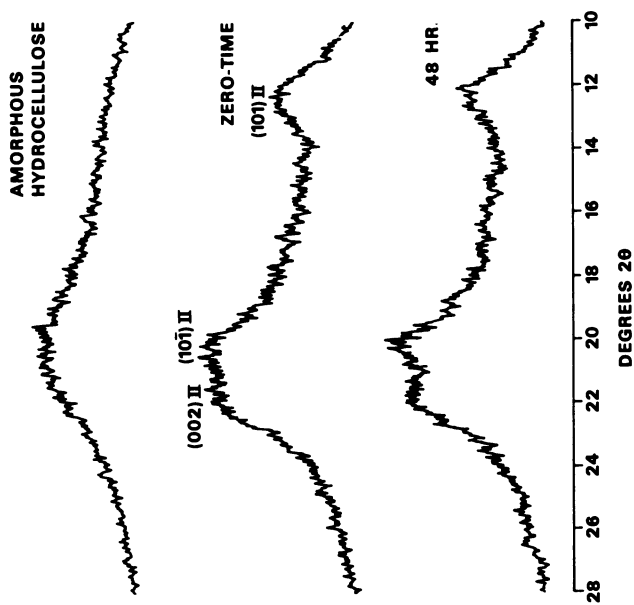


Figure 3. X-ray diffractograms of the amorphous hydrocellulose during degradation in 1.0M NaOH at 80°C.

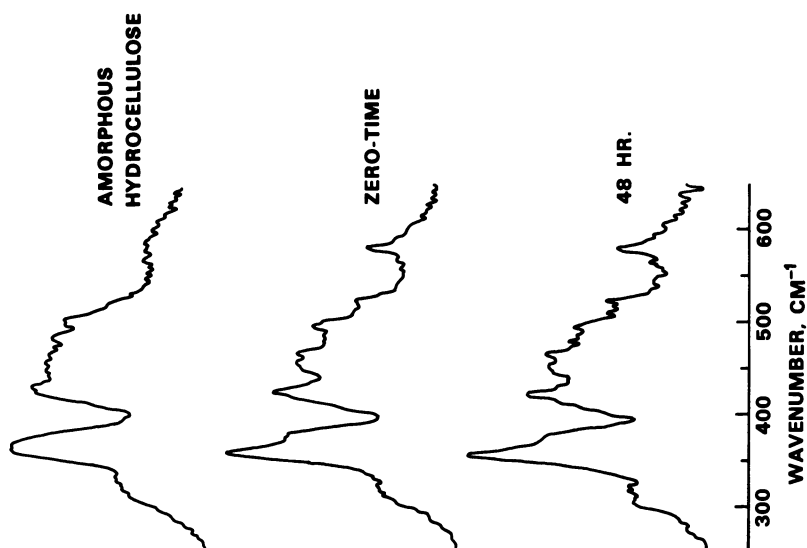


Figure 5. Raman spectra of the amorphous hydrocellulose during degradation in 1.0M NaOH at 80°C.

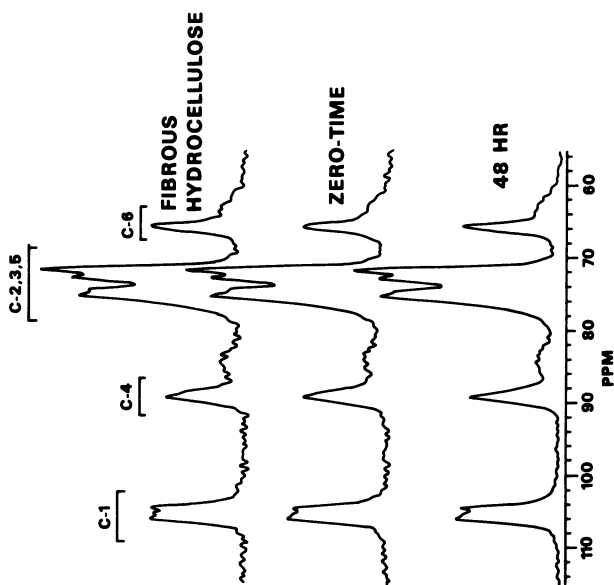


Figure 6. Solid-state ^{13}C -NMR spectra of the fibrous hydrocellulose during degradation in 1.0M NaOH at 80°C.

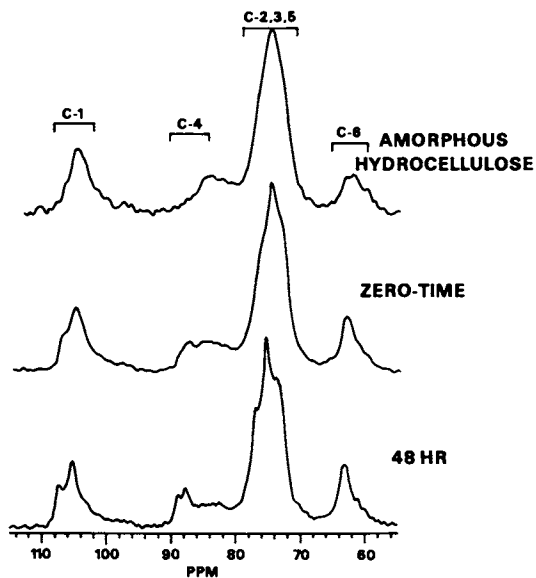


Figure 7. Solid-state ^{13}C -NMR spectra of the amorphous hydrocellulose during degradation in 1.0M NaOH at 80°C.

Resonance locations and multiplicities are characteristic of the cellulose II allomorph, confirming the results of x-ray diffraction and Raman spectroscopy.

The absence of change in the physical structure of the fibrous hydrocellulose during degradation suggests three alternative hypotheses. First, selective degradation of amorphous cellulose could have occurred but to an extent not detectable by the methods applied. Second, removal of amorphous material could have been accompanied by a comparable amount of decrystallization of cellulose I domains. Finally, cellulose removed during degradation may have displayed partial cellulose I character. This would involve molecules in slightly distorted cellulose I domains (tilted or twisted segments of elementary fibril) and at crystallite surfaces (20), since removal of either would not result in detectable changes in physical structure. Alkaline reaction data presented in the following section tend to support the latter hypothesis.

The increase in cellulose II character and decrease in accessibility of the amorphous hydrocellulose upon exposure to the alkaline medium and during the reaction interval definitely indicate partial recrystallization. However, selective removal of amorphous cellulose may have occurred simultaneously. This additional possibility is consistent with the alkaline reaction data.

Peeling and Stopping Reactions. The yield loss during alkaline degradation was more rapid and extensive for the amorphous hydrocellulose than for the fibrous hydrocellulose, at both 60 and 80°C (Figure 8). However, the evolution of yield loss with time was different at 60 and 80°C. While at 60°C yield loss occurred throughout the time interval studied (168 hr), the yield of both substrates leveled off after ca. 48 hours at 80°C. While small amounts of pectic material are probably lost during the degradations, such losses are insignificant relative to yield losses due to peeling (10).

Direct comparison of yield data for the two substrates is not possible due to the differences in initial accessible reducing end-group contents (Table I). The kinetic model used by Haas, et al. (5) was therefore employed to provide a basis for comparison of reaction rates of molecules within the two substrates. This model incorporates pseudo-first-order rate expressions for peeling (Equation 1), chemical stopping (Equation 2), and physical stopping (Equation 4); our notation differs from that of Haas, et al. In all three rate expressions, the reaction rates are related to the number of accessible reducing endgroups by pseudo-first-order rate coefficients. Thus, the rate coefficients reflect the reactivities of accessible reducing endgroups occupying different structural environments.

Since the yield losses were predominantly due to peeling (10), the pseudo-first-order rate expression for peeling can be written:

$$d[Y_1]/dt = k_p[ARE_t] \quad (1)$$

where $[Y_1]$ = Yield loss, as mole fraction of total monomer units at zero-time

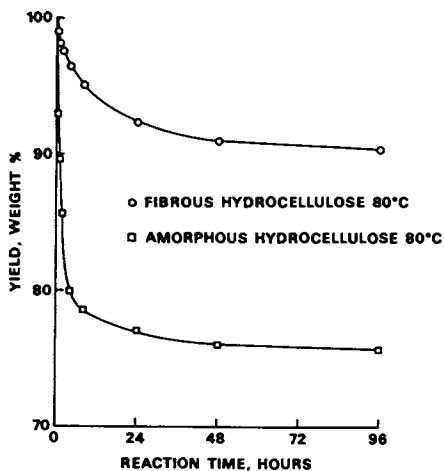
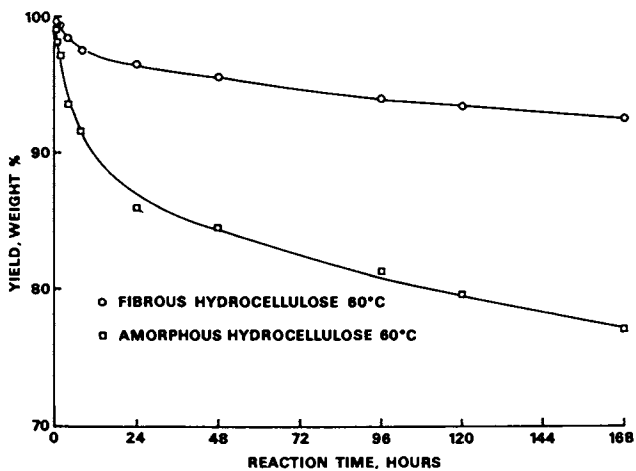


Figure 8. Hydrocellulose yield during degradation in 1.0M NaOH.

- t = Time, hr
 k_p = Rate coefficient for peeling, hr^{-1}
 $[\text{ARE}]_t$ = Accessible reducing endgroup content at time " t ,"
as mole fraction of total monomer units at zero-time

The derivative in Equation 1 was evaluated at selected reaction times from the slopes of plots of yield loss versus reaction time. Values of k_p , calculated from Equation 1, are listed in Table II.

Table II. Rate Coefficients for Peeling^a

Reaction Time, hr	60°C		80°C	
	Fibrous	Amorphous	Fibrous	Amorphous
0	4.13	6.16	27.9	40.4
2	3.28	5.52	8.91	13.6
4	2.74	4.16	8.06	6.23
48	0.48	0.60	1.38	0.19
96	0.38	0.53	0.60	0.14

^a k_p, hr^{-1} .

In all cases, k_p decreased with reaction time. Thus, the accessible reducing endgroups in both hydrocelluloses were more reactive initially, apparently due to their location in less ordered regions of the respective physical structures. As the less ordered material was removed, the accessible reducing endgroups occupied increasingly ordered regions of the structures and were therefore less reactive.

The higher k_p values for the amorphous hydrocellulose throughout the 60°C reaction and during the initial period of the 80°C reaction indicate that the accessible reducing endgroups were more reactive than those in the fibrous hydrocellulose. This coincides with the periods during which the accessibility decreased (Figure 1), suggesting that selective removal (peeling) of amorphous material did occur. Thus, the less ordered environment occupied by the degrading molecules in the amorphous hydrocellulose clearly rendered them more susceptible to peeling.

During the later period of the 80°C reaction, the amorphous hydrocellulose exhibited a lower value of k_p than the fibrous hydrocellulose. Since this corresponds to the period during which the hydroxyl accessibility of the amorphous hydrocellulose leveled-off (Figure 1), it appears that the population of degradable chains with accessible reducing endgroups had been depleted. Consequently, peeling was probably occurring close to cellulose II domains where it was significantly inhibited. In contrast, peeling progressed more slowly toward the cellulose I domains of the fibrous hydrocellulose, for example, in slightly distorted cellulose I domains, but was also strongly inhibited at the faces of more perfect cellulose I crystallites. The degree of inhibition of peeling is evidenced by the convergence of 60 and 80°C k_p values for both substrates at longer reaction times.

In the case of chemical stopping, the rate of formation of carboxylic acid endgroups is also proportional to the number of accessible reducing endgroups. The pseudo-first-order rate expression is given by:

$$[AE]/dt = k_{CS}[ARE_t] \quad (2)$$

where [AE] = Carboxylic acid endgroup content, as mole fraction of total monomer units at zero-time

k_{CS} = Rate coefficient for chemical stopping, hr^{-1}

Carboxylic acid endgroup contents were first corrected for losses of carboxylic acid groups associated with pectic material lost during the reactions (10). Values of k_{CS} were then determined at specific time intervals by the same graphical procedure as outlined for k_p ; the values of k_{CS} are given in Table III.

Table III. Rate Coefficients for Chemical Stopping^a

Reaction time, hr	60°C		80°C	
	Fibrous	Amorphous	Fibrous	Amorphous
0	0.0142	0.0302	0.106	0.262
2	0.0112	0.0271	0.0338	0.107
4	0.0094	0.0204	0.0305	0.0808
48	0.0015	0.0057	0.0119	0.0225
96	0.0010	0.0055	0.0073	0.0205

^a k_{CS}, hr^{-1} .

The rate coefficients for chemical stopping decreased with time for both substrates in a pattern similar to that for peeling. Thus, as the accessible reducing endgroups occupied progressively more ordered regions of the structures, their reactivity toward chemical stopping also decreased.

The amorphous hydrocellulose exhibited higher values of k_{CS} throughout both the 60 and 80°C reactions. During the early period of the 80°C reaction and throughout the 60°C reaction, when the rate coefficient for peeling was higher for the amorphous substrate (Table II), its higher k_{CS} value can be primarily attributed to the reaction occurring in less ordered regions of the structure. However, this could not account for the behavior in the later period of the 80°C reactions, where peeling was apparently hindered to similar extents by the crystalline regions of both structures. Therefore, it is concluded that the cellulose II domains in the amorphous substrate did not inhibit chemical stopping as drastically as the cellulose I domains in the fibrous substrate.

Further clarification of these differences is provided by comparing the relative rates of peeling and chemical stopping for the two substrates. Average values of k_p/k_{CS} (Table IV) were calculated using Equation 3, derived by dividing Equation 1 by Equation 2.

where [IRE] = Inaccessible reducing endgroup content, as mole fraction of total monomer units at zero-time
 k_{ps} = Pseudo-first-order rate coefficient for physical stopping

Although physical stopping is not a chemical reaction, per se, k_{ps} values determined using Equation 4 may be compared to k_{cs} values, providing a measure of the relative importance of the two modes of stopping. Furthermore, comparison of k_{ps} values for two substrates gives an indication of the relative extent of structural hindrance to peeling.

In both the 60 and 80°C reactions, the fibrous hydrocellulose exhibited higher k_{ps} values than the amorphous hydrocellulose (Table V). This appears to be due to the involvement of more molecules in crystalline domains of the fibrous substrate. The greater inhibition of chemical stopping by cellulose I than cellulose II domains may also have contributed to this effect by allowing more molecules in the fibrous hydrocellulose to peel to a point where the reducing endgroup would be inaccessible.

Table V. Rate Coefficients for Physical Stopping^a

Reaction Time, hr	60°C		80°C	
	Fibrous	Amorphous	Fibrous	Amorphous
0	0.0410	0.0142	0.363	0.154
2	0.0218	0.0137	0.0812	0.0700
4	0.0157	0.0132	0.0543	0.0195
48	0.0032	0.0021	0	0
96	0.0028	0.0019	0	0

^a k_{ps}, hr^{-1} .

At 80°C and for longer reaction times, both hydrocelluloses ceased physical stopping. This may be an indication that each physical structure has some maximum number of potential physical stopping sites. As a consequence, inaccessible reducing endgroups could become accessible as adjacent molecules are removed by peeling, giving rise to a steady state distribution of accessible and inaccessible reducing endgroups.

Except for the later period of the 80°C reactions, the fibrous hydrocellulose exhibited a higher value of k_{ps} (Table V) than k_{cs} (Table IV). Consequently the degradation of a majority of the molecules in the fibrous hydrocellulose was terminated by physical rather than chemical stopping processes. In contrast, chemical stopping was the dominant mechanism of stabilization in the amorphous hydrocellulose.

Random Chain Cleavage Reaction. In addition to peeling, cellulose is also reported to undergo random cleavage of glycosidic linkages in alkaline media (1,2). This reaction results in the formation of

one reducing and one nonreducing endgroup. Since reducing endgroups can also be involved in peeling and stopping reactions, it is not possible to monitor directly their formation due to random chain cleavage. However, the rate of chain cleavage can be characterized by monitoring increases in the total number of endgroups. Accurate characterization of the reaction does require that no other changes in the total number of endgroups occur, as for example, from loss of molecules by complete peeling or dissolution.

During degradation of the fibrous hydrocellulose, no changes in total endgroup content were detected (Table VI). This is consistent with results of previous studies (6,7) in which chain cleavage was found to be important in native cellulose only above 100°C.

Table VI. Total Endgroup Contents^a of Hydrocelluloses

Reaction Time, hr	60°C		80°C	
	Fibrous	Amorphous	Fibrous	Amorphous
0	1.94	4.13	1.88	4.51
2	1.94	3.57	1.90	4.28
4	1.92	3.44	1.96	4.35
8	2.04	3.52	1.96	4.44
24	1.95	3.59	1.89	4.96
48	1.92	3.65	1.89	5.05
96	1.86	3.76	1.90	5.35
168	1.89	4.09	--	--

^aExpressed as $10^3 \times$ mole fraction of total monomer units at zero-time.

In contrast, the amorphous hydrocellulose underwent initial decline in total endgroup content (Table VI) which may be attributed to complete peeling and/or dissolution of low DP molecules. After the initial periods, total endgroup contents increased gradually at both 60 and 80°C, indicating that random chain cleavage occurred. Random chain cleavage must also have occurred during the initial periods but was probably masked by the more substantial negative effects of complete peeling or dissolution on the total endgroup contents.

The amorphous substrate suffered the most rapid decline in hydroxyl accessibility (Figure 1) during the same periods in which total endgroup losses occurred. This indicates that complete peeling or dissolution primarily involved molecules existing entirely within amorphous regions and became insignificant once the majority of highly accessible chains had been removed or chemically stabilized. Further support is thus provided for the hypothesis that selective peeling of amorphous material contributes to the higher rate coefficient of peeling in the case of the amorphous hydrocellulose (Table II). The comparative lack of similar losses from the fibrous substrate suggests that the large majority of molecules were embedded to some extent in crystalline regions.

Because endgroup losses occurred simultaneously with random chain cleavage during the initial periods, analysis of the total endgroup data for kinetics of chain cleavage was confined to the later reaction periods. Since the total number of monomer units, or yield, is essentially equal to the number of glycosidic linkages, the pseudo-first-order rate expression for random chain cleavage can be written as:

$$d[TE]/dt = k_{CC}[Y_t] \quad (5)$$

where [TE] = Total endgroup content, as mole fraction of total monomer units at zero-time
 k_{CC} = Rate coefficient for random chain cleavage, hr^{-1}
 $[Y_t]$ = Yield, as mole fraction of total monomer units at time "t"

Rate coefficients for random chain cleavage in the 60°C amorphous hydrocellulose reaction decreased gradually from 8 to 168 hours (Table VII). At 80°C, the decrease in k_{CC} occurred more rapidly between 2 and 48 hours, with a more gradual decline up to 96 hours. This reflects the more rapid decline in accessibility of the amorphous hydrocellulose at 80°C (Figure 1). Thus, random chain cleavage appears to be inhibited by the larger cellulose II fraction that formed in the amorphous substrate at 80°C.

Table VII. Rate Coefficients^a for Random Chain Cleavage

Reaction Time, hr	60°C		80°C	
	Fibrous	Amorphous	Fibrous	Amorphous
0	0	ND	0	ND
2	0	ND	0	5.78×10^{-5}
8	0	8.42×10^{-6}	0	5.31×10^{-5}
48	0	8.38×10^{-6}	0	0.82×10^{-5}
96	0	8.34×10^{-6}	0	0.49×10^{-5}
168	0	7.53×10^{-6}	--	--

^a k_{CC}, hr^{-1} .

ND = Rate coefficients not determined due to simultaneous complete peeling or dissolution

The absence of chain cleavage in the fibrous hydrocellulose suggests that its disordered regions were more highly structured than the corresponding regions of the amorphous hydrocellulose. This is consistent with the results of a previous study (6) in which mercerized cellulose was found to be more susceptible to random chain cleavage than native cellulose. Another implication is that the disordered regions associated with the two crystalline polymorphs display different degrees of structural order, giving rise to differences in reactivity. Thus, in addition to molecular mobility and accessibility, the particular molecular conformation

appears to influence susceptibility to the random chain cleavage reaction.

Conclusions

Alkaline peeling and chemical stopping occur more rapidly in the amorphous regions of amorphous hydrocellulose than in the disordered regions of fibrous hydrocellulose. In addition, random chain cleavage at 60 and 80°C occurs only in amorphous hydrocellulose. Therefore, it is proposed that the disordered regions of the fibrous hydrocellulose consist of less reactive molecules at crystallite surfaces and in slightly distorted crystalline domains, as previously suggested (20).

Peeling is inhibited to similar extents by the crystalline order of both cellulose I and II allomorphs, while chemical stopping is significantly more inhibited in the cellulose I allomorph. This is consistent with the higher ratio of the rate of chemical stopping to that of peeling typically reported for mercerized cellulose in comparison to native cellulose (3,6-8).

Physical stopping, that is, formation of inaccessible reducing endgroups, occurs when peeling of molecular chains reaches the crystalline domains in both cellulose I and II. The relative rates of physical and chemical stopping are dictated by the number of molecules involved in crystalline domains. In a previous study (5), cellulose molecules were reported to maintain constant reactivity toward peeling and chemical stopping unless physical stopping occurred. However, the results of the present study indicate that reactivity diminishes gradually as reactions approach more highly ordered regions of physical structure. Simultaneously, abrupt physical stopping can occur.

The rate of chemical stopping increases with temperature relative to peeling in both fibrous and amorphous hydrocellulose. This observation is consistent with previous findings (5).

Experimental

Cellulose Substrates. Raw cotton fiber cut in ca. 0.25 inch lengths was purified by extraction with chloroform, 95% ethanol, boiling 1% (w/w) sodium hydroxide (oxygenfree), and diethylene triamine-pentaacetic acid (0.15% w/v, pH 9) (10). Fibrous hydrocellulose was prepared by treating the purified fibers (60 g) with 0.1M hydrochloric acid (6L) at 40°C for 20 hours, washing with distilled water (until neutral), and then freeze-drying. Amorphous hydrocellulose was prepared by dropwise addition of a DMSO-PF solution of the fibrous hydrocellulose (0.2%, w/v, cellulose/DMSO, 3.5L) to 0.2M sodium methoxide-isopropoxide solution (1:1, v/v, methanol:isopropanol, 14L) (9,10). The resulting precipitate was washed with 0.2M sodium methoxide-isopropoxide, methanol (until neutral), 0.1M hydrochloric acid, and distilled water (until neutral), and then freeze-dried. Both the fibrous and amorphous hydrocelluloses were further dried in vacuo over phosphorus pentoxide to constant weight.

Degradation Procedure. Alkaline degradations were conducted in 316 stainless steel laboratory digesters (10). Hydrocellulose substrate

(400 mg) and oxygen-free 1.0M sodium hydroxide (40 mL) were sealed in the reaction vessels under nitrogen, and the vessels were rotated end-over-end at ca. 3 rpm in a constant temperature oil bath. The reaction mixtures were maintained at 60 or 80°C for the specified time interval, cooled to 20°C, and neutralized with 1.0M hydrochloric acid. Zero-time samples were prepared by limiting the time at the reaction temperature to ca. one minute. Degraded hydrocellulose was washed with 0.1M hydrochloric acid and distilled water (until neutral), and then freeze-dried. Yield was determined after further drying in vacuo over phosphorus pentoxide to constant weight.

Analytical Methods. Carboxylic acid endgroup contents were determined by methylene blue absorption using TAPPI Standard Method T237 su-63 with minor modifications (10). Accessible reducing endgroups were detected by reduction with sodium borohydride-³H, and total reducing endgroups were determined similarly after regenerating the cellulose from the DMSO-PF solvent (9,10). Inaccessible reducing endgroup contents were calculated as total less accessible reducing endgroup contents.

Cellulose hydroxyl accessibility was measured by the deuteration method of Rouselle and Nelson (13), but the deuteration time (in liquid D₂O) was extended to 12 hours (10). X-ray diffractograms were collected on a Norelco diffractometer, using nickel-filtered, CuK α radiation. Raman spectra were acquired with a Jobin Yvon Ramanor Spectrometer, utilizing the 5145 Å line of an argon laser operated, at 100 mw, as the exciting source. Solid-state ¹³C-NMR spectra were obtained on a General Electric S-100 instrument employing the combined techniques (16,17) of proton-carbon cross polarization, high power proton decoupling, and magic-angle sample spinning.

Acknowledgments

The authors wish to thank Dr. T. Early of GE-NMR Instruments Company, Inc. for obtaining the solid-state ¹³C-NMR spectra and Mr. C. Woitkovich for acquiring the Raman spectra. V. M. Gentile sincerely appreciates fellowship support from The Institute of Paper Chemistry during this work.

References

1. Meller, A. Holzforschung 1960, 14, 78 and references cited therein.
2. Richards, G. N. In Cellulose and Cellulose Derivatives; Part V, p. 1007 and references cited therein, N. Bikales and L. Segal (Eds.), Wiley-Interscience, New York, 1971.
3. Machell, G.; Richards, G. N. Tappi 1958, 41, 12.
4. Colbran, R. L.; Davidson, G. F. J. Textile Inst. 1961, 52, T73.
5. Haas, D. W.; Hrutfiord, B. F.; Sarkanen, K. V. Appl. Polymer Sci. 1967, 11, 587.
6. Lai, Y.-Z.; Sarkanen, K. V. Cellulose Chem. Technol. 1967, 1, 517.

7. Franzone, O.; Samuelson, O. Svensk Papperstid. 1957, 60, 872.
8. Christofferson, K.; Samuelson, O. Svensk Papperstid. 1962, 65, 571.
9. Gentile, V. M.; Schroeder, L. R.; Atalla, R. H. J. Wood Chem. 1986, 6, 1.
10. Gentile, V. M. Doctoral Dissertation, The Institute of Paper Chemistry, Appleton, Wisconsin (1986).
11. Nicholson, M. D.; Johnson, D. C.; Haigh, F. C. Appl. Polymer Symp. 1976, 28, 931.
12. Baker, T. J.; Schroeder, L. R.; Johnson, D. C. Cellulose Chem. Technol. 1981, 15, 311.
13. Rouselle M. A.; Nelson, M. L. Textile Res. J. 1971, 41, 599.
14. Wadsworth, L.C.; Cuculo, L. C. In Modified Cellulosics, Part III, p. 117, R. M. Rowell and R. A. Young (Eds.), Academic Press, New York, 1978.
15. Atalla, R. H. J. Appl. Polymer Sci. (Appl. Polymer Symp.) 1983, 37, 295.
16. Earl, W. L.; VanderHart, D. L. Macromolecules 1981, 14, 570.
17. VanderHart, D. L.; Atalla, R. H. Macromolecules 1984, 17, 1465.
18. Tripp, V. M. In Cellulose and Cellulose Derivatives, Part IV, p. 305, N. Bikales and L. Segal (Eds.), Wiley-Interscience, New York, 1981.
19. Howsmon, J. A.; Sisson, W. A. In Cellulose, Part I, 2nd Ed., p. 231, E. Ott and H. M. Spurlin (Eds.), Interscience Publishers, New York, 1954.
20. Rowland, S. P. In Modified Cellulosics, Part III, p. 162, and references cited therein, R. M. Rowell and R. A. Young (Eds.), Academic Press, New York, 1978.

RECEIVED March 5, 1987

Chapter 17

Intra- and Intermolecular Hydrogen Bonds in Native, Mercerized, and Regenerated Celluloses Reflection in Patterns of Solubility and Reactivity

A. Isogai¹, A. Ishizu¹, J. Nakano¹, and Rajai H. Atalla²

¹Department of Forest Products, Faculty of Agriculture, University of Tokyo,
Bunkyo-ku, Tokyo 113, Japan

²Institute of Paper Chemistry, Appleton, WI 54912

An unusual pattern of dissolution of cellulose and related polysaccharides in the SO₂-amine-DMSO system has been observed, and interpreted in terms of distinctive hydrogen bonding patterns. In particular, it was found that only native and mercerized cellulose dissolve in this system, while regenerated celluloses, glucomannan, xylan, starch, pectin and curdlan are insoluble. The pattern for the celluloses has been correlated with relative reactivities of hydroxyl groups in etherification reactions in different environments, and with results of solid state ¹³C NMR studies on the celluloses and related oligosaccharides and polysaccharides. They suggest that the solvent system acts at particular sites involving cooperative hydrogen bonding incorporating, among others, the primary hydroxyl group at C6 and the linkage oxygen.

Our proposal has the key implication that regenerated and mercerized celluloses have different patterns of intermolecular hydrogen bonding, even though they may have similar heavy atom lattices. This is analogous to what has been proposed as the key difference between the I_α and I_β forms of native cellulose. Taken together these findings suggest that the organization and packing of the heavy atom lattices in celluloses are dominated by the shapes of the molecules in their different conformations, and that more than one stable pattern of intermolecular hydrogen bonding is consistent with each heavy atom lattice.

The supermolecular structures of cellulose have been investigated extensively by many techniques including x-ray and electron diffraction, electron microscopy, IR and Raman spectroscopy, broad-line proton NMR and solid-state ¹³C-NMR. Nevertheless, many questions remain concerning the solid-state structures.

0097-6156/87/0340-0292\$06.00/0
© 1987 American Chemical Society

During our studies on cellulose chemistry (1-5), we have encountered an unusual pattern of solubilities of various celluloses and related polysaccharides in one of the nonaqueous cellulose solvent systems we investigated, the SO₂-diethylamine(DEA)-dimethylsulfoxide(DMSO) system. In this paper, we propose an interpretation of this pattern in terms of intra- and intermolecular hydrogen bonds in native, mercerized and regenerated celluloses. We also consider parallels with the relative reactivities of hydroxyl groups in glucose residues of cellulose toward etherification, under basic conditions, and the data from solid-state ¹³C-NMR reported by Atalla and others (6-9).

Experimental

Sample Preparations. The native celluloses used were Avicel, cotton linters and ramie. Degrees of polymerization of Avicel and the cotton linters determined by the copperethylenediamine viscosity method (10) were 250 and 1360, respectively. Mercerized samples were prepared from these celluloses by stirring in 24% NaOH solution containing 1% NaBH under a nitrogen atmosphere for 20 hrs at room temperature. The samples were washed on a 1G2 glass filter with large amounts of water, dilute acetic acid, large amounts of water again and, finally, acetone. They were dried at 40°C in vacuo for 1 day. Regenerated samples were prepared from native celluloses by dissolving in cadoxene (11), and regenerating by dropwise addition to dilute acetic acid. The regenerated cellulose was filtered and washed with large amounts of water. Half of each sample was washed with acetone and dried at 40°C in vacuo for 1 day, and the other half was subjected to lyophilization followed by drying at 40°C in vacuo for 1 day.

Amylose and starch, both derived from potato, were commercial samples. Glucomanan and xylan were isolated from spruce and beech holocelluloses, respectively, and purified by the usual method (12). Pectin was isolated and purified from the midrib of *Nicotiana tabacum* and kindly provided by Dr. Shigeru Eda at The Central Research Institute, Japan Tobacco Inc. (5).

The solubility of the polysaccharides was tested by dispersing 1g of a dried sample in 42 ml DMSO, and then adding the SO₂/DMSO solution containing 1.19 g of SO₂ (4.09 ml of 0.291 g SO₂/ml DMSO solution) and 1.92 mo DEA, in this order at room temperature. Successful dissolution was judged by visual examination after stirring for 1 day.

Results and Discussion

1. Solubilities of celluloses and other polysaccharides in the SO₂-DEA-DMSO system

In our previous work on the derivatizations of cellulose (1-5), we have found the SO₂-DEA-DMSO system to be the most effective nonaqueous cellulose solvent medium for the preparation of highly substituted cellulose ethers. The solubilities of various cellulosic samples and other polysaccharides in this nonaqueous solvent system were tested in the course of the investigations. As shown in

Table I, native celluloses such as ramie, cotton linters and Avicel, both before and after mercerization dissolved completely in this solvent system. More recently we have established that highly crystalline algal celluloses are also readily dissolved in this system.

Table I. Solubilities of Various Polysaccharides in SO_2 -diethylamine-DMSO System

Soluble	Native celluloses (ramie, linter, Avicel) Mercerized celluloses (ramie, linter, Avicel)
Insoluble	Amylose, starch, glucomannan, xylan, pectin Regenerated cellulose (ramie, linter, Avicel)

In sharp contrast, regenerated cellulose samples prepared from ramie, cotton linters and Avicel do not dissolve, even after decrystallization by ball-milling. Furthermore, amylose, starch, glucomannan, xylan and pectin were also found to be insoluble in this system. Our finding concerning regenerated samples consistent with the report by Yamazaki and Nakao (13) that commercially available rayons, even with DPv as low as 300, are insoluble in all SO_2 -amine-organic solvent systems. The patterns of solubility, or lack thereof, are curious because regenerated celluloses generally have lower crystallinities than native ones. Moreover, the other polysaccharides so far examined have lower molecular weights and crystallinities than native celluloses. In addition, amylose and starch are soluble in DMSO alone above 60°C . All the cellulose samples and the polysaccharides used in this work are soluble in other nonaqueous cellulose solvent systems such as paraformaldehyde-DMSO (14), LiCl - dimethylacetamide (15), N-methylmorpholine N-oxide (16) (containing small amounts of water) and others. Thus, the insolubility of regenerated celluloses was observed only for the SO_2 -amine systems. We believe that the differences in solubility reported in Table I may reflect different patterns of intra- and intermolecular hydrogen bonding in different celluloses.

In the previous work in which ^1H - and ^{13}C -NMR were used (17), the dissolution of cellulose in the SO_2 -DEA-DMSO system has been explained in terms of complex formation between the -OH of cellulose, and SO_2 and DEA, as shown in Figure 1. The pattern of solubilities noted earlier suggests that the complex formation reaction in Figure 1 is specific to particular intra- and/or intermolecular hydrogen bonding patterns peculiar to native and mercerized celluloses.

The dissolution characteristics of native, mercerized and regenerated celluloses, and their interpretation in terms of hydrogen bonding differences, point to some interesting relationships. Native and mercerized celluloses would seem to have some common hydrogen bonding patterns, although they have different x-ray diffraction patterns. On the other hand, mercerized and regenerated celluloses would differ from each other with respect to intermolecular hydrogen bonds, although they have the same x-ray pattern.

Recently, VanderHart and Atalla (18) proposed, on the basis of CP-MAS ^{13}C NMR of different cellulose samples, that all native cellulose are composites of two crystalline modifications, cell I_α and I_β , even though they have similar x-ray patterns. These have been interpreted in terms of similar heavy atom lattices with different hydrogen bonding patterns (19,20). Thus, it may well be that mercerized and regenerated celluloses differ in the same way and can have different intermolecular hydrogen bonding patterns, which result in differences in their solubility in the SO_2 -DEA-DMSO system.

2. Relative reactivities of hydroxyl groups in glucose residues of cellulose toward etherifications under basic conditions

We have previously reported studies on the distribution of substituents in partially etherified celluloses which were prepared from heterogeneous alkali cellulose and from homogeneous nonaqueous cellulose solutions (21). In the latter case, partially substituted cellulose ethers such as methyl- and carboxymethyl-celluloses were prepared from SO_2 -DEA-DMSO solutions of cellulose by additions of powdered NaOH as a base.

When the nonaqueous cellulose solvent was used as a medium, the order of reactivities was $6\text{-OH} > 2\text{-OH} > 3\text{-OH}$. This order is similar to observations in the case of simple alcohols. Thus, although the primary hydroxyl group 6-OH has the highest reactivity, and the secondary hydroxyl groups 2-OH and 3-OH have almost equal reactivities, the difference of reactivities between 6-OH, 2-OH and 3-OH is small. On the other hand, when heterogeneous alkali cellulose systems were used, where cellulose was swollen in aqueous alkali rather than being in solution, the order of reactivity was $2\text{-OH} > 6\text{-OH} > 3\text{-OH}$ at all concentrations of aqueous alkali (22). This order is not consistent with the pattern for lower molecular weight compounds and suggests consideration of effects of intra- and intermolecular hydrogen bonds which may remain even in swollen alkali cellulose. The secondary hydroxyl group 2-OH has a higher reactivity than the primary alcohol 6-OH, and there is a remarkable difference in reactivities between the secondary alcohols 2-OH and 3-OH. These results suggest that some of the intramolecular hydrogen bonds between the 3-OH groups and O-5 in the adjacent anhydroglucose residues, known to occur in native celluloses, are retained even in swollen alkali cellulose, and thus have an effect on the etherification process.

The resistance to disruption by alkali also suggests some strong intermolecular hydrogen bonds in cellulose. Such strong hydrogen bonds may well be the key to retention of the fiber form of alkali cellulose at all concentrations of alkali. In the case of most polymers, swelling and dissolution in solvents proceed in sequence. That is, first the accessible parts are swollen by a solvent and this is followed by dissolution. However, in the case of cellulose in aqueous alkali, although it is swollen and undergoes a lattice transformation, it does not dissolve. If the hydroxyl groups are solvated with aqueous alkali and if all intra- and intermolecular hydrogen bonds are cleaved, cellulose fibers cannot be expected to keep their form nor to form a new lattice. This suggests that

some of the strong intermolecular hydrogen bonds in native cellulose may survive in swollen alkali celluloses and contribute to the definition of the new lattice. Such a proposal seems a plausible alternative to that of Na^+ stabilization of the lattice.

It has been proposed that in alkali cellulose, alkali (NaOH) and water bridge the cellulose molecules (23). However, it does not seem likely that all direct intermolecular hydrogen bonds in alkali cellulose are disrupted, inasmuch as the fibrous morphology is retained. Additionally, there have not been any reports of any precipitates of complexes between oligomers and alkali in aqueous solutions.

There has been another proposal that plane-structures consisting of cellulose molecules in the 101 plane of native cellulose are held together by hydrophobic interactions even in the presence of alkali, and that hydrophilic surfaces of the 101 plane-structures are solvated with alkali and water (24). However, if such planar structures were solvated with aqueous alkali, they would be expected to result in the formation of a dispersion of micelles. It seems to us more likely that some strong or sterically protected intermolecular hydrogen bonds of native cellulose survive even in alkali cellulose. On the other hand, since some hydrogen bonds are cleaved by NaOH and water which penetrate into the crystalline lattice of cellulose, new lattice planes can be formed as, for example, in Na-Cellulose I or other soda celluloses.

In assessing the stability of intermolecular hydrogen bonds, the pattern of chemical reactivity of the hydroxyl groups may be an indicator. On the basis of the results of relative reactivities of the hydroxyl groups in the anhydroglucose residues, the more stable intermolecular hydrogen bonds of cellulose appear likely to involve 6-OH, because it often shows lower reactivity for etherifications than the 2-OH.

3. Solid-state ^{13}C -NMR data of various cellulose samples

^{13}C -NMR spectral shifts for cellulose and some oligomers are summarized in Figure 2 (6-9). Horii *et al.* (9) discussed the chemical shifts of C-6 carbons, and proposed that the difference between Cellulose I and Cellulose II is caused by conformational differences at the 6-OH groups. The shifts in the crystalline parts of Cellulose I were assigned to t-g conformations (ca. 66 ppm for C-6), and those for Cellulose II and the amorphous parts of all celluloses to g-t conformations (ca. 63 ppm for C-6).

In contrast, chemical shifts of the C-4 carbons change largely depending on whether cellulose is in a solid state or in solution (Figure 2). Horii *et al.* (25) suggested that this change in the chemical shift of C-4 is also caused by conformational difference. However, such a high downfield shift of C-4 carbons ($\Delta = \text{ca. } 10 \text{ ppm}$) seems unlikely to arise from a conformational difference alone. Changes in chemical shifts of carbons in low molecular sugars, which have been reported by Horii *et al.* (9), were explained mainly in terms of changes in shielding due to different hydrogen bonding patterns associated with different conformations.

The solid-state ^{13}C -NMR spectra of curdlan, amylose and chitin have also been reported (26), and generally C-1 and C-4, or C-3 in

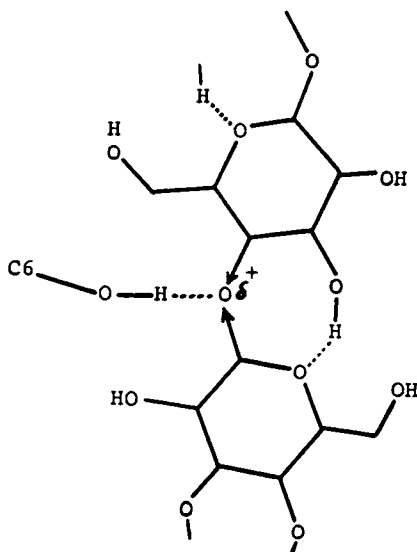


Figure 1. Dissolution mechanism of cellulose in SO_2 -amine-DMSO systems.

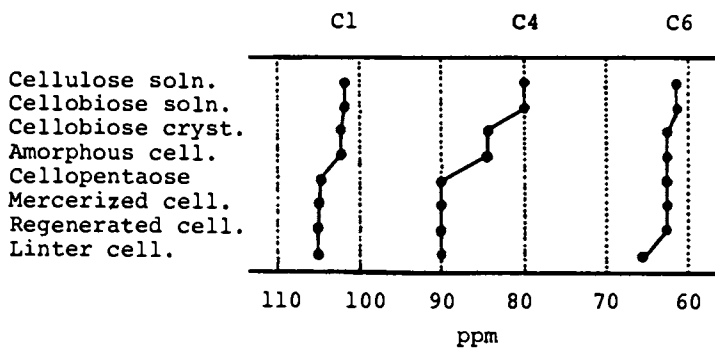


Figure 2. ^{13}C -chemical shifts of carbon in various cellulose samples.

the case of curdlan, have high chemical shifts in their solid states in comparison with shifts in solution. Table II shows the difference (Δ) between the chemical shifts in the solid state and in solution for the above glucans as well as cellulose. The table shows that Δ for C-1 carbons ranges from 1.0 to 3.0 ppm. In the case of amylose and chitin Δ 's for C-4, and in the case of curdlan Δ for C-3, are only slightly higher (4.1-4.5 ppm). On the other hand, cellulose has a much larger Δ of 10 ppm for C-4. This exceptionally high chemical shift for C-4 suggests a special difference for solid-state structures of celluloses.

Table II. Difference (Δ , ppm) of ^{13}C -Chemical Shifts Between Solid and Solution States

Sample	Linkages	Δ , ppm		
		C-1	C-3	C-4
Curdlan	(1-3)- β -D-glucan	1.0	4.2	
Amylose	(1-4)- α -D-glucan	2.3		4.5
Chitin	(1-4)- β -D-2-acetamido-2-deoxy-glucan	2.3		4.1
Cellulose	(1-4)- β -D-glucan	3.0		10.0

We propose here a possible explanation for the high value of the chemical shifts of C-4 in crystalline cellulose, namely, as represented in Figure 3, an exceptionally strong intermolecular hydrogen bond between a 6-OH and a glycosidic linkage oxygen atom. We speculate that it is the 6-OH of an adjacent chain because of the anomalously low reactivity of the primary hydroxyls in soda celluloses. Stabilization of such an intermolecular hydrogen bond can be facilitated by a transfer of electron density to the glycosidic oxygen atom from the C-4 carbon. This, in turn, can reduce the shielding at C-4 and result in the downfield shift of its resonance. Electron density at C-1 is clearly too low for it to make a significant contribution because of its anomeric character; this is reflected in its downfield shift beyond 100 ppm. Strong intermolecular hydrogen bonds stabilized by the shift of electron density could be resistant to cleavage even in concentrated aqueous alkali, and thus stabilize the morphology of the fiber.

Discussion

The results discussed in the previous sections suggest one property common to native and mercerized celluloses which is not shared by regenerated celluloses. That is their solubility in the SO_2 -amine-DMSO system. On the other hand, mercerized cellulose and regenerated cellulose possess very similar x-ray diffraction patterns, though their response to the solvent system is not the same. These patterns suggest differences between mercerized and regenerated celluloses analogous to the differences between I_α and I_β , among the components of native celluloses. Thus it is proposed that, although

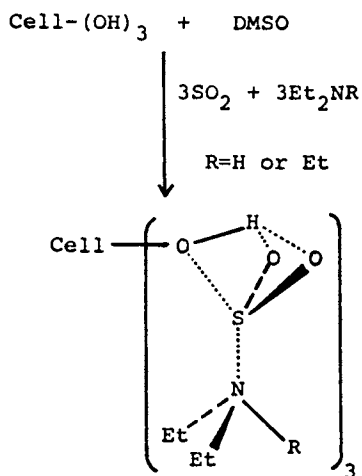


Figure 3. Possible intermolecular hydrogen bond in cellulose.

mercerized and regenerated celluloses possess the same or very similar heavy atom lattices, the patterns of hydrogen bonding developed during regeneration are unlike those which result from mercerization. Furthermore, it appears that the system of hydrogen bonds that is the specific site of attack of the SO₂-amine-DMSO system is not formed during the regeneration of cellulose from solution.

Whether the hydrogen bond of the primary hydroxyl to the glycosidic linkage oxygen is a part of this system remains an open question, since the unusually high downfield shift of the ¹³C-NMR resonance of C-4 also occurs in regenerated cellulose. It seems more likely that this hydrogen bond is part of a system of hydrogen bonds that act in concert and result in a cooperative stabilization of the system for native and mercerized celluloses. Thus, while the C-6 hydroxyl hydrogen bond to the glycosidic linkage may be formed in regeneration, the other components of the cooperative hydrogen bond system do not occur. If the action of the SO₂-amine-DMSO solvent is particularly attuned to the cooperative hydrogen bonding effect, its inability to solubilize regenerated cellulose, or any of the other polysaccharides can be accounted for.

The proposal we make here is a speculative one. We believe it valuable to present it, however, particularly in view of the differences in hydrogen bonding patterns of the I_α and I_β celluloses alluded to above. The implications of our proposal are quite important in the context of structural studies on cellulose in general, for it follows from the proposal that the packing of the heavy atom lattice is determined primarily by the shape of the molecules in their different conformations and that more than one stable pattern of hydrogen bonding is possible for each of the heavy atom lattices.

References

1. Isogai, A.; Ishizu, A.; Nakano, J. J. Appl. Polym. Sci. 1984, 29, 2097.
2. Isogai, A.; Ishizu, A.; Nakano, J. ibid. 1984, 29, 3873.
3. Isogai, A.; Ishizu, A.; Nakano, J. ibid. 1985, 30, 345.
4. Isogai, A.; Ishizu, A.; Nakano, J. ibid. in press.
5. Isogai, A.; Ishizu, A.; Nakano, J.; Eda, S.; Kato, K. Carbohydr. Res. 1985, 138, 99.
6. Atalla, R. H.; Gast, J. C.; Sindorf, D. W.; Bartuska, V. J.; Maciel, G. E. J. Am. Chem. Soc. 1980, 102, 3249.
7. Earl, W. L.; VanderHart, D. L. ibid. 1980, 102, 3251.
8. Kunze, J.; Scheler, G.; Schroter, B.; Phillip, B. Polym. Bull. 1983, 10, 56.
9. Horii, F.; Hirai, A.; Kitamaru, R. ibid. 1983, 10, 357.
10. TAPPI Standard, T 230 om-82 (1985).
11. Jayme, G.; Lang, F. Methods in Carbohydr. Chem., Vol III, Academic Press, New York, p. 80 (1963).
12. Timell, T. E. Methods in Carbohydr. Chem., Vol V, Academic Press, New York, p. 134, 137 (1965).
13. Yamazaki, S.; Nakao, O. Sen-i Gakkaishi 1974, 30, T234.
14. Gruber, E.; Gruber, R. Cellulose Chem. Technol. 1978, 12, 345.
15. Gagnaire, D.; Germain, J. S.-; Vincendon, M. J. Appl. Polym. Sci., Appl. Polym. Symp. 1983, 87, 261.

16. Chanzy, H.; Noe, P.; Paillet, M.; Smith, P. ibid. 1983, 87, 239.
17. Isogai, A.; Ishizu, A.; Nakano, J. J. Appl. Polym. Sci. under contribution.
18. VanderHart, D. L.; Atalla, R. H. Macromolecules 1984, 17, 1465.
19. Atalla, R. H. Proceedings of Paper Making Raw Materials, Vol. III, Oxford p. 59 (1985).
20. Wiley, J. H.; Atalla, R. H. Paper in this ACS Symposium Series.
21. Isogai, A.; Ishizu, A.; Nakano, J. Sen-i Gakkaishi 1984, 40, T504.
22. Rowland, S. P. Cellulose Chem. Technol. 1980, 14, 423.
23. For example, T. Okano and A. Sarko J. Appl. Polym. Sci. 1985, 30, 325.
24. For example, F. J. Kolpak and J. Blackwell Macromolecules 1976, 9, 275.
25. Horii, F.; Hirai, A.; Kitamaru, R. ACS Symposium Series, No. 1984, 260, p. 27.
26. Saito, H.; Tabeta, R.; Hirano, S. Proceedings of the Second International Conference on Chitin and Chitosan in 1982 (Japan), p. 72.

RECEIVED March 5, 1987

Author Index

- Atalla, Rajai H., 1,88,151,272,292
Bertoniere, Noelle R., 255
Blackwell, John, 199
Bresee, Randall R., 214
Chanzy, H., 189
Eckhardt, B., 68
Fateley, William G., 214
Fellers, John F., 233
Fink, H.-P., 178
French, A. D., 15,68
Gentile, Victor M., 272
Hatano, Masahiro, 135
Hayashi, Jisuke, 135
Henrissat, Bernard, 38
Hirai, A., 119
Horii, F., 119
Ishizu, A., 292
Isogai, A., 292
Kitamaru, R., 119
Kon, Hiroshi, 135
Kunze, J., 178
Kurz, David, 199
Lee, David M., 199
Lin, J. S., 233
Miller, D. P., 15
Nakano, J., 292
Nishimura, Hisao, 169
Nozawa, Tsunenori, 135
Okano, Takeshi, 169
Perenich, Theresa A., 214
Perez, Serge, 38
Philipp, B., 178
Quenin, I., 189
Roughhead, W. A., 15
Sakthivel, A., 68
Sarko, Anatole, 169
Schroeder, Leland R., 272
Su, Mao-Yao, 199
Takai, Mitsuo, 135
Tang, Ming-Ya, 233
Tvaroska, Igor, 38
VanderHart, D. L., 88
Wiley, James H., 151
Winter, William T., 38
Yang, Charles Q., 214
Young, R. A., 68
Zeronian, S. Haig, 255

Affiliation Index

- Academy of Sciences of the German
Democratic Republic, 178
Case Western Reserve University, 199
Centre National de la Recherche
Scientifique, 38,189
Clemson University, 15
Georgia Institute of Technology, 68
Hokkaido University, 135
Institute of Paper
Chemistry, 1,88,151,272,292
Kansas State University, 214
Kyoto University, 119
National Bureau of Standards, 88
Oak Ridge National Laboratory, 233
Southern Regional Research
Center, 255
State University of New York, 169
Tohoku University, 135
U.S. Department of Agriculture, 15,68
University of California--Davis, 255
University of Georgia, 214
University of Tennessee, 233
University of Tokyo, 292

Subject Index

- A
- Accessibility
 calculation for moisture-regain method, 264
 cotton, 264t
 endgroups in alkaline degradation, 283
 fibrous hydrocellulose, 274-275
 mercerized cotton, 264t
 See also Hydroxyl accessibility
- Acetobacter xylinum
 bacteria cellulose, 89
 carbon-13 CP-MAS spectra, 96f
 crystalline native cellulose, 11
 nascent fibril of cellulose, 130
 NMR spectra, 113
- Acid hydrolysis
 cellulose, 257
 effect on cotton linters, 98f
 effect on spectral changes of cotton linters, 97
 See also Hydrolysis
- Algal cellulose
 crystalline polymorphy, 115
 orientation, 156f
 unit cell, 153
 See also Rhizoclonium hieroglyphicum
- Alkali treatment, cellulose, 178-187
- Alkaline degradation
 description, 272
 hydrocellulose, 280f
 structure changes, 274-281
- Alkaline peeling--See Peeling
- Allomorphs
 carbon-13 NMR spectra, 146-149
 cellulose, 3
 cellulose II family, 142
 CH₂ stretching bands, 141t
 Cladophora cellulose, 105-106
 glucose ring stretching, 144t
 infrared spectra, 138-146
 irreversibility of cellulose I, 135-136
 magnetically inequivalent sites, 110
 native celluloses, 88-116
 OH stretching bands, 138,141t
 spectra changes from mechanical beating, 97
- Amorphous fraction, cellulose sample, 263
- Amylose
 effect of water on CP-MAS spectra, 124
- Amylose--Continued
 polymorphs, 189
- Angular modulation frequency, FT-IR-PAS, 217
- Anhydroglucose
 assignment of carbon-13 resonances, 95
 nonequivalence along chains, 113
 unit cell, 111
- Anisotropic bulk magnetic susceptibility, mechanism, 90-91
- Anisotropy, cellulose orientation, 166
- Anselme Payen, 2
- Antiparallel model
 cellotetraose, 82-83t,86
 cellulose I, 200
 cellulose I-ethylenediamine complexes, 207
 cellulose II, 200-203
 X-ray diffraction patterns for cellotetraose, 76f,85f
- Attenuated total reflectance, cellulose textile materials, 214
- Availabilities, hydroxyl groups, 261-262
- B
- Bacterial cellulose
 CP-MAS NMR spectra, 129f
 crystalline spectra, 126
 nascent microfibrils, 149
 Raman spectra, 158,162f
 size of the crystallites, 161-164
- Band assignments, Raman spectroscopy, 161
- Biosynthesis, cellulose, 4
- Bromine sorption, measurement of accessibility, 265
- Browning's method, 94
- C
- Carbon-13 chemical shifts
 cellulose, 297f
 See also Chemical shifts
- Carbon-13 longitudinal relaxation time, observations, 102-106

- Carbon-13 NMR spectra
 allomorphs, 146-149
 cellotetraose, 63-64
 cellulose, 296
 cellulose disordering by alkali
 treatment, 178
 cellulose resonance
 multiplicities, 90-91
 cotton
 linters, 180f, 181f, 182-184, 186f
 guanidonium hydroxide-treated
 cellulose, 184-185
 hydrocellulose, 275
 hydrocellulose during alkaline
 degradation, 279f, 280f
 isolation of crystalline core, 100
 methyl β -D-cellobioside, 63-64
 native cellulose, 88-116, 153
 procedure in alkali treatment
 study, 179
 structural irreversibility
 study, 138
 viscose fiber, 180f
 Carbon-13 spin exchange
 Dante sequence, 94
 hydrocellulose from cotton
 linters, 110-111
 Cell symmetry
 ramie cellulose, 18-19
 See also Symmetry
 Cellobiose
 charge densities, 47-48
 conformational energy well, 44f
 conformations, 45
 crystalline state, 50f
 energy map, 45
 numbering of atoms and torsion
 angles, 39
 packing in crystals, 48
 preparation in structural study, 41
 relative energies of stable
 conformers, 45t
 schematic representation, 39f
 Cellodextrins
 conformations, 62f
 X-ray diffraction, 39
 Cellotetraose
 antiparallel orientation, 63
 computer model building, 73
 crystal data, 55t
 crystallization, 42
 fractional coordinates of atoms, 60t
 micrograph of microcrystals, 57f
 molecular formula, 73
 projection onto base plane, 61f
 Rietveld crystal structure
 application, 7
 similarity to cellulose II, 68
 small-angle powder diffraction, 71f
 space group, 68-69, 74
 structure, 39, 59t, 63
 unit cell content, 61f
 Cellotetraose--Continued
 wide-angle neutron powder
 diffractogram, 56f
 wide-angle X-ray powder
 diffraction, 71f
 X-ray diffraction data, 55-58
 Cellulose
 acid hydrolysis, 257
 algae, crystalline composite
 hypothesis, 93
 alkali treatment, 178-187
 alkaline degradation
 procedure, 289-290
 allomorphs, 3
 amorphous, alkaline degradation, 281
 antiparallel models, 75
 availability of hydroxyl
 groups, 261-262
 band assignment in vibrational
 spectrum, 161
 biosynthesis, 4
 carbon-13 chemical shifts, 297f
 chain axis, orientation, 154
 chains
 glycosidic
 linkages, 8-9, 185, 286-287
 mobility in hydrated
 state, 128-130
 chemical characterization, 255-269
 comparison of structural types, 12
 complexes
 formation in structural study, 204
 X-ray studies, 199-212
 conformation, 167
 conformational stability in
 derivatization reactions, 10
 contributions from crystalline and
 noncrystalline regions, 124-126
 correlations between chemical shifts
 and dihedral angles, 10
 CP-MAS carbon-13 NMR study, 119-133
 cross-section spectra, 166
 crystal structure, 18, 126-133, 35
 crystalline allomorph, 3, 110-111, 234
 crystallinity
 determinations, 255-257
 crystallite length, 265
 crystallization in molecular weight
 study, 190
 crystals
 electron micrographs, 195f
 two-step growth pattern, 197
 description, 119, 234
 deuterated, 142
 diffractometric studies, 5-7
 dissolution, 294, 297f
 effect of acid hydrolysis, 113-114
 effect of complexing agent, 211
 esters, irreversible
 conversions, 136
 etherifications, 295-296
 families, chain conformation, 148

Cellulose--Continued

fiber
 composition, 174
 photoacoustic infrared spectra, 220f
 first recognized, 2
 formylation, 257-258
 frame relaxation times, 100
 glycosidic linkage treatment, 185
 hydrogen bonds, 197,299f
 hydroxyl accessibility
 measurement, 290
 lateral order distribution, 266
 line positions after alkali treatment, 180t
 low and high temperature polymorphs, 190
 mercerized, hydrogen bonds, 292-300
 microcrystallites, 251
 microfibrils, biosynthesis, 203
 mobility of crystal chains, 114-115
 morphology of
 recrystallized, 196-198
 NMR spectra of
 alkali-treated, 179-185
 oligomers
 CP-MAS, 54f
 structures, 58-65
 organic solvents, 199
 orientation, 164-167
 parallel chains, 200
 parallel-up models, 75
 polymorphy, 161-164,196
 pore volume fraction, 249t
 preparation in CP-MAS carbon-13 NMR study, 130
 recrystallized
 polymorphic and morphological aspects, 189-198
 X-ray diagram, 193f
 regenerated, hydrogen bonds, 292-300
 resemblance to mannan crystals, 196-197
 resistance to disruption by alkali, 295
 SAXS source, 245
 solid-state carbon-13 NMR spectra, 296-298
 solid-state structural changes, 187
 solubilities in SO₂-DEA-DMSO system, 293-295
 spectroscopy, 7-10
 spectrum of fully deuterated, 158
 structural models, 2,132f
 structure
 description, 1-12,234-235
 determination difficulties, 2
 future directions, 11-12
 multidisciplinary studies, 10
 questions of general interest, 19
 Valonia ventricosa, 4
 tetramer packing, 75

Cellulose--Continued

textile materials
 chemical additive examination, 230
 FT-IR-PAS, 214-230
 threefold helices, 172
 transformation to cellulose II, 135
 transformation to Na-cellulose, 171f
 treatment with aqueous guanidonium hydroxide, 185
 uniformity of chemical additives, 221-226
 unit cell symmetry, 5
 vibrational spectrum, 155-161
 X-ray diffraction studies, 15
 Cellulose I
 base plane of the unit cell, 16
 chain geometry, 136
 chemical stopping in alkaline degradation, 284-285
 conversion to Na-cellulose I, 174
 crystalline forms, 126-128
 difference from cellulose II, 296
 difference from Na-cellulose I, 170
 intra-chain hydrogen bonds, 142
 nonequivalent glycosidic linkages, 8
 parallel packing, 137
 peeling inhibition, 289
 polarity of adjacent chains, 200
 Raman spectroscopy, 8
 refinements of structures, 6
 spectrum, 111
 structural irreversibility, 135-149
 structure, 200,201f
 unit cell, 16,17f
 See also Native cellulose
 Cellulose I-1,3-diaminopropane complex, structure, 210f
 Cellulose I-ethylenediamine complex, structure, 207,208f
 Cellulose II
 cellotetraose similarity, 68
 chain conformation, 148
 chain geometry, 136
 chemical stopping in alkaline degradation, 284-285
 conversion product of Na-cellulose IIB, 176
 crystal structure, 64
 crystals, electron micrographs, 193f
 differences from native cellulose, 164
 diffraction, 191
 effect of degree of polymerization on morphology, 197
 family, parallel dichroism, 142-144
 models, 63
 peeling inhibition, 289
 preparation in irreversibility study, 137
 Raman spectra, 154
 spectra of high crystallinity samples, 9

- Cellulose II--Continued
 stability compared with cellulose I, 203
 structural difference to cellulose I, 8
 structure, 38-65,202f
 unit cell, 200-203
- Cellulose II-hydrazine complex A, 212f
- Cellulose III
 preparation in irreversibility study, 137
 unit cell, 148
- Cellulose IV
 preparation in irreversibility study, 137
 X-ray diffraction, 191,192
- Cellulose-diaminopropane complexes, unit cells, 206t
- Cellulose-ethylenediamine complexes, unit cells, 206t
- Cellulose-hydrazine complexes, unit cells, 206t
- Cellulose triacetate, fibers, spectral characteristics, 219
- Cellulose trinitrate I, saponified into cellulose I, 136
- Chain axes, cellulose II, 192
- Chain cleavage
 pseudo-first-order rate expression, 288
 rate coefficients, 288t
- Chain conformation
 cellulose, 140f,146
 cellulose I, 4,138-141,200
 cellulose I-ethylenediamine complex, 205
 cellulose II, 4,138-141,148,200-203
 cellulose II-hydrazine complex, 211
 Na-cellulose I, 170
 ramie cellulose, 18
 unit cell, 142
 use of carbon-13 NMR spectra, 178
- Chain packing
 Na-cellulose IV, 172
 polarity of cellulose I and Na-cellulose I, 170-172
- Chain polarity
 cellulose, 4
 transformation from cellulose I to Na-cellulose, 170
- Chain stacking, cellulose, 176
- Chemical microstructural analysis, description, 258-262
- Chemical shifts
 allomorphs, 146-148
 cellulose, dependence on packing and hydrogen bonding, 122-124
 crystalline cellulose, 298
See also Carbon-13 chemical shifts
- Chemical stopping
 alkaline degradation of hydrocellulose, 284-286
- Chemical stopping--Continued
 rate coefficients, 284t
- Chitin
 cellulose II complex similarity, 211
 structure, 207
- Cladophora cellulose
 allomorphs, 105-106,116
 carbon-13 NMR spectra, 97-99,104f,111
 candidates for CP-MAS spectra, 112f
 changes in lineshape, 105
 hydrolysis, 115
 multiple crystalline forms, 100
See also Cladophora glomerata
- Cladophora glomerata
 beating of algal cellulose, 94
 spectra, 95-97
See also Cladophora cellulose
- Coefficient of variation,
 crystallinity of cotton by X-ray determination, 257
- Computer techniques, X-ray diffraction data, 4-7,21-25
- Conformational analysis, cellulose II structural study, 41-42,45-47
- Conformations, celluloses I and II, 137
- Contrast variation, technique, 235
- Cotton
 accessibility, 264t
 aggregate fractals, 250-252
 permeability limits, 267t
 SAXS, 234
 structural similarity to ramie, 16
 thermal diffusion length, 227t
 volume accessible to water, 267t
See also Greige cotton
- Cotton cellulose
 aggregate structure, 251-252
 CP-MAS carbon-13 NMR spectra, 124,125f,127f,131f
 growth process, 235
 SAXS, 236-238
 spectra
 crystalline components, 126-133
 noncrystalline components, 128-130
 use, 214
 WAXD, 238-245
- Cotton fabrics
 carbonyl peak intensities, 226t
 distribution of the finishing agents, 224
 finishing agents, 224
 wrinkle recovery properties, 224-226
- Cotton fiber
 chemical microstructural analysis, 262
 methine orientation, 166
 Raman spectra, 154
- Cotton hydrocellulose
 CP-MAS spectra, 103f
 spectra as function of delay time, 102

- Cotton linters
 carbon-13 NMR spectra, 92f,179-185
 cellulose I WAXS pattern, 182
 spectral changes accompanying acid hydrolysis, 97
- Cotton yarn
 carbonyl peak after sizing, 223t,224t
 depth of sizing agent examined, 226-230
 photoacoustic infrared spectra, 220f,222f,225f,228f,229f
 sizing agent detection, 219-221
- Cross polarization (CP), use in NMR studies, 9
- Cross-polarization-magic angle spinning (CP-MAS)
 cellulose oligomers, 54f
 cellulose I, 147f
 cellulose II, 47-48,148f
 crystalline allomorphs, 92f
 measurements, 120
 native celluloses, 95-97
 structural analysis of cellulose, 119-133
 solid carbohydrates, 47
See also Magic angle spinning (MAS)
- Crystal structure
 cellulose, 18,126-133
 native cellulose, 126
 ramie cellulose, 126
 regenerated cellulose, 128
 Rietveld method, 68-86
- Crystalline alkali-cellulose complexes, mercerization intermediates, 169-171
- Crystalline cellulose, chemical shifts, 298
- Crystalline regions, definition, 263
- Crystallization
 effect of temperature, 189
 measurement methods, 257
- Cupra rayon, CP-MAS NMR spectra, 128,129f,131f
- Curdlan, carbon-13 NMR spectra, 296-298
- D
- Dante irradiation, description, 93-94
- Degree of polymerization
 effect on cellulose morphology, 197
 hydrocellulose, 273-274
 native celluloses, 293,294t
 relationship to hydrocellulose weight after hydrolysis, 268f
- Depth profiling technique,
 FT-IR-PAS, 226-230
- Desizing
 effectiveness, 223
 FT-IR-PAS, 221
- Deuteration, cellulose samples, 137-138
- Dichroism, complications, 155
- Diffraction studies, cellulose, 5-7
- Dimethyloldihydroxyethyleneurea, structure, 218
- Dipolar coupling, protons, 100
- Disaccharides
 carbon-13 chemical shifts, 124
 chemical shifts and torsion angles, 122
 preparation in CP-MAS carbon-13 NMR study, 130
 structures, 7
- Disorder, measurement in cellulose, 255-256
- E
- Electron density
 methyl β -D-cellobioside in crystal conformation, 49t
 relationship to chemical shift, 48
- Electron micrographs, cellulose crystals, 193f,195f
- Endgroups
 accessibility in alkaline treatment, 283
 alkaline degradation of hydrocelluloses, 287
 analytical determination, 290
- Equatorial layer line, X-ray diffraction data, 28t
- Etherifications, cellulose, 295-296
- F
- Fibrils, algal species, 95-97
- Foam finishing techniques, description, 224
- Formylation, cellulose, 257-258
- Fortisan cellulose II-hydrazine complex A, structure, 209
- Fourier transform infrared spectrometer, 216f
- Fourier transform infrared photoacoustic spectroscopy (FT-IR-PAS)
 advantages, 215
 depth profiling, 226-230
 disadvantages, 230
 procedure in textile material study, 218-219

Fourier transform infrared
photoacoustic spectroscopy
(FT-IR-PAS)--Continued
scheme of operation, 215
See also Photoacoustic spectroscopy
Fractal analysis, cotton
cellulose, 233-252
Fractals
cellulose aggregates, 252
characterization, 235

G

Glaucoecystis, microfibrils, 203
Glucans, carbon-13 chemical
shifts, 298t
Glucmannan polymers, molecular weight
influence on polymorphism, 196
 β -D-Glucose
carbon-13 NMR spectra, 121f
charge densities, 47-48
Glucose ring stretching, allomorphs of
cellulose, 144t
 β -1,4-Glycosidic linkage
cellulose chains, 8-9
cleavage in alkaline media, 286-289
distributions in torsion angles, 130
stable conformations, 8
symmetry, 148
Gold colloids, fractal structure, 236
Greige cotton
Guinier plots, 241f
isointensity contour
plots, 239f, 242f
scattering intensity data, 240f
See also Cotton
Guanidinium hydroxide treatment,
cellulose, 184-185

H

Hausdorff dimension, 235
Higher plant celluloses
allomorphs, 116
CP-MAS spectra, 96f
similarity, 113
Hydrocellulose
alkaline degradation, 280f
amorphous and fibrous
structures, 274-281
carbon-13 NMR spectra during
degradation, 279f
cellulose II character, 281
CP-MAS spectra, 104f, 112f
degree of polymerization, 273-274
effect of physical structure on
alkaline degradation, 272-290

Hydrocellulose--Continued
fibrous and amorphous peeling, 285
fibrous changes during
treatment, 281
hydroxyl accessibility during
degradation, 276f
longitudinal relaxation time, 102
preparation in alkaline degradation
study, 273
Raman spectra, 275, 278f
random chain cleavage, 288
spectra, 101
X-ray diffractograms, 275, 277f
Hydrocellulose II
Guinier plots, 241f
isointensity contour plots, 239f
scattering intensity in SAXS, 245
specific inner surface, 250
structural parameters, 246t
Hydrogen bonding
alkali-treated cellulose, 296
cellulose, 138-141, 292-300
differences among lattice
packings, 300
unit cell, 11-12
Hydrolysis
Cladophora glomerata, 94-95
relationship between residue weight
and time, 259t
See also Acid hydrolysis
Hydroxyl accessibility
alkaline degradation, 274, 287
hydrocellulose during alkaline
degradation, 276f
See also Accessibility
Hydroxyl groups
availabilities in cellulose, 262t
hydrogen bonding
information, 258-262
reactivity in glucose residues of
cellulose, 295-296

I

Incident light, plane of polarization
in Raman spectra, 155
Infrared spectroscopy, infrared
absorption spectrum, 214
Inositols, vibrational spectra, 12
Intensity ratios, two-unit-cell
model, 128
Invariant values, cellulose, 247-249
Iodine sorption, measurement of
accessibility, 265
IR spectra, 138, 140f, 143f

L

Lateral order distribution,
cellulose, 266

- Leveling-off degree of
polymerization, 265-266
- Linked-Atom Least-Squares (LALS)
program
cellotetraose, 55-58
molecular model generation, 43
use, 20,26t
X-ray intensities, 200
- M
- Magic angle spinning (MAS)
diagrams of rotors, 121f
speeds in native cellulose study, 93
use, 39
See also Cross-polarization-magic
angle spinning (CP-MAS)
- Mannan, polymorphism, 196
- Mercerization
crystalline alkali-cellulose
complexes as
intermediates, 169-171
effect on pore volume fraction, 249
mechanism, 202-203
transformations, 174
- Mercerized cellulose
hydrogen bonding patterns, 294
random chain cleavage, 288
similarity to regenerated
cellulose, 298
- Mercerized cotton
accessibility, 264t
crystalline fraction, 264
permeability limits, 267t
volume accessible to water, 267t
- Mercerized ramie
conformation, 167
Raman spectra, 162f,164
- Methyl β -D-cellobioside
charge densities, 47-48
crystalline state, 50f
packing in crystals, 48
relative energies of stable
conformers, 45t
- Methyl β -D-cellobioside
crystal data, 51t
crystal structure, 53f,63
diffraction methods, 42-43
diffraction pattern, 51
hexagonal crystalline platelet, 52f
model for cellulose II, 51
structure, 63
X-ray diffraction, 52f
- Meyer-Misch cell, 33
- Microfibrils
cellulose I, 174
definition, 234
- Miller indices, 38
- MM2 CARB program, 41,46t
- Moisture regain, definition, 263
- Moisture-regain technique, measurement
of cellulose disorder, 256
- Molecular conformations, celluloses I
and II, 12
- Molecular weight
effect on internal water accessible
to solute, 268f
effect on polymorphism, 189-198
- Monomeric geometries, effect in rigid
models, 27t
- Monosaccharides
carbon-13 chemical shifts, 124
preparation in CP-MAS carbon-13 NMR
study, 130
- MULTAN program, use, 42
- N
- Na-cellulose, transition to celluloses
I and II, 185
- Na-cellulose I
antiparallel structure, 174
fibrous orientation, 170
X-ray fiber diffraction, 171f
- Na-cellulose IIB
crystal structure, 172
threefold helical structure, 174
unit cell, 173f
X-ray fiber diffraction, 171f
- Na-cellulose IV
crystal structure, 172
unit cell, 173f
X-ray fiber diffraction, 171f
- Native cellulose
allomorphs, 89,111,295
antiparallel chain arrangement, 4
carbon-13 NMR spectra, 9,95-97,153
categories of Raman spectra, 158
crystal structure,
88-89,126,130-133,169,234
crystalline polymorphy, 11,102
differences of cellulose, 164
distributions in torsion angles, 130
hydrogen bonds, 292-300
OH stretching bands, 142
peeling, 272-273
preparation in irreversibility
study, 137
Raman spectra, 9
structural complexity, 11
surface layers of the
crystallites, 91
unit cell parameters, 90
See also Cellulose I
- Near-neighbor spectra
allomorph contributions, 110
isolation, 106-113
source, 106

- Near-surface analysis, cellulose
fibers, 219-221
NMR--See also Carbon-13 NMR spectra
- O
- Oligomers
packing features, 48
X-ray crystallography, 63
Organic solvents, cellulose, 199
- P
- Packing
cellulose I-ethylenediamine
complexes, 207
celluloses I and II, 154
ramie cellulose, 18,29,31t,35
use of carbon-13 NMR spectra, 178
See also Parallel packing
Parallel dichroism, cellulose II
family, 142-144
Parallel-down model
description, 32t,34t
See also Parallel model
Parallel-down structure,
description, 18
Parallel model
cellotetraose, 80-81t,86
cellulose I, 200
cellulose I-ethylenediamine
complexes, 207
diffraction patterns for
cellotetraose, 85f
X-ray diffraction patterns for
cellotetraose, 76f
See also Parallel-down model
Parallel packing
cellulose I, 137
See also Packing
Parallel-up structure, description, 18
Peeling
pseudo-first-order rate
expression, 281-283
rate coefficients, 283t
rates for hydrocellulose, 285t
reactions, alkaline degradation of
hydrocellulose, 281-283
Periodate oxidation,
description, 258-262
Permeability limits
cotton, 267t
mercerized cotton, 267t
Perturbative Configuration Interaction
with Localized Orbitals (PCILO)
charge densities, 47-48
description, 41
Photoacoustic sample cell unit, 216f
- Photoacoustic spectroscopy
effective sampling depth, 217
See also Fourier transform infrared
photoacoustic spectroscopy
(FT-IR-PAS)
Physical stopping
description, 285
maximum number of sites, 286
peeling reaction, 274
pseudo-first-order rate
equation, 285-286
rate coefficients for
hydrocellulose, 286t
rate factors, 289
PITMOS, molecular drawings, 43
Plant cell walls, molecular
organization, 151-152
Polyethylene, carbon-13 NMR chemical
shifts, 64
Polymer hypothesis, evolution, 3
Polymeric fibers, structural studies,
difficulty, 5
Polymers
computer programs, 20
spectra of nonrandomly oriented, 154
structure analyses precision, 2
Polymorphs
cellulose I, 153
composition, 192f
near-neighbor spectrum results, 107
parameters, 189
recrystallized cellulose, 189-198
Polysaccharides
crystallization behavior, 189
solubilities, 292-300
Pore size, methods for cellulose
samples, 250
Pore structure,
characterization, 266-269
Pore volume fraction, cellulose, 249t
Porod's law
deviation, 246-247
SAXS, 246
Potassium bromide pellet method,
cellulose analysis, 214
Power law behavior, SAXS, 245
Principle of economy, 6
Proton-spin diffusion,
observations, 100-102
Protons, dipolar coupling, 100
PS-79 program, 20,26t
- R
- R factors
parallel-down chains, 23f
SRRC, 22t,34
symmetrical models, 31t
X-ray diffraction studies, 20-21
See also R values

- R values
 cellotetraose, 75
 ramie cellulose, 35
 Rietveld method, 72-73
 weighting schemes, 21
 See also R factors
- Raman microprobe
 experiments, 156f
 purpose, 151
- Raman spectra
 band assignments, 153
 categories for cellulose, 166
 celluloses, 151-167
 hydrocellulose, 275,278f,279f
 native celluloses, 9,158
 Valonia, 161t
- Raman spectroscopy, 7-9
- Ramie cellulose
 cell symmetry, 18-19
 chain conformation, 18
 cross-sectional Raman spectra, 165f
 crystal structure, 126
 differences from Valonia
 cellulose, 161-164
 monomeric geometry, 25
 packing, 18
 Raman spectra, 155,161t,162f
 selection in X-ray diffraction
 study, 15-16
 unit cell, 16
- Ramie cellulose I, X-ray diffraction
 studies, 15-36
- Ramie cellulose I-1,3-diaminopropane
 complex, structure, 209
- Ramie cellulose I-ethylenediamine,
 X-ray diffraction studies, 205-208
- Ramie fiber, Raman spectra, 159f
- Rayon
 recrystallized, 191
 solubility in SO₂-amine-organic
 solvent systems, 294
- REFIN program, 72
- Regenerated cellulose, crystal
 structure, 128
- Resonance intensity
 emphasis in crystalline
 interior, 100
 hydrocellulose, 101
- Rhizoclonium cellulose
 CP-MAS spectra, 108f
 crystalline lateral dimensions, 110
 crystalline polymorphism, 107-109
 isolation of near-neighbor
 spectra, 106-108
 See also Rhizoclonium hieroglyphicum
- Rhizoclonium hieroglyphicum
 spectra, 95-97,103f
 See also Algal cellulose,
Rhizoclonium cellulose
- Rietveld method
 antiparallel model for
 cellotetraose, 79f
- Rietveld method--Continued
 cellotetraose, 68-86
 description, 70-72
 important features, 72
 parallel model for
 cellotetraose, 77f
 termination of refinement, 72
 use, 69
- S
- Scan velocity, Fourier transform
 infrared spectrometer, 218t
- Scanning transmission electron
 micrographs, fibrillar network of
 native celluloses, 99
- Scattering, intensity, cellulose in
 SAXS, 245
- SHELX program
 description and use, 19-20
 R values, 34
 R-value calculation, 25
- Silica particles, fractal
 structure, 236
- Single-crystal diffraction, use, 39
- Sizing agent
 amount removed by desizing, 223
 degree of penetration, 223
 detection by FT-IR-PAS, 219-221
 warp yarns, 219
- Small-angle X-ray scattering (SAXS)
 cotton cellulose, 233-252
 procedure in cellulose study, 237
 scattering source for cellulose, 245
- SO₂-diethylamine-dimethyl sulfoxide
 (SO₂-DEA-DMSO), solubilities of
 cellulose, 292-300
- Soda cellulose, conversion to
 cellulose I, 136
- Solid-state NMR, use in cellulose II
 structural study, 41
- Solubilities, polysaccharides, 292-300
- Solvent crystallization, role in
 polymorphism, 189
- Sorption
 deuteration method, 262-263
 moisture-regain method, 263-265
- Southern Regional Research Center
 (SRRC) program
 R factors, 22t,34
 R-value calculations, 21
 temperature factors, 32t
 use, 20
 X-ray diffraction data for ramie
 cellulose, 26t,29
- Space group
 cellotetraose, 55,68-69
 parameters, cellotetraose structural
 study, 74-75
Valonia cellulose, 200

Specific inner surface, hydrocellulose
 II and Valonia, 250
 Spectral subtraction technique,
 application, 221
 Spectroscopy, cellulose, 4-5,7-10
 Structural analyses, problems, 2
 Structural irreversibility, celluloses
 I and II, 135-149
 Structural levels, cellulose, 3
 Structural models, cellulose, 2
 Symmetry
 unit cell, 5
See also Cell symmetry, Twofold
 screw axis symmetry

T

Temperature factor
 importance in X-ray diffraction
 studies, 31
 SRRC program, 32t
 Temperature of crystallization, effect
 on cellulose II-cellulose IV
 ratios, 191
 Thermal diffusion length
 cotton, 227t
 photoacoustic spectroscopy, 217
 Torsion angles
 determination, 119
 distributions about β -1,4-glycoside
 linkages, 130
 relationship to chemical
 shifts, 120-124
 Two-crystal model, intensity
 ratios, 128
 Two-unit-cell model, intensity
 ratios, 128
 Twofold screw axis symmetry
 cellulose, 18
 coincidence with molecular chain
 axis, 6
 validity of assumption, 5
See also Symmetry

U

Unit cell
 algal cellulose, 153
 anhydroglucose sites, 113
 anhydroglucose units, 105,111
 cellotetraose, 69,86
 cellulose I, 17f,172,175f,200
 cellulose I-1,3-diaminopropane
 complex, 209
 cellulose I-hydrazine complexes, 205
 cellulose II, 200-203

Unit cell--Continued

cellulose II-hydrazine
 complex, 209-211
 cellulose III, 148
 cellulose-diaminopropane
 complexes, 206t
 cellulose-ethylenediamine
 complexes, 206t
 cellulose-hydrazine complexes, 206t
 celluloses I and II, 141,175f
 chain conformations, 142
 8-chain versus 2-chain, 36
 conformation to crystallographic
 convention, 35
 crystal structure, 115
 hydrogen bonding pattern, 11-12
 inequivalences, 115
 Na-cellulose IIB, 173f
 Na-cellulose IV, 173f
 native cellulose, 11
 parameters, 74-75,90,153
 spectral lines, 109
 tetramers of cellotetraose, 75-78
Valonia, 91,154
 X-ray diffraction studies, 16-18

V

Valonia cellulose

crystalline spectra of dry and
 hydrated, 126
 Guinier plots, 241f
 iso-intensity contour plots, 240f
 preparation in SAXS study, 236-237
 Raman spectra, 157f,161-164
 scattering intensity in SAXS, 245
 specific inner surface, 250
 spectra, 159f
 structural parameters, 246t
 transformation of cellulose I to
 II, 138
 X-ray diffraction data for ramie
 cellulose, 25
See also Valonia macrophysa,
Valonia ventricosa

Valonia macrophysa

aggregates, 155
 carbon-13 NMR spectra, 95-97
See also Valonia cellulose

Valonia ventricosa

carbon-13 NMR spectra, 95-97
 cellulose structure, 4
 description, 237
 resonance multiplets, 91
 X-ray intensity data, 200
See also Valonia cellulose

Vibrational spectra, inositols, 12

W

- Warp yarns, sizing agents, 219
- Water
 effect on cotton
 cellulose, 124-126,128-130
 sorption equation, 264
- Weighting schemes, R values, 21
- Wide-angle X-ray diffraction (WAXD)
 data, cotton cellulose, 244f
- Wide-angle X-ray scattering (WAXS)
 alkali-treated cellulose, 182,184t
 cotton linters treated with
 alkali, 184
 procedure in alkali treatment
 study, 179
 procedure in cellulose study, 238
- X
- X-ray crystallography, oligomers, 63

- X-ray diffraction
 ability to distinguish models, 32
 cellodextrins, 39
 cellotetraose, 56f,76f,78-86
 cellulose crystallites, 154,191
 change in distance due to chain
 rotation, 33t
 crystalline oligomers, 48-50
 dependence on models, 39
 methyl β -D-cellobioside, 52f
 Na-cellulose, 170,171f
 procedure in cellulose complexes
 study, 204-205
 structural irreversibility
 study, 138
 use in Rietveld method, 69
- X-ray diffractogram
 cellulose I, 138,139f
 cellulose II, 138,139f
 hydrocellulose, 275,277f,278f
- X-ray studies, cellulose
 complexes, 199-212

Production by Barbara J. Libengood
Indexing by Keith B. Belton
Jacket design by Carla L. Clemens

Elements typeset by Hot Type Ltd., Washington, DC
Printed and bound by Maple Press Co., York, PA